New Procedures in Spinal Interventional Neuroradiology
Series Editor: Luigi Manfrè

Luigi Manfrè *Editor*

Vertebral Lesions

EXTRAS ONLINE

Springer

New Procedures in Spinal Interventional Neuroradiology

Series Editor
Luigi Manfrè
Catania, Italy

In recent years, the dramatically increasing demand for new minimally invasive procedures for the treatment of spinal diseases has led to the development of a wide variety of new devices designed to foster a new "covert" surgical approach that is based on only a small incision, without major muscle involvement and with excellent maintenance of normal anatomy. The use of a CT guided technique (with performance of surgery in a CT unit rather than in a conventional operating room) offers a wide range of new possibilities and many advantages in comparison to conventional open surgical procedures. These include in particular the reduction of side effects and complications, shortening of the operative time, lowering of the risks of anesthesia (especially in severely ill or elderly patients), and decreased total cost. This series provides up-to-date information on these important advances and their application in different scenarios. It will consist of 5 handy volumes designed for ease of consultation. Each volume will include a concise but comprehensive introduction on biomechanics, relevant clinical syndromes, and diagnostic imaging. The principal emphasis of the series, however, will be description of the various procedures using either an X-ray or a CT guided approach. Owing to its practical orientation, the series will fill a gap in the literature and meet the need, identified by numerous specialists (including interventional neuroradiologists and radiologists, neurosurgeons, and orthopedists), for topical and handy guides that specifically illustrate the materials and methods presently available within spinal interventional neuroradiology.

More information about this series at http://www.springer.com/series/13394

Luigi Manfrè
Editor

Vertebral Lesions

Springer

Editor
Luigi Manfrè
Minimal Invasive Spine Therapy
Cannizzaro Hospital
Catania, Italy

New Procedures in Spinal Interventional Neuroradiology
ISBN 978-3-319-52632-4 ISBN 978-3-319-52634-8 (eBook)
DOI 10.1007/978-3-319-52634-8

Library of Congress Control Number: 2017946479

Printed on acid-free paper

This Springer imprint is published by Springer Nature
The registered company is Springer International Publishing AG
The registered company address is: Gewerbestrasse 11, 6330 Cham, Switzerland

To my two lovely twins Costanza and Ottavia, luce dei miei occhi

Contents

Vertebral Lesions: Imaging

1

Simon Nicolay, Johan W. Van Goethem, Luc van den Hauwe, Paul M. Parizel, and Pia C. Maly Sundgren

1.1 Imaging Strategy

1.1.1 Introduction

A wide variety of lesions can be found in the vertebral column. The lesions can be solitary or multiple and include both benign and malignant lesions. The differential diagnosis of a vertebral tumour can be narrowed down based on the age of the patient, the number of lesions, the location in the vertebra, the location in the spinal column, the morphology and the imaging characteristics (Algorithms 1 and 2).

S. Nicolay (✉) • L. van den Hauwe • P.M. Parizel
Department of Radiology, University Hospital Antwerp,
Wilrijkstraat 10, 2650 Edegem, Belgium
e-mail: simon.nicolay@uza.be

J.W. Van Goethem
Department of Radiology, University Hospital Antwerp,
Wilrijkstraat 10, 2650 Edegem, Belgium

Department of Radiology, AZ Nikolaas, Moerlandstraat 1,
9100 Sint-Niklaas, Belgium

P.C. Maly Sundgren
Department of Diagnostic Radiology, Clinical Sciences Lund,
Lund University, Lund, Sweden

Center for Medical Imaging and Physiology, Skåne University Hospital,
221 85 Lund, Sweden

L. Manfrè (ed.), *Vertebral Lesions*, New Procedures in Spinal Interventional Neuroradiology, DOI 10.1007/978-3-319-52634-8_1

Algorithm 1

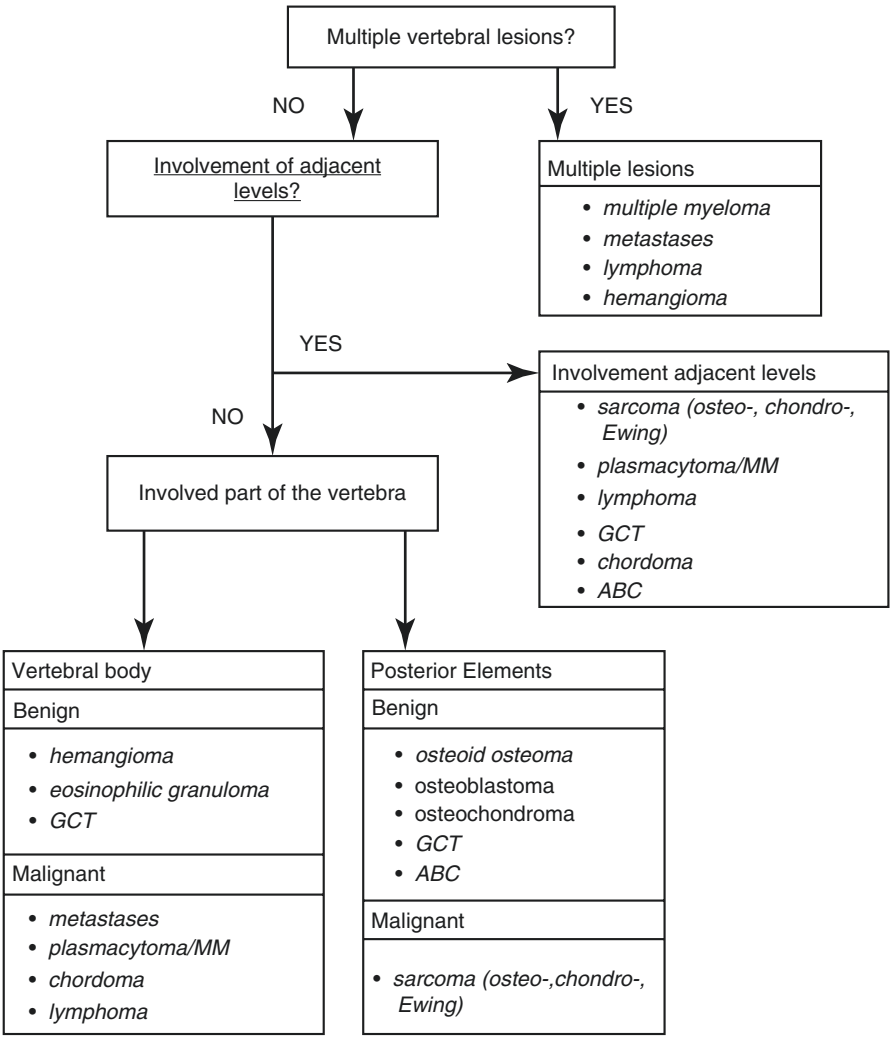
Multiple vertebral lesions?
NO
YES
Involvement of adjacent levels?
Multiple lesions
multiple myeloma
metastases
lymphoma
hemangioma
YES
Involvement adjacent levels
sarcoma (osteo-, chondro-, Ewing)
plasmacytoma/MM
lymphoma
GCT
chordoma
ABC
NO
Involved part of the vertebra
Vertebral body
Benign
hemangioma
eosinophilic granuloma
GCT
Malignant
metastases
plasmacytoma/MM
chordoma
lymphoma
Posterior Elements
Benign
osteoid osteoma
osteoblastoma
osteochondroma
GCT
ABC
Malignant
sarcoma (osteo-,chondro-, Ewing)

Algorithm 2

Age
0-10 • Eosinophilic granuloma
10-20 • Osteoid osteoma • ABC
20-50 • GCT
40-60 • plasmacytoma • chordoma • hemangioma
50-70 • *MM* • *metastasis*

Initial imaging usually consists of plain radiography. This is not very sensitive mainly because of the poor two-dimensional tissue separation due to the complex three-dimensional anatomy of the spine. The sensitivity to specify a vertebral lesion on an X-ray is difficult as well. Magnetic resonance imaging (MRI) is the imaging modality of choice when it comes to detecting and characterizing tumours of the osseous spine. MRI has the advantage of superior soft tissue characterization, the possibility of multiplanar imaging and the ability of evaluating present neurological compromise. Computed tomography (CT) is superior in detecting calcifications or cortical bone lesions. Since this technique offers multiplanar imaging too, it is very well suited to evaluate the complex anatomy of the posterior vertebral elements and assess some typical lesions in this anatomical region. Furthermore CT plays an important role in biopsy guidance or therapeutic ablation of certain tumours.

1.1.2 Age and Clinical History

The patient's age is a very important piece of information when it comes to differentiating a vertebral tumour (Algorithm 2). For example, osteoid osteoma, aneurysmal bone cyst (ABC) and Ewing sarcoma are predominantly found in young people, giant cell tumour (GCT) in the middle-aged and chordoma in the elderly.

The value of a thorough clinical history and examination should not be underestimated. Multiple vertebral body lesions in a patient with a known primary tumour will most likely be metastases. Depending on the extent and location of the tumour, clinical symptoms may arise. Osteoid osteoma, aggressive haemangioma and malignancies are typically symptomatic.

1.1.3 Number of Lesions

Determining the multiplicity of vertebral bone pathology offers a valuable clue to narrow down the differential diagnosis. Solitary vertebral lesions are less common than lesions in multiple locations. Pathology with multiple vertebral lesions will most frequently be metastases from breast and lung tumours in woman and prostate and lung tumours in men (Fig. 1.1). A medical history of a primary tumour supports this diagnosis even more. Multiple lesions are seen in 30% of vertebral metastases [1]. Multiple primary vertebral lesions are most commonly lymphoproliferative disorders such as lymphoma or multiple myeloma (Fig. 1.2). Other multifocal lesions include eosinophilic granuloma in children, fibrous dysplasia and haemangioma (Fig. 1.3). MRI and bone scintigraphy or single positron emission computed tomography (SPECT) are most sensitive in the detection of multiple lesions. Radiologists should, however, be aware that MRI is normal in as much as 20% of cases of multiple myeloma [1].

Solitary vertebral tumours are less common. The differential diagnosis is much broader than for multiple lesions. This stresses the importance of a thorough analysis of the imaging features in order to come to the correct diagnosis or narrow down the differential diagnosis.

1.1.4 Location

The location of the tumour(s) in the spine is another helpful tool in the assessment of the nature of the lesion. The cervical spine is favoured by osteoblastoma, osteochondroma and eosinophilic granuloma. The thoracic spine is a predilection site for haemangioma, enostosis and chondrosarcoma [1–3]. ABC is frequently found in the thoracic spine but even more in the lumbosacral spine. Enostosis and osteoid osteoma are most commonly found in the lumbar spine [4]. The sacrum is often affected by chordoma and plasmacytoma (Fig. 1.4). Giant cell tumours (GCT) are the most common benign sacral tumours [5, 6]. Rarely Ewing sarcoma occurs in the sacrum [7].

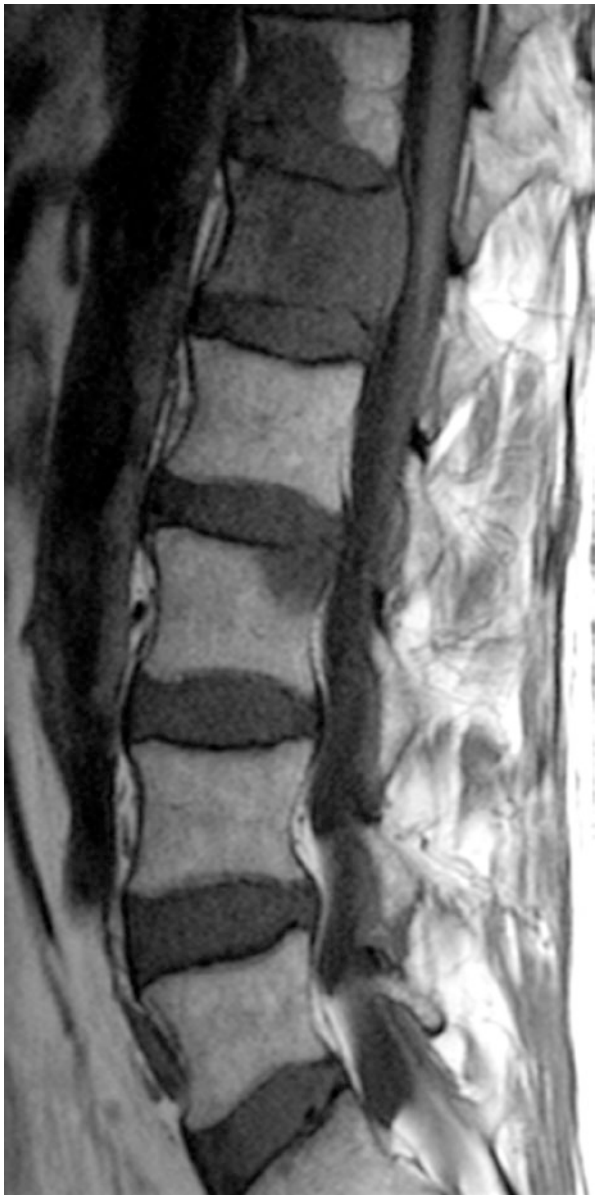

Fig. 1.1 Sagittal T1-WI in a patient with a known primary neoplasm showing multiple hypointense vertebral metastases

The next feature to look for is the site of the lesion within the vertebra. Haemangioma, enostosis and GCT have a strong predilection for the vertebral body. Only 10% of haemangiomas are found in the posterior elements. Chordomas and Ewing sarcomas have a predilection for the vertebral body too, usually eccentrically. GCT tends to lie more centrally. Benign lesions of the posterior vertebral elements comprise osteoblastoma, osteoid osteoma, ABC and

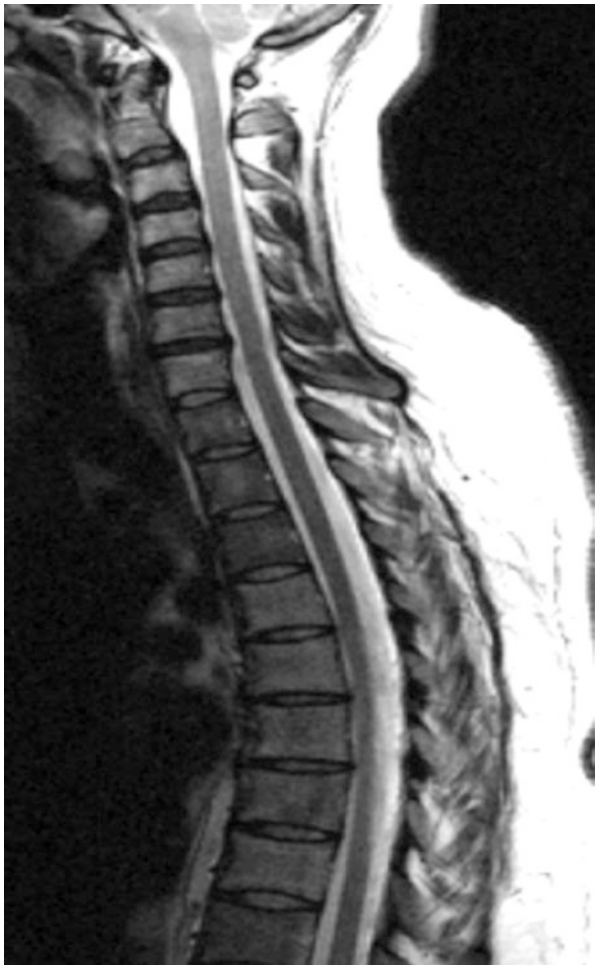

Fig. 1.2 Sagittal T2-WI in a patient with lymphoma showing multiple lesions

osteochondroma (Figs. 1.5, 1.6 and 1.7). Some lesions affect the vertebral body as well as the posterior elements. ABC prefers the pedicles but sometimes extends into the vertebral body (Fig. 1.8). On the other hand, plasmacytoma and multiple myeloma mainly affect the vertebral body but tend to spread to the posterior elements.

1.1.5 Morphology

1.1.5.1 Border

The border of a lesion is a good indicator of its biological activity. Benign lesions like haemangioma, enostosis, osteoid osteoma, osteoblastoma and ABC have a clear demarcation, known as *geographic* appearance (Fig. 1.8). In contrast,

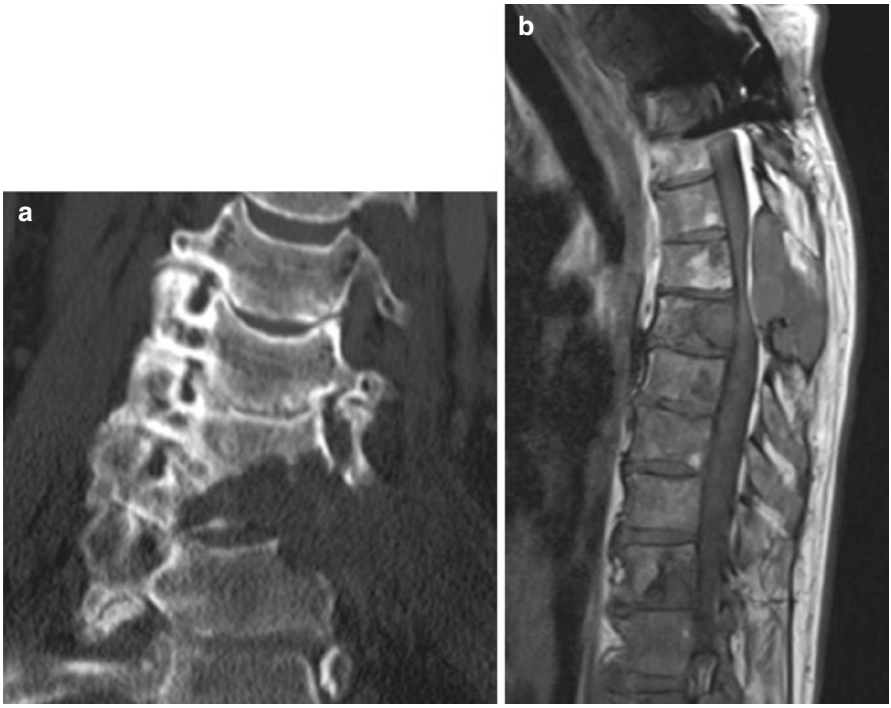

Fig. 1.3 (**a**, **b**) Coronal CT reconstruction showing an aggressive vertebral haemangioma extending over multiple vertebral levels (**a**). Multilevel involvement in a patient with fibrous dysplasia, illustrated on a sagittal T1-weighted MRI image (**b**)

aggressive benign lesions like aggressive haemangioma and malignant lesions such as osteosarcoma, Ewing sarcoma and metastases have a large transition zone. Cortical destruction is also a sign of aggressiveness.

1.1.5.2 Matrix

The structure or matrix of a tumour can help the radiologist in diagnosing tumours arising from the bone or cartilage.

Osteoblastic tumours contain amorphous ossifications on plain radiography or CT. The matrix lacks an organized trabecular pattern and is usually less dense than normal bone. Dense osteoblastic lesions display a low T1–T2 signal intensity pattern on MR imaging. Enostosis is characterized by solid, dense, cortical bone within the spongy bone of the vertebral body. A typical feature of osteoid osteoma is calcification within a lucent nidus with surrounding reactive sclerosis (Fig. 1.6). Osteoblastoma is histologically similar to osteoid osteoma, with areas of calcification in the matrix, but is larger and more expansive (Fig. 1.5).

Cartilage-forming tumours typically show punctate, arc or ring calcifications at radiography and CT. These calcifications appear as low-signal-intensity foci at MR imaging. Chondroid tissues with ring- and arc-type calcifications are typical for

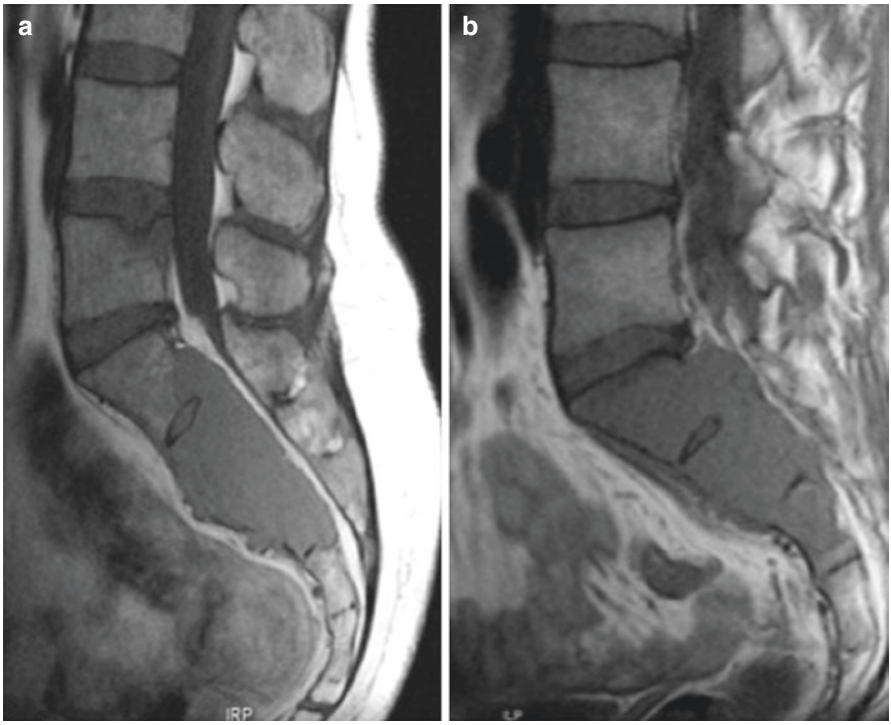

Fig. 1.4 (**a**, **b**) Sagittal T1-WI demonstrating the typical sacral localization of plasmacytoma (**a**) and GCT (**b**). These tumours can be difficult to distinguish from each other on imaging alone, often stressing the need for a correlation with age and symptoms. In the case insufficient biopsy, this might be needed to make a diagnosis

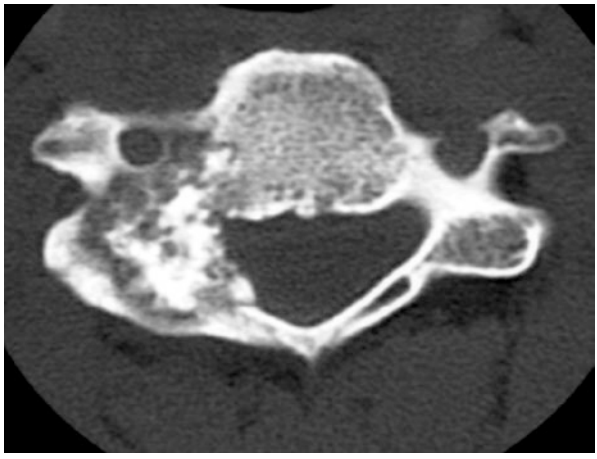

Fig. 1.5 Axial CT image in a patient with an osteoblastoma in the cervical spine. The tumour has a calcified or ossified matrix and is typically located in the posterior elements, in this case the right pedicle and lamina

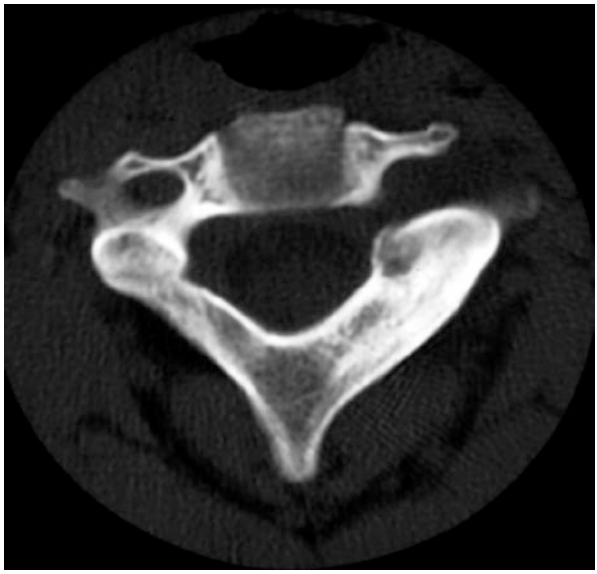

Fig. 1.6 Axial CT image in a patient with an osteoid osteoma in the left lamina of a cervical vertebra. The characteristic morphology with a lucent central nidus surrounded by dense sclerotic bone can easily be depicted

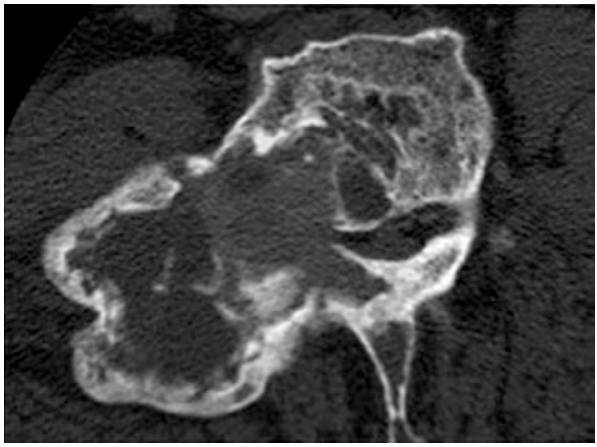

Fig. 1.7 Osteochondroma localized both in the posterior elements and body of a vertebra, showing typical continuity of marrow and cortex with the underlying native bone

osteochondroma and chondrosarcoma. This pattern may, however, also occur in osteoblastoma and chondroid types of chordoma (Fig. 1.5).

1.1.5.3 Expansion

ABC, osteoblastoma and to a lesser extent aggressive haemangioma can have an expansive nature (Figs. 1.5 and 1.8). Malignant lesions such as Ewing sarcoma and chondrosarcoma demonstrate expansion in combination with soft tissue extension, a feature that may, sometimes, be found in benign lesions like osteoblastoma and GCT as well.

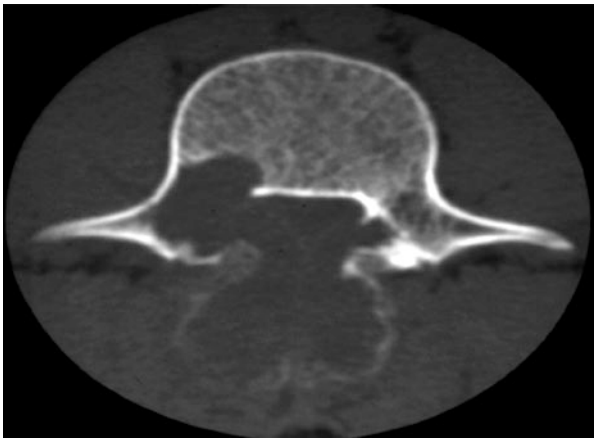

Fig. 1.8 Aneurysmal bone cyst. A well-defined, geographic, expansive, osteolytic lesion is found on CT. The tumour is located in the vertebral body as well as in the posterior elements

1.1.5.4 Soft Tissue Component

A soft tissue component can be seen in malignant lesions like Ewing sarcoma but also in benign lesions like osteoblastoma. Aggressive haemangiomas can also be accompanied by a large soft tissue component. These lesions are frequently symptomatic.

1.1.6 Imaging Features

1.1.6.1 CT/X-ray Imaging Features

Distinction between lesions can be made based on their osteoblastic or osteolytic nature (Table 1.1). The amount and degree of matrix mineralization in osteoblastic lesions is widely variable; thus the appearance on plain radiography or CT may range from densely blastic to nearly completely lytic. The differential diagnosis of osteoblastic tumours includes osteoblastic metastasis, bone island, lymphoma and osteosarcoma. Osteoid osteoma and osteoblastoma are essentially no bone-forming tumours but display a high density due to adjacent reactive bone sclerosis.

As in osteoblastic lesions, a gradient in osteolytic lesions exists. A very lytic appearance is usually associated with a more aggressive behaviour. Less lytic lesions tend to be less aggressive. The differential diagnosis of a lytic vertebral lesion, ranked from moderately lytic to extremely lytic, includes ABC, chordoma, GCT, lymphoma, metastasis, plasmacytoma/multiple myeloma and sarcoma.

A SPECT study is very sensitive to osteoblastic activity. Osteoblastic and less aggressive osteolytic lesions with partial osteoblastic activity will be detected using this technique. Purely osteolytic tumours might escape detection (Table 1.2).

In some cases the density of a lesion on CT facilitates further characterization. A low density (−50 to −100 HU) can be found in fatty lesions like lipomas and haemangiomas. By measuring the density, fat-containing lesions can be differentiated from air (−800 to −1000 HU), occasionally seen in degenerative disc disease. A very dense tumour in the spongy vertebral bone with a density similar to cortical bone will most likely be a bone island, also known as enostosis (Fig. 1.9).

Table 1.1 List of vertebral lesions that are predominantly osteolytic and those that are predominantly osteoblastic

Osteolytic vertebral lesions	Osteoblastic vertebral lesions
ABC	Osteoid osteoma (reactive sclerosis)
Chordoma	Osteoblastoma (reactive sclerosis)
Giant cell tumour	Enostosis
Lymphoma	Lymphoma
Metastasis	Hemangioma
Plasmacytoma/multiple myeloma	Metastasis (breast, prostate)
Sarcoma (osteo-, chondro-, Ewing)	Osteosarcoma

Table 1.2 Vertebral lesions that are purely osteolytic in nature and therefore might escape detection on SPECT examination

Bone lesions that can be negative on SPECT
Multiple myeloma
Aggressive metastasis
Chordoma

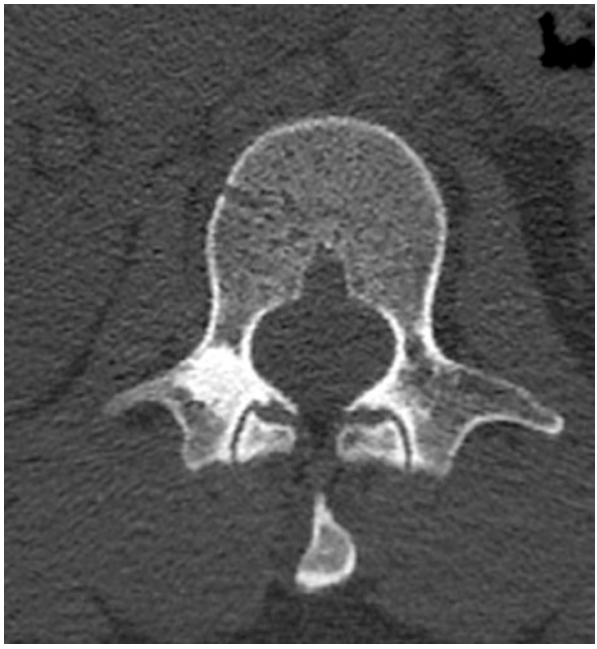

Fig. 1.9 Axial CT image showing an enostosis in the right pedicle of L1, which appears very dense, similar in density to cortical bone

1.1.6.2 MR Imaging Features

The behaviour of a lesion on T1-weighted and T2-weighted MRI sequences is another important parameter. The majority of pathological lesions have low signal intensity on T1-WI and high signal intensity on T2-WI (Fig. 1.10). However, a few exceptions exist (Table 1.3). Haemangioma and eosinophilic granuloma contain fat and will be bright on T1-WI (Figs. 1.11 and 1.12). Another exception is the dark

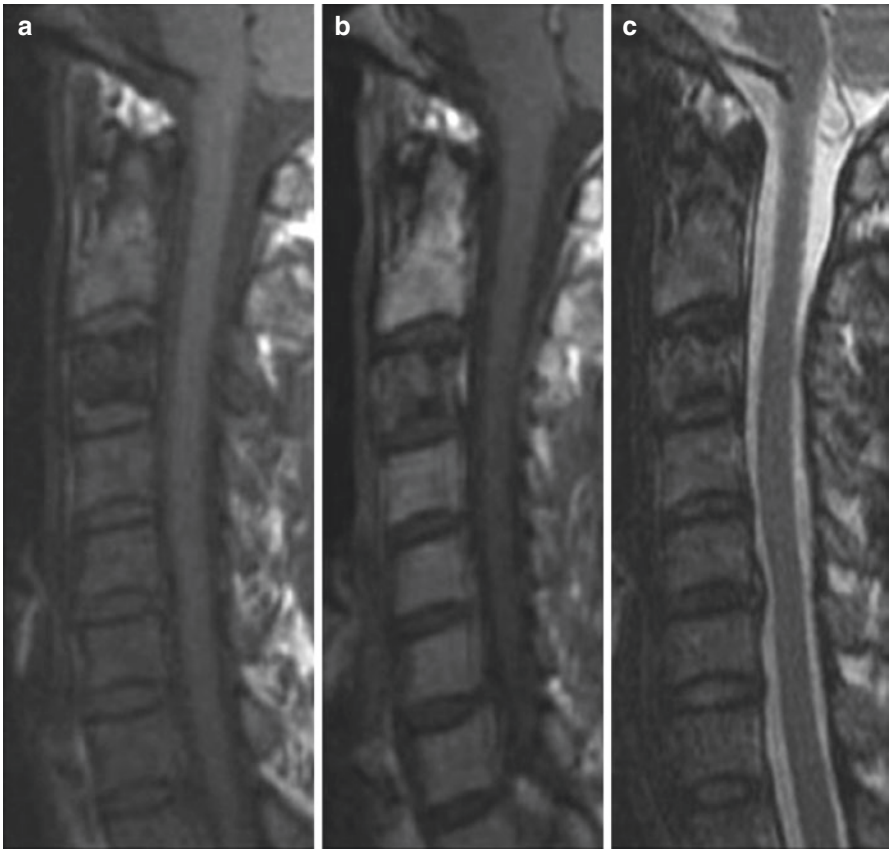

Fig. 1.10 (**a**–**c**) Ewing sarcoma in the body of C3, demonstrating a low signal on T1-WI (**a**), a high signal on T2-WI (**c**) and a moderate enhancement after gadolinium administration (**b**)

Table 1.3 Vertebral lesions that do not follow the general rule of low signal intensity on T1-WI and high signal intensity on T2-WI

Lesions with high signal intensity on T1-WI	Lesions with low signal intensity on T2-WI
Haemangioma	Giant cell tumour
Eosinophilic granuloma	Enostosis

appearance of a GCT on T2-WI due to the high cellularity and collagen and haemosiderin content [8]. Bone islands are dark on both T1-WI and T2-WI since they are histologically identical to cortical bone.

The enhancement pattern after the administration of a gadolinium chelate can be very suggestive in some cases, like a ring and arc pattern in chondroid tumours (Fig. 1.13).

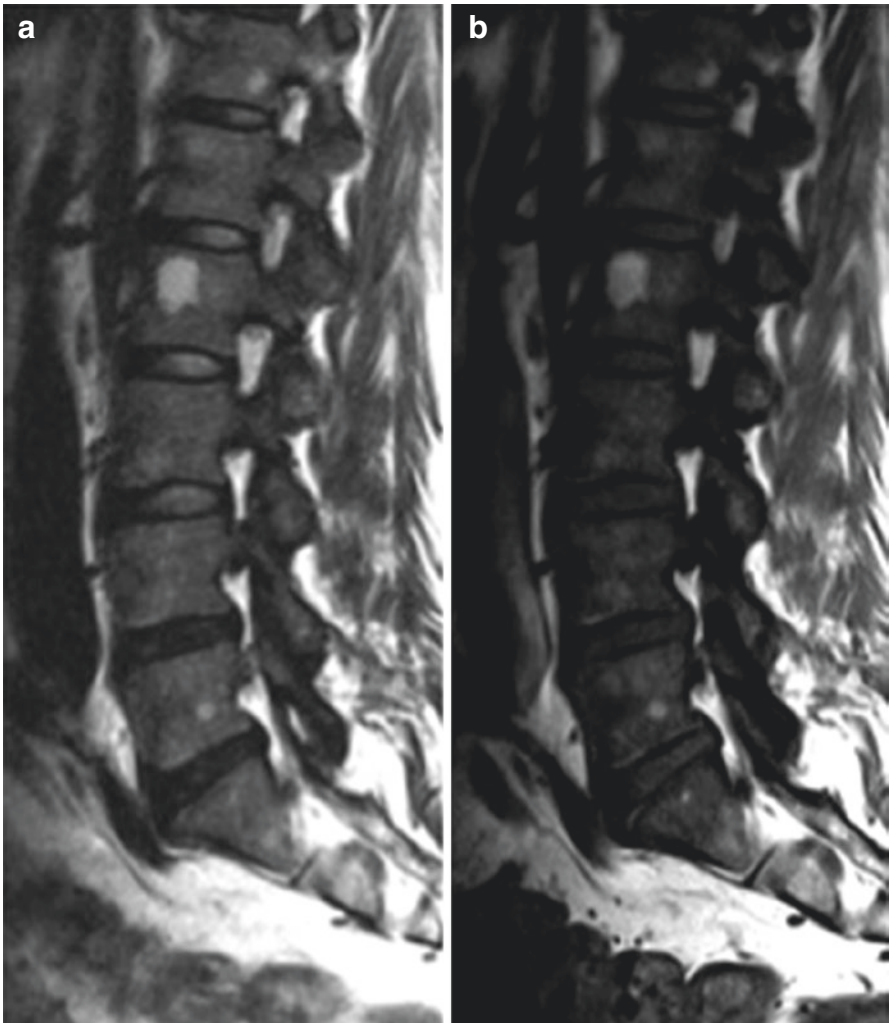

Fig. 1.11 (**a**, **b**) Multiple vertebral haemangiomas. These lesions typically have a high signal on T2-WI (**a**) but also on T1-WI (**b**), due to fatty contents

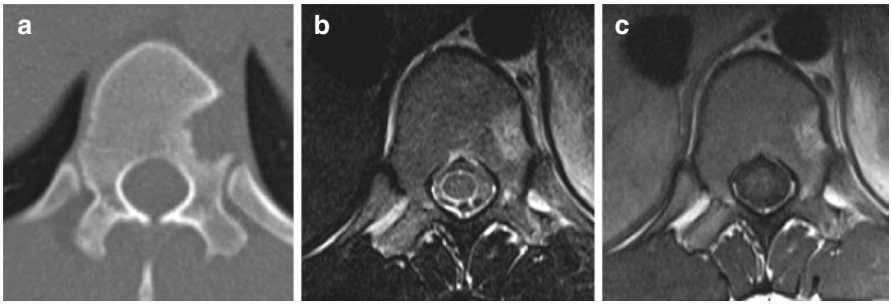

Fig. 1.12 (**a**–**c**) Eosinophilic granuloma. A well-demarcated lytic lesion is noted eccentrically in the body of a thoracic vertebra. A high signal intensity on T2-WI as well as T1-WI is typical

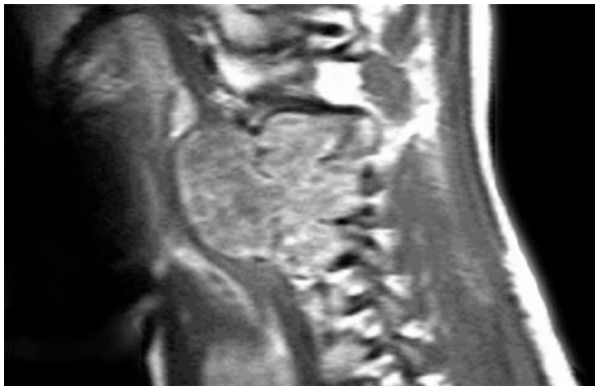

Fig. 1.13 Sagittal contrast-enhanced T1-WI image in a patient with a vertebral chordoma. The tumour extends across multiple cervical segments and has a large dumbbell-shaped soft tissue component. Heterogeneous enhancement with ring and arc pattern of the chondroid matrix is noted

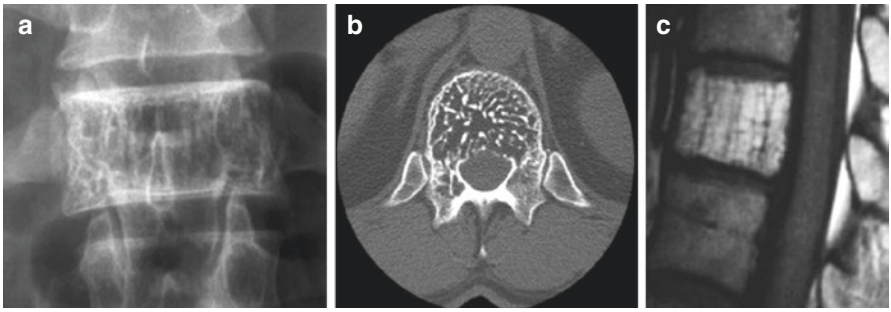

Fig. 1.14 (**a**–**c**) Thickening of bone trabeculae in a classic, nonaggressive haemangioma resulting in a "jail bar" or "honey-combing" appearance on plain radiography (**a**) and corresponding "polka-dot" sign on axial CT images (**b**). Sagittal T1-WI image (**c**) also showing the "jail bar" appearance, as well as a high signal intensity due to the fatty component of the lesion

1.1.6.3 Specific Patterns

Some morphological patterns can offer, if present, a very specific diagnosis or differential diagnosis. It is, however, important to interpret these findings with caution and correlate them with all other features. *Vertebra plana* is characteristic for EG but can also be seen in rare cases of other tumours like GCT. A *polka-dot* pattern on axial CT images is very typical for a haemangioma (Fig. 1.14b). Osteoid osteoma displays a specific morphology that can be detected on radiography, CT and MRI: prominent reactive sclerosis surrounding a lucent central nidus (with variable central calcification) (Fig. 1.6). Paget's disease and lymphoma may result in an expanded vertebra with marked sclerosis, known as an *ivory vertebra*. Although typically linked to ABC fluid–fluid levels, a result of sedimentation of blood degradation products can sometimes be found in osteoblastoma, chondroblastoma, telangiectatic osteosarcoma and rarely in GCT and fibrous dysplasia (Fig. 1.15) [9]. On axial MR images, a plasmacytoma may resemble the morphology of the brain, called *mini-brain* appearance [10]. Chordomas may be shaped as a *dumbbell* or *mushroom*, preserving the disc space (Fig. 1.13). The spider pattern can be observed in plasmacytoma but also in haemangioma (Fig. 1.16).

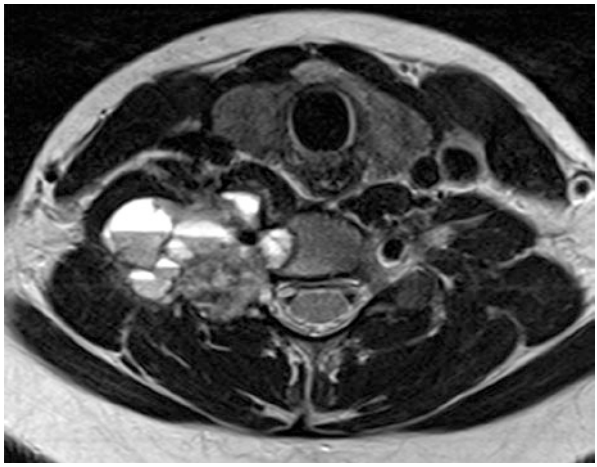

Fig. 1.15 Aneurysmal bone cyst (ABC) in the right lateral parts of C6. T2-weighted MRI shows a large, expansive tumour with cystic components showing fluid–fluid levels. This is a typical finding for ABC but may also occur in other tumours

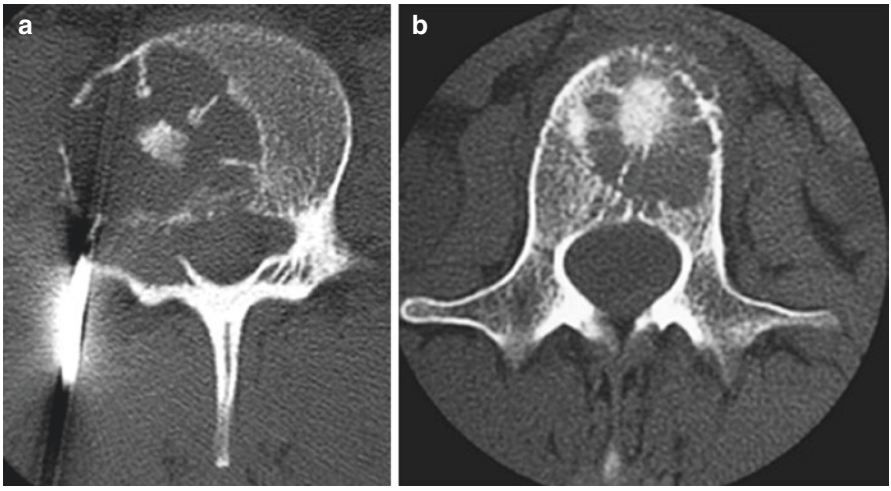

Fig. 1.16 (**a**, **b**) Axial CT image of a vertebra containing an osteolytic lesion with central dense bone and extending dense spider-leg appearance. This pattern is frequently observed in plasmacytoma (**a**) but also in haemangioma (**b**)

1.2 Primary Vertebral Lesions

1.2.1 Vertebral Haemangioma

1.2.1.1 General

Haemangioma is the most common benign vertebral tumour. Its incidence increases with age, with a peak around 40–60 years of age. The majority of haemangiomas are asymptomatic and discovered incidentally. In rare cases an aggressive behaviour is noted with a soft tissue mass that can cause neurological compromise. This lesion

primarily affects the thoracic spine (>50%), a smaller portion is found in the lumbar spine (30%), and the cervical spine and sacrum are involved in the remainder. There is a strong affection for the vertebral body, but in 10% of the cases, spread to the posterior elements occurs. One third are multiple.

1.2.1.2 Imaging

This vascular tumour causes trabecular bone resorption. In response reactive trabecular thickening occurs in unaffected bone. The thickened vertically oriented bone trabeculae give the tumour its typical *jail bar* appearance on plain radiography and *polka-dot* pattern on axial CT (Fig. 1.14a, b). On MRI a well-demarcated lesion with a bright signal on T2-WI as well as on T1-WI, due to fatty content, will be seen (Figs. 1.11 and 1.14c) [11]. In contrast, the aggressive type will be dark on T1-WI. Haemangiomas show enhancement after gadolinium administration, most marked in the aggressive type.

1.2.2 Plasmacytoma

1.2.2.1 General

Solitary plasmacytoma of bone is a localized tumour in the bone comprised of a single clone of plasma cells in the absence of other features of multiple myeloma (anaemia, hypercalcaemia, renal insufficiency or multiple lytic bone lesions). It is found in 3–7% of patients with plasma cell neoplasms. Men are more affected than women. The peak incidence is in the 5th to 6th decade. Local or irradiating pain is the most frequent complaint. This tumour has a predilection for the thoracic spine. The lumbar spine is less involved and the cervical spine and the sacrum are rarely affected. The lesion arises in the vertebral body, but the posterior vertebral elements are virtually always involved. The majority are solitary.

1.2.2.2 Imaging

On plain radiography this lesion has a lytic, often expansive, multicystic appearance, frequently accompanied by thickened trabeculae [12]. Fractures or total collapse may occur.

A low signal intensity on T1-WI and a high signal on T2-WI are found in the entire vertebral body. Usually there is diffuse enhancement after gadolinium administration, but peripheral enhancement is sometimes seen (Fig. 1.17). Because of the slow-growing nature of this tumour, reactive thickened cortical bone forms typical curvilinear low-signal-intensity structures resembling brain sulci, known as the *mini-brain* appearance (Fig. 1.18) [10].

1.2.3 Multiple Myeloma

1.2.3.1 General

Multiple myeloma, a monoclonal proliferation of malignant plasma cells, is the most frequent primary malignant vertebral tumour. It is mostly found in the 6th to 7th decade. The majority are asymptomatic and are incidentally discovered during

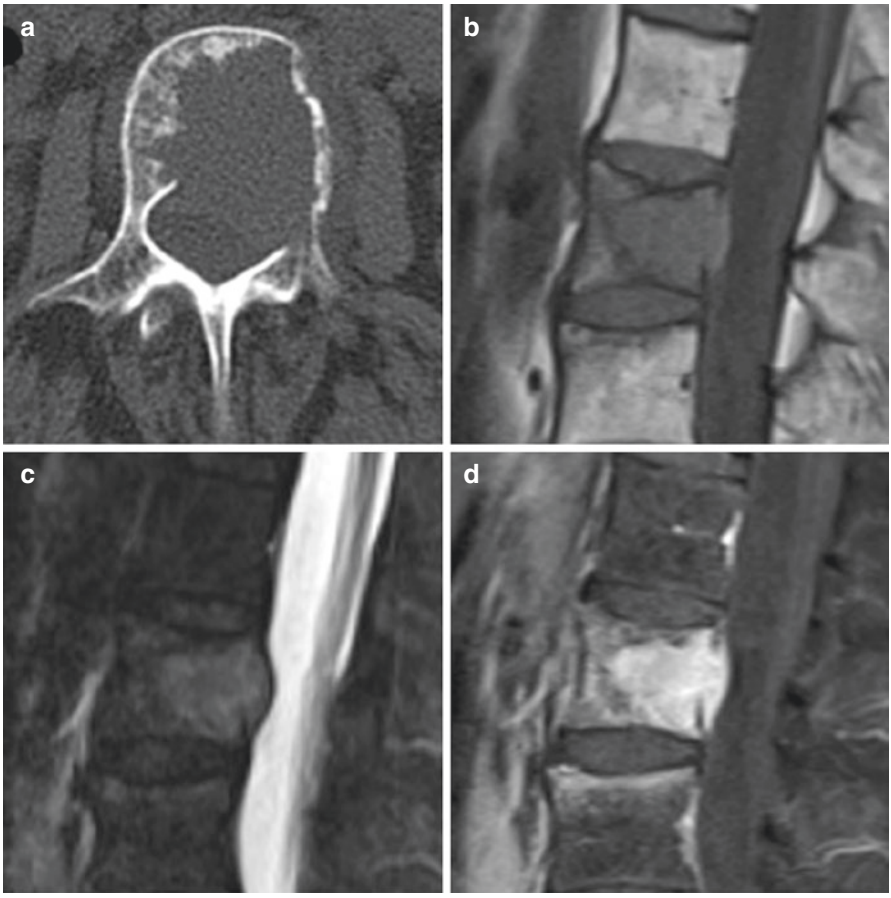

Fig. 1.17 (**a**–**d**) Plasmacytoma presenting on axial CT as a lytic, expansive lesion of the vertebral body with typical involvement of the posterior elements, in this case the left pedicle (**a**). Corresponding sagittal MRI images with a low signal intensity on T1-WI (**b**), intermediate signal intensity on STIR (**c**) and diffuse enhancement with intravenous contrast medium (**d**)

examination for other medical problems. The most common symptom is bone pain due to local extension. The lesion favours the vertebral body, often with epidural extension.

1.2.3.2 Imaging

Radiography and CT characteristically show punched out lytic lesions, osteopenia and fractures (Fig. 1.19a, b). Osteosclerosis is rare. Furthermore, compared with conventional radiography and MRI, CT is superior in estimating potential instabilities and risk of fractures [13, 14]. The fracture risk can be classified according to the volume of osteolysis. In cases in which more than 50% of the vertebral body is destroyed, the risk is classified as high [15]. On MRI different patterns are possible, ranging from normal appearance to focal disease or diffuse vertebral infiltration. Usually multiple myelomas show low signal intensity on T1-WI and contrast enhancement (Fig. 1.19c, d).

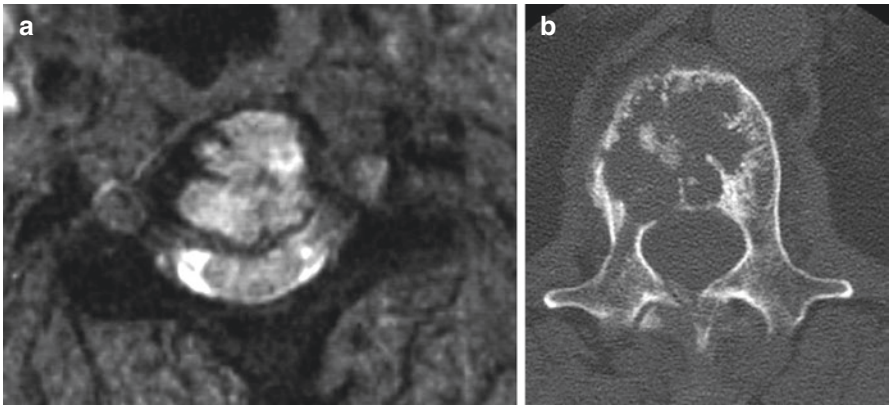

Fig. 1.18 Typical "mini-brain" appearance of a plasmocytoma in a cervical vertebral body on a T2-weighted image (**a**) and in a thoracic vertebral body on CT (**b**) (Courtesy image **b**; J.A. Jacobson, Department of Radiology, University of Michigan, Ann Arbor, USA)

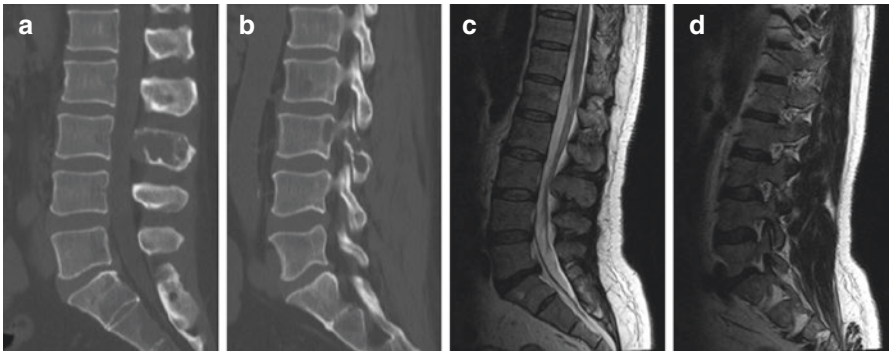

Fig. 1.19 (**a**–**d**) Sagittal CT reconstructions in a patient with multiple myeloma revealing multiple lytic lesions, most pronounced in the posterior vertebral elements of L3 (**a**, **b**). Sagittal T1-WI MRI in the same patient shows multiple low intensity lesions (**c**, **d**)

Radiologists should be aware that MRI is normal in 20% of cases with proven bone marrow infiltration. This is why initial staging should be performed using both MRI and CT.

1.2.4 Chordoma

1.2.4.1 General

Chordoma is a malignant tumour deriving from a notochord remnant. It is composed of fibrous, mucoid, necrotic, calcified and bony components. A hyaline cartilage component is found in the chondroid-type chordoma. Men are more affected

than women with a peak incidence around 50–60 years of age [16, 17]. The most common symptom is local pain due to local invasion. Only in large tumours compression of the spinal cord or nerve roots may be present. The tumour arises in the midline of the axial skeleton and has a predilection for the sacrum, accounting for 50% of cases. The clivus is involved in 35% and the remainder are found in the vertebrae [18].

1.2.4.2 Imaging

Radiographic examination shows bone destruction frequently accompanied by amorphous calcifications. These calcifications are due to necrosis, not bone formation. CT can show paravertebral and epidural extension [19].

Due to the various components, the tumour is heterogeneous on MRI, usually predominantly isointense on T1-WI and hyperintense on T2-WI. Enhancement is variable, ranging from discrete to markedly (Fig. 1.13). Septations or capsules are frequently present. Haemorrhage and cyst formation may also be seen.

1.2.5 Osteoid Osteoma

1.2.5.1 General

Osteoid osteoma is a benign osteoblastic lesion representing 10% of all tumours found in the osseous spine. Young men between 10 and 20 years of age are typically affected. Women are less affected. This tumour is known for its characteristic central nidus, composed by vascular fibrous connective tissue, surrounded by a dense osteoid matrix. The classic clinical presentation is night pain relieved by aspirin in a teenager or young adult. Spinal osteoid osteoma is an important cause of painful scoliosis. A strong predilection for the posterior vertebral elements, especially the pedicles, exists. The lumbar spine is most frequently involved, in descending order followed by the cervical, the thoracic and sacral levels [4]. One of the treatment options of osteoid osteoma is interventional radiology with radio frequency ablation.

1.2.5.2 Imaging

Plain radiography characteristically shows a lucent nidus, sometimes with small central calcifications, surrounded by dense bone sclerosis. The same features are found on CT (Fig. 1.6). CT is more sensitive in case of extensive bone sclerosis [20, 21].

Bone scintigraphy is highly sensitive but not specific. It will show the *double density* sign representing intense uptake centrally in the region of the nidus and adjacent reactive uptake corresponding to sclerosis. It can be difficult to see osteoid osteoma on MRI alone. The sclerosis and calcifications display a low signal on both T1-WI and T2-WI, while the nidus is high on T2 and enhances after gadolinium administration.

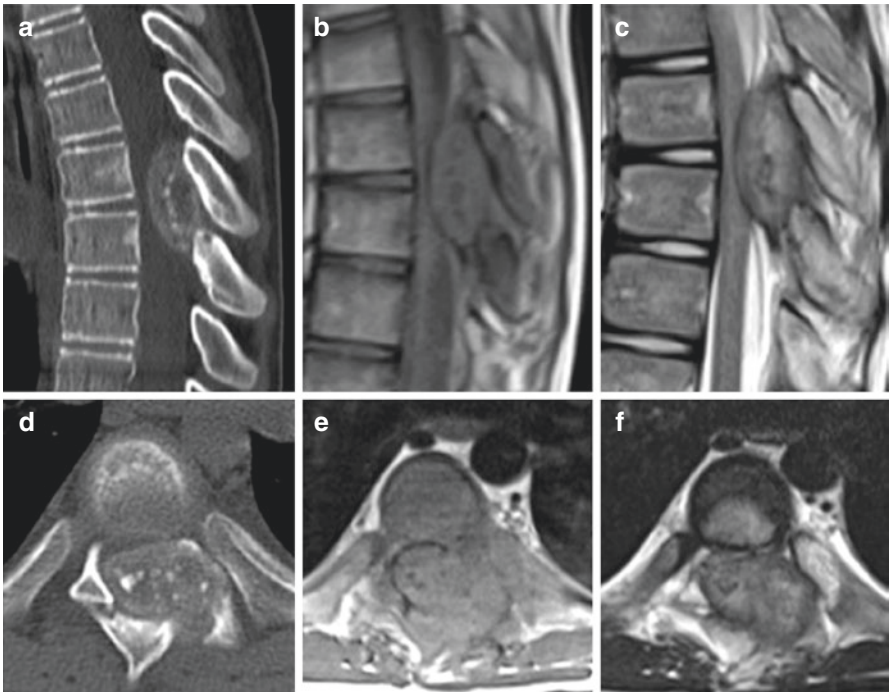

Fig. 1.20 (**a**–**f**) Osteoblastoma in the posterior elements of a thoracic vertebra, incidentally found in a young patient on a CT investigation after trauma (**a**, **d**). The tumour extends into the spinal canal and has a calcified or ossified matrix. On MRI an isointense signal is seen on T1-WI (**b**, **e**) and a heterogeneous iso- to hyperintense signal on T2-WI (**c**, **f**)

1.2.6 Osteoblastoma

1.2.6.1 General

Osteoblastomas are benign osteoid-producing tumours that are histologically related to osteoid osteomas and are always larger than 1.5 cm in size. It also occurs in adolescents or young adults and presents with pain. In contrast to osteoid osteomas, these lesions are more aggressive and more recurrent and aspirin does not relieve the pain. Osteoblastomas may also occur primarily in the posterior vertebral elements (Figs. 1.5 and 1.20), anywhere along the spine. Secondary ABC may be seen in association with osteoblastoma.

1.2.7 Aneurysmal Bone Cyst

1.2.7.1 General

Aneurysmal bone cysts (ABCs) are benign tumours of unknown aetiology that have a tendency to affect children and adolescents, slightly more frequent in women than in men. Histologically it is made of blood-filled sinusoids and solid

fibrous elements. This tumour is multiloculated and as its name suggests it has an expansive nature. Sometimes an ABC arises within a pre-existing tumour. This is important to consider if an aggressive lesion is biopsied and the pathology returns ABC, as this may imply that the true lesion was not sampled. Depending on the size and location, pain and neurological symptoms may occur. Pathological fractures are sometimes seen too. The lumbosacral spine is the most common site involved. ABCs favour the posterior vertebral elements, sometimes spreading to the vertebral body.

1.2.7.2 Imaging

Plain film and CT show an expansive, osteolytic lesion with thin cortical bone lining. Multiloculated tumours with fluid–fluid levels, due to the presence of blood degradation products, are seen on CT and MRI (Fig. 1.15). Internal septations or lobulations are sometimes present.

1.2.8 Giant Cell Tumour

1.2.8.1 General

This tumour, equally affecting men and women in the fourth to fifth decade, is the most frequent benign tumour of the sacrum. In some cases it has a locally aggressive behaviour and can even show malignant transformation after incomplete resection in 10% of cases. It is impossible to differentiate behaviour based on the appearance of the primary lesion. Pathologically they are often indistinguishable from brown tumours and look very similar to other lesions like chondroblastoma, ABC, chondromyxoid fibroma and osteosarcoma. Local pain is usually present, not infrequently accompanied by neurological symptoms. The sacrum is by far the most involved part of the spine (Fig. 1.4b). In rare cases a GCT is found in the vertebrae (Fig. 1.21). Multifocal giant cell tumours can be seen in Paget's disease or in hyperparathyroidism.

1.2.8.2 Imaging

A lytic, expansive tumour, characteristically in the sacrum, is seen on plain radiography. On MRI an inhomogeneous, multiloculated cystic mass is noted. As a result of blood degradation products and high cellularity, the signal intensity on T2-WI can be quite low.

1.2.9 Eosinophilic Granuloma

1.2.9.1 General

Eosinophilic granuloma is a tumour of unknown aetiology and is a part of the spectrum of Langerhans cell histiocytosis. It typically affects children in the first decade; boys are more frequently affected than girls. The mid-cervical spine in children and the second cervical vertebrae (C2) in adults are predilection sites [22]. Usually the

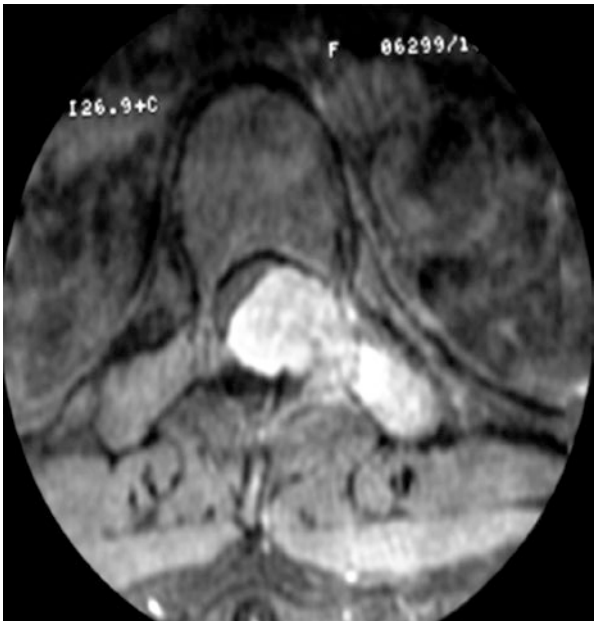

Fig. 1.21 Axial fat-suppressed T1-WI after gadolinium administration showing a GCT of the transverse process extending into the spinal canal

entire vertebral body is involved. The clinical presentation is very variable ranging from asymptomatic to pain and even neurological complications. Usually a good response to NSAIDs is seen.

1.2.9.2 Imaging

On plain radiography and CT, eosinophilic granuloma is noted as a well-defined, lytic lesion (Fig. 1.12a). A rare but typical presentation is a so-called vertebra plana, which is complete collapse of a single vertebral body. On MRI the tumour has high signal intensity on T2-WI, variable signal intensity on T1-WI (Fig. 1.12b, c) [23] and a strong enhancement after contrast administration.

1.2.10 Enostosis

1.2.10.1 General

Enostosis, commonly called bone island, is an asymptomatic lesion discovered incidentally in patients of all ages. They are not true neoplasms and represent dense compact bone within spongiosa. They are believed to be a developmental abnormality.

1.2.10.2 Imaging

Radiography and CT demonstrate round osteoblastic lesions with spiculated periphery (Fig. 1.9). Enostoses have low signal intensity at T1- and T2-weighted MR

imaging. Bone scintigraphy is normal in the majority of cases. The diagnosis is, usually, easy to make based on imaging characteristics. However, rarely it may be difficult to differentiate it from an osteoblastic metastasis, osteoid osteoma or a low-grade sarcoma. Since enostoses vary in size, a giant variant may also be difficult to distinct from a low-grade osteosarcoma.

1.3 Vertebral Metastasis

1.3.1 General

The vertebral column is the most common location for bone metastasis and metastases are the most common tumours of the spine [24, 25]. Osseous metastases are over ten times more common than primary bone tumours. In 50% of cancer patients bone metastases occur, 40–70% of which are found in the vertebrae. Ten percent of patients with a malignant neoplasm have vertebral metastases [26]. In no less than 10–40% of these patients, the metastatic lesions are responsible for the first symptoms, e.g. compression fracture or neurological symptoms. Metastases favour sites with high vascular bone marrow, like the vertebrae. Fat cells of the bone marrow are replaced by tumour cells. The presence of tumours cells causes osteoclastic and osteoblastic activation with subsequent osteolysis (70%), osteosclerosis (9%) or both (21%). The responsible primary tumours are, in descending order, breast carcinoma, lung carcinoma, prostate carcinoma and gastrointestinal tumours [24, 27] (Table 1.4).

Metastases reach the spine through several pathways. Direct extension and haematogenous spread is seen in lung tumours. Breast and prostate tumours invade the spine through the venous system via Batson's plexus, the former most frequently in the thoracic spine and the latter in the lumbar spine. Metastases can occur at all ages, but the majority of vertebral metastases are found starting from the fifth decade and increasing with age. There is no gender predilection. The thoracic spine is the most common location, followed by the lumbar spine and the cervical spine. The lesions are more frequently lytic than sclerotic. In some case a mixed composition is found. The clinical presentation of vertebral metastases is very variable. Pain is frequently encountered, e.g. as a result of a compression fracture of the affected vertebrae. Depending on the location in the spine and in the vertebra, neurological symptoms may be present. Sometimes metastatic lesions are asymptomatic and detected during routine screening investigations.

Table 1.4 Most common primary tumors that give vertebral metastases

Vertebral metastases most commonly originate from:
1. Breast carcinoma (21%)
2. Lung carcinoma (14%)
3. Prostate carcinoma (7.5%)
4. Gastrointestinal tumours (5%)

1.3.2 Imaging

Imaging has multiple purposes regarding metastases. In the first place, imaging is used to detect lesions and assess their location. It can, however, also be very valuable in evaluation of different therapeutic options [28]. When it comes to detection of metastases in the osseous spine, MRI is more sensitive than MDP scintigraphy [29]. MRI is positive in 15% of negative bone scans and detects 20% more lesions in patients with positive bone scans. It will also be negative if there is no osteoblastic turnover within the lesion, as seen in some lung and breast tumours. Still bone scintigraphy has a relatively high sensitivity and is as such a useful tool for screening asymptomatic cancer patients. Since high osteoblastic turnover is absent in some lung and breast tumour metastases, some authors recommend MRI for screening [30, 31]. CT is not suited as a screening technique because of the use of ionising radiation. It can be used to confirm a suspected lesion on scintigraphy, showing trabecular or cortical bone destruction but also invasion of paraspinal tissues. MRI is the recommended imaging tool in case of neurological symptoms and is capable of whole spine investigation. Osteolytic lesions will display low signal intensity on T1-WI because of the high contrast of tumour (hypointense) with fatty bone marrow (hyperintese). A corresponding high signal on T2-WI is usually noted. On fat suppression sequences like STIR, the hyperintense tumour contrasts nicely to the suppressed surrounding bone marrow, making this sequence very sensitive (Fig. 1.22) [32]. Furthermore negative STIR excludes metastasis and makes the use of a contrast medium unnecessary [33]. Another feature of lytic lesions is the loss of out-of-phase signal decrease. In contrast osteosclerotic metastases have low signal intensity on both T1-WI and T2-WI. In case of an infiltrating component, a high signal on T2-WI may be seen. When the tumour destructs the vertebral cortex, the normal hypointense vertebral lining is lost. After the administration of gadolinium-chelate osteolytic metastases will enhance prominently, sclerotic lesions will show a more heterogeneous, peripheral enhancement. An advantage of the use of contrast is the improved evaluation of extraosseous components. The ADC calculated from diffusion-weighted MR (DW-MR) images is probably a reliable parameter to distinguish vertebral metastases from normal vertebrae [34]. In a recent study, whole-body DW-MR imaging is said to be more sensitive in the detection of osseous metastases than skeletal scintigraphy and CT bone survey [35].

1.3.3 Differential Diagnosis

Some non-tumoural lesions may mimic metastasis. Some bone marrow changes, physiological and pathological, may have low signal intensity on T1-WI. Examples are an inverted ratio of red and fat marrow in young people, medullary hyperplasia in anaemia and smokers or stimulated haematopoiesis. Another pitfall is the presence of red bone marrow islands. These bone marrow changes are usually less hypointense and do not enhance after contrast medium administration. Degenerative changes like bone marrow oedema in degenerative osteochondritis with intense

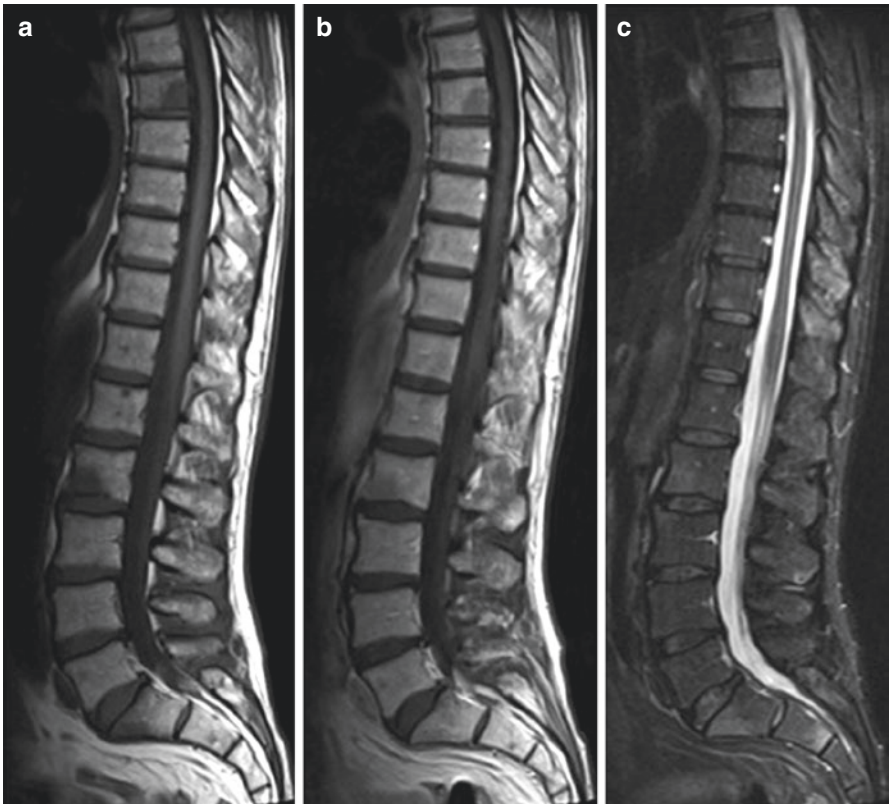

Fig. 1.22 (**a**–**c**) Multiple metastases in a patient with primary breast cancer. The lesions are characteristically hypointense on T1-WI (**a**). After gadolinium administration mild enhancement is noted (**b**). A corresponding high signal is seen on STIR (**c**)

contrast enhancement may mimic metastatic disease. The presence of osteophytosis can be helpful in the differential diagnosis in these patients.

The presence of a recent Schmorl herniation in a vertebral endplate with oedema could also resemble a metastatic lesion. Identifying the depressed cortical bone by the disc herniation will facilitate the diagnosis. It can be difficult to differentiate a pathological vertebral body fracture, associated with an underlying tumour, from an osteoporotic fracture. The main affected population, the elderly, are commonly affected by osteoporosis as well as vertebral metastatic lesions. The differential diagnosis is not clear-cut and can sometimes be very difficult [36]. In both cases low signal intensity on T1-WI and high signal intensity on T2-WI and STIR are noted. A band-like hypointensity on T1-WI under the endplate is suggestive of benignity [37]. A metastatic collapse will show intense, heterogeneous enhancement, while an arranged linear enhancement pattern is seen in osteoporosis. The use of contrast medium will also facilitate detection of an epidural tumoural component or other tumoural lesions [36]. On CT signs of a benign vertebral collapse include the

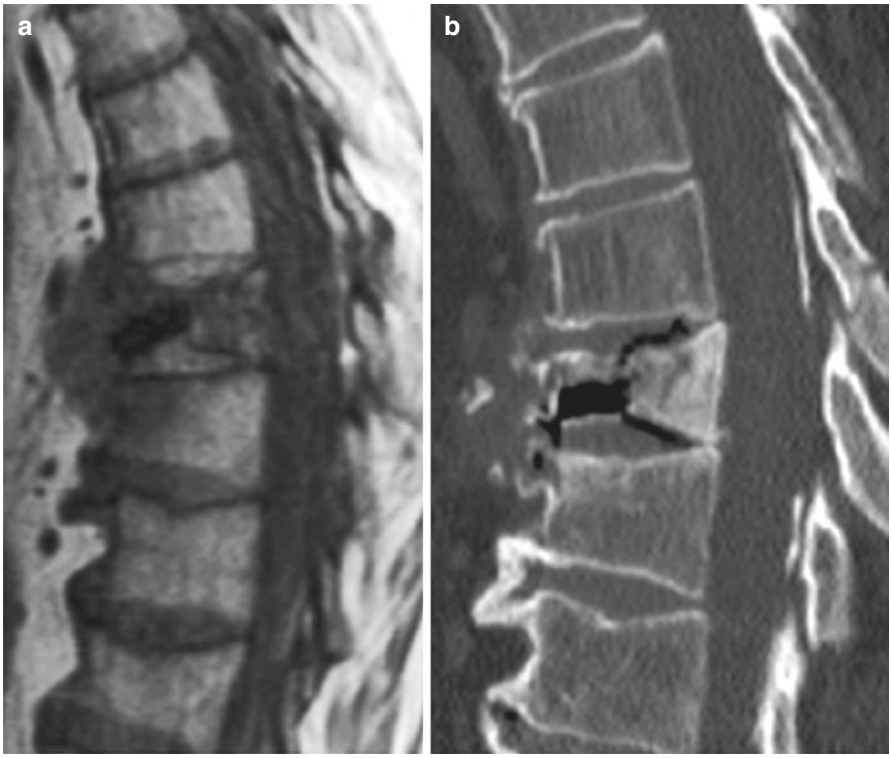

Fig. 1.23 (**a**, **b**) Sagittal T1-WI in a patient with an acute compression fracture (**a**). The presence of an intervertebral vacuum cleft sign on CT (**b**) confirmed the diagnosis of an osteoporotic fracture

absence of cortical destruction, retropulsion of a bone fragment, a vertebral vacuum sign and the absence of a soft tissue mass (Fig. 1.23) [38]. Signs of a malign vertebral lesion on CT are the presence of other lesions, posterior vertebral element involvement, cortical lysis and the presence of a soft tissue mass or local invasion [38]. On MRI reassuring features are the presence of a low-signal band on T1-WI and T2-WI, the retropulsion of a fragment, normal bone marrow signal and other compression fractures. MRI features suggestive of a malignant vertebral collapse include a convex posterior border, the involvement of posterior vertebral elements, the presence of an epidural or paraspinal mass and other suspicious lesions (Fig. 1.24). Disappearance of the basivertebral vein is usually a sign of epidural tumour spread [29]. The use of diffusion-WI (DWI) to distinguish between benign or malignant lesion is still controversial [39–41].

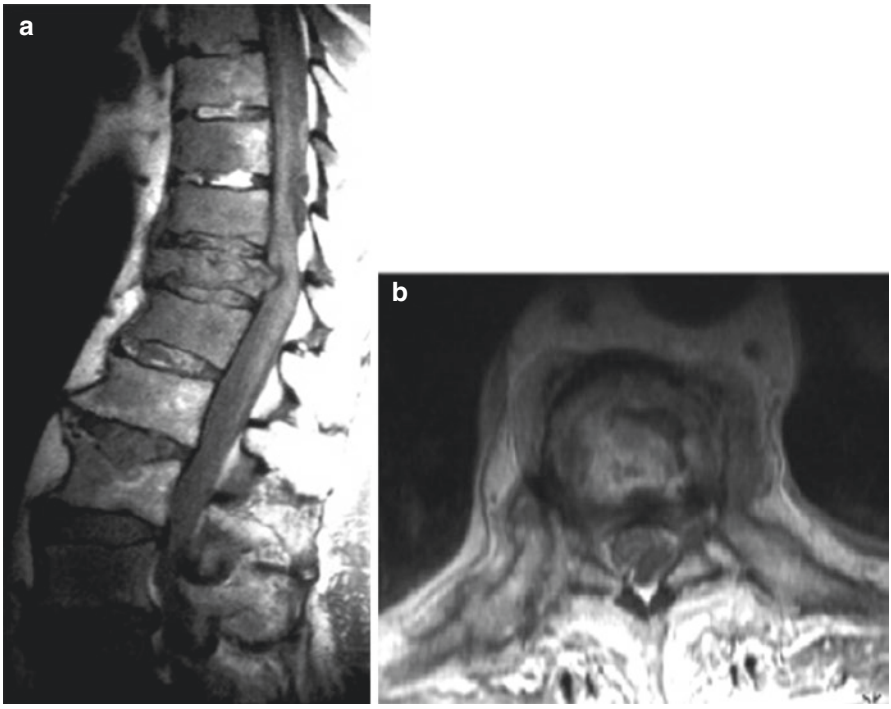

Fig. 1.24 (**a**, **b**) Metastatic compression fracture with a convex posterior border. Multiple vertebral lesions are visible (**a**). Axial images show the presence of an epidural mass and a lesion in the left pedicle (**b**)

1.4 Summary

A wide variety of lesions can be found in the osseous spine. Metastatic bone disease usually presents as multiple vertebral body lesions and is the most common vertebral tumour. In a clear clinical context, the diagnosis can be easily made. However, in case of an isolated spine lesion, making a diagnosis is much more challenging. The age of the patient and the clinical history usually narrow the differential diagnosis. Other important parameters include the number of lesions, location of the lesion in the vertebra, lesion morphology and imaging features. Radiologists should recognize the fundamental morphological features of tumours affecting the spine.

MR imaging has become the primary tool in the evaluation of spine tumours owing to its phenomenal capability for contrast discrimination of bone marrow and delineation of soft tissue involvement.

References

1. Van Goethem JW, van den Hauwe L, Ozsarlak O, De Schepper AM, Parizel PM. Spinal tumors. Eur. J. Radiol. 2004;50:159–76.
2. Flemming DJ, Murphey MD, Carmichael BB, Bernard SA. Primary tumors of the spine. Semin. Musculoskelet. Radiol. 2000;4:299–320.
3. Murphey MD, Andrews CL, Flemming DJ, Temple HT, Smith WS, Smirniotopoulos JG. From the archives of the AFIP. Primary tumors of the spine: radiologic-pathologic correlation. Radiographics. 1996;16:1131–58.
4. Ozaki T, Liljenqvist U, Hillmann A, Halm H, Lindner N, Gosheger G, Winkelmann W. Osteoid osteoma and osteoblastoma of the spine: experiences with 22 patients. Clin. Orthop. 2002;397:394–402.
5. Disler DG, Miklic D. Imaging findings in tumors of the sacrum. AJR Am. J. Roentgenol. 1999;173:1699–706.
6. Gerber S, Ollivier L, Leclère J, Vanel D, Missenard G, Brisse H, de Pinieux G, Neuenschwander S. Imaging of sacral tumours. Skelet. Radiol. 2008;37(4):277–89.
7. Ilaslan H, Sundaram M, Unni KK, Dekutoski MB. Primary Ewing's sarcoma of the vertebral column. Skelet. Radiol. 2004;33:506–13.
8. Murphey MD, Nomikos GC, Flemming DJ, Gannon FH, Temple HT, Kransdorf MJ. From the archives of the AFIP. Imaging of giant cell tumor and giant cell reparative granuloma of bone: radiologic-pathologic correlation. Radiographics. 2001;21:1283–309.
9. Keenan S, Bui-Mansfield LT. Musculoskeletal lesions with fluid-fluid level: a pictorial essay. J. Comput. Assist. Tomogr. 2006;30(3):517–24.
10. Major NM, Helms CA, Richardson WJ. The "mini brain": plasmacytoma in a vertebral body on MR imaging. AJR Am. J. Roentgenol. 2000;175(1):261–3.
11. Baudrez V, Galant C, Vande Berg BC. Benign vertebral hemangioma: MR-histological correlation. Skelet. Radiol. 2001;30(8):442–6.
12. Shah BK, Saifuddin A, Price GJ. Magnetic resonance imaging of spinal plasmacytoma. Clin. Radiol. 2000;55(6):439–45.
13. Lecouvet FE, Malghem J, Michaux L, Michaux JL, Lehmann F, Maldague BE, Jamart J, Ferrant A, Vande Berg BC. Vertebral compression fractures in multiple myeloma. Part II Assessment of fracture risk with MR imaging of spinal bone marrow. Radiology. 1997;204(1):201–5.
14. Derlin T, Bannas P. Imaging of multiple myeloma: current concepts. World J. Orthop. 2014;5(3):272–82.
15. Horger M, Claussen CD, Bross-Bach U, Vonthein R, Trabold T, Heuschmid M, Pfannenberg C. Whole-body low-dose multidetector row-CT in the diagnosis of multiple myeloma: an alternative to conventional radiography. Eur. J. Radiol. 2005;54(2):289–97.
16. Thornton E, Krajewski KM, O'Regan KN, Giardino AA, Jagannathan JP, Ramaiya N. Imaging features of primary and secondary malignant tumours of the sacrum. Br. J. Radiol. 2012;85(1011):279–86.
17. York JE, Kaczaraj A, Abi-Said D, Fuller GN, Skibber JM, Janjan NA, Gokaslan ZL. Sacral chordoma: 40-year experience at a major cancer center. Neurosurgery. 1999;44(1):74–9.
18. Smolders D, Wang X, Drevelengas A, Vanhoenacker F, De Schepper AM. Value of MRI in the diagnosis of non-clival, non-sacral chordoma. Skelet. Radiol. 2003;32:343–50.
19. Wippold FJ, Koeller KK, Smirniotopoulos JG. Clinical and imaging features of cervical chordoma. Am. J. Roentgenol. 1999;172(5):1423–6.
20. Iyer RS, Chapman T, Chew FS. Pediatric bone imaging: diagnostic imaging of osteoid osteoma. AJR Am. J. Roentgenol. 2012;198(5):1039–52.
21. Youssef BA, Haddad MC, Zahrani A, Sharif HS, Morgan JL, al-Shahed M, al-Sabty A, Choudary R. Osteoid osteoma and osteoblastoma: MRI appearances and the significance of ring enhancement. Eur. Radiol. 1996;6(3):291–6.
22. Bertram C, Madert J, Eggers C. Eosinophilic granuloma of the cervical spine. Spine. 2002;27(13):1408–13.

23. De Schepper AM, Ramon F, Van Marck E. MR imaging of eosinophilic granuloma: report of 11 cases. Skelet. Radiol. 1993;22:163–6.
24. Harrington KD. Metastatic disease of the spine. J. Bone Joint Surg. A. 1986;68:1110–5.
25. Shah LM, Salzman KL. Imaging of spinal metastatic disease. Int. J. Surg. Oncol. 2011:769753.
26. Schiff D, O'Neill BP, Suman VJ. Spinal epidural metastasis as the initial manifestation of malignancy: clinical features and diagnostic approach. Neurology. 1997;49:452–6.
27. Schick U, Marquardt G, Lorenz R. Intradural and extradural spinal metastases. Neurosurg. Rev. 2001;24:1–5.
28. Andreula C, Murrone M. Metastatic disease of the spine. Eur. Radiol. 2005;15:627–32.
29. Algra PR, Jl B, Verboom LJ, et al. MRI vs scintigraphy in the detection of vertebral metastases. Radiographics. 1991;11:219–32.
30. Layer G, Stuedel A, Schuller H, van Kaick G, Grunwald F, Reiser M, Schild HH. Magnetic resonance imaging to detect bone marrow metastases in the initial staging of small cell lung carcinoma and breast carcinoma. Cancer. 1999;85:1004–9.
31. Steinborn MM, Heuck AF, Tilling R, et al. Whole body bone marrow MRI in patients with metastatic disease to the skeletal system. JCAT. 1999;23:123–9.
32. Mehta RC, Marks MP, Hinks RS, et al. MR evaluation of vertebral metastases: T1-weighted, short-inversion-time inversion recovery, fast spin echo, and inversion-recovery fast spin-echo sequences. AJNR Am. J. Neuroradiol. 1995;16:281–8.
33. Mahnken AH, Wildberger JE, Adam J, et al. Is there a need for contrast-enhanced T1-weighted MRI of the spine after inconspicuous short tau inversion recovery imaging? Eur. Radiol. 2005;15:1387–92.
34. Herneth AM, Philipp MO, Naude J, Funovics M, Beichel RR, Bammer R, Imhof H. Vertebral metastases: assessment with apparent diffusion coefficient. Radiology. 2002;225(3):889–94.
35. Del Vescovo R, Frauenfelder G, Giurazza F, Piccolo CL, Cazzato RL, Grasso RF, Schena E, Zobel BB. Role of whole-body diffusion-weighted MRI in detecting bone metastasis. Radiol. Med. 2014;119(10):758–66.
36. Cicala D, Briganti F, Casale L, Rossi C, Cagini L, Cesarano E, Brunese L, Giganti M. Atraumatic vertebral compression fractures: differential diagnosis between benign osteoporotic and malignant fractures by MRI. Musculoskelet. Surg. 2013;97(2):169–79.
37. Kuisma M, Karppinen J, Niinimäki J, Kurunlahti M, Haapea M, Vanharanta H, Tervonen O. A three-year follow-up of lumbar spine endplate (Modic) changes. Spine. 2006;31:1714–8.
38. Sattari A, Quillard A, Laredo JD. Benign nontraumatic osteolytic vertebral collapse simulating malignancy. Eur. Radiol. 2008;18(3):631–8.
39. Baur A, Dietrich O, Reiser M. Diffusion-weighted imaging of the spinal column. Neuroimaging Clin. N. Am. 2002;12(1):147–60.
40. Castillo M, Arbelaez A, Smith JK, Fisher LL. Diffusion weighted MR imaging offers no advantage over routine noncontrast MR imaging in the detection of vertebral metastases. Am. J. Neuroradiol. 2000;21:948–53.
41. Maeda M, Sakuma H, Maier SE, et al. Quantitative assessment of diffusion abnormalities in benign and malignant vertebral compression fractures by line scan diffusion-weighted imaging. AJR Am. J. Roentgenol. 2003;181:1203–9.

Biomechanics of Vertebral Fracture

2

Cari M. Whyne, Stewart McLachlin, Mikhail Burke, and Michael Hardisty

2.1 The Spine as a Biomechanical System

The spine is a complex mechanical system complete with levers, pivots, passive restraints and actuators in the form of vertebrae, intervertebral discs and facet joints, ligaments and muscles, respectively [1, 2]. The bony spine consists of 24 vertebrae (7 cervical, 12 thoracic and 5 lumbar), the sacrum and coccyx. Each vertebra consists of a vertebral body (the primary load-bearing structure) and posterior elements. Vertebrae protect the neural canal and form the primary load-bearing structure within the spine.

The study of spinal biomechanics and injury dates back to the Egyptian empire during the time of the construction of the pyramids [2, 3]. Modern biomechanical studies aim to better understand the mechanics of musculoskeletal motion and the mechanical behaviour of biological tissues and structures including the spine. The importance of biomechanics is present both at structural and tissue levels in physiologic, pathologic and traumatic injury scenarios. Each element of the spine is intricate with respect to its structure, function and its interactions within the system as a whole. Biomechanical analysis is important in understanding vertebral fracture risk, the impact of treatments on the bone and the design and performance of implants and minimally invasive repair techniques for the spine. This chapter will specifically focus on the biomechanics of vertebral fracture in the spine.

C.M. Whyne, Ph.D. (✉)
Orthopaedic Biomechanics Laboratory, Holland Musculoskeletal Program, Sunnybrook Research Institute, 2075 Bayview Avenue, Room S620, Toronto, ON, Canada, M4N3M5

Department of Surgery, IBBME and IMS, University of Toronto, Toronto, ON, Canada
e-mail: cari.whyne@sunnybrook.ca

S. McLachlin, Ph.D. • M. Burke, B.A.Sc. • M. Hardisty, Ph.D.
Orthopaedic Biomechanics Laboratory, Holland Musculoskeletal Program, Sunnybrook Research Institute, 2075 Bayview Avenue, Room S620, Toronto, ON, Canada, M4N3M5

L. Manfrè (ed.), *Vertebral Lesions*, New Procedures in Spinal Interventional Neuroradiology, DOI 10.1007/978-3-319-52634-8_2

2.2 Vertebral Structure

Vertebrae consist of four main structural components: the trabecular centrum, the cortical shell, the bony endplate composing the vertebral body and the posterior elements.

2.2.1 Trabecular Centrum

The trabecular centrum is the principal load-bearing component of the vertebra [4–7]. Trabecular bone density varies with location, spinal level, age, sex and pathology [4, 8–11]. Loss of density is reflected through both trabecular thinning and loss of trabeculae, leading to architectural changes from plates to rods with a sparser network of longer vertical and horizontal struts.

2.2.2 Cortical Shell

The thickness of the cortical shell ranges from 0.3 to 0.4 mm and is thickest near the endplates [12–14]. While the mechanical properties of the cortical shell are reported to be comparable to cortical bone at other anatomic sites [15, 16], its microstructure is more representative of condensed trabecular bone [13, 17, 18]. The cortical shell has been reported to support from 10% to 75% of spinal axial compressive loading [5, 19, 20]. However there is a mechanical interaction between the cortical shell and the centrum [21]. Intervertebral disc degeneration increases the structural role of the cortical shell, and the shell may also support more load at the mid-vertebral transverse cross-section than nearer to the endplates [22].

2.2.3 Endplates

Vertebral endplate thickness ranges from 0.4 to 0.8 mm [12–14]. The morphology of the vertebral endplate is altered with advancing disc degeneration. While early research suggested age-related thickening of the vertebral endplates, more recent microCT-based analysis has shown disc degeneration leads to decreases in endplate thickness and increases in porosity [23–25]. Failure loads and stiffness measurements are consistent with changes in endplate thickness with axial position (level) and across the endplate (thinner central portion). Mechanical testing has shown a significant decrease in endplate stiffness and strength in the vertebrae adjacent to more degenerated discs [26, 27]. Vertebrae may also demonstrate ‘double endplates’, most commonly adjacent to grade 2 or 3 degenerated discs [25, 28]. With the transfer of load through the intervertebral disc, the endplates deform transferring load to the underlying trabecular centrum.

2.2.4 Posterior Elements

The posterior elements consist of two pairs of facet (apophyseal) joints connecting adjacent vertebrae in the inferior and superior directions. The posterior elements play a significant role in torsion, transverse shear and extension loading modes [29]. The orientation of the facets varies with spinal level, enabling a wide range of movement in the cervical spine (flexion, extension, lateral flexion and rotation), limiting flexion/extension movements in the thoracic spine and preventing rotation in the lumbar spine. The posterior ligamentous complex functions as a tension band and protects against hyperflexion. While only a small portion of the compressive load on the spine is carried by posterior elements under physiologic loading (<10%), in cases of disc degeneration, this rises substantially (≥40%) [29, 30].

2.3 Vertebral Bone

2.3.1 Composition

The majority of the vertebral body is composed of trabecular bone (70–80%), which is made up of microstructural rods and plates connected in a 3D network generating an open porous cellular solid [31]. The pores are filled with bone marrow. The orientation of the trabecular microstructure in the vertebra is anisotropic with an inferior–superior principal material directionality. Trabecular bone is highly porous and as a result much less rigid (90–400 MPa) than cortical bone.

The trabecular bone tissue is similar to cortical bone, but is arranged in packets of lamellar bone [32] rather than osteons as in cortical bone. The bone tissue is composed of a mineral phase, 43% by volume (hydroxyapatite); an organic phase, 32% by volume (primarily type I collagen); and interstitial fluid, 25% by volume. The apparent mineral density of human trabecular bone ranges from 0.1 to 1.0 g/cm^3. Both density and architecture play an important role in determining the mechanical properties of trabecular bone [33–35]. This may include potential detrimental effects of increased variability in trabecular thickness and number within trabecular bone specimens [36, 37]. Material properties in trabecular bone decrease more rapidly with disease and ageing than in cortical bone because of higher rates of turnover.

2.3.2 Mechanical Behaviour

It is the composite nature of the bone and its intricate structure that creates its remarkable mechanical properties: stiff, strong and tough. The organic phase of the bone governs the plastic behaviour of the material and is responsible for much of the bone's toughness and ductility. The mineral phase of the bone controls its elastic

behaviour and largely determines the bone's stiffness and strength. This division of mechanical properties between the two phases is evident from experiments whereby one of the constituents is damaged. The bone without collagen (due to protease treatment or ashing) or with damaged collagen (due to KOH treatment, irradiation or heat treatment) retains its stiffness [38–41]; however, it is very brittle, failing at lower strains with little mechanical energy input. The bone's collagen matrix has better mechanical properties (strength, stiffness, fracture toughness) due to mineralization. Experimentally removing the mineral phase in the bone leads to greatly reduced stiffness, with half of the bone's toughness retained [42].

Mineralization occurs after osteoid (new bone) is formed, but the degree of mineralization in bone tissue is not constant, with the stiffness of the bone increasing with the presence of more mineral. The organic phase of the bone governs the plastic behaviour of the material influencing its toughness and ductility. The bone exhibits directional differences in both strength and toughness.

The apparent stress–strain behaviour of vertebral trabecular bone exhibits an initial linear region followed by apparent yield and failure. Vertebral trabecular bone is anisotropic in both modulus and strength, although the strength of vertebral trabecular bone is only slightly lower in tension than compression [43]. However, its post-elastic behaviour is quite different.

Bone structures damage with everyday loading; however, damage within the bone does not prevent the bone from performing its mechanical function. Bone damage during the linear phase of loading is likely involved in the regulation of bone turnover. Both the resistance to crack creation and growth are important in understanding bone mechanical failure. Vertebral trabecular bone fractures at apparent strains of approximately 1.5% in tension [44]. Under compressive loading, there is a long post-yield plateau in which fractured trabeculae fill the marrow spaces, after which additional loading yields an increase in modulus [45]. Vertebral trabecular bone is transversely isotropic with substantially higher modulus and strength in the inferior–superior direction (similar to the microstructural orientation). There is a strong linear correlation between the stress at which the bone fails and its elastic modulus, whereas there is little to no dependency of failure strain on density [44]. As such, simple strain-based failure criteria are commonly applied to the bone, independent of orientation, loading or density [14].

Mechanistically, bone fracture has been described to occur through strain-controlled failure, indicating ductile behaviour [46–48]. The mineral component of the bone contributes its strength and stiffness; however, as mineralization increases, bone tissue becomes brittle, reducing the energy required for failure [49–53]. Many studies have demonstrated strong correlations between mineral content and strength/stiffness [49, 51, 52, 54].

Cyclic loading and its associated damage and strain accumulation can weaken vertebrae [55–57]. Cyclic loading tests have indicated failure through a gradual creep-like increase in mean displacement and rapid crack propagation from the cortical shell to the interior of the vertebral body [58]. Microdamage and microfractures commonly seen in human vertebrae likely result from cyclic loading that may be accentuated by occasional overloads and may act as a stimulus to remodelling

[14]. The process of cumulative 'fatigue failure' of the vertebral body has been investigated in human cadaver spines, with the force required to cause fatigue failure decreasing as the number of loading cycles increases [58–61]. Clinical evidence of fatigue failure is observed in the presence of individual fractured and healing trabeculae in many cadaveric vertebral bodies [62].

The compressive strength of human thoracolumbar vertebrae ranges from 2 to 8 kN, based on bone density and cross-sectional area [14, 59, 63–68]. Vertebral compressive strength increases caudally mainly due to increases in vertebral cross-sectional area [68, 69]. Regional distribution of bone density and vertebral geometry also impact strength [5, 8, 59, 63, 68].

2.3.3 Bone Quality

From a biomechanical perspective, the impact of bone quality on fracture risk has gained much recent attention. Where BMD describes only how much bone is present, bone quality describes the mechanical properties encompassing both the inherent structural and material properties within a vertebra. As such bone quality evaluation considers mineralization, composition, remodelling, connectivity and architecture. Together these structural and material factors can be used to determine the load-bearing capacity of a vertebra (failure load) and can reflect the impact of pathological processes (i.e. osteoporosis, diabetes, metastatic disease) or treatments (i.e. bisphosphonates, radiation) on vertebral stability. However, many of these factors are difficult and impractical to measure clinically because of the invasive (bone biopsy) or harmful (high-dose radiation) tests needed to make measurements.

2.3.4 Age-Related Changes

Vertebral body strength decreases by ~12% per decade [67]. The bone is highly affected by ageing with a loss of bone mass of up to 50% from 20 to 80 years of age, influenced by gender, hormonal changes and anatomic site, with negative consequences to its ultimate strength. Architectural changes in the trabecular centrum of vertebrae occur with age, both through thinning and loss of trabeculae. Increase in bone fragility may occur from replacement of plate-like closed trabecular structures with more open structures composed of rods. The more porous trabecular bone appearance results due to reduced horizontal cross-linking struts, further diminishing the buckling strength of vertically oriented (longer and thinner) trabeculae [69]. Reducing bone density by 10% through the removal of longitudinally oriented trabecular elements has been shown to create a 50% greater reduction in bone strength than an equivalent density reduction via trabecular thickness [70]. This implies that maintenance of trabecular number is critical in the preservation of bone strength with ageing [71]. The loss of bone density may be offset in part by subtle increases in bone size in men; however, no age-related changes in cross-sectional area have been found for women [6].

Trabecular microarchitecture has been shown to be highly associated with whole-vertebral biomechanical behaviour, mediated by bone mineral content but not by cross-sectional area or the cortical shell [72]. The role of trabecular microarchitecture is more accentuated in low-strength vertebrae and involves mostly the degree of anisotropy, with variations in vertebral strength primarily due to the bone volume fraction of vertically oriented trabeculae [72]. Localized bending of slender vertical trabeculae has been shown to lead to concentrated yielding at a tissue level in low-density vertebral bone.

Ageing is accompanied by osteoarthritic changes around the intervertebral disc and endplates (i.e. osteophytes) and disc degeneration [73, 74]. Bone density distribution is impacted as well, with more uniform distributions in vertebrae adjacent to degenerated discs [9].

Damage and remodelling of trabeculae are normal physiologic processes that can elevate osteoporotic fracture risk [55, 75]. Decreased structural strength in aged bone is affected by changes in the remodelling/repair rate, resulting in faster damage accumulation for continuous cyclic loading [76]. Ageing slows remodelling, and during remodelling cycles, there is a net loss in bone mass leading to deterioration in crack-initiation and crack-growth toughness. Lower turnover leads to higher mineralization that may contribute to the brittle nature of aged bone tissue.

It is also proposed that elderly vertebrae, with low bone mineral density (BMD), may deform gradually under constant load by a quasi-continuous 'creep' mechanism [61, 77]. The bone is a 'viscoelastic' material, with repeated loading of small bone samples demonstrating residual deformation that recovers slowly, if at all [78–80]. Since BMD and trabecular density tend to be lower in the anterior vertebral body, creep may contribute in osteoporotic vertebrae to anterior wedge deformities [61].

2.3.5 Impact of Intervertebral Disc

Vertebral body endplate stresses depend on the state of the adjacent intervertebral discs. A healthy disc is composed of a gelatinous nucleus pulposus surrounded by a fibre-reinforced annulus fibrosis. Degenerated discs present with a loss in hydration and height with a nucleus similar to the annulus fibrosis material [81]. Healthy discs preferentially load the interior of the trabecular centrum in axial compression; degenerated discs load the cortical shell in axial compression with an increased load on the anterior body under bending [82, 83]. As such, healthy spinal motion segments tend to fail via central endplate ruptures, whereas low-density vertebrae with degenerated discs fail more commonly in wedge-type fracture patterns [84].

2.4 Spinal Column Classification

Spinal column classifications have been developed to assist in describing fractures from an anatomical perspective. The spine has been described as a two-column structure [85, 86] and a three-column structure [87, 88, 89]. Where the two-column

theory divides the vertebrae to the vertebral body and the posterior elements, the three-column concept introduces a middle column, containing the dorsal half of the vertebral body, posterior longitudinal ligament, and dorsal annulus fibrosus. The middle column allows for the specific assessment of the neutral axis, which bears a significant portion of the axial load and about which spinal element distraction or compression does not excessively occur with flexion or extension [90]. The instantaneous axis of rotation (IAR) is generally located within the neutral axis. The posterior column is the most important column for spinal stability, and compromise of any two columns that include the posterior column is generally mechanically unstable.

2.5 Spinal Stability

All joints in the human body are defined by an inherent stability. In the spine, stability relies on the intervertebral disc and ligamentous structures to provide passive restraint and active stabilization from the surrounding musculature. In a healthy spine, the osseous anatomy provides little intrinsic stability, beyond constraining the limits of motion through the facet joints. Instability of the spine is difficult both to define and quantify [91]. Mechanical stability may be defined as the ability of the spine to bear physiological loads, whereas clinical stability encompasses both mechanical instability and the associated pain or neurological damage. Historically, White and Panjabi defined clinical instability of the spine as changes in the patterns of motion under physiological loads which may result in neurologic deficit, excessive deformity and/or pain, acutely or with time [57]. They further described kinematic instability as excessive change in physiologic motion, axis of rotation or in the coupling characteristic of the spine.

2.6 Vertebral Fractures

Spinal fractures can vary widely with respect to both severity and injury pattern and occur more commonly in the thoracic and lumbar spine, including the thoracolumbar junction. Fractures may occur traumatically due to high-impact loading (including motor vehicle accidents, falls from heights and sport-related collisions) or under physiologic loading levels when inherent weakening of the vertebrae is present due to pathologic conditions (such as osteoporosis or metastatic disease).

2.7 Traumatic Injuries

Traumatic spinal injuries cover a large spectrum, including minor sprains and strains, herniated discs (tears in the annulus causing leakage), subluxations, fractures and dislocations of the facet joint [92–95]. In general, spinal trauma is the result of high-speed injuries and is most common among the younger male

population [93]. Damage to the spinal cord is present in only a small percentage of these injuries [96, 97].

Early spinal trauma classification systems focused on anatomical, morphological and mechanistic criteria of the trauma [95]. Sir Francis Holdsworth described 1000 patients with facet fractures and dislocations in a widely referenced historical classification system [85]. More complex classification systems have since been developed; however, none is considered ideal [92, 94]. For example, the Allen-Ferguson system divides traumatic injuries of the cervical spine into six phylogenies, compressive flexion, vertical compression, distractive flexion, compressive extension, distractive extension, and lateral flexion, and has been shown to be an effective diagnostic tool [92, 98]. The newer subaxial injury classification (SLIC) system is also largely based around mechanisms of injury but provides evidence on the morphology of fractures, assessment of the discoligamentous complex and neurologic status [94]. The international group AOSpine has provided updated classification guidelines on cervical spine injuries based on common presentations [99]. Soft tissue injuries to the spine can result from hyperflexion which typically results in posterior injuries whereas hyperextension causes anterior ligamentous and disc disruption. Flexion distraction injuries have a spectrum of injury based on facet joint distraction, ranging from subluxation and fracture to dislocation injuries (which have a high propensity to include spinal cord damage). Incidence of these injuries has been shown to result from the location of the force vector applied, shifting from posterior element fracture to bilateral facet dislocation. Additional classification systems exist for the axis and odontoid.

For thoracolumbar injuries, Denis classified five different types of spinal fractures considering the anatomic site of injury, the mechanism of injury and the level at which the injuries tend to occur [88]. The McAfee and Magerl classifications for thoracolumbar spinal fractures are similarly based on the three-column concept of the spine (anterior, middle and posterior), with instability predicted depending on the columnar disruption [100, 101]. More recently, the thoracolumbar injury classification and severity score was developed based on injury morphology (compression fracture, burst fracture, translational rotational injury or distraction injury), posterior ligamentous complex integrity (intact to injured) and patient neurology (intact to cauda equina) [102]. These classifications are designed to help guide operative vs. non-operative management of patients [103].

2.7.1 Osteoporotic Fractures

Vertebral fractures are the most common type of osteoporotic fracture. They are associated with increased morbidity and mortality (20% increase in 5 years) [104]. The prevalence of vertebral compression fracture increases the subsequent risk of fracture in both the spine and hip [105–107]. The high rate of subsequent vertebral fracture following an initial fracture is referred to as the ‘vertebral fracture cascade’ [108]. Only one third of osteoporotic vertebral fractures come to medical attention. Moderate trauma is associated with many painful vertebral fractures, but studies

have reported from 50% to 73% as occurring 'spontaneously' without any known cause or due to only low-energy trauma [109, 110].

2.7.2 Pathologic Fractures

The vertebral column is the most frequent site of metastatic involvement of the skeleton, occurring in up to one third of all cancer patients [111]. Bone metastases contribute to both morbidity (pain and skeletal-related events) and mortality [112, 113]. Pain management and the prevention of pathologic spinal fractures are critical elements in the preservation of quality of life in individuals with vertebral metastases. Vertebral metastatic disease uncouples physiologic osteoclastic and osteoblastic cell interactions leading to abnormal bone turnover, impacting architecture, density, bone quality and stability [114, 115]. Vertebral metastases can be present as bone destructive (osteolytic), as bone generating (osteoblastic) or as a mixture of osteolytic and osteoblastic disease. In some cancer types (i.e. breast), the incidence of pure osteolytic metastases has declined, likely at least in part, due to the widespread use of bisphosphonates in patients with skeletal disease [116]. Pathologic sequelae can be found in the vertebrae as distinct focal regions and areas with more diffuse involvement throughout entire vertebrae. The time-dependent risk of skeletal-related events, including fracture, is increased with metastatic involvement [117, 118]. Fracture can occur in the metastatic spine under physiologic loading conditions resulting in wedge or burst fracture patterns.

2.8 Fracture Types

2.8.1 Compression Fractures

Compression fractures can present with an anterior wedge, biconcave or crush morphology. Cadaveric studies have shown that some degree of endplate disruption occurs in all types of vertebral compression fracture, suggesting its role as a 'weak link' in the spine [10, 119–122]. Wedge fractures, characterized by failure of the anterior wall of the vertebral body, are the most common type of thoracolumbar spinal fracture (~50%). Such fractures generally result from axial compressive loading which may be combined with forward bending moments. Compressive forces applied ventral to the IAR often result in wedge compression fractures [90]. They are generally considered a single-column injury and as such are deemed to be relatively stable. They are largely unreported but can present with pain and loss of mobility. They can be classified as mild, moderate or severe depending on the loss of vertebral height. The most common pathology leading to wedge fractures is osteoporosis, but such injuries can also result from metastatic disease and secondary to trauma. In wedge fractures, an underlying cause of anterior weakening may be 'stress shielding' of the anterior vertebral body by the neural arch, following intervertebral disc narrowing [123]. In this scenario, even moderate flexion can disengage the neural

arches, concentrating over 50% of the applied compressive force on to the weakened anterior vertebral body. Bone loss in the anterior vertebral body may also result due to limited bending in the elderly coupled with reduced responsiveness to mechanical stimuli of old compared with younger bone [61, 124, 125].

Initial failure of the vertebra is often associated with the development of high tensile strains within the endplate, which in turn is influenced by the material behaviour of the disc [72]. Biaxial tension generated in the endplate may be particularly harmful with respect to limiting microdamage and crack propagation [72]. Biconcave fractures result from both endplates bulging into the vertebral bodies with increasing age [126, 127]. This may occur in middle age, when only the central nucleus pulposus exhibits a true hydrostatic pressure [128], which acts on the weak central region of the vertebral endplates leading to the central region of the endplates bulging into their vertebral bodies when the spine is compressed [10, 121, 122, 129]. Both disc degeneration and vertebral endplate damage can cause a reduction in pressure in the nucleus pulposus of the adjacent disc [130], concentrating compressive stress on the annulus and neural arch. If moderate spinal flexion disengages the apophyseal joints [131], then compressive overload can result in a crush fracture that primarily involves the vertebral body cortex [61].

2.8.2 Burst Fractures

Burst fractures have a similar appearance to crush fractures but with additional radial outward displacement of the cortex. Burst fractures generally occur from high-impact loading in young healthy spines. Pure axial loading in line with the IAR leads to a burst fracture pattern. The mechanism of burst fracture has been described as a pressurization of the vertebral body under rapid loading due to failure of the endplates and entry of the nucleus pulposus into the vertebral trabecular centrum [85]. This pressurization leads to radial bursting of the vertebral body, which can cause pieces of bone to retropulse into the spinal canal causing neurologic damage. This mechanism can also occur in cancer-involved bone under physiologic loading conditions due to pressurization of osteolytic tumour tissue leading to the retropulsion of the bone and/or tumour into the spinal canal [132].

2.8.3 Flexion Distraction Injuries

Distraction forces placed dorsal to the IAR can generate ligamentous or bony ‘Chance’ fractures [90]. The magnitude of the applied bending moment (related to the perpendicular distance of the force relative to the IAR) impacts the extent of the fracture. The most common cause of this injury pattern is deceleration with restraint by a single lap belt. Hyperextension-shear injuries result from compressive forces behind the IAR [90]. Flexion distraction-type injuries have been classified into four stages, based on the severity of post-injury translational displacement [92]. The stages range from (1) representing an isolated posterior ligamentous injury resulting

in facet subluxation only in association with post-traumatic flexion to (2) a unilateral facet injury and ultimately gross instability with (3) and (4) which include bilateral facet dislocation/subluxation. Each stage may exhibit a variety of injury patterns including facet fractures, facet subluxation/dislocation (pure ligamentous injury) and vertebral body fractures. The more recent SLIC adds some additional consideration to this injury pattern (considered hyperflexion) for facet subluxations and perched facets [94]. However, the combination of fractures and ligamentous injury that can produce the various stages of injury and the resulting instability pattern remains poorly understood [133].

2.8.4 Facet Joint Injuries

Traumatic facet joint injuries can result in a spectrum of soft and bony tissue disruption [134]. As a primary stabilizer for axial rotation of the head and neck, facet joint injuries are the results of high-energy injuries with flexion rotation moments (unilateral facet injury) and hyperflexion/distraction (bilateral facet injury) [134, 135]. Facet subluxation describes joint motion extending beyond its physiologic range of motion. Excessive facet subluxation can result in facet fractures that can occur in the inferior articular process of the superior vertebrae or in the superior articular process of the inferior vertebrae (a more common occurrence) [93]. Facet perch describes subluxation immediatly prior to dislocation where the ends of the joint are atop one another [94]. Facet dislocation, which can occur unilaterally or bilaterally, is when the joint surfaces have slid past each other and are in a locked position.

2.8.5 Fractures of the Odontoid Process

The most frequent cervical spine injury in the elderly is a fracture of the odontoid process, often referred to as a ‘dens’ fracture, of the second cervical vertebra (C2) [136]. The odontoid process is a unique bony prominence or peg of the C2 vertebrae about which the C1 vertebra rotates. In the elderly population, this fracture type is common in low-energy impacts that occur during a fall from a standing height as a result of weakened bone due to osteoporosis and change in force vectors due to osteoarthritis [136, 137]. The low-energy mechanism of this fracture typically leaves the surrounding ligamentous complex intact which gives support that these fractures are inherently stable [138]. However increased mobility of the C1/C2 complex can result in spinal cord injury and fusion may be required.

2.8.6 Classification of Fracture Instability

Many classification schemes of spinal fracture instability exist, but in general, instability is referred to as acute (overt or limited) or chronic [90]. Acute instability is most frequently encountered in traumatic, infectious, and/or neoplastic conditions.

Chronic instability may result from an acute process or degenerative changes. Classification systems for fracture instability aim to determine which fractures are overtly unstable (require surgical stabilization), which fractures have limited instability but with a likelihood of chronic progression (require surgical stabilization) and which fractures are grossly stable (do not require surgical intervention). Overt instability is defined as the inability of the spine to support the torso during normal activity and requires loss of integrity of the vertebral body or disc and the posterior elements. Limited instability refers to the loss of either ventral or dorsal spinal integrity (not both) with overall stability sufficient to support most normal activities. The most widely described mechanistic scheme is the AO classification [100]. Based on the two-column theory, the AO system describes fractures as Type A (ventral column injuries resulting from axial loading with or without flexion), Type B (ventral and dorsal column injury from flexion or extension, with distraction) and Type C (ventral and dorsal column injury from rotational forces). This classification scheme is extensive with subgroups and specifications providing categories for the majority of spine fractures.

2.9 Fracture Risk Prediction

2.9.1 Bone Mineral Density

Bone mineral density (BMD) estimation based on dual-energy X-ray absorptiometry (DXA) remains the clinical standard of care used to estimate osteoporotic fracture risk in the spine. DXA is a 2D imaging technique that yields an 'areal' measure of BMD (units g/cm^2) obtained by dividing the bone mineral content by the area of a standardized region of interest. DXA measurements alone explain only ~60% of the variation in vertebral strength [63]. Vertebral fractures occur in individuals with BMD values outside the range of osteoporosis in up to 50% of all cases [139]. Correlations between compressive strength of cadaveric vertebrae and BMD are modest (r^2 from 0.62 to 0.69).

2.9.2 Clinical Factors

Fracture risk prediction tools have been developed which rely both on BMD and validated clinical risk factors, such as FRAX developed by the World Health Organization [140]. The FRAX® algorithms give a 10-year probability of hip fracture and overall osteoporotic fracture (spine, forearm, hip or shoulder) based on hip BMD and clinical risk factors (age, sex, height, weight, previous fracture, smoking, alcohol, glucocorticoids and rheumatoid arthritis). In particular, a history of a fragility fracture (vertebral or hip) is a powerful predictor of future fracture independent of BMD and is considered in such risk analysis tools [105, 141]. However, the added benefit of such tools beyond BMD alone for the assessment of vertebral fracture risk has not been conclusive in the literature [141, 142].

2.9.3 Quantitative Computed Tomography

Quantitative computed tomography (QCT) is a 3D X-ray-based method of bone density assessment that provides a true measure of volumetric bone mineral density (units g/cm^3). QCT can isolate measurements to the trabecular centrum and yield measures of vertebral geometry, such as cross-sectional area and total volume. However, QCT versus compressive strength of cadaveric vertebrae have yielded only weak to moderate correlations (r^2 from 0.23 to 0.66) with some improvement when both density and cross-sectional area are considered [63, 65, 69]. Neither DXA nor QCT measures of BMD are strong predictors of whether an individual will suffer an osteoporotic vertebral fracture in vivo [143].

2.9.4 Structural Rigidity

Structural rigidity is a measure based upon engineering beam theory that integrates both the material and geometric properties of an object, defining its ability to resist axial, bending and twisting loads via axial (EA), bending (EI) and torsional (GJ) rigidities, respectively. On the basis of the principle that the weakest section dictates the load capacity for a structure, algorithms have been developed and implemented to calculate the minimal rigidity of the bones [144, 145]. CT-based structural rigidity analysis (CTRA) uses serial, transaxial CT images to measure tissue mineral density and cross-sectional geometry and calculates EA, EI and GJ by summing up the modulus-weighted area of each pixel within the bone contour by the position of the pixel relative to the centroid of the bone cross-section [144]. Based on composite beam theory, CTRA does not, however, predict the exact failure load or pinpoint the exact location of an impending fracture but rather seeks to determine a fracture risk threshold for whole bones using simple and reproducible measures. CTRA has been correlated to failure load ($R^2 = 0.69$) in cadaveric vertebrae with simulated metastatic defects [145] and with yield load (R^2 = 0.89 to 0.62) in rat vertebrae with osteolytic and mixed osteolytic/osteoblastic metastases [146]. However, no relationship was found for healthy rat vertebrae, and the structural rigidity predicted yield load was considerably higher than the experimental yield load in all groups. In a prospective study of vertebral metastatic breast cancer, CTRA demonstrated 100% sensitivity with specificity from 44% to 70% [147].

2.9.5 Finite Element Analysis

Finite element analysis (FEA) is a numerical technique that is used to find approximate solutions to boundary value problems for partial differential equations. In FEA, a large or complex problem is divided into smaller simpler parts (finite elements) which can be modelled with simple equations. The finite elements are then assembled into a larger system of equations that represents the whole problem. FEA allows parametric representation of complex geometric and material property distributions which occur in musculoskeletal modelling and are difficult to represent with

other analytical or experimental techniques. FE models can also be parametrically analyzed to investigate changes in loading conditions, geometries, material property definitions/distributions or pathologies. FEA has been successful in predicting failure loads and fracture patterns for bone structures [148, 149]. FEA based on idealized geometries has been used to generate guidelines for vertebral fracture risk prediction in healthy and pathologic scenarios [150].

QCT-based FEA has been proposed as an improved method for estimating fracture risk in the spine [151]. QCT-based FEA has been shown to be highly correlated with ex vivo compressive stiffness and strength [152–157]. It has been shown to perform better than QCT BMD with and without transverse plane cross-sectional area with respect to ex vivo vertebral compressive strength evaluation ($r^2 = 0.86$) and is associated with fracture even after adjusting for BMD [153, 157, 158]. QCT-based FEA of lumbar vertebrae has also been shown to better discriminate between osteoporotic and non-osteoporotic individuals and fracture and non-fracture cohorts than BMD alone [156, 157, 159]. However, less encouraging results have been found under anterior flexion loading and in predictions of failure patterns and post-yield behaviour [160–162]. The highly non-uniform loading applied through the intervertebral discs and facets may impact these predictions [163–167]. As well, while QCT yields information on the architecture and mineralization of bone structures, it does not provide information on the organic components of the bone, which impacts its plastic behaviour, nor on the fracture resistance of bone tissue.

2.9.6 Damage

The bone is full of small defects and cracks, and the interaction of these cracks within its microstructure influences how both trabecular and cortical bone fail, leading to whole bone fracture. Fracture risk can be increased by the presence of damage by two mechanisms: (1) damage leading to a reduction in material properties locally leading to catastrophic failure or (2) damage leading to systemic changes that decrease bone mass ultimately translating into less structurally sound bone structures.

Under tensile loading, cracks can open, limiting strength and leading to catastrophic failure. In contrast, compression loads may cause cracks to close or compaction of failed bone tissue allowing maintenance of load-bearing capacity. Both the mineral and organic phases contribute to fracture resistance, through multiple mechanisms at multiple-scale levels, including crack deflection, uncracked ligament bridging, collagen fibril bridging, microcracking, sacrificial bonds, fibrillar sliding and molecular uncoiling [168]. Microdamage in age-related fractures may be due to repetitive loading of the bone, likely initiating at the level of the collagen fibre or below and may include collagen fibre–matrix debonding, disruption of the mineral–collagen aggregate and failure of the collagen fibre itself [55].

Overloading of trabecular bone causes damage that leads to large reductions in apparent modulus [169]. In vertebral specimens loaded in compression to 15% strain, the primary mechanism of failure was found to be microscopic cracking as opposed to fracture of individual trabeculae [170]. Fracture of trabeculae is primarily in elements oriented transversely to the loading direction. Microdamage, rather

than microfracture, is likely the mechanism for the large apparent reductions in mechanical properties after compressive overloading [171]. The impact of microdamage on bone strength supports the elevated risk for vertebral osteoporotic fractures in those who have previously sustained osteoporotic fractures. Further, musculoskeletal injury has been shown to lead to a loss in systemic bone mass and specifically decreased stiffness in trabecular bone [108].

Studies have evaluated the impact of age and bone diseases on cross-linking [172]. Interfacial bonding between the mineral and organic phases of bone tissue may also be important to the strength and stiffness of the bone; however, the nature of collagen–mineral interactions in the bone remains less characterized [173–175]. The biomechanical impact of collagen in the bone has been shown to be related to the content present, its extent of cross-linking (interfibrillar pyrrole or intrafibrillar pyridinoline) and gene polymorphisms [176–181]. Collagen cross-linking has also been shown to affect the mineralization process and influence microdamage formation [172]. Fracture energy is highly affected by collagen fibre orientation. The angle between collagen and crack propagation direction influences toughening mechanisms [48]. Woven bone, consisting of unorganized collagen fibrils, shows reduced mechanical properties versus lamellar bone, despite mineralization, highlighting the importance of collagen fibre orientation [182].

The mechanical properties of the bone's collagen fibril matrix can be influenced by inter- and intrafibrillar cross-links. These cross-links can be formed enzymatically through the action of lysyl oxidase or non-enzymatically through glycation or potentially oxidative stress [111, 183]. Whereas the presence of enzymatic cross-links has been positively correlated to mechanical performance with minimal content changes throughout adulthood [176, 184], increased non-enzymatic cross-linking in the collagen matrix has been shown to degrade the mechanical properties of the bone. Glycation, both in vivo (Advanced Glycation End Products) and ex vivo (ribosylation), changes how the collagen matrix can deform and alter apparent yield strain, strength, as well as changing how microdamage accumulates without affecting the initial stiffness [185–188]. Fragility of ribose-treated bone has been shown to be reversible with a sugar cross-links cleaver (N-phenacylthiazolium bromide) [189]. It has been further verified that increased cross-linking between collagen fibres lowers toughness [189]. High densities of these resulting advanced glycation end products (AGEs) increase trabecular bone fragility, decreasing post-yield strain energy absorption and specifically decrease the energy dissipation within the organic phase [187]. Pentosidine, an AGE-based non-enzymatic cross-link, has been correlated with the strength of individual trabeculae [190]. Pentosidine levels have been shown to increase significantly with age and pathological conditions making it a potential biomarker for bone quality [191, 192].

2.9.7 Loading

The loading applied to the spine is also a critical component of vertebral fracture risk prediction. Both the magnitude and direction of the applied loads are key factors in fracture risk evaluation and in the mechanism of failure. This includes

traumatic loading and repetitive loading at physiologic load levels (fatigue failure) [10, 60, 193]. Estimated forces applied to the thoracolumbar spine in older individuals range from approximately 400 to 2100 N for typical activities [71]. Subtle changes in body position can dramatically alter spinal loading. Lifting while standing straight with outstretched arms in comparison to a position with knees bent and arms in greatly increases spinal loads. Forward flexion further increases compressive loading. Activities of daily living such as bending, lifting and rising from a seated position can generate high forces on the spine [71].

A factor of risk can be determined by comparing the load-bearing requirement of the spine to its load-bearing capacity. The ratio of the load on the spine to the failure load of the bone indicates whether fracture is likely during a given activity [193]. A high factor of risk can result from weakened bone (low failure load) or the application of large forces. The likelihood for nonphysiologic spinal loading may be increased through work- or sport-related exposure or pathological processes which may increase the propensity for falling. The relationship between fall risk and skeletal fracture has received much attention in the context of osteoporosis. Muscle weakness, impaired balance and slower reaction times in fall prevention have been suggested as contributors to osteoporotic fracture incidence [108, 193].

2.9.8 Spinal Alignment

While a straight spine would theoretically be an ideal axial loading spinal configuration, it would not tolerate eccentric loads and would provide limited flexibility [90]. The spine has a curvilinear sagittal conformation with a primary kyphotic thoracic curve, compensated by secondary cervical and lumbar lordotic curves of equal summative magnitude, yielding a balanced configuration necessary for a bipedal upright posture [90]. Increases in thoracic kyphosis or the loss of lumbar lordosis results in an increased moment arm generating greater bending moments at each vertebral segment [90]. As such, increased deformity resulting from vertebral fracture can increase the moment arm length, leading to higher bending moments and increased risk for subsequent fracture.

2.10 Vertebral Metastases

2.10.1 Strength and Fracture Risk

Many methods have been employed towards assessing metastatically involved vertebral strength including clinical, experimental, image-based and computational analyses [132, 145, 150, 194–208]. Clinically, preoperative condition influences outcome in the metastatic spine [195]. Qualitative (radiographic-based), experimental and computational modelling of osteolytic vertebrae have found tumour size to be the most important risk factor for vertebral body failure, yet measures of tumour

size alone have not been able to completely explain the strength reductions [145, 150, 194, 196, 197, 199, 200, 203].

The presence of contained tumour tissue causes an increased propensity for vertebrae to pressurize and burst into the spinal canal [132]. Osteolytic tumour tissue consists of both solid extracellular matrix and interstitial fluid and can be modelled as a poroelastic material [209]. Vertebral pressurization has been shown at physiologic load levels in specimens with simulated metastases, causing the development of increased tensile hoop strains and tensile axial strains on the vertebral cortex, leading to narrowing of the spinal canal [194]. Digital image correlation under axial compressive loading has shown that higher strains result in the presence of osteolytic tumour, particularly adjacent to the dorsal wall which may correspond to an increased burst fracture risk [204]. At high loading rates, the presence of a large fluid-rich relatively incompressible osteolytic tumour can provide axial support to the vertebral body while increasing pressure, vertebral bulge and tensile hoop strain (indicative of an elevated risk of burst fracture prior to endplate failure). Validated 3D poroelastic FEA of the metastatic spine has demonstrated that while the strongest (exponential) factor is tumour size, lower BMD, pedicle disruption and focal osteolytic disease (in contrast to more diffuse lesions) in the posterior vertebral body also increase burst fracture risk [194, 203, 206]. Additional structural and geometric factors including upper thoracic vertebral level, a reduced degree of kyphosis, removing the stabilization of the rib cage and axial compressive loading lead to a higher risk of burst fracture initiation [206–208].

Experimental in vitro testing has shown metastatic compromise of the posterior elements to cause decreases in vertebral strength, whereas the impact of defect location has been less clear [37, 197]. However, the majority of the mechanical testing protocols have modelled defects as voids or with unconstrained simulated tissue, reducing any potential effects due to the mass and fluid behaviour of tumour material and the ability to study burst fracture patterns [145, 196–200, 202].

Minimum failure load calculated based on axial and bending rigidity has been successful in predicting fracture prospectively in cadaveric studies of vertebrae with simulated and actual lesions and in retrospective evaluation of clinical imaging data [147, 201]. This approach has been shown to be highly sensitive and moderately specific to vertebral fracture [147]. FEA has also been used to develop biomechanically-based guideline equations to quantify burst fracture risk in metastatically involved vertebrae based on load-bearing capacity and load exposure [150, 194]. The equation-based guidelines were able to describe the mechanical behaviour of the metastatically involved vertebral FE model ($R^2 = 0.97$) reflecting the in vitro risk and mechanism of fracture and yielding a clear clinical threshold for burst fracture risk in a retrospective clinical data set [210].

Micro-FEA has also demonstrated elevated stresses and strains in regions of microdamage identified through histological and barium sulphate ($BaSO_4$) staining within healthy and osteolytic vertebral vertebrae as compared to undamaged regions [211]. Damaged regions of metastatic vertebrae are more extensive and experience significantly higher local stresses and strains than those in the damaged regions of healthy specimens.

2.10.2 Impact on Material Properties

Cancerous regulation has been shown to lead to a decrease in mineralization and increased fracture risk [212, 213]. In metastatic bone, measurement of the tissue-level material properties has been performed on human bone cores demonstrating significant reductions in tissue density, average BV fraction, mineralization, hardness and tissue elastic modulus as compared to normal bone [213]. The large material changes had little effect on macroscopic mechanical properties when compared to BV fraction. These observations therefore do not explain the high incidence of fracture observed in osteoblastic disease. Uncertainty with respect to treatment received by patients from whom bone specimens were harvested (i.e. bisphosphonates and/or external beam radiation therapy, both of which significantly influence macroscopic- and tissue-level material properties) and grouping of data from heterogeneous disease (osteolytic/osteoblastic/mixed) may have implications with respect to these findings [192].

Recent preclinical work evaluating the impact of collagen and mineral parameters within metastatically involved rat vertebrae has demonstrated that metastatic involvement has a clear impact on the formation of specific non-enzymatic and mature enzymatic cross-links in vertebral bone [192]. This includes increases in the formation of pentosidine and decreases in the formation of the enzymatic cross-link deoxypryridinoline within osteolytic vertebrae compared to mixed osteolytic/osteoblastic vertebrae, decreased crystallinity, increased carbonation and collagen quality (1660/1690 sub-band) ratio with osteolytic bone compared to mixed bone and healthy controls, along with an observed increase in proline hydroxylation with metastatic involvement. The mineral:matrix ratio was also found to be decreased in both osteolytic and mixed bone compared to healthy controls.

2.11 Treatment Effects

Anti-resorptive drug therapies, such as bisphosphonates are commonly used in the treatment of both osteoporosis and skeletal metastatic disease. In their use in osteoporosis, they have been shown to produce average increases in areal BMD of 5–8% and decreases in fracture incidence of up to 60% [143, 214, 215]. These treatments affect bone strength rather than applied loading, suggesting that osteoporotic fracture risk may be dominated by the load-bearing capacity of the bone as opposed to loading conditions. A number of studies have looked at the effects of bisphosphonates on trabecular bone biomechanics in large animals, reporting preservation or improvement of trabecular microarchitecture and strength but with increased microdamage accumulation [216–223]. In considering differences in bone mechanical properties relative to density, no findings showed significant changes in the relationships as a result of treatment [224–226].

Spine stereotactic body radiotherapy (SBRT) provides ablative doses of radiation delivered in just a few treatments as opposed to conventional radiation therapy given in many treatments over several weeks. This technique is increasingly applied to spine

metastases with evidence supporting greater rates of local control. However SBRT has demonstrated elevated rates of late toxicity in the bone presenting as spine SBRT-induced vertebral compression fractures (from 11 to 39% with SBRT as compared to ~5% with conventional radiation) [227–231]. Gamma irradiation of the bone has been shown to lead to decreases in ultimate strength, ductility, toughness, fracture toughness and fatigue resistance of the bone through damage to collagen [41, 232, 233]. This embrittlement can predispose the bone to fracture. The destruction of collagen connectivity in the bone treated with gamma irradiation may contribute to the loss of ultimate strength, ductility and fracture toughness [234–236]. Separation surgery represents an approach that combines SBRT treatment with surgical mechanical stabilization to combat the radiation-induced loss of strength in the bone tissue [237].

2.11.1 Minimally Invasive Cement-Based Vertebral Stabilization

In both vertebroplasty and kyphoplasty, bone cement is injected percutaneously into the vertebral cancellous bone to provide mechanical reinforcement to a weakened vertebra. These procedures have been used in osteoporotic and metastatically involved vertebrae, for pain relief and mechanical stabilization. From a biomechanical perspective, strength or load-bearing capacity of a single vertebra has been shown to be significantly increased following augmentation when compared to the intact strength, while the impact on stiffness has been varied (increased, decreased or no change) [238]. FEA and experimental studies have shown that the volume of cement injected affects the restoration of strength and stiffness, but the type of cement appears to have less of an effect [239]. Where smaller volumes can equalize stress in the disc, larger volumes may be required to increase compressive stiffness and reduce loading of the neural arch [61, 240]. Location of cement deposition is also critical in vertebrae with osteolytic metastases [241, 242].

Clinical and biomechanical reports suggest, however, that cement augmentation may cause an increase in fracture in vertebrae adjacent to augmented levels. Higher cement rigidity causes a ‘pillar effect’ which reduces the endplate bulge of the augmented vertebra leading to higher intervertebral disc pressure, intensifying the mechanical loading on adjacent vertebrae and elevating the risk of fracture [238, 243]. However, some clinical reviews have found no differences in the incidence of secondary fractures between vertebral augmentation techniques and conservative treatment for patients with osteoporotic vertebral compression fractures [244]. Rapid pain relief afforded by the cement augmentation may allow for higher levels of physical activities, which are associated with greater risks of vertebral fracture [245]. Fractures may also occur at a higher rate as a consequence of the normal progression of osteoporosis and the fracture cascade [108, 243]. Vertebroplasty does not restore vertebral height, and as such, suboptimal spinal kinetics, including an increased flexion moment arm, may also contribute to increased fracture incidence post-augmentation. Overall, a Cochrane review conducted in 2015 resolved that based upon moderate quality evidence, there was no sufficient support for vertebroplasty for treating osteoporotic vertebral fractures in routine practice [246].

In contrast, vertebral cement augmentation has been described as an effective procedure for treating prophylactic and painful vertebral body fractures caused by metastasis and multiple myeloma [247]. Percutaneous vertebroplasty is effective in decreasing vertebral bulge (as a surrogate for burst fracture risk) if the tumour is surrounded posteriorly with cement [241, 242]. However, injecting cement into the posterior third of the vertebral body is not without risk due to potential extravasation into the canal. As no correlation has been shown between the amount of injected cement and pain relief, excessive cement injection should be avoided to prevent leakage [247]. Elimination of tumour prior to cement injection in osteolytic vertebrae creates a cavitary defect that facilitates cement fill, enhances biomechanical stability and reduces the risk of cement extravasation [248, 249].

2.12 Summary

Overall, the use of clinical, experimental, preclinical, image analysis and computational research methods has led to a better understanding of the biomechanics of vertebral fracture. However, knowledge gaps remain with respect to the occurrence and impact of tissue-level changes to the bone resulting from ageing, pathologic changes, and local and systemic treatments. High-fidelity biomechanical analysis combined with clinical factors may ultimately combine to yield benefit by better determination of vertebral fracture risk and directing treatment towards the enhancement of spinal stability as a whole.

References

1. Bernhardt M, White AA, Panjabi MM, et al. Biomechanical considerations of spinal stability. In: Rothman RH, Simeone FA, editors. The Spine. 3rd ed. Philadelphia: WB Saunders; 1992. p. 1167–95.
2. Kowalski RJ, Ferrara LA, Benzel EC. Biomechanics of the Spine. Neurosurg. Q. 2005;15(1):42–59.
3. Hippocrates. The Genuine Works of Hippocrates. [translated from the Greek by F. Adams]. Baltimore: Williams & Wilkins; 1993:231–241.
4. Hansson T, Roos B, Nachemson A. The bone mineral content and ultimate compressive strength of lumbar vertebrae. Spine. 1980;5:46–55.
5. McBroom RJ, Hayes WC, et al. Prediction of vertebral body compressive fracture using quantitative computed tomography. J. Bone Joint Surg. 1985;67-A:1206–14.
6. Mosekilde L, Mosekilde L. Normal vertebral body size and compressive strength: relations to age and to vertebral and iliac trabecular bone compressive strength. Bone. 1986;7:107–11.
7. Yoganandan N, Myklebust JB, et al. Functional biomechanics of the thoracolumbar vertebral cortex. Clin. Biomech. 1988;3:11–8.
8. Cody DD, Goldstein SA, Flynn MJ, Brown EB. Correlations between vertebral regional bone mineral density (rBMD) and whole bone fracture load. Spine. 1991;16:146–54.
9. Keller TS, Hansson TH, et al. Regional variations in the compressive properties of lumbar vertebral trabeculae: effects of disc degeneration. Spine. 1989;14:1012–9.
10. Brinckmann P, Biggemann M, Hilweg D. Prediction of the compressive strength of human lumbar vertebrae. Spine. 1989;14:606–10.

11. Edmondston SJ, Singer KP, et al. Ex vivo estimation of thoracolumbar vertebral body compressive strength: the relative contributions of bone densitometry and vertebral morphometry. Osteoporos. Int. 1997;7:142–8.
12. Edwards WT, Zheng YG, Ferrara LA, Yuan HA. Structural features and thickness of the vertebral cortex in the thoracolumbar spine. Spine. 2001;26:218–25.
13. Silva MJ, Keaveny TM, Hayes WC. Direct and computed tomography thickness measurements of the human lumbar vertebral shell and endplate. Bone. 1994;15:409–14.
14. Keaveny TM, Buckley JM. Biomechanics of vertebral bone. In: Kurtz SM, Edidin AA, editors. Spine technology handbook. New York: Academic Press; 2006.
15. Reilly DT, Burstein AH. The elastic and ultimate properties of compact bone tissue. J. Biomech. 1975;8:393–405.
16. Turner CH. Yield behavior of bovine cancellous bone. J. Biomech. Eng. 1989;111:256–60.
17. Mosekilde L. Vertebral structure and strength in vivo and in vitro. Calcif. Tissue Int. 1993;53:S121–6.
18. Roy ME, Rho JY, et al. Mechanical and morphological variation of the human lumbar vertebral cortical and trabecular bone. J. Biomed. Mater. Res. 1999;44:191–7.
19. Rockoff SD, Sweet E, Bleustein J. The relative contribution of trabecular and cortical bone to the strength of human lumbar vertebrae. Calcif. Tissue Res. 1969;3:163–75.
20. Silva MJ, Keaveny TM, Hayes WC. Load sharing between the shell and centrum in the lumbar vertebral body. Spine. 1997;22:140–50.
21. Eswaran SK, Gupta A, Adams MF, Keaveny TM. Cortical and trabecular load sharing in the human vertebral body. J. Bone Miner. Res. 2006;21:307–14.
22. Homminga J, Weinans H, et al. Osteoporosis changes the amount of vertebral trabecular bone at risk of fracture but not the vertebral load distribution. Spine. 2001;26:1555–61.
23. Nachemson A, Lewin T, Maroudas A, et al. In vitro diffusion of dye through the end-plates and the annulus fibrosus of human lumbar inter-vertebral discs. Acta Orthop. Scand. 1970;41(6):589–607.
24. Bernick S, Cailliet R. Vertebral end-plate changes with aging of human vertebrae. Spine. 1982;7(2):97–102.
25. Rodriguez AG, Rodriguez-Soto AE, Burghardt AJ, Berven S, Majumdar S, Lotz JC. Morphology of the human vertebral endplate. J. Orthop. Res. 2012 Feb;30(2):280–7.
26. Grant JP, Oxland TR, Dvorak MF, et al. The effects of bone density and disc degeneration on the structural property distributions in the lower lumbar vertebral endplates. J. Orthop. Res. 2002;20(5):1115–20.
27. Keller TS, Ziv I, Moeljanto E, et al. Interdependence of lumbar disc and subdiscal bone properties: a report of the normal and degenerated spine. J. Spinal Disord. 1993;6(2):106–13.
28. Fields AJ, Sahli F, Rodriguez AG, Lotz JC. Seeing double: a comparison of microstructure, biomechanical function, and adjacent disc health between double- and single-layer vertebral endplates. Spine (Phila Pa 1976). 2012 Oct 1;37(21):E1310–7.
29. Adams MA, Hutton WC. The mechanical function of the lumbar apophyseal joints. Spine. 1983;8:327–30.
30. Pollintine P, Dolan P, Tobias JH, Adams MA. Intervertebral disc degeneration can lead to 'stress-shielding' of the anterior vertebral body: a cause of osteoporotic vertebral fracture? Spine. 2004;29:774–82.
31. Eastell R, Mosekilde L, Hodgson SF, Riggs BL. Proportion of human vertebral body bone that is cancellous. J. Bone Miner. Res. 1990 Dec;5(12):1237–41.
32. Choi K, Goldstein SA. A comparison of the fatigue behavior of human trabecular and cortical bone tissue. J. Biomech. 1992;25:1371–81.
33. Rice JC, Cowin SC, Bowman JA. On the dependence of the elasticity and strength of cancellous bone on apparent density. J. Biomech. 1988;21(2):155–68.
34. Keaveny TM, Hayes WC. A 20-year perspective on the mechanical properties of trabecular bone. J. Biomech. Eng. 1993;115:534–42.
35. Gibson L. The mechanical behaviour of cancellous bone. J. Biomech. 1985;18:317–28.

36. Yeh OC, Keaveny TM. Biomechanical effects of intraspecimen variations in trabecular architecture: A three-dimensional finite element study. Bone. 1999;25(2):223–8.
37. Kothari M, Keaveny TM, Lin JC, Newitt DC, Majumdar S. Measurement of intraspecimen variations in vertebral cancellous bone architecture. Bone. 1999;25(2):245–50.
38. Wang X, Li X, Bank RA, Agrawal CM. Effects of collagen unwinding and cleavage on the mechanical integrity of the collagen network in bone. Calcif. Tissue Int. 2002;71(2):186–92.
39. Yan J, Daga A, Kumar R, Mecholsky JJ. Fracture toughness and work of fracture of hydrated, dehydrated, and ashed bovine bone. J. Biomech. 2008;41(9):1929–36.
40. Wynnyckyj C, Willett T. Changes in bone fatigue resistance due to collagen degradation. J. Orthop. Res. 2011;29(2):197–203.
41. Barth HD, Launey ME, Macdowell AA, Ager JW, Ritchie RO. On the effect of X-ray irradiation on the deformation and fracture behavior of human cortical bone. Bone. 2010;46(6):1475–85.
42. Wang X, Bank RA, TeKoppele JM, Agrawal CM. The role of collagen in determining bone mechanical properties. J. Orthop. Res. 2001;19(6):1021–6.
43. Mosekilde L, Mosekilde L, Danielsen CC. Biomechanical competence of vertebral trabecular bone in relation to ash density and age in normal individuals. Bone. 1987;8(2):79–85.
44. Kopperdahl DL, Keaveny TM. Yield strain behavior of trabecular bone. J. Biomech. 1998;31:601–8.
45. Hayes WC, Bouxsein ML. Biomechanis of cortical and trabecular bone: implications for assessment of fracture risk. In: Mow VC, Hayes WC, editors. Basic orthopaedic biomechanics. 2nd ed. Philadelphia: Lippincott-Raven Publishers; 1997.
46. Keaveny TM, Morgan EF, Niebur GL, Yeh OC. Biomechanics of trabecular bone. Annu. Rev. Biomed. Eng. 2001;3:307–33.
47. Nalla RK, Kinney JH, Ritchie RO. Mechanistic fracture criteria for the failure of human cortical bone. Nat. Mater. 2003;2(3):164–8.
48. Peterlik H, Roschger P, Klaushofer K, Fratzl P. From brittle to ductile fracture of bone. Nat. Mater. 2006;5(1):52–5.
49. Burr DB. The contribution of the organic matrix to bone's material properties. Bone. 2002;31(1):8–11.
50. Burstein AH, Zika JM, Heiple KG, Klein L. Contribution of collagen and mineral to the elastic-plastic properties of bone. J. Bone Joint Surg. 1975;57-A:956–61.
51. Currey JD. The mechanical consequences of variation in the mineral content of bone. J. Biomech. 1969;2:1–11.
52. Currey JD. The effect of porosity and mineral content on the Young's modulus of elasticity of compact bone. J. Biomech. 1988;21:131–9.
53. Currey JD, Brear K, Zioupos P. The effects of aging and changes in mineral content in degrading the toughness of human femora. J. Biomech. 1996;29:257–60.
54. Bailey AJ, Knott L. Molecular changes in bone collagen in osteoporosis and osteoarthritis in the elderly. Exp. Gerontol. 1999;34:337–51.
55. Burr DB, Forwood MR, et al. Bone microdamage and skeletal fragility in osteoporotic and stress fractures. J. Bone Miner. Res. 1997;12:6–15.
56. Kopperdahl DL, Pearlman JL, Keaveny TM. Biomechanical consequences of an isolated overload on the human vertebral body. J. Orthop. Res. 2000;18:685–90.
57. White AA, Panjabi MM. Clinical biomechanics of the spine. Philadelphia: Lippincott; 1990.
58. Liu YK, Njus G, Buckwalter J, Wakano K. Fatigue response of lumbar intervertebral joints under axial cyclic loading. Spine. 1983;8:857–65.
59. Brinckmann P, Biggemann M, Hilweg D. Fatigue fracture of human lumbar vertebrae. Clin. Biomech. 1988;3(Suppl 1):S1–S23.
60. Hansson TH, Keller TS, Spengler DM. Mechanical behaviour of the human lumbar spine. II. Fatigue strength during dynamic compressive loading. J. Orthop. Res. 1987;5(4):479–87. (published erratum appears in J Orthop Res 1988;6(3):465).
61. Adams MA, Dolan P. Biomechanics of vertebral compression fractures and clinical application. Arch. Orthop. Trauma Surg. 2011;131:1703–10.

62. Vernon-Roberts B, Pirie CJ. Healing trabecular microfractures in the bodies of lumbar vertebrae. Ann. Rheum. Dis. 1973;32(5):406–12.
63. Cheng XG, Nicholson PHF, et al. Prediction of vertebral strength in vitro by spinal bone densitometry and calcaneal ultrasound. J. Bone Miner. Res. 1997;12:1721–8.
64. Ebbesen EN, Thomsen JS, et al. Lumbar vertebral body compressive strength evaluated by dual-energy X-ray absorptiometry, quantitative computed tomography, and ashing. Bone. 1999;25:713–24.
65. Eriksson SA, Isberg BO, Lindgren JU. Prediction of vertebral strength by dual photon absorptiometry and quantitative computed tomography. Calcif. Tissue Int. 1989;44:243–50.
66. Moro M, Hecker AT, Bouxsein ML, Myers ER. Failure load of thoracic vertebrae correlates with lumbar bone mineral density measured by DXA. Calcif. Tissue Int. 1995;56:206–9.
67. Mosekilde L, Mosekilde L. Sex differences in age-related changes in vertebral body size, density and biomechanical competence in normal individuals. Bone. 1990;11:67–73.
68. Singer K, Edmondston S, et al. Prediction of thoracic and lumbar vertebral body compressive strength: correlations with bone mineral density and vertebral region. Bone. 1995;17:167–74.
69. Edmondston SJ, Singer KP, et al. The relationship between bone mineral density, vertebral body shape and spinal curvature in the elderly thoracolumbar spine: an in vitro study. Br. J. Radiol. 1994;67:969–75.
70. Silva M, Gibson L. Modeling the mechanical behavior of vertebral bone: effects of age-related changes in microstructure. Bone. 1997;21:191–9.
71. Bouxsein M. Biomechanics of age related fractures. In: Marcus R, Feldman D, Kelsey J, editors. Osteoporosis, vol. 1. 2nd ed. San Diego, CA: Academic Press; 2001.
72. Aaron Joseph Fields. Trabecular microarchitecture, endplate failure, and the biomechanics of human vertebral fractures. UC Berkeley thesis, 2010.
73. Antonacci MD, Hanson DS, Leblanc A, Heggeness MH. Regional variation in vertebral bone density and trabecular architecture are influenced by osteoarthritic change and osteoporosis. Spine. 1997;22:2393–401. discussion 2392–2401.
74. Vernon-Roberts B, Pirie CJ. Degenerative changes in the intervertebral discs of the lumbar spine and their sequelae. Rheumatol. Rehabil. 1977;16:13–21.
75. Keaveny TM, Wachtel EF, Kopperdahl DL. Mechanical behavior of human trabecular bone after overloading. J. Orthop. Res. 1999;17:346–53.
76. Ferguson SJ, Steffen T. Biomechanics of the aging spine. Eur. Spine J. 2003;12(S2): S97–S103.
77. Pollintine P, Luo J, Offa-Jones B, Dolan P, Adams MA. Bone creep can cause progressive vertebral deformity. Bone. 2009;45(3):466–72.
78. Currey JD. Anelasticity in bone and echinoderm skeletons. J. Exp. Biol. 1965;43:279–92.
79. Mercer C, He MY, Wang R, Evans AG. Mechanisms governing the inelastic deformation of cortical bone and application to trabecular bone. Acta Biomater. 2006;2(1):59–68.
80. Yamamoto E, Paul Crawford R, Chan DD, Keaveny TM. Development of residual strains in human vertebral trabecular bone after prolonged static and cyclic loading at low load levels. J. Biomech. 2006;39(10):1812–8.
81. Iatridis JC, Setton LA, Weidenbaum M, Mow VC. Alterations in the mechanical behavior of the human lumbar nucleus pulposus with degeneration and aging. J. Orthop. Res. 1997;15:318–22.
82. Kurowski P, Kubo A. The relationship of degeneration of the intervertebral disc to mechanical loading conditions on lumbar vertebrae. Spine. 1986;11:726–31.
83. Horst M, Brinckmann P. 1980 Volvo award in biomechanics: measurement of the distribution of axial stress on the end-plate of the vertebral body. Spine. 1981;6:217–32.
84. Hansson T, Roos B. The relation between bone-mineral content, experimental compression fractures, and disk degeneration in lumbar vertebrae. Spine. 1981;6:147–53.
85. Holdsworth FW. Fractures, dislocations, and fracture-dislocations of the spine. J. Bone Joint Surg. 1963;45B:6–20.
86. Kelly RP, Whitesides TE. Treatment of lumbodorsal fracture-dislocations. Ann. Surg. 1968;167:705–17.

87. Louis R. Spinal stability as defined by the three-column spine concept. Anat. Clin. 1985;7:33–42.
88. Denis F. The three column spine and its significance in the classification of acute thoracolumbar spinal injuries. Spine. 1983;8:817–31.
89. Denis F. Spinal instability as defined by the three-column spine concept in acute spinal trauma. Clin. Orthop. Relat. Res. 1984 Oct;189:65–76.
90. Roger EP, Jone GA, Benzel EC. Biomechanics of spinal column failure. In: Amar AP, editor. Surgical management of spinal cord injury: controversies and consensus. Hoboken, NJ: Blackwell Publishing; 2007.
91. Reeves NP, Narendra KS, Cholewicki J. Spine stability: the six blind men and the elephant. Clin. Biomech. (Bristol, Avon). 2007;22(3):266–74. Review.
92. Allen BL, Ferguson RL, Lehmann TR, O'Brien RP. A mechanistic classification of closed, indirect fractures and dislocations of the lower cervical spine. Spine. 1982;7:1–27.
93. Dvorak MF, Fisher CG, Aarabi B, Harris MB, et al. Clinical outcomes of 90 isolated unilateral facet fractures, subluxations, and dislocations treated surgically and nonoperatively. Spine. 2007;32:3007–13.
94. Vaccaro AR, Hulbert RJ, Patel AA, Fisher C, et al. The subaxial cervical spine injury classification system: a novel approach to recognize the importance of morphology, neurology, and integrity of the disco-ligamentous complex. Spine. 2007;32:2365–74.
95. McLachlin SD. 2013. An Investigation of subaxial cervical spine trauma and surgical treatment through biomechanical simulation and kinematic analysis. Thesis, University of Western Ontario.
96. Kwon BK, Vaccaro AR, Grauer JN, Fisher CG, Dvorak MF. Subaxial cervical spine trauma. J. Am. Acad. Orthop. Surg. 2006;14:78–89.
97. Lowery DW, Wald MM, Browne BJ, Tigges S, et al. Epidemiology of cervical spine injury victims. Ann. Emerg. Med. 2001;38:12–6.
98. Nakashima H, Yukawa Y, Ito K, Machino M, Kato F. Mechanical patterns of cervical injury influence postoperative neurological outcome: a verification of the allen system. Spine. 2011;36:E441–6.
99. Vaccaro AR, Koerner JD, Radcliff KE, Oner FC, Reinhold M, Schnake KJ, Kandziora F, Fehlings MG, Dvorak MF, Aarabi B, Rajasekaran S. AO spine subaxial cervical spine injury classification system. Eur. Spine J. 2015:1–12.
100. Magerl F, Aebi M, Gertzbein SD, Harms J, Nazarian S. A comprehensive classification of thoracic and lumbar injuries. Eur. Spine J. 1994;3(4):184–201.
101. McAfee PC, Yuan HA, Fredrickson BE, Lubicky JP. The value of computed tomography in thoracolumbar fractures: an analysis of one hundred consecutive cases and a new classification. J. Bone Joint Surg. Am. 1983;65:461–73.
102. Vaccaro AR, Lehman RA Jr, Hurlbert RJ, Anderson PA, Harris M, Hedlund R, Harrop J, Dvorak M, Wood K, Fehlings MG, Fisher C. A new classification of thoracolumbar injuries: the importance of injury morphology, the integrity of the posterior ligamentous complex, and neurologic status. Spine. 2005;30(20):2325–33.
103. Vaccaro AR, Zeiller SC, Hulbert RJ, Anderson PA, Harris M, Hedlund R, Harrop J, Dvorak M, Wood K, Fehlings MG, Fisher C. The thoracolumbar injury severity score: a proposed treatment algorithm. J. Spinal Disord. Tech. 2005;18(3):209–15.
104. Burge R, Dawson-Hughes B, Solomon DH, Wong JB, King A, Tosteson A. Incidence and economic burden of osteoporosis-related fractures in the United States, 2005–2025. J. Bone Miner. Res. 2007 Mar;22(3):465–75.
105. Klotzbuecher CM, Ross PD, Landsman PB, et al. Patients with prior fractures have an increased risk of future fractures: a summary of the literature and statistical synthesis. J. Bone Miner. Res. 2000;15:721–39.
106. Cooper C, O'Neill T, Silman A. The epidemiology of vertebral fractures. European Vertebral Osteoporosis Study Group. Bone. 1993;14(Suppl 1):S89–97. Review.
107. Cauley JA, Hochberg MC, Lui LY, Palermo L, Ensrud KE, Hillier TA, Nevitt MC, Cummings SR. Long-term risk of incident vertebral fractures. J. Am. Med. Assoc. 2007 Dec 19;298(23):2761–7.

108. Christiansen BA, Bouxsein ML. Biomechanics of vertebral fractures and the vertebral fracture cascade. Curr. Osteoporos. Rep. 2010 Dec;8(4):198–204.
109. Cooper C, Atkinson EJ, O'Fallon WM, Melton LJ 3rd. Incidence of clinically diagnosed vertebral fractures: a population-based study in Rochester, Minnesota, 1985–1989. J. Bone Miner. Res. 1992;7:221–7.
110. Freitas SS, Barrett-Connor E, Ensrud KE, et al. Rate and circumstances of clinical vertebral fractures in older men. Osteoporos. Int. 2008;19:615–23.
111. Wong DA, Fornasier VL, McNab I. Spinal metastases: the obvious, the occult, and the imposters. Spine. 1990;15(1):1–3.
112. Toma S, Venturino A, Sogno G, et al. Metastatic bone tumors. Nonsurgical treatment. Outcome and survival. Clin. Orthop. Relat. Res. 1993;295:246–51.
113. Gainford MC, Dranitsaris G, Clemons M. Recent developments in bisphosphonates for patients with metastatic breast cancer. BMJ (Clin. Res. Ed.). 2005;330(7494):769–73.
114. Guise TA. Molecular mechanisms of action of osteolytic bone metastases. Cancer. 2000;88:2892–8.
115. Whyne CM. Biomechanics of metastatic disease in the vertebral column. Neurol. Res. 2014;36(6):493–501.
116. Skrinskas T, Clemons M, Freedman O, Weller I, Whyne CM. Automated CT-based analysis to detect changes in the prevalence of lytic bone metastases from breast cancer. Clin. Exp. Metastasis. 2009;26:97–103.
117. Du Y, Cullum I, Illidge TM, Ell PJ. Fusion of metabolic function and morphology: sequential [18F] fluorodeoxyglucose positron-emission tomography/computed tomography studies yield new insights into the natural history of bone metastases in breast cancer. J. Clin. Oncol. 2007;25(23):3440–7.
118. Vassiliou V, Kalogeropoulou C, Petsas T, Leotsinidis M, Kardamakis D. Clinical and radiological evaluation of patients with lytic, mixed and sclerotic bone metastases from solid tumors: is there a correlation between clinical status of patients and type of bone metastases? Clin. Exp. Metastasis. 2007;24(1):49–56.
119. Perey O. Fracture of the vertebral endplate. A biomechanical investigation. Acta Orthop. Scand. 1957;28(Supp 25):1–107.
120. Hutton WC, Adams MA. Can the lumbar spine be crushed in heavy lifting? Spine. 1982;7(6):586–90.
121. Yoganandan N, Larson SJ, Gallagher M, Pintar FA, Reinartz J, Droese K. Correlation of microtrauma in the lumbar spine with intraosseous pressures. Spine. 1994;19(4):435–40.
122. Jiang G, Luo J, Pollintine P, Dolan P, Adams MA, Eastell R. Vertebral fractures in the elderly may not always be “osteoporotic”. Bone. 2010;47(1):111–6.
123. Adams MA, Pollintine P, Tobias JH, Wakley GK, Dolan P. Intervertebral disc degeneration can predispose to anterior vertebral fractures in the thoracolumbar spine. J. Bone Miner. Res. 2006;21(9):1409–16.
124. Turner CH, Takano Y, Owan I. Aging changes mechanical loading thresholds for bone formation in rats. J. Bone Miner. Res. 1995;10(10):1544–9.
125. Bassey EJ, Rothwell MC, Littlewood JJ, Pye DW. Pre- and postmenopausal women have diVerent bone mineral density responses to the same high-impact exercise. J. Bone Miner. Res. 1998;13(12):1805–13.
126. Twomey L, Taylor J. Age changes in lumbar intervertebral discs. Acta Orthop. Scand. 1985;56(6):496–9.
127. Mok FP, Samartzis D, Karppinen J, Luk KD, Fong DY, Cheung KM. ISSLS prize winner: prevalence, determinants, and association of Schmorl nodes of the lumbar spine with disc degeneration: a population-based study of 2449 individuals. Spine (Phila Pa 1976). 2010;35(21):1944–52.
128. Adams MA, McNally DS, Dolan P. ‘Stress’ distributions inside intervertebral discs. The eVects of age and degeneration. J. Bone Joint Surg. Br. Vol. (London). 1996;78(6):965–72.
129. Holmes AD, Hukins DW, Freemont AJ. End-plate displacement during compression of lumbar vertebra-disc-vertebra segments and the mechanism of failure. Spine. 1993;18(1):128–35.
130. Adams MA, Freeman BJ, Morrison HP, Nelson IW, Dolan P. Mechanical initiation of intervertebral disc degeneration. Spine. 2000;25(13):1625–36.

131. Adams MA, May S, Freeman BJ, Morrison HP, Dolan P. Effects of backward bending on lumbar intervertebral discs. Relevance to physical therapy treatments for low back pain. Spine. 2000;25(4):431–7. discussion 438.
132. Whyne CM, Hu SS, Lotz JC. Parametric finite element analysis of vertebral bodies affected by tumors. J. Biomech. 2001 Oct;34(10):1317–24.
133. Rasoulinejad P, McLachlin SD, Bailey SI, Gurr KR, Bailey CS, Dunning CE. The importance of the posterior osteoligamentous complex to subaxial cervical spine stability in relation to a unilateral facet injury. Spine J. 2012;12(7):590–5.
134. Nadeau M, McLachlin SD, Bailey SI, Gurr KR, Dunning CE, Bailey CS. A biomechanical assessment of soft-tissue damage in the cervical spine following a unilateral facet injury. J. Bone Joint Surg. 2012;94(21):e156.
135. Vaccaro AR, Schroeder GD, Kepler CK, Cumhur Oner F, Vialle LR, Kandziora F, Koerner JD, Kurd MF, Reinhold M, Schnake KJ, Chapman J, Aarabi B, Fehlings MG, Dvorak MF. The surgical algorithm for the AOSpine thoracolumbar spine injury classification system. Eur. Spine J. 2016 Apr;25(4):1087–94.
136. Chapman J, Bransford R. Geriatric spine fractures: an emerging healthcare crisis. J. Trauma Acute Care Surg. 2007;62(6):S61–2.
137. Malik SA, Murphy M, Connolly P, O'Byrne J. Evaluation of morbidity, mortality and outcome following cervical spine injuries in elderly patients. Eur. Spine J. 2008;17(4):585–91.
138. McCabe CMJ, McLachlin SD, Bailey SI, Gurr KR, Bailey CS, Dunning CE. The effect of soft-tissue restraints after type II odontoid fractures in the elderly: a biomechanical study. Spine. 2012;37(12):1030–5.
139. Kanis JA, et al. A new approach to the development of assessment guidelines for osteoporosis. Osteoporos. Int. 2002;13:527–36.
140. http://www.shef.ac.uk/FRAX/
141. Hillier TA, Cauley JA, Rizzo JH, Pedula KL, Ensrud KE, Bauer DC, Lui LY, Vesco KK, Black DM, Donaldson MG, Leblanc ES, Cummings SR. WHO absolute fracture risk models (FRAX): do clinical risk factors improve fracture prediction in older women without osteoporosis? J. Bone Miner. Res. 2011 Aug;26(8):1774–82.
142. Trémollieres FA, Pouillès JM, Drewniak N, Laparra J, Ribot CA, Dargent-Molina P. Fracture risk prediction using BMD and clinical risk factors in early postmenopausal women: sensitivity of the WHO FRAX tool. J. Bone Miner. Res. 2010 May;25(5):1002–9.
143. Cummings SR, Bates D, Black DM. Clinical use of bone densitometry: scientific review. JAMA. 2002 Oct 16;288(15):1889–97. Review. Erratum in: JAMA 2002 Dec 11;288(22):2825.
144. Villa-Camacho JC, Iyoha-Bello O, Behrouzi S, Snyder BD, Nazarian A. Computed tomography-based rigidity analysis: a review of the approach in preclinical and clinical studies. Bonekey Rep. 2014 Nov 5;3:587. doi:10.1038/bonekey.2014.82. eCollection 2014. Review.
145. Whealan KM, Kwak SD, Tedrow JR, Inoue K, Snyder BD. Noninvasive imaging predicts failure load of the spine with simulated osteolytic defects. J. Bone Joint Surg. Am. 2000;82(9):1240–51.
146. Hojjat SP, Beek M, Akens MK, Whyne CM. Can micro-imaging based analysis methods quantify structural integrity of rat vertebrae with and without metastatic involvement? J. Biomech. 2012 Sep 21;45(14):2342–8.
147. Snyder BD, Cordio MA, Nazarian A, Kwak SD, Chang DJ, Entezari V, et al. Noninvasive prediction of fracture risk in patients with metastatic cancer to the spine. Clin. Cancer Res. 2009;15:7676–83.
148. Huiskes R, Hollister SJ. From structure to process, from organ to cell: recent developments of FE-analysis in orthopaedic biomechanics. J. Biomech. Eng. 1993;115(4B):520–7.
149. Lotz JC, Cheal EJ, Hayes WC. Fracture prediction for the proximal femur using finite element models: part II – nonlinear analysis. J. Biomech. Eng. 1991;113(4):361–5.
150. Whyne CM, Hu SS, Lotz JC. Biomechanically derived guideline equations for burst fracture risk prediction in the metastatically involved spine. J. Spinal Disord. Tech. 2003;16(2):180–5.

151. Zysset PK, Dall'ara E, Varga P, Pahr DH. Finite element analysis for prediction of bone strength. Bonekey Rep. 2013 Aug;7(2):386.
152. Bozic KJ, Keyak JH, Skinner HB, Bueff HU, Bradford DS. Three-dimensional finite element modeling of a cervical vertebra: an investigation of burst fracture mechanism. J. Spinal Disord. 1994 Apr;7(2):102–10.
153. Crawford RP, Cann CE, Keaveny TM. Finite element models predict in vitro vertebral body compressive strength better than quantitative computed tomography. Bone. 2003;33:744–50.
154. Buckley JM, Loo K, Motherway J. Comparison of quantitative computed tomography based measures in predicting vertebral compressive strength. Bone. 2007;40:767–74.
155. Dall'Ara E, Pahr D, Varga P, Kainberger F, Zysset P. QCT-based finite element models predict human vertebral strength in vitro significantly better than simulated DEXA. Osteoporos. Int. 2012 Feb;23(2):563–72.
156. Imai K, Ohnishi I, Bessho M, Nakamura K. Nonlinear finite element model predicts vertebral bone strength and fracture site. Spine (Phila Pa 1976). 2006 Jul 15;31(16):1789–94.
157. Wang X, Sanyal A, Cawthon PM, Palermo L, Jekir M, Christensen J, Ensrud KE, Cummings SR, Orwoll E, Black DM. Osteoporotic fractures in men (MrOS) Research Group, Keaveny TM. Prediction of new clinical vertebral fractures in elderly men using finite element analysis of CT scans. J. Bone Miner. Res. 2012 Apr;27(4):808–16.
158. Kopperdahl DL, Aspelund T, Hoffmann PF, Sigurdsson S, Siggeirsdottir K, Harris TB, Gudnason V, Keaveny TM. Assessment of incident spine and hip fractures in women and men using finite element analysis of CT scans. J. Bone Miner. Res. 2014 Mar;29(3):570–80.
159. Faulkner KG, Cann CE, Hasegawa BH. Effect of bone distribution on vertebral strength: assessment with patient-specific nonlinear finite element analysis. Radiology. 1991; 179:669–74.
160. Buckley JM, Cheng L, Loo K, Slyfield C, Xu Z. Quantitative computed tomography-based predictions of vertebral strength in anterior bending. Spine (Phila Pa 1976). 2007 Apr 20;32(9):1019–27.
161. Dall'Ara E, Schmidt R, Pahr D, Varga P, Chevalier Y, Patsch J, Kainberger F, Zysset P. A nonlinear finite element model validation study based on a novel experimental technique for inducing anterior wedge-shape fractures in human vertebral bodies in vitro. J. Biomech. 2010 Aug 26;43(12):2374–80.
162. Jackman TM, Alex M, DelMonaco AM, Morgan EF. Accuracy of finite element analyses of CT scans in predictions of vertebral failure patterns under axial compression and anterior flexion. J. Biomech. 2016;49:267–75.
163. Adams MA, Roughley PJ. What is intervertebral disc degeneration, and what causes it? Spine (Phila Pa 1976). 2006 Aug 15;31(18):2151–61. Review.
164. Clouthier AL, Hosseini HS, Maquer G, Zysset PK. Finite element analysis predicts experimental failure patterns in vertebral bodies loaded via intervertebral discs up to large deformation. Med. Eng. Phys. 2015 Jun;37(6):599–604.
165. Hussein AI, Mason ZD, Morgan EF. Presence of intervertebral discs alters observed stiffness and failure mechanisms in the vertebra. J. Biomech. 2013 Jun 21;46(10):1683–8.
166. Jones AC, Wilcox RK. Finite element analysis of the spine: towards a framework of verification, validation and sensitivity analysis. Med. Eng. Phys. 2008 Dec;30(10):1287–304.
167. Maquer G, Schwiedrzik J, Huber G, Morlock MM, Zysset PK. Compressive strength of elderly vertebrae is reduced by disc degeneration and additional flexion. J. Mech. Behav. Biomed. Mater. 2015 Feb;42:54–66.
168. Launey ME, Chen PY, McKittrick J, Ritchie RO. Mechanistic aspects of the fracture toughness of elk antler bone. Acta Biomater. 2010 Apr;6(4):1505–14.
169. Wachtel EF, Keaveny TM. Dependence of trabecular damage on mechanical strain. J. Orthop. Res. 1997 Sep;15(5):781–7.
170. Fyhrie DP, Schaffler MB. Failure mechanisms in human vertebral cancellous bone. Bone. 1994 Jan–Feb;15(1):105–9.
171. Yeh OC, Keaveny TM. Relative roles of microdamage and microfracture in the mechanical behavior of trabecular bone. J. Orthop. Res. 2001 Nov;19(6):1001–7.

172. Saito M, Marumo K. Collagen cross-links as a determinant of bone quality: a possible explanation for bone fragility in aging, osteoporosis, and diabetes mellitus. Osteoporos. Int. 2010;21(2):195–214. [Review].
173. Beniash E. Biominerals – hierarchical nanocomposites: the example of bone. Wiley Interdiscip. Rev. Nanomed. Nanobiotechnol. 2011;3(1):47–69. Review.
174. Thompson JB, Kindt JH, Drake B, Hansma HG, Morse DE, Hansma PK. Bone indentation recovery time correlates with bond reforming time. Nature. 2001;414(6865):773–6.
175. Walsh WR, Guzelsu N. Compressive properties of cortical bone: mineral-organic interfacial bonding. Biomaterials. 1994;15(2):137–45.
176. Bailey AJ, Sims TJ, Ebbesen EN, Mansell JP, Thomsen JS, Mosekilde L. Age-related changes in the biochemical properties of human cancellous bone collagen: relationship to bone strength. Calcif. Tissue Int. 1999;65:203–10.
177. Langdahl BL, Ralston SH, Grant SFA, Eriksen RF. An Sp1 binding site polymorphism in the COL1A1 gene predicts osteoporotic fractures in both men and women. J. Bone Miner. Res. 1998;13:1384–9.
178. Mann V, Hobson EE, Li B, Stewart TL, Grant SFA, Robins SP, et al. A COL1A1 Sp1 binding site polymorphism predisposes to osteoporotic fracture by affecting bone density and quality. J. Clin. Invest. 2001;197:899–907.
179. Oxlund H, Mosekilde L, Ortoft G. Reduced concentration of collagen reducible cross links in human trabecular bone with respect to age and osteoporosis. Bone. 1996;19:479–84.
180. Viguet-Carrin S, Garnero P, Delmas PD. The role of collagen in bone strength. Osteoporos. Int. 2006;17(3):319–36. [Review].
181. Zioupos P, Currey JD, Hamer AJ. The role of collagen in the declining mechanical properties of aging human cortical bone. J. Biomed. Mater. Res. 1999;45:108–16.
182. Marotti G, Muglia MA, Palumbo C. Structure and function of lamellar bone. Clin. Rheumatol. 1994;13(Suppl 1):63–8. 109.
183. Bird TA, Levene CI. Lysyl oxidase: evidence that pyridoxal phosphate is a cofactor. Biochem. Biophys. Res. Commun. 1982 Oct 15;108(3):1172–80.
184. Oxlund H, Mosekilde L, Ortoft G. Reduced concentration of collagen reducible crosslinks in human trabecular bone with respect to age and osteoporosis. Bone. 1996;19:479–84.
185. Zimmermann EA, Schaible E, Bale H, Barth HD, Tang SY, Reichert P, et al. Age-related changes in the plasticity and toughness of human cortical bone at multiple length scales. Proc. Natl. Acad. Sci. U. S. A. 2011;108(35):14416–21.
186. Tang SY, Vashishth D. Non-enzymatic glycation alters microdamage formation in human cancellous bone. Bone. 2010;46(1):148–54.
187. Tang SY, Vashishth D. A non-invasive in vitro technique for the three-dimensional quantification of microdamage in trabecular bone. Bone. 2007;40(5):1259–64.
188. Vashishth D, Gibson GJ, Khoury JI, Schaffler MB, Kimura J, Fyhrie DP. Influence of nonenzymatic glycation on biomechanical properties of cortical bone. Bone. 2001;28(2):195–201.
189. Bradke, B. S., Tang, S., & Vashid, D. (2009). An Agent Cleaving Sugar-derived Collagen Cross-links Decreases Bone Fragility. In Orthopaedic Research Society Meeting (p. Poster 695). Las Vegas: ORS.
190. Hernandez CJ, Tang SY, Baumbach BM, Hwu PB, Sakkee AN, van der Ham F, et al. Trabecular microfracture and the influence of pyridinium and non-enzymatic glycation-mediated collagen cross-links. Bone. 2005;37(6):825–32.
191. Odetti P, Rossi S, Monacelli F, Poggi A, Cirnigliaro M, Federici M, Federici A. Advanced glycation end products and bone loss during aging. Ann. N. Y. Acad. Sci. 2005 Jun;1043:710–7.
192. Burke M, Atkins A, Akens M, Willett T, Whyne C. Osteolytic and mixed cancer metastasis modulates collagen and mineral parameters within rat vertebral bone matrix. J. Orthop. Res. 2016;34(12):2126–36.
193. Myers ER, Wilson SE. Biomechanics of osteoporosis and vertebral fracture. Spine (Phila Pa 1976). 1997 Dec 15;22(24 Suppl):25S–31S. Review.
194. Whyne CM, Hu SS, Lotz JC. Burst fracture in the metastatically involved spine: Development, validation, and parametric analysis of a three-dimensional poroelastic finite-element model. Spine. 2003;28(7):652–60.

195. Constans JP, de Divitiis E, Donzelli R, Spaziante R, Meder JF, Haye C. Spinal metastases with neurological manifestations. Review of 600 cases. J. Neurosurg. 1983;59(1):111–8.
196. Dimar JR 2nd, Voor MJ, Zhang YM, Glassman SD. A human cadaver model for determination of pathologic fracture threshold resulting from tumorous destruction of the vertebral body. Spine. 1998;23(11):1209–14.
197. Ebihara H, Ito M, Abumi K, Taneichi H, Kotani Y, Minami A, et al. A biomechanical analysis of metastatic vertebral collapse of the thoracic spine: A sheep model study. Spine. 2004;29(9):994–9.
198. Hong J, Cabe GD, Tedrow JR, Hipp JA, Snyder BD. Failure of trabecular bone with simulated lytic defects can be predicted non-invasively by structural analysis. J. Orthop. Res. 2004;22(3):479–86.
199. McGowan DP, Hipp JA, Takeuchi T, White AA 3rd, Hayes WC. Strength reductions from trabecular destruction within thoracic vertebrae. J. Spinal Disord. 1993;6(2):130–6.
200. Silva MJ, Hipp JA, McGowan DP, Takenchi T, Hayes WC. Strength reductions of thoracic vertebrae in the presence of transcortical osseous defects: Effects of defect location, pedicle disruption, and defect size. Eur. Spine J. 1993;2(3):118–25.
201. Windhagen HJ, Hipp JA, Silva MJ, Lipson SJ, Hayes WC. Predicting failure of thoracic vertebrae with simulated and actual metastatic defects. Clin. Orthop. Relat. Res. 1997;344:313–9.
202. Windhagen H, Hipp JA, Hayes WC. Postfracture instability of vertebrae with simulated defects can be predicted from computed tomography data. Spine. 2000;25(14):1775–81.
203. Taneichi H, Kaneda K, Takeda N, Abumi K, Satoh S. Risk factors and probability of vertebral body collapse in metastases of the thoracic and lumbar spine. Spine. 1997;22(3):239–45.
204. Hardisty MR, Whyne CM. Whole bone strain quantification by image registration: a validation study. J. Biomech. Eng. 2009;131(6):064502.
205. Mizrahi J, Silva MJ, Hayes WC. Finite element stress analysis of simulated metastatic lesions in the lumbar vertebral body. J. Biomed. Eng. 1992;14(6):467–75.
206. Tschirhart CE, Nagpurkar A, Whyne CM. Effects of tumor location, shape and surface serration on burst fracture risk in the metastatic spine. J. Biomech. 2004;37(5):653–60.
207. Tschirhart CE, Finkelstein JA, Whyne CM. Metastatic burst fracture risk assessment based on complex loading of the thoracic spine. Ann. Biomed. Eng. 2006;34(3):494–505.
208. Tschirhart CE, Finkelstein JA, Whyne CM. Biomechanics of vertebral level, geometry, and transcortical tumors in the metastatic spine. J. Biomech. 2007;40(1):46–54.
209. Whyne CM, Hu SS, Workman KL, Lotz JC. Biphasic material properties of lytic bone metastases. Ann. Biomed. Eng. 2000;28(9):1154–8.
210. Roth SE, Mousavi P, Finkelstein J, Chow E, Kreder H, Whyne CM. Metastatic burst fracture risk prediction using biomechanically based equations. Clin. Orthop. Relat. Res. 2004;419:83–90.
211. Choudhari C, Chan K, Akens MK, Whyne CM. μFE models can represent microdamaged regions of healthy and metastatically involved whole vertebrae identified through histology and contrast enhanced μCT imaging. J. Biomech. 2016 May 3;49(7):1103–10.
212. Sone T, Tamada T, Jo Y, Miyoshi H, Fukunaga M. Analysis of three-dimensional microarchitecture and degree of mineralization in bone metastases from prostate cancer using synchrotron microcomputed tomography. Bone. 2004;35(2):432–8.
213. Nazarian A, von Stechow D, Zurakowski D, Muller R, Snyder BD. Bone volume fraction explains the variation in strength and stiffness of cancellous bone affected by metastatic cancer and osteoporosis. Calcif. Tissue Int. 2008;83(6):368–79.
214. Bates DW, Black DM, Cummings SR. Clinical use of bone densitometry: clinical applications. J. Am. Med. Assoc. 2002 Oct 16;288(15):1898–900.
215. Delmas PD, Seeman E. Changes in bone mineral density explain little of the reduction in vertebral or nonvertebral fracture risk with anti-resorptive therapy. Bone. 2004 Apr;34(4):599–604.
216. Acito AJ, Kasra M, Lee JM, Grynpas MD. Effects of intermittent administration of pamidronate on the mechanical properties of canine cortical and trabecular bone. J. Orthop. Res. 1994;12:742–6.

217. Mashiba T, Turner CH, Hirano T, Forwood MR, Johnston CC, Burr DB. Effects of suppressed bone turnover by bisphosphonates on microdamage accumulation and biomechanical properties inclinically relevant skeletal sites in beagles. Bone. 2001;28:524–31.
218. Hu JH, Ding M, Soballe K, Bechtold JE, Danielsen CC, Day JS, Hvid I. Effects of short-term alendronate treatment on the three-dimensional microstructural, physical, and mechanical properties of dog trabecular bone. Bone. 2002;31:591–7.
219. Borah B, Dufresne TE, Chmielewski PA, Gross GJ, Prenger MC, Phipps RJ. Risedronate preserves trabecular architecture and increases bone strength in vertebra of ovariectomized minipigs as measured by three-dimensional microcomputed tomography. J. Bone Miner. Res. 2002;17:1139–47.
220. Komatsubara S, Mori S, Mashiba T, Ito M, Li J, Kaji Y, Akiyama T, Miyamoto K, Cao Y, Kawanishi J, Norimatsu H. Long-term treatment of incadronate disodium accumulates microdamage but improves the trabecular bone microarchitecture in dog vertebra. J. Bone Miner. Res. 2003;18:512–20.
221. Ding M, Day JS, Burr DB, Mashiba T, Hirano T, Weinans H, Sumner DR, Hvid I. Canine cancellous bone microarchitecture after one year of high-dose bisphosphonates. Calcif. Tissue Int. 2003;72:737–44.
222. Day JS, Ding M, Bednarz P, van der Linden JC, Mashiba T, Hirano T, Johnston CC, Burr DB, Hvid I, Sumner DR, Weinans H. Bisphosphonate treatment affects trabecular bone apparent modulus through micro-architecture rather than matrix properties. J. Orthop. Res. 2004;22:465–71.
223. Muller R, Hannan M, Smith SY, Bauss F. Intermittent ibandronate preserves bone quality and bone strength in the lumbar spine after 16 months of treatment in the ovariectomized cynomolgus monkey. J. Bone Miner. Res. 2004;19:1787–96.
224. Lafage MH, Balena R, Battle MA, Shea M, Seedor JG, Klein H, Hayes WC, Rodan GA. Comparison of alendronate and sodium fluoride effects on cancellous and cortical bone in minipigs. A one-year study. J. Clin. Invest. 1995;95:2127–33.
225. Balena R, Toolan BC, Shea M, Markatos A, Myers ER, Lee SC, Opas EE, Seedor JG, Klein H, Frankenfield D, et al. The effects of 2-year treatment with the aminobisphosphonate alendronate on bone metabolism, bone histomorphometry, and bone strength in ovariectomized nonhuman primates. J. Clin. Invest. 1993;92:2577–86.
226. Eswaran SK, Allen MR, Burr DB, Keaveny TM. A computational assessment of the independent contribution of changes in canine trabecular bone volume fraction and microarchitecture to increased bone strength with suppression of bone turnover. J. Biomech. 2007;40(15):3424–31.
227. Cunha MV, Al-Omair A, Atenafu EG, et al. Vertebral compression fracture (VCF) after spine stereotactic body radiation therapy (SBRT) analysis of predictive factors. Int. J. Radiat. Oncol. Biol. Phys. 2012;84:e343–9.
228. Rose PS, Laufer I, Boland PJ, et al. Risk of fracture after single fraction image-guided intensity-modulated radiation therapy to spinal metastases. J. Clin. Oncol. 2009;27:5075–9.
229. Boehling NS, Grosshans DR, Allen PK, et al. Vertebral compression fracture risk after stereotactic body radiotherapy for spinal metastases. J. Neurosurg. Spine. 2012;16:379–86.
230. Chow E, Harris K, Fan G, Tsao M, Sze WM. Palliative radiotherapy trials for bone metastases: a systematic review. J. Clin. Oncol. 2007;25:1423–36.
231. Sahgal A, Whyne CM, Ma L, Larson DA, Fehlings MG. Vertebral compression fracture after stereotactic body radiotherapy for spinal metastases. Lancet Oncol. 2013 Jul;14(8):e310–20.
232. Barth HD, Zimmermann EA, Schaible E, Tang SY, Alliston T, Ritchie RO. Characterization of the effects of X-ray irradiation on the hierarchical structure and mechanical properties of human cortical bone. Biomaterials. 2011;32:8892–904.
233. Currey JD, Foreman J, Laketic I, Mitchell J, Pegg DE, Reilly GC. Effects of ionizing radiation on the mechanical properties of human bone. J. Orthop. Res. 1997;15:111–7.
234. Burton B, Gaspar A, Josey D, Tupy J, Grynpas MD, Willett TL. Bone embrittlement and collagen modifications due to high-dose gamma-irradiation sterilization. Bone. 2014 Apr;61:71–81.

235. Zioupos P, Currey JD, Hamer AJ. The role of collagen in the declining mechanical properties of aging human cortical bone. J. Biomed. Mater. Res. 1999;45:108–16.
236. Zioupos P. Accumulation of in-vivo fatigue microdamage and its relation to biomechanical properties in ageing human cortical bone. J. Microsc. 2001;201:270–8.
237. Moussazadeh N, Laufer I, Yamada Y, Bilsky MH. Separation surgery for spinal metastases: effect of spinal radiosurgery on surgical treatment goals. Cancer Control. 2014 Apr;21(2):168–74. Review.
238. Baroud G, Bohner M. Biomechanical impact of vertebroplasty. Postoperative biomechanics of vertebroplasty. Joint, Bone, Spine. 2006 Mar;73(2):144–50.
239. Wilcox RK. The biomechanics of vertebroplasty: a review. Proc. Inst. Mech. Eng. Part H. 2004;218(1):1–10.
240. Luo J, Daines L, Charalambous A, Adams MA, Annesley-Williams DJ, Dolan P. Vertebroplasty: only small cement volumes are required to normalize stress distributions on the vertebral bodies. Spine (Phila Pa 1976). 2009;34(26):2865–73.
241. Ahn H, Mousavi P, Roth S, Reidy D, Finkelstein J, Whyne C. Stability of the metastatic spine pre and post vertebroplasty. J. Spinal Disord. Tech. 2006 May;19(3):178–82.
242. Tschirhart CE, Roth SE, Whyne CM. Biomechanical assessment of stability in the metastatic spine following percutaneous vertebroplasty: effects of cement distribution patterns and volume. J. Biomech. 2005 Aug;38(8):1582–90.
243. Baroud G, Vant C, Wilcox R. Long-term effects of vertebroplasty: adjacent vertebral fractures. J. Long-Term Eff. Med. Implants. 2006;16(4):265–80.
244. Song D, Meng B, Gan M, Niu J, Li S, Chen H, Yuan C, Yang H. The incidence of secondary vertebral fracture of vertebral augmentation techniques versus conservative treatment for painful osteoporotic vertebral fractures: a systematic review and meta-analysis. Acta Radiol. 2015 Aug;56(8):970–9.
245. Sisodia GB. Methods of predicting vertebral body fractures of the lumbar spine. World J. Orthop. 2013 October 18;4(4):241–7.
246. Buchbinder R, Golmohammadi K, Johnston RV, Owen RJ, Homik J, Jones A, Dhillon SS, Kallmes DF, Lambert RG. Percutaneous vertebroplasty for osteoporotic vertebral compression fracture. Cochrane Database Syst. Rev. 2015 Apr 30;4:CD006349.
247. Dalbayrak OMR. Yilmaz M, Naderi S. Clinical and radiographic results of balloon kyphoplasty for treatment of vertebral body metastases and multiple myelomas. J. Clin. Neurosci. 2010 Feb;17(2):219–24.
248. Ahn H, Mousavi P, Chin L, Roth S, Finkelstein J, Vitken A, Whyne C. The effect of pre-vertebroplasty tumor ablation using laser-induced thermotherapy on biomechanical stability and cement fill in the metastatic spine. Eur. Spine J. 2007 Aug;16(8):1171–8.
249. Pezeshki PS, Davidson S, Murphy K, McCann C, Slodkowska E, Sherar M, Yee AJ, Whyne CM. Comparison of the effect of two different bone-targeted radiofrequency ablation (RFA) systems alone and in combination with percutaneous vertebroplasty (PVP) on the biomechanical stability of the metastatic spine. Eur. Spine J. 2016;25(12):3990–6.

Spine Biopsy

3

Alessandro Cianfoni and Giannantonio Pellicanò

3.1 Introduction

Percutaneous spine biopsy, with modern devices and imaging-guidance techniques, is a safe, effective, and minimally invasive procedure to obtain tissue samples of bone, intervertebral discs, and paraspinal soft tissues, of the whole spine, from the cervical to the sacral regions. A spine biopsy is generally indicated to obtain tissue diagnosis of a focal or diffuse imaging abnormality of uncertain nature, to differentiate a benign osteoporotic versus a malignant vertebral fracture, to further histologically characterize a metastatic spine lesion in a known neoplastic patient, to diagnose an infectious versus a sterile spondylodiscitis, or to isolate the microbiological agent of an infectious lesion.

Although some literature supports the concept of higher accuracy in surgical open biopsies, the degree of invasiveness and correlated potential complications is much lower for percutaneous image-guided biopsies, and the procedure is usually performed under local anesthesia and as an outpatient procedure if desired; moreover the use of large-caliber biopsy needles and coaxial technique, allowing multiple sampling passes, ensures high rate of diagnostic results. Proper technique and state-of-the-art imaging guidance, in the hands of skilled operators, are strongly recommended to guarantee patients' safety and tolerability and high diagnostic rate.

A. Cianfoni, M.D. (✉)
Neuroradiology-Neurocenter of Southern Switzerland, Ospedale Regionale di Lugano, Via Tesserete 46, 6900 Lugano, Switzerland
e-mail: alessandro.cianfoni@eoc.ch

G. Pellicanò, M.D.
Radiodiagnostic 2-3, Azienda Ospedaliero-Universitaria, Careggi, Florence, Italy
e-mail: Gianni.pellicano@ifi.it

L. Manfrè (ed.), *Vertebral Lesions*, New Procedures in Spinal Interventional Neuroradiology, DOI 10.1007/978-3-319-52634-8_3

This chapter will cover main principles and indication of imaging guidance techniques, materials, and approaches to the sacral, lumbar, thoracic, and cervical vertebrae.

3.2 Imaging Guidance Modalities

Spine biopsies can be assisted and guided by X-ray, fluoroscopy, CT, or hybrid navigation systems. While fluoroscopy is versatile, rapid, and efficient, allowing real-time assessment of needle positioning, CT is preferred when a small lesion in the bone has to be targeted, in areas with unclear fluoroscopic landmarks (such as the sacrum or the posterior elements of thoracic and lumbar spine), when the area is poorly visible on fluoroscopy (such as the high thoracic region in some patients), or when an extraosseous paraspinal soft tissue lesion has to be targeted. Navigation systems rely on the use of volumetric data sets initially acquired, either via CT scan or flat-panel rotational fluoroscopy, and are then used to guide needle positioning, virtually with no radiation exposure of the operator, but rely on the absolute immobility of the patient, and lack real-time or intermittent control, and are therefore not very suitable for procedures in awake patients. MR guidance is technically possible, but availability of compatible materials is limited and is not a widely used technique in most centers. The choice of imaging method further rests on operator's experience and preference.

3.2.1 Fluoroscopy Guidance

Fluoroscopy armamentarium to safely perform spine biopsies should contemplate the capability of obtaining good spinal column views in the anteroposterior (AP), latero-lateral (LL), and oblique views. These characteristics can be offered by c-arms, single-plane, and biplane angiography units. By no means one should undertake these procedures with the aid of only a fixed fluoroscopy unit. The fluoroscopy table should be completely radiotransparent. True level-specific AP and LL views of the vertebral body to be targeted should be obtained. These views are irrespective of any predetermined tube angulation and, depending on patient's body positioning and spine curvatures, such as scoliosis, lordosis, or kyphosis, should only be defined by the actual fluoroscopic appearance of the vertebral body at the level of interest. Angulation of the tube along two axes, right to left (RL) and craniocaudal (CC), is required to obtain both AP and LL views.

Based on precise AP and LL views, depending on the desired needle path, specific oblique fluoroscopic views are obtained, and the so-called "I-I" or "bull's eye" technique is utilized (Fig. 3.1). Aligning the needle along the X-ray beam, from the skin to the target, the needle will appear as a single radiopaque dot superimposed to the target. The depth of the needle tip can be checked on intermittent LL views, and its final correct position on the target must be confirmed by the two correct AP and LL views, as defined above. Thorough knowledge of AP, LL, and oblique fluoroscopic landmarks and strict adherence to this technique guarantee the safest and most reproducible needle approach to spine targets.

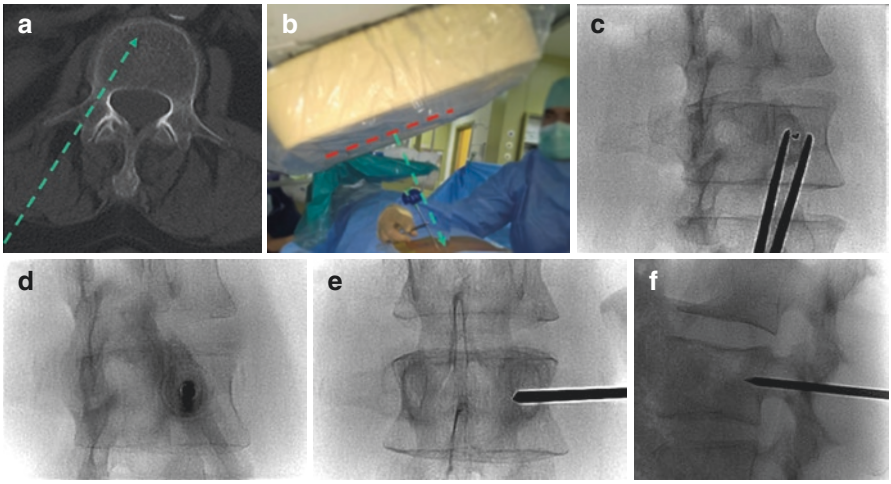

Fig. 3.1 "Bull's eye" technique with fluoroscopic guidance: based on a desired anatomical access (in this case right pedicular access to the vertebral body) (**a**), the fluoroscopic unit is rotated to recreate the obliquity of the desired needle access, aided by known fluoroscopic landmarks (in this case the eye of the "Scottie dog"), and the needle is inserted to the target parallel to the X-ray beam (*green dashed arrow* on **b**), perpendicular to the image intensifier (I-I, *red dashed line* on **b**) (**b**). The use of a needle holder avoids radiation exposure to the operator's hands. The needle on the target appears as a dot (**c** and **d**). The exact position of the needle in space is checked on AP (**e**) and LL (**f**) views

3.2.2 CT Guidance

A CT apparatus with a tiltable gantry (usually 20°–30° in both directions) is preferred, while multidetector technology, CT fluoroscopy, and a screen inside the CT room are optional additional and potentially useful features, based on operator's preference. On the initial volumetric scout views in two orthogonal projections, based on the desired CC angulation of the needle access to the target, **the gantry is tilted as necessary**, and the localizing scan encompassing the region of interest is performed. The axial slice visualizing the target and an accessible needle path is selected, and the skin is marked at the chosen needle entry site. A radiopaque grid with vertical bars can be applied to the skin and used to define the exact needle entry point on the RL axis. Sliding the CT cradle, the marked skin point is placed under the laser light of the CT gantry, and the needle is aligned from its entry into the skin to its hub with the laser light. If this technical tip is correctly applied, the **gantry-needle-target alignment** is obtained; the whole needle shaft, from the skin entry point to the tip, and the target are in-plane with the gantry and are visible on one single axial slice; moreover the projected path of the needle is well discernible and predictable (Fig. 3.2). While the needle-gantry alignment controls the CC angulation of the needle, the RL obliquity is left to the operator's ability, and usually rapidly adjusted after few trials and errors in the superficial tissues, unless some recently available guiding devices are used. It is imperative that the control CT views obtained intermittently during the procedure show the whole length of the inserted needle, with one slice above and one below in which no needle be visualized; if this

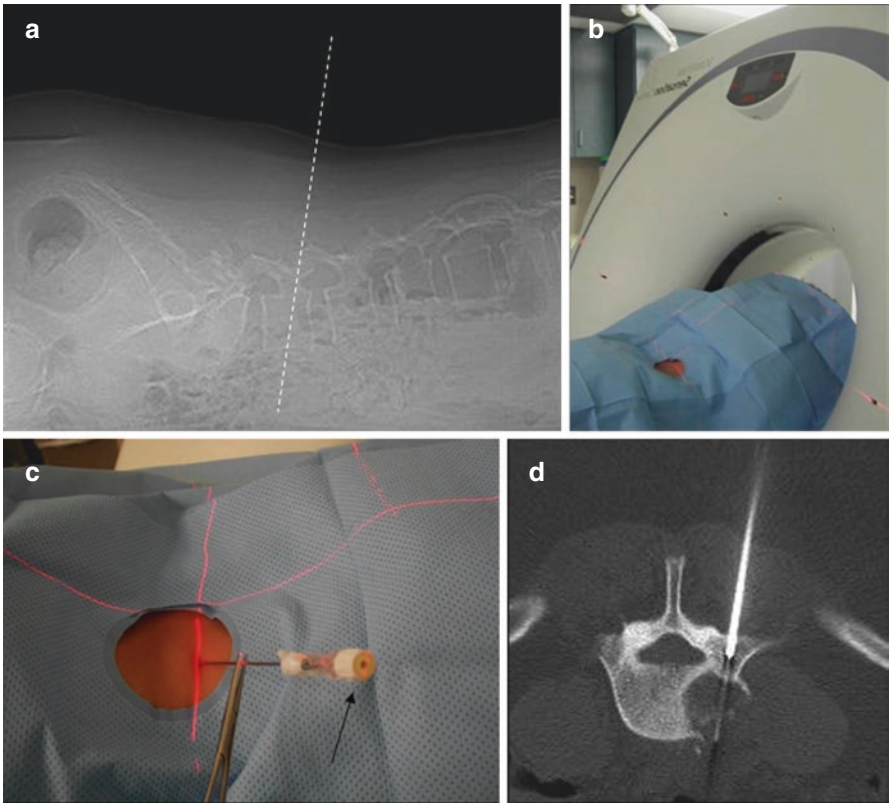

Fig. 3.2 Gantry-needle-target alignment with CT guidance: on the lateral scout view (**a**), the desired access obliquity is defined, and the CT gantry is accordingly tilted (**b**), to acquire the localizing axial scan. Once the axial access slice is selected and the skin marked and prepped, the needle is aligned with the gantry using the gantry laser light. The laser light projects along the whole needle shaft (**c**), from the skin entry point to the needle hub (*black arrow* on **c**). The control CT scan shows the needle on one single slice, from the skin to the target (**d**)

safety condition is not respected, there is risk for a not perfectly in-plane needle, or for a needle tip slightly curved, to be inadvertently advanced off-plane and out of the operator control and sight, with risk of injury in a complex and delicate anatomical region such as the spine. Strict immobility of the patient is also required between localizing scan and skin marking and also strongly desired during the whole procedure; in fact even small patient's movements during the procedure may render the CT-guided needle-access complex, lengthy, and in worst-case scenario imprecise.

Note that sterile prepping and draping usually precede skin marking if fluoroscopic guidance is used, while the opposite occurs if CT guidance is favored.

3.3 Materials

A wide variety of devices, produced by different vendors, each with its own specific features, can be used to obtain spine biopsies (Fig. 3.3). We recommend the use of coaxial systems, composed of an access cannula, which can be a trocar needle, a bone

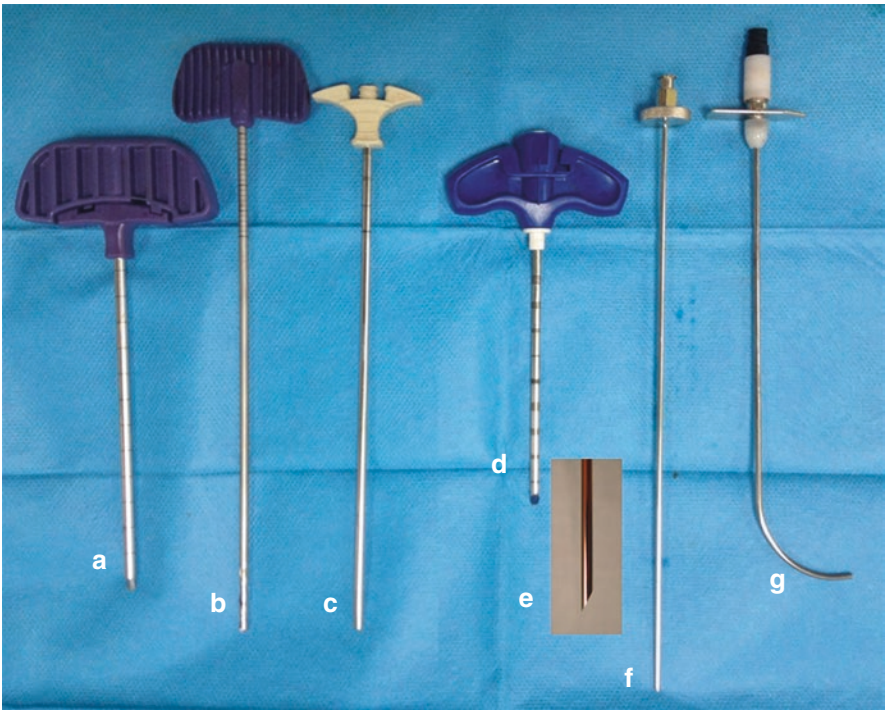

Fig. 3.3 Vertebral biopsy devices: coaxial biopsy systems composed of vertebral access cannula (**a**, 8 G and **d**. 10 G), coaxial drill (**b**) to create a path through sclerotic bone, coaxial biopsy cannulas (**c** and **f**), to retrieve large-caliber core bone samples. A curved nitinol flexible biopsy cannula is shown (**g**) that can be used coaxially, through the access cannula, to sample different regions of the lesion. The access cannula can have a diamond tip (**a**) or a beveled tip (**d** and **e**)

access needle, and a vertebroplasty needle, with diamond or beveled tip, and a biopsy device, to be used coaxially. A beveled tip allows slight steerability of the access cannula during positioning in the vertebra. The coaxial systems allow multiple biopsy passes through the same access, if necessary. The access cannula, of large caliber, can be slightly redirected in a different RL or CC direction, and the coaxial biopsy device inserted along different directions to obtain sampling from a wider region. Coaxial nitinol curved-tip biopsy cannulas exist to obtain multiple samples from different regions of the target lesion, once the access cannula has been placed. The biopsy device can be a cannula with a trephinated or a fish-mouth tip, if an osseous lesion is to be sampled, or a cutting spring-loaded needle, if a soft tissue lesion is being targeted. In case a sclerotic bone has to be traversed, the use of a coaxial drill can be used to create a path for the access cannula; in some cases the use of a surgical hammer is necessary to obtain access-cannula penetration through cortical or sclerotic bone.

In case of osseous lesions with heterogeneous density, it might be advisable to sample the lesion in multiple small increments (5–8 mm) to avoid the risk that a more proximal sclerotic sample in the biopsy cannula crashes the rest of the sample when the cannula is further advanced in the lesion (Fig. 3.4).

We suggest to advance and then to retrieve the biopsy cannula under constant vacuum suction. Vacuum can be easily obtainable with a set of small tubing

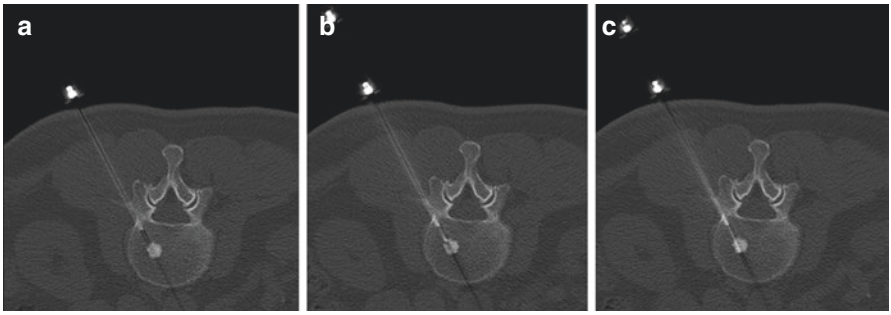

Fig. 3.4 Sampling bone of different densities: it is advisable to proceed with small incremental advancements (**a-b-c**), followed by retrieval and collection of the short core of tissue, to maximize the chances to obtain a representative osseous biopsy core and avoid sample crushing

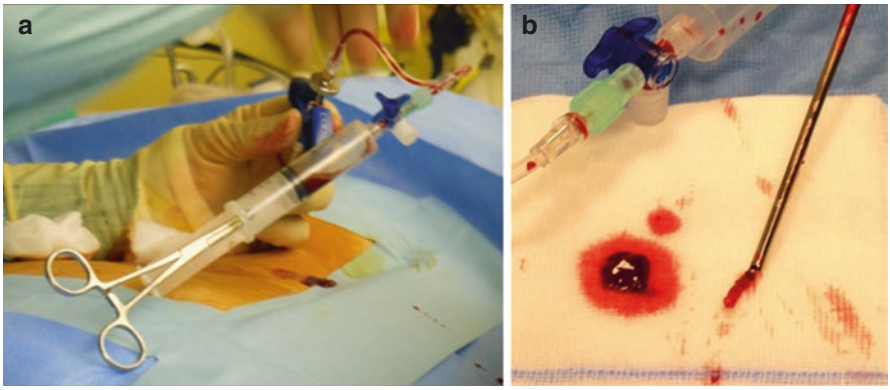

Fig. 3.5 Vacuum suction: (**a**) a 20 mL Luer lock syringe is connected via a three-way stopcock to a short tubing, attached with a Luer lock to the biopsy cannula during advancement and retrieval; negative pressure is maintained in the system with a needle holder clamped to the plunger in aspiration. (**b**) Fluid and tissue samples can be obtained in this way

attached with a Luer lock junction at the cannula and with a three-way stopcock at a large-volume (20–60 mL) syringe. Suction can be held by a second operator, while the first operator handles the biopsy cannula, by locking the syringe in vacuum with a needle holder or by the use of a dedicated self-locking vacuum syringe (Fig. 3.5). Spinal needles of different lengths, usually 22 G in caliber, are used to perform local anesthesia on the periosteum; scalpels are used to make small incision to the skin and if necessary to the fascia, for easier access of the cannulas. In some cases k-wires can be used to adopt the Seldinger technique, in case cannulas of different lengths and/or caliber have to be exchanged without the need to perform a new percutaneous access. We suggest the use of rather large-caliber systems, typically from 11 to 8 G cannulas for bone access, which allows the use of adequate size coaxial biopsy devices to obtain large core biopsy samples (see Fig. 3.3).

3.4 Positioning, Prepping, Draping, Anesthesia, and Contraindications

Positioning of the patient is individualized based on the planned access, typically in the prone position for access to the sacral, lumbar, thoracic, and posterior elements of the cervical spine, while in the supine position for anterior access to the lower cervical spine and for paramaxillary or trans-oral approaches to the upper cervical spine. Lateral decubitus can be used in selected cases. Bolsters strategically placed under patient's body can be used to favorably alter spine curves and render certain spine accesses easier (see Fig. 3.6). A typical example is a bolster under the lower

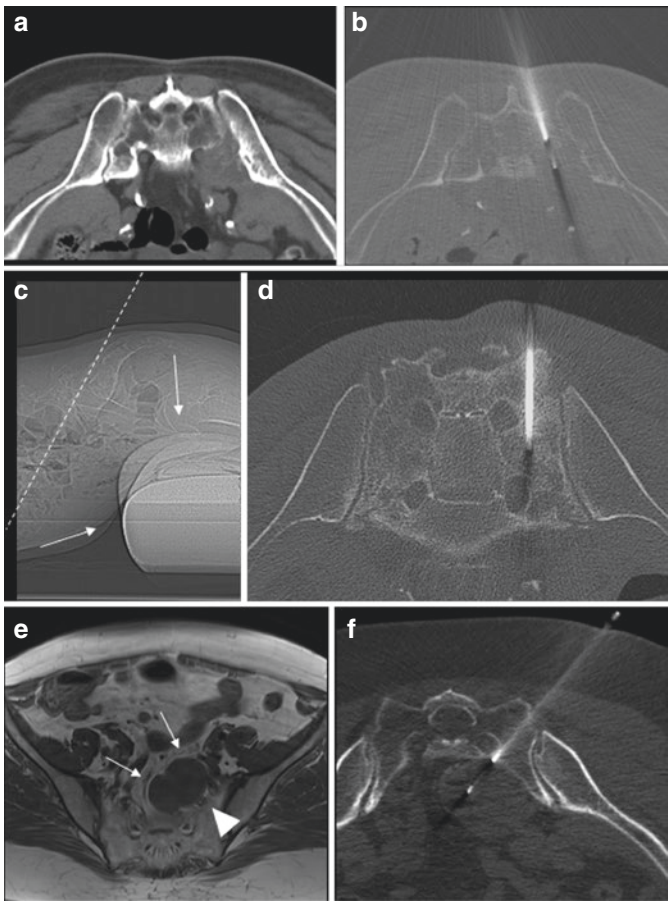

Fig. 3.6 CT-guided sacral biopsies: (**a, b**) a lytic lesion of the sacral wing, eroding the contours of the neuroforamen biopsied through a short-axis access, just lateral to the expectable border of the sacral foramen. (**c, d**) Extensive permeative lytic and sclerotic changes of the sacral wing, biopsied through a long-axis access. A bolster placed under the hips (*arrows* on **c**) serves to render the sacrum more vertical, so that the gantry tilt can reproduce the obliquity of the sacrum long axis. (**e, f**) Trans-sacral approach to biopsy a presacral mass (*arrows* on **e**); the access was planned to spare the sciatic nerve coursing just ventral to the sacrum (*arrowhead* on **e**); a cutting spring-loaded biopsy needle was used coaxially to sample this soft tissue lesion

abdomen in a prone patient to flatten the lumbosacral lordosis and facilitate access to an otherwise steeply oblique L5–S1 disc space. A general principle is also to favor a decubitus the patient can reasonably hold remaining still and comfortable for the expected duration of the whole procedure, if the biopsy is conducted on an awake patient; for example, a prolonged prone decubitus can be problematic for an obese patient with respiratory problems. Prepping of the skin should be wide and thorough to ensure sterility; when the skin is marked at the entry site with an indelible marker, alcoholic prepping solutions should be avoided, due to the ability of alcohol to promptly delete ink from the skin. We recommend full draping and the use of full gown, gloves, hat, and mask for the operator, in every bone or disc access, due to the heightened risk of infection. Local anesthesia should be delivered to the sensitive tissues, such as the skin, fascia, and periosteum. **Local anesthesia close to the nerve roots should be avoided if the needle access has the potential risk of injury to the nerve**; for example, no anesthesia should be delivered in the neuroforamen or in the region of the lumbar plexus if a posterolateral direct access to the vertebral body is being performed; the nerves should remain awake and sensitive, so that they serve as a warning if the needle course is too close to them. For the same reason, such accesses should not be attempted in a patient unconscious or under general anesthesia.

General but all relative contraindications to a spine biopsy are an uncooperative patient, unlikely to remain still during the procedure, coagulopathy, low platelet count, and treatment with anticoagulants or antiplatelet agents (spine biopsies are usually performed in patients treated with ASA or other NSAIDs).

3.5 Sacral Vertebral Biopsies

The sacrum has a complex tridimensional conformation, and fluoroscopy does not recognize clear and safe landmarks, since the sacral foramina are "V-shaped" channels, and the sacroiliac joints have wavy contours. Fluoroscopy can still be used to guide short- and long-axis needle accesses, especially when a sacroplasty is to be performed, but we recommend CT guidance to biopsy the sacrum, for practicality, precision, and safety (Fig. 3.6). Planning the biopsy, the lesion in the sacrum is viewed in three planes, with multiplanar CT-reconstructed images, and the most suitable access is chosen, ideally along the long axis of the lesion, so that a satisfactory sample can be obtained, keeping the needle path away from the sacral central canal and neuroforamina. When a lytic lesion destroys the cortical margins of the neuroforamen, the needle should strictly avoid the expected course of the nerve root (see Fig. 3.6). In such cases it is advisable to carefully analyze pre-procedural MRI images, commonly able to depict the position of the nerve root even when the foramen has been invaded by a mass. Rather rarely an access through the iliac wing will be necessary to reach a lesion in the sacrum. Trans-sacral approach can also be used when a retroperitoneal presacral mass needs to be biopsied (see Fig. 3.6). Attention should be paid to avoid the nervous structures of the sacral plexus that lie just anterior to the sacral alae. As usual, after bone access, the guiding cannula is

placed adjacent to the margins of the lesion, and the biopsy can be performed with a coaxial device, depending on the consistency of the target lesion.

3.6 Lumbar Vertebral Biopsy

The lumbar vertebrae are characterized by rather large and squared vertebral bodies, pedicles horizontally aligned parallel to the superior end plate, projecting over the superior half of the vertebral body, progressively larger and posterolaterally oblique from L1 to L5 (in fact it should be noted that L1 pedicles can be very thin and straight, so that an oblique trans-pedicular needle access might be impossible), and thin, long, and straight transverse processes. Spatial orientation of the vertebrae, along lordotic and/or scoliotic curves, strongly influences needle accesses.

3.6.1 Trans-pedicular Approach

The most common and safe approach to the lumbar vertebral body is trans-pedicular, and when the pedicle size allows it, with various degree of CC and RL access obliquity, different parts of the vertebral body can be reached (Fig. 3.7). The pedicle is usually accessed with a posterior oblique approach at the junction between transverse process and superior articular process. At this site the periosteum is infiltrated

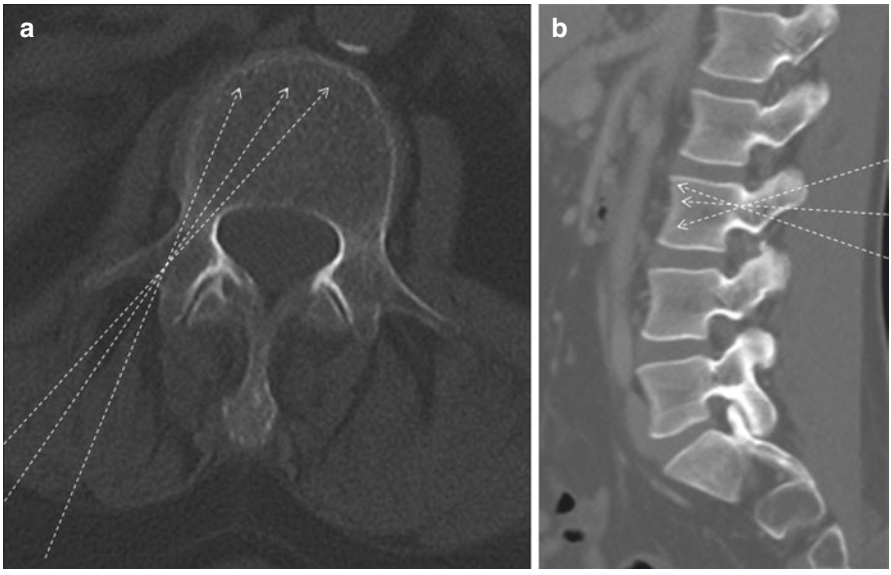

Fig. 3.7 Trans-pedicular access to the lumbar vertebral body: the needle access is usually at the junction between the transverse process and the articular process; with large pedicles, different RL and/or CC obliquities allow to reach different regions of the vertebral body (*dashed arrows* on **a** and **b**); exceptions might occur at L1 where pedicles can be quite thin

with local anesthetics, the access cannula perforates the cortical bone, is stabilized, and then advanced through the pedicle to reach the posterior vertebral wall. During the controlled maneuvers to dock the cannula through the cortex, the needle can inadvertently slide cranial to the pedicle toward the disc space or, more dangerously, caudally to approach the neuroforamen; in such cases the needle has to be retrieved and repositioned (Fig. 3.8). While advancing the cannula through the pedicle, special attention should be paid not to breach the cortex of the pedicle (especially the medial and inferior cortex, which mark the boundary with the central canal and the neuroforamen, respectively). Once the vertebral body is reached, the access cannula is advanced just proximal to the target, and then the biopsy cannula is coaxially inserted to obtain the tissue sample from the target lesion (Fig. 3.9).

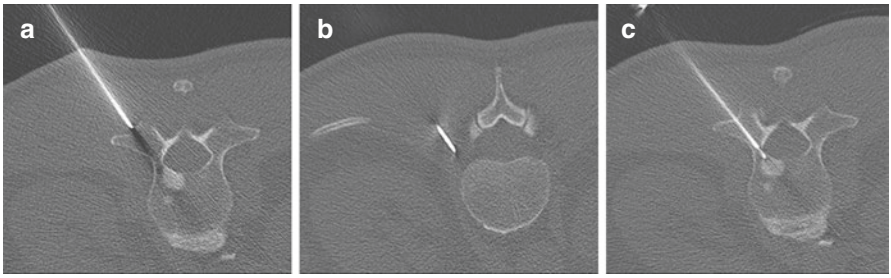

Fig. 3.8 Possible complication during pedicular access: docking of the needle tip through the cortical bone in the pedicular access (**a**), the needle is felt to advance but appears deviated caudally off-plane; a control scan shows the needle tip off-plane and in the neuroforamen (**b**). The needle has to be retrieved, realigned in-plane, and correctly docked through the pedicle (**c**)

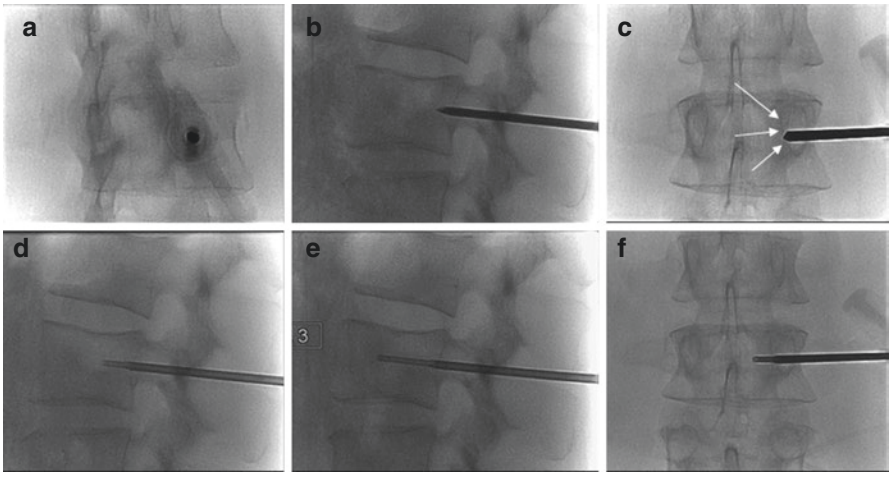

Fig. 3.9 Trans-pedicular biopsy of the right side of the L3 vertebral body: using fluoroscopic guidance, the needle is inserted through the right pedicle using "bull's eye" technique (**a**) to pass the posterior wall (**b**) without passing the medial border of the pedicle on AP view (*arrows* on **c**). A coaxial biopsy cannula is inserted to obtain a core sample of the posterior third of the vertebral body (**d**) and then of the middle third of the vertebral body (**e**). The AP view displays the needle tip on the right side of the vertebral body (**f**)

3.6.2 Extra-Pedicular Approach

If an extra-pedicular access is desired, some additional anatomical consideration should be kept in mind. The segmental arteries and veins run around the lumbar vertebral body at its waist, which is located along the lateral borders, at mid-height of the vertebral body, and the nerves of the lumbar plexus course from the upper portion of the foramina, below the pedicle, anterolaterally, along the lateral borders of the vertebral bodies, medial to the psoas muscle. To avoid these structures, we recommend the access point to be in the upper half of the vertebral body height, no more caudal than the axial level of the pedicles and, as dorsal as possible, ideally not more ventral than the junction between pedicle and vertebral body (Fig. 3.10). Moreover the access-cannula path should either be through the transverse process, then just lateral to the pedicle, or tangent and just above the transverse process, with a craniocaudal obliquity to course lateral to the pedicle. The access should not course below the transverse process and should not enter the vertebral body too ventral along its lateral border (Fig. 3.11). The extra-pedicular access has the potential to

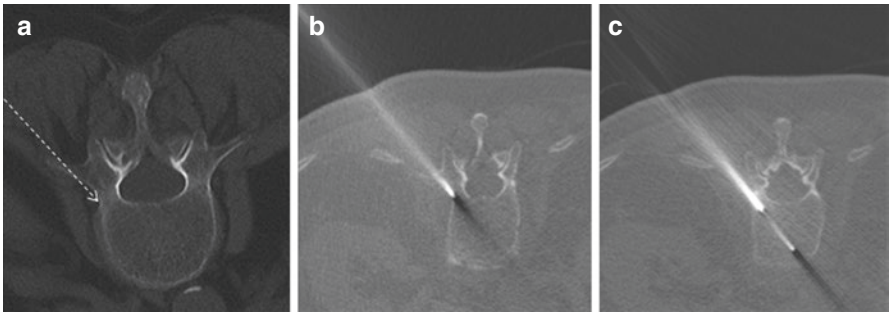

Fig. 3.10 Extra-pedicular access to the lumbar vertebral body: the needle course either through or just above the transverse process and should enter the vertebral body no more ventral than the junction between pedicle and vertebral body (**a** and **b**). This access allows a great degree of RL obliquity and easily allows to reach across midline (**c**)

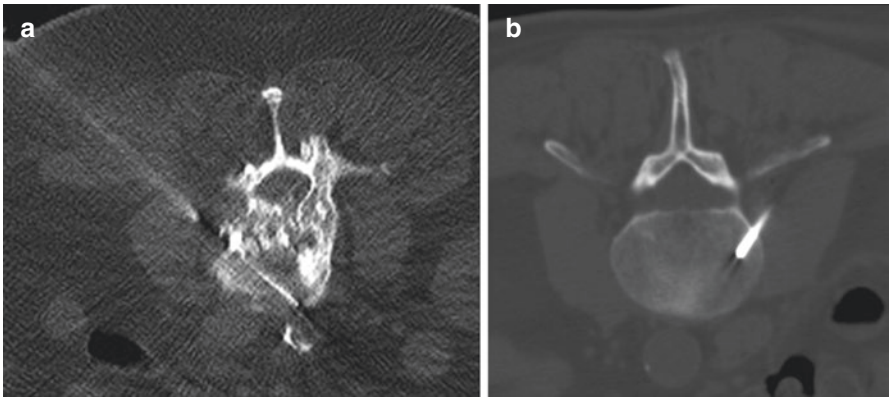

Fig. 3.11 Incorrect extra-pedicular lumbar access: (**a** and **b**) two examples in which the access is ventral to the junction between the pedicle and the vertebral body, carrying the risk to injure the segmental vessels and the nervous structures of the lumbar plexus, running medial to the psoas muscle

carry more discomfort to the patient since local anesthesia to the periosteum is less easily performed (if an access through the transverse process is chosen, the needle perforates three times the sensitive periosteum, at the dorsal and ventral aspect of the transverse process and at the vertebral body posterolateral corner), and infiltrating local anesthetics along the lateral border of the vertebral body has the potential to numb nervous structures, which can be then inadvertently injured by the access cannula (see "Positioning, Prepping, Draping, Anesthesia, and Contraindications"). As an additional technical consideration, the posterolateral border of the vertebral body might facilitate undesired ventral and tangential sliding of the access cannula along the lateral border of the vertebral body during docking maneuvers; therefore an assertive and firm pressure should be applied in an oblique medially oriented direction, to access the vertebral body at the point of contact with the needle tip.

3.6.3 Fluoroscopic Guidance

To access the lumbar vertebral body with fluoroscopic guidance, we use the I-I technique. First, a true level-specific AP view is obtained, with the spinous process projecting over the midline, and the disc end plates well profiled ("box view"); with this view, at the lumbar levels, the pedicles of the index vertebral body are projected over the upper half of the box. Depending on the desired CC access obliquity, the fluoroscopic tube is accordingly rotated in the CC direction; if access to the inferior half of the vertebral body is desired, the tube is tilted from the true AP projection more cranially, so that the pedicles project more caudally over the vertebral body. From this projection the tube is rotated RL ipsilateral to the access' side so that the "Scottie dog" projection is obtained. The more the tube is rotated RL, the more the eye of the Scottie dog superimposes toward the center of the box and the more the needle access will be medially directed toward midline or across midline of the vertebral body. For a trans-pedicular access, the target is the center of the eye of the Scottie dog, while for an extra-pedicular access, the target is just outside of the eye of the Scottie dog, at 1–3 o'clock for a right-sided access and at 9–11 o'clock for a left-sided access (Fig. 3.12). Slight adjustments of the CC and RL obliquity of the I-I view are crucial while precisely directing the needle toward a specific area of the vertebral body, as is the case in biopsies of focal lesions or, when obliged by distorted anatomy, such as in compression fracture deformities. As a general rule, when visible, the final target should be superimposed upon the access landmark (either trans-pedicular or extra-pedicular) on the I-I fluoroscopic view (Fig. 3.13).

The exact position of the needle tip has to be confirmed intermittently with true AP and LL views (see Figs. 3.1 and 3.9).

Important **safety landmarks** during needle insertion: (1) in a trans-pedicular access, the needle tip has to project in the AP view always lateral to the medial border of the pedicle, until it has reached the posterior wall on the LL view (see Fig. 3.9) (this avoids dangerous access to the central canal); (2) in an extra-pedicular access, the needle tip has to project in the AP view lateral to the lateral border of the pedicle when it is at the posterior wall on the LL view, but it has to be seen on the AP view

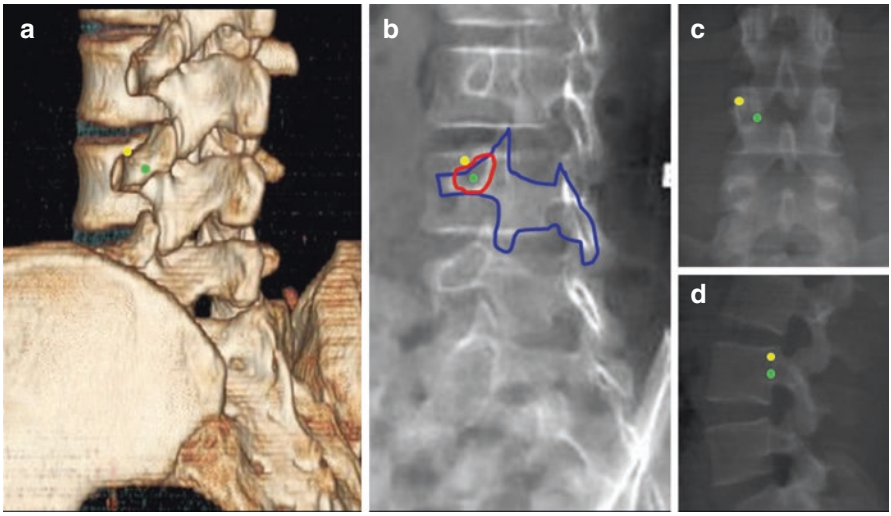

Fig. 3.12 Fluoroscopic landmarks for lumbar trans- and extra-pedicular access: (**a**) volume-rendering 3D CT posterolateral *left* oblique view of the lumbar spine displaying an anatomical view of the "Scottie dog", with its fluoroscopic correlate (**b**). AP (**c**) and LL (**d**) fluoroscopic views of the lower lumbar spine. In **b** the *left* L3 "Scottie dog" is contoured in *blue*, with the eye, representing the pedicle, contoured in *red*. The *yellow dot* and the *green dot* represent the target for extra-pedicular and trans-pedicular approach, respectively, on 3D view, I-I fluoroscopic view, AP and LL views

progressively entering in the box when it is advanced more ventrally on the LL view (this avoids sliding along the lateral edge of the vertebral body medially to the psoas muscle); and (3) for both accesses, once the needle tip is placed in the vertebral body, it can be safely advanced ventrally, as checked on the LL view, up to the junction between anterior and middle third of the vertebral body.

3.6.4 CT Guidance

The use of CT guidance to access a lumbar vertebral body might seem more straightforward with respect to anatomy landmarks, but attention should be paid to the 3D orientation in space of the lumbar vertebral bodies accordingly to the lordotic curvature. Therefore we stress the importance of tilting the gantry as necessary to obtain the desired CC obliquity of the axial view, which will then reflect the obliquity of the needle access. Otherwise a common pitfall is the undesired access of a disc space, instead of a vertebral body access, from a trans-pedicular approach, if the vertebra has a lordotic position (Fig. 3.14). On CT axial images, the landing zone of the needle for a trans-pedicular approach, at the junction between transverse process and superior articular process, seems flat and wide: this is actually misleading, since that surface, if seen tridimensionally, might be rather ragged and uneven and might cause the needle tip to slide cranially or caudally in an off-plane slice; we

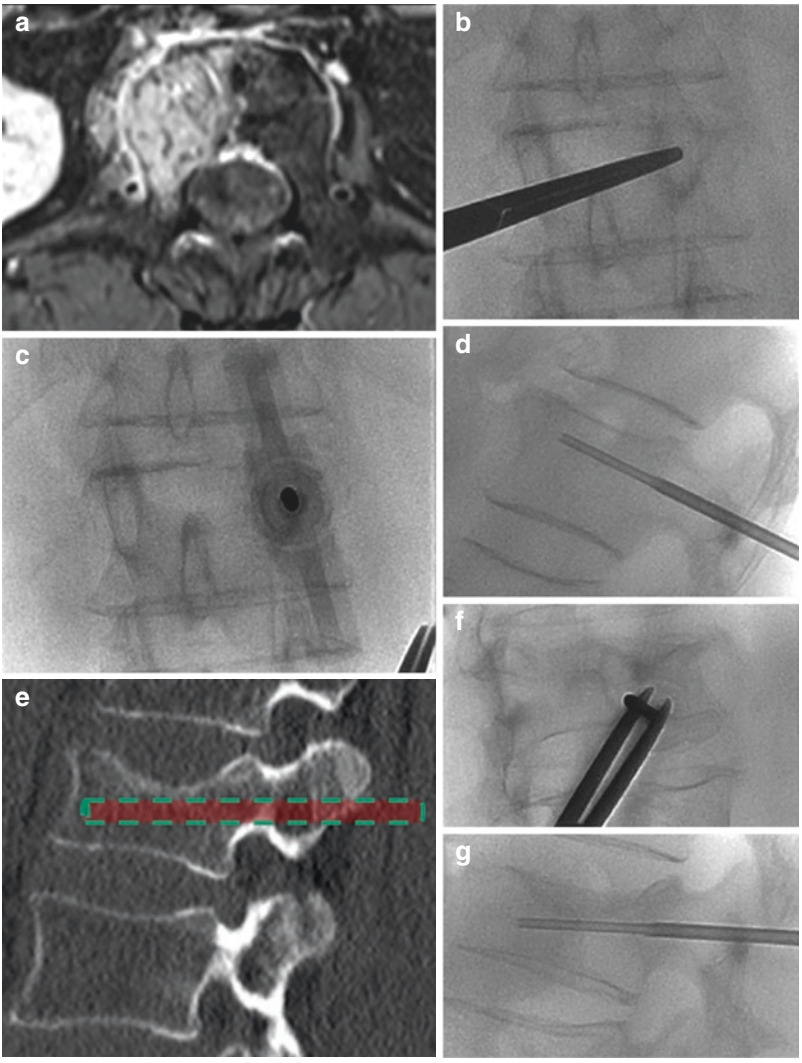

Fig. 3.13 Superimposing access landmark and target on the "bull's eye" view, two examples: in the first case (**a–d**), the lesion to be biopsied is in the right half of the vertebral body, as seen on contrast-enhanced fat-suppressed T1-W axial MRI (**a**). On fluoroscopy with slight right obliquity, the access landmark for this trans-pedicular approach, the center of the eye of the "Scottie dog", is superimposed on the right side of the vertebral body, which appears lytic, and this access point is marked on the skin with the use of a needle -holder (**b**); the needle is then advanced through the pedicle using the I-I technique (**c**). The coaxial biopsy cannula is then advanced to the vertebral body to collect the bone sample (**d**). In the second case (**e–g**), the vertebral body to be biopsied is deformed by a compression fracture, which limits the trans-pedicular access to a craniocaudal oblique access through the inferior half of the pedicle (**e**). The fluoroscopy unit is then rotated in CC and RL direction to obtain a view of the Scottie dog, with the eye superimposing on the fluoroscopic image of the deformed vertebral body, and the access is through the inferior portion of the eye, which represents the inferior half of the pedicle (**f**). With this access the biopsy cannula course is entirely in the vertebral body, with no straying through the disc space (**g**)

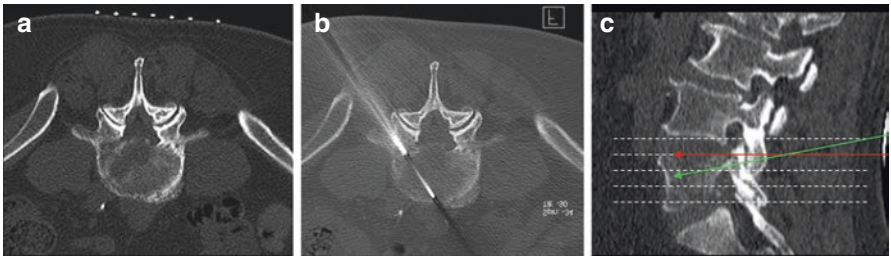

Fig. 3.14 Common pitfall in CT-guided biopsy of vertebral body: during biopsy of a pathological fracture of the L5 vertebral body, axial localizing scans were acquired, and a slice was chosen as access-slice where both pedicle and vertebral body were visible (**a**). Results of the biopsy through the soft-tissue density area thought to be in the vertebral body (**b**) returned as disc material and cartilage. Review of the procedure showed that the axial localizing scan, acquired with no gantry tilt (*dashed white lines* on **c**), was not respective of the lordotic position of the L5 vertebra, and although the access was through the pedicle, the biopsy most likely was through the L4–L5 disc space (*red arrow* on **c**). A repeat biopsy, with gantry tilt, guided the biopsy through the pedicle and the L5 vertebral body (*green arrow* on **c**), resulting in the diagnosis of metastases from renal cell cancer

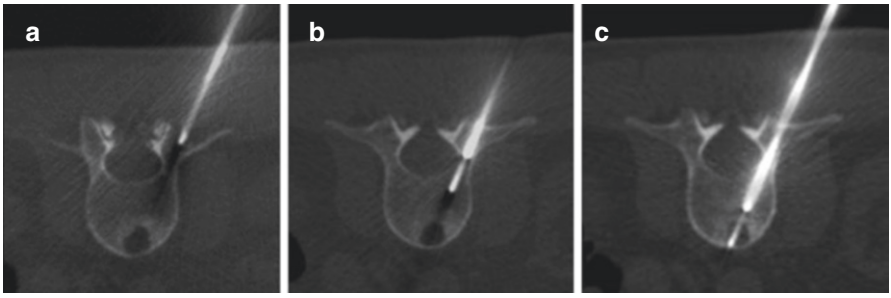

Fig. 3.15 Trans-pedicular lumbar biopsy with CT-guidance: the access cannula is docked through the cortex of the pedicle at the junction between transverse process and articular process (**a**); a first biopsy is performed with a coaxial device in the trabecular bone of the vertebral body (**b**); then the cannula is advanced and another coaxial biopsy is performed on a lytic lesion in the anterior third of the vertebral body (**c**)

recommend not to accept this initial deviation of the needle, but rather insist on repositioning the needle in-plane and obtaining a precise docking of the needle tip through the cortical bone, and then precisely and safely advance it through the pedicle with a good gantry-needle alignment (see "Imaging Guidance Modalities," "CT Guidance," and Fig. 3.8). Forward adjustments of the devices will be performed at small increments and intermittently checked with CT scans (Fig. 3.15).

3.7 Thoracic Vertebral Biopsy

The thoracic vertebrae are characterized by progressively caudo-cranially smaller vertebral bodies, pedicles that are thin and straight in the dorsoventral direction but obliquely oriented in respect of the disc end plate. The upper thoracic vertebral

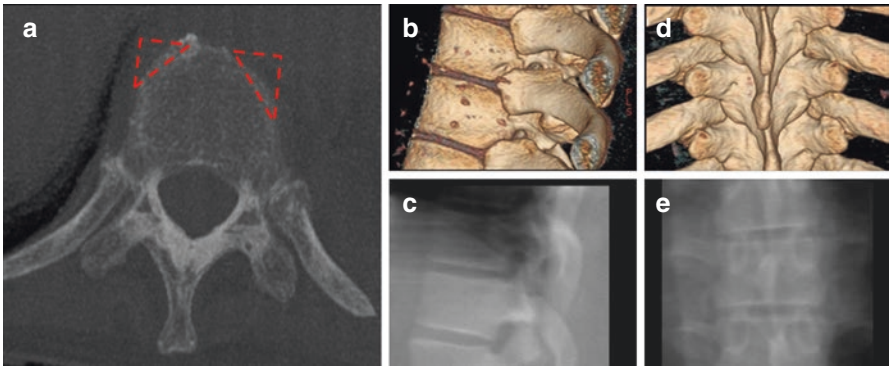

Fig. 3.16 Relevant anatomy of the thoracic vertebrae: cross-sectional (**a**), 3D volume-rendering (**b** and **d**), and respective fluoroscopic images (**c** and **e**) show the bare areas at the anterolateral corners of the vertebral body (*red dashed triangles* on **a**), the thin, straight, and upward oriented pedicles, the thick and dorsally oriented transverse processes. The ribs articulate with the pedicles at the disc level (**b**). The posterior 3D view (**d**) shows the relationship between ribs and transverse processes, which is important to consider for both trans-pedicular and extra-pedicular accesses

bodies may have a triangular shape on the axial plane, with so-called bare areas along their anterolateral aspects. The transverse processes are long and thick, steeply oriented dorsally. Pedicles are larger, and transverse processes are small in the lower thoracic vertebrae. The transverse processes transition to the laminae with no interposition of articular masses. Ribs articulate with vertebrae at the junction between pedicle and vertebral body, at the level of the disc space, and with the superior and ventral aspect of the transverse process (Fig. 3.16). As in the lumbar spine, spatial orientation of the vertebrae, along kyphotic and/or scoliotic curves, strongly influence needle accesses.

3.7.1 Trans-pedicular Approach

The size and orientation of thoracic pedicles limit, especially in the upper thoracic region, the needle access to the vertebral body. The pedicle is usually accessed with a posterior oblique approach at the midpoint or apex of the transverse process. During the controlled maneuvers to dock the cannula through the cortex, the needle can inadvertently slide medially and ventrally along the steep transverse process at the junction with the lamina, but from this point only a straight dorsoventral access is possible, in order to avoid the central canal (Fig. 3.17). With such an access, it is impossible to reach the midline of the vertebral body, and, if the bare areas are prominent, the needle cannot be advanced ventral to the posterior half of the vertebral body. In case this is not the desired access, the needle needs to be retrieved and the transverse process cortex has to be perforated at the desired entry point, in order to allow a more lateral to medial obliquity (Fig. 3.18). The use of a beveled-tip needle can be of help in such instances. While advancing the cannula through the

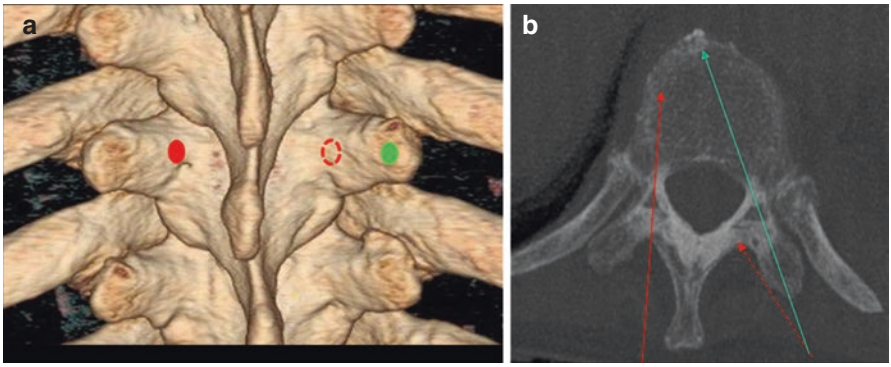

Fig. 3.17 Trans-pedicular access to the thoracic vertebral body and pitfalls: to achieve obliquity and access the midline of the vertebral body, the cannula is usually docked at the apex or at the midpoint of the transverse process (*green dot* on **a** and *green arrow* on **b**); it can occur that the tip of the needle instead of perforating the bone cortex slides along the dorsal aspect of the transverse process at its junction with the lamina (*red dashed circle* on **a** and *dashed red arrow* on **b**), which cannot be accepted because it poses at risk of violating the central canal. A direct access to the pedicle from the junction between transverse process and lamina (*red dot* on **a**) will result in a more straight approach to the ipsilateral half of the vertebral body (*red arrow* on **b**). Note that the more oblique access (*green arrow*) reaches the most anterior portion of the vertebral body, while the more straight access (*red arrow*) risks to violate the bare areas

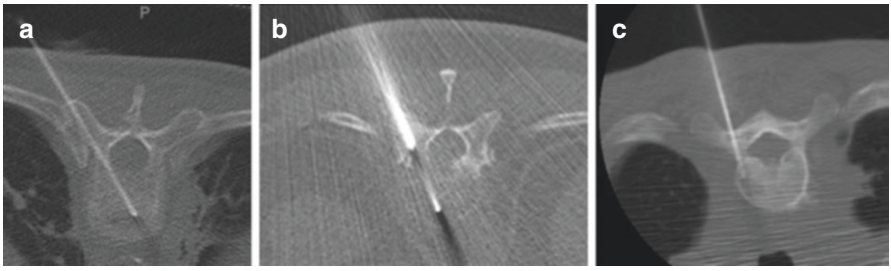

Fig. 3.18 Trans-pedicular thoracic approaches: oblique accesses to reach the midline of the vertebral body, in the mid-thoracic spine (**a**) and in the lower thoracic spine (**b**). Straight access to reach the ipsilateral half of the vertebral body in the upper thoracic region (**c**)

pedicle, special attention should be paid not to breech the medial cortex of the pedicle (boundary with the central canal). Once the vertebral body is reached, the access cannula is advanced just proximal to the target, and then the biopsy cannula is coaxially inserted to obtain the tissue sample from the target lesion.

3.7.2 Extra-Pedicular Approach

The extra-pedicular access is commonly used to access the thoracic vertebral bodies and is especially useful above T8, when small size and straight AP orientation of the

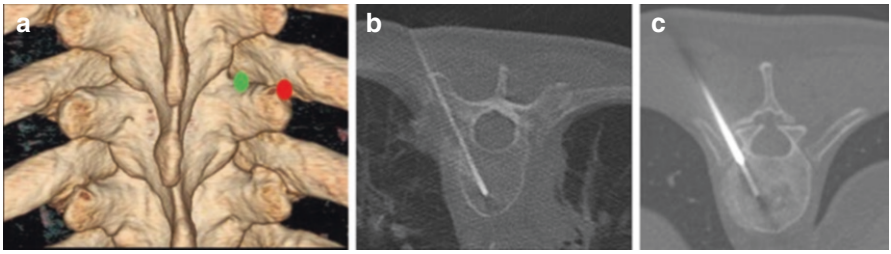

Fig. 3.19 Extra-pedicular accesses to the thoracic vertebral body: the needle access between the rib and the transverse process (*red dot* on **a** and example on **b**) might appear similar to the access shown on Fig. 3.18a, but the needle is, in this case, in its entire course extra-pedicular. The access through the costo-pedicular fibrous junction (*green dot* on **a** and example on **c**) requires the needle to pass above and tangent to the transverse process and be oblique, with rather steep craniocaudal angulation

pedicles prevents sufficiently oblique pedicular access to reach the midline of the vertebral body.

The access can be between the transverse process and the rib or, with an access oriented more steeply craniocaudally from dorsal to ventral, sliding above the transverse process, along the lateral aspect of the pedicle and the medial aspect of the rib head, in the so-called costo-pedicular junction (Fig. 3.19). This is often felt as a fibrous firm non-osseous structure, until true bone contact is made with the postero-superior-lateral aspect of the vertebral body. Once bone contact is made, the needle can be advanced into the anterior 1/3 of the vertebral body, toward its midline. This access poses some difficulty if the superior aspect of the vertebral body is the target, due to the steep cranio-caudal angulation to pass above the transverse process. As an additional technical consideration, when the needle enters the costo-pedicular junction, the tip of the needle is at the cranial and lateral aspect of the posterior wall, but it is not inserted in the bone yet, and the posterolateral border of the vertebral body might facilitate undesired ventral and tangential sliding of the access cannula along the lateral border of the vertebral body during docking maneuvers; therefore an assertive and firm pressure should be applied in an oblique medially oriented direction, to access the vertebral body at the point of contact with the needle tip. The presence of the lung has always to be kept in mind to avoid perforation of the pleural space.

3.7.3 Fluoroscopic Guidance

To access the thoracic vertebral body with fluoroscopic guidance, we strongly recommend to use the I-I technique, because it allows to profile the rib head and the pleural line and safely helps keep the needle away from the pleural space. In fact, alike, but even more importantly than in the lumbar access, the distance from the midline of the skin access, and the lateral to medial and CC obliquity of the needle access, is largely variable, depending on the thickness of the soft tissues dorsal to

the spinal column and the degree of kyphotic curvature of the spine at the target level.

First a true level-specific AP view is obtained, with the spinous process projecting over the midline, and the disc end plates well profiled ("box view"); with this view, at the thoracic levels, the pedicles of the index vertebral body are usually partially superimposed to the adjacent cranial disc space. Depending on the desired CC access obliquity, the fluoroscopic tube is accordingly rotated in the CC direction; if access to the inferior half of the vertebral body is desired, the tube is tilted from the true AP projection more cranially, so that the pedicles project more caudally over the vertebral body. From this projection the tube is rotated RL ipsilateral to the access' side. For a trans-pedicular access, the target is the center of the pedicle. It is important to consider that due to the straight AP orientation of the pedicles, the oblique fluoroscopic view might not precisely represent the I-I view of the pedicle. In such case aiming at this oval target with the needle might pose the risk of violation of the central canal rather than a safe trans-pedicular approach (Fig. 3.20). Intermittent double check in AP view is always recommended if a trans-pedicular approach to the thoracic vertebral body is chosen. For an extra-pedicular access, the target is the costo-pedicular joint, located at the superolateral aspect (2 o'clock for a right access, 10 o'clock for a left access) of the pedicle, where a concave lateral aspect of the pedicle is noted (Figs. 3.20 and 3.21). The exact position of the needle tip has to be confirmed intermittently with true AP and LL views.

Important **safety landmarks** during needle insertion: (1) in a trans-pedicular access, the needle tip has to project in the AP view always lateral to the medial border of the pedicle, until it has reached the posterior wall on the LL view (this avoids dangerous access to the central canal); (2) in an extra-pedicular access, the needle tip should strictly remain medial to the rib head and pleural line on the I-I view and

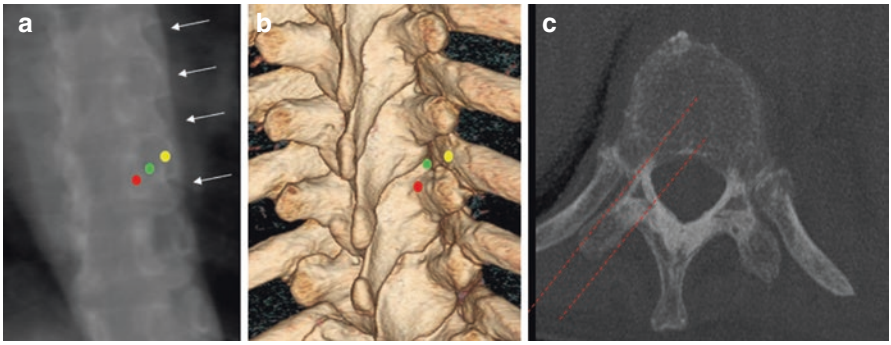

Fig. 3.20 Fluoroscopic landmarks in thoracic spine: on this oblique right I-I fluoroscopic view of the mid-thoracic spine (**a**), with its respective volume-rendering 3D view (**b**), the *yellow dot* marks the rib head, the *green dot* is the target for extra-pedicular approach to the thoracic vertebral body, whereas the *red dot*, looking like a pedicle, might not precisely reflect the bull's eye view of the pedicle, and targeting it as the pedicle, as safe in the lumbar spine, could actually expose to the risk of violating the central canal (**c**). *White arrows* on (**a**) mark the pleural line

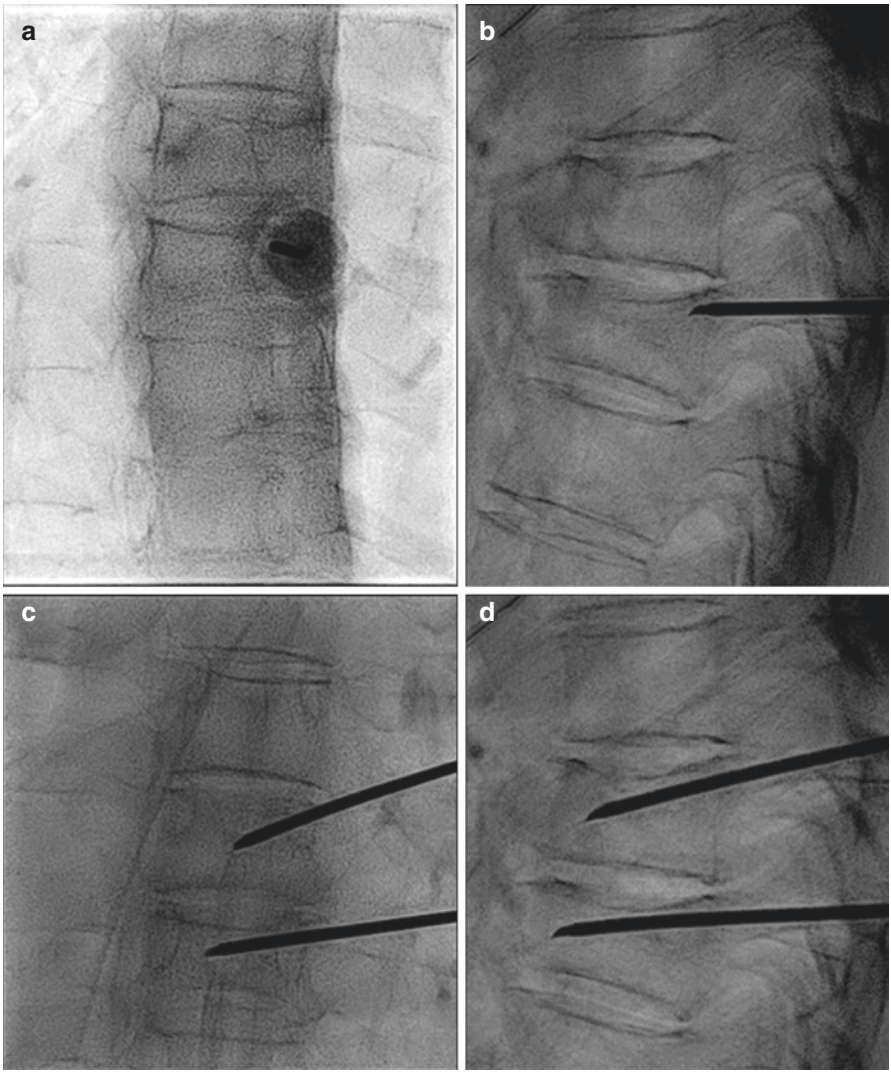

Fig. 3.21 Example of fluoroscopic-guided extra-pedicular approach to the thoracic spine: on the I-I view (**a**) obtained with ipsilateral RL obliquity and pronounced CC cranial angulation, the oval image of the pedicle-transverse process is superimposed to the image of the vertebral body, and the target is the lucent area between rib head and oval image. When bone contact is made, the needle tip on AP view (not shown) is at the lateral border of the pedicle, while on the LL view (**b**), it is at the superior aspect of the posterior wall. From this position the needle can be advanced to the anterior third of the vertebral body, along *midline* (**c** and **d**)

has to project in the AP view lateral to the lateral border of the pedicle when it is at the posterior wall on the LL view, but it has to be seen on the AP view progressively entering in the box when it is advanced more ventrally on the LL view (this avoids sliding along the lateral edge of the vertebral body in the subpleural space); and (3)

for both accesses, once the needle tip is placed in the vertebral body, it can be safely advanced ventrally, as checked on the LL view, up to the junction between anterior and posterior half of the vertebral body. It is important to consider that on LL fluoroscopic view the vertebral body has a rectangular shape and that fluoroscopy is unable to represent the bare areas at the anterior aspect of some thoracic vertebral bodies; therefore the needle tip can be advanced to the anterior half of the vertebral body on LL view only if it safely oriented toward midline on the AP view. If the needle is inserted with no sufficient lateral to medial obliquity and is seen on AP view rather along the lateral half of the vertebral body, it should not be advanced to the anterior half of the vertebral body, to avoid breaching the anterolateral vertebral body cortex and stray in the prevertebral bare-areas, where the aorta courses. Careful assessment of local anatomy on pre-procedural axial cross-sectional images is strongly recommended to plan the procedure.

3.7.4 CT Guidance

The use of CT guidance to access a thoracic vertebral body, similar to what has been said in the paragraph regarding lumbar spine access, might seem more straightforward with respect to anatomy landmarks, but attention should be paid to the 3D orientation in space of the thoracic vertebral bodies accordingly to the kyphotic curvature. Therefore we stress the importance of tilting the gantry as necessary to obtain the desired CC obliquity of the axial view, which will then reflect the obliquity of the needle access. The same general rules described in the lumbar spine access paragraph apply when using CT guidance to access the thoracic spine. CT guidance displays more clearly than fluoroscopy the anatomic landmarks of a transpedicular access, of an extra-pedicular access between rib and transverse process, and of an extra-pedicular access above the transverse process and of the bare areas (see Figs. 3.16, 3.17, 3.18, 3.19, and 3.20).

3.8 Cervical Vertebral Biopsy

Cervical procedures carry the risk of injuries to the regional delicate vital structures.

Thorough knowledge of the normal, fluoroscopic, and cross-sectional anatomy, adherence to a rigorous image guidance and procedural technique, and considerable operator experience are strongly recommended to reduce the potential for serious complications.

The cervical spine is characterized by lordotic curvature and by opposite CC angulation of the anterior and posterior vertebral elements. The C1 and C2 vertebrae have a unique and peculiar shape which is beyond the scope of this chapter to illustrate, but that should be thoroughly known altogether with the relationships between osseous structures, nerves, spinal cord, and vertebral arteries, before engaging in any invasive maneuver in this region. The cervical vertebrae from C3 to C7 have a small squared vertebral body, with uncinate processes along the lateral

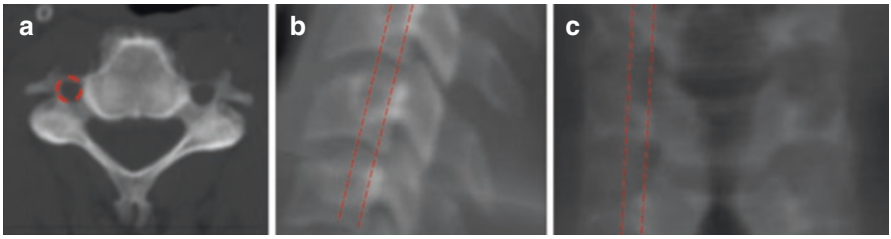

Fig. 3.22 Course of the vertebral artery in the foramen transversarium: the course of the vertebral artery in the foramen transversarium, from C6 to C3 (in some individual also at C7), is shown on cross-sectional axial (**a**), LL (**b**), and AP (**c**) fluoroscopic images with *red dashed lines*. The course at C2–C1 is not shown here, but typically better depicted on cross-sectional CT images

aspects of the superior disc end plates; the pedicles are thin, with a marked obliquity, and their junction with the vertebral body is along the inferior aspect of the vertebral body, with the foramen coursing above the pedicle. The transverse processes have a more ventral position than in the thoracic and lumbar spine and are located along the lateral aspects of the vertebral body. The foramen transversarium, located in the transverse process, hosting the course of the vertebral artery, is located lateral to the uncinate process (Fig. 3.22). The pedicles are thin, with thick cortical margins; the vertebral arteries run along the anterolateral aspect of the pedicles, entering the foramen transversarium at C6 and upward in the majority of patients.

There is a substantial individual variability in the neck appearance (short versus long); visibility with image guidance; anatomy of the visceral neck, with vessels' tortuosity; and therefore percutaneous accessibility.

3.8.1 Anterolateral Approach

This access is used in the infrahyoid neck to access the vertebral bodies from C4 to C7. Most of the delicate and vital structures are located anterior and anterolateral to the cervical spine. The airway is located midline, is easily seen on CT and fluoroscopy, and can be manually mobilized sideways. The hypopharynx-esophagus, located midline behind the trachea and in front of the prevertebral space, can be mobilized by deep palpation, more easily toward the left side. The carotid artery and the jugular vein are contained within the carotid space, along with cranial nerve X in the infrahyoid neck, course anterolateral to the trachea, and can be palpated and mobilized laterally. The vertebral artery's course, unprotected out of the transverse foramen, needs to be considered when accessing C7.

The patient is positioned supine, with slight head hyperextension; general anesthesia is strongly recommended to ensure comfort and safety.

The access is anterolateral oblique, anterior to the sternocleidomastoid muscle, between the common carotid artery laterally and the trachea and esophagus medially. The access is more easily and safely performed from the right side, due to the slight off-midline course on the left side of the esophagus. The thyroid gland is often traversed at the C7 level. This access is limited below C7 by the anterior and

medial course of the common carotid and above C4 by the carotid bifurcation and the mandible.

The first access can be performed in this delicate environment with a long 22 G spinal needle, inserted to get bone contact with the anterior aspect of the vertebral body, just medial to the ipsilateral uncinate process; after removal of the hub, the needle can serve as a k-wire for coaxial insertion of an access cannula. The cannula perforates the anterior cortex of the vertebral body just medial to the uncinate process, so that oblique path of the coaxial biopsy cannula traverses the center of the vertebral body. **Safety margins** to be avoided are the posterior vertebral body wall and the boundaries with the transverse foramen, just lateral to the uncinate process.

3.8.1.1 Fluoroscopic Guidance

Biplane fluoroscopy is desirable. True lateral and AP views to profile the vertebral body and the disc space at the level of interest are obtained. No I-I views are used.

The access is preferentially from the right side (to avoid esophagus and easier for right-handed operators). The left hand palpates the pulsatile carotid, retracts it laterally, and reaches deep with the finger tips for the anterior aspect of the spine, protecting the foramen transversarium laterally and splaying trachea and esophagus medially. The right hand inserts the needle under real-time biplane fluoroscopy and docks it into the target (brief radiation exposure to hands) (Fig. 3.23). Alternatively, the use of a "prong deflector" has been described to avoid left hand radiation exposure. The vertebral body access should be medial to the uncovertebral joint, which

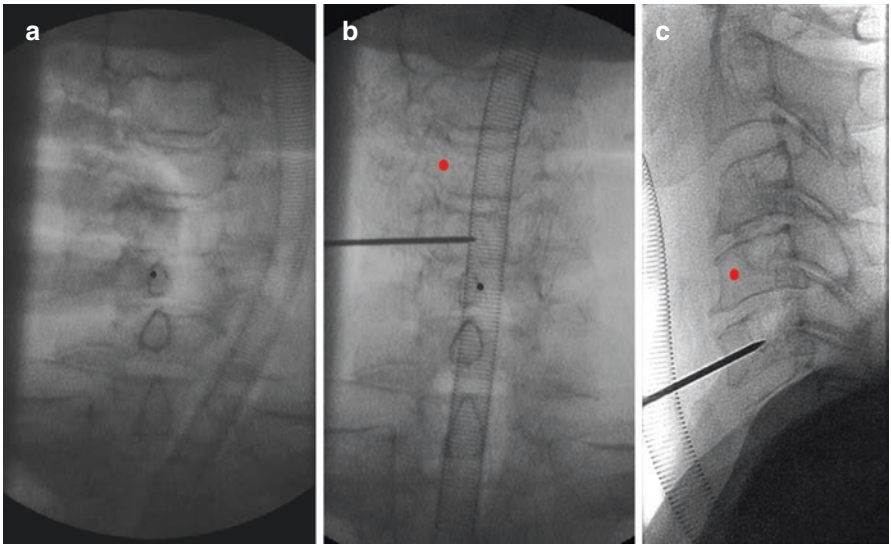

Fig. 3.23 Anterolateral cervical spine access (C5) with fluoroscopic guidance: the left hand palpates the right common carotid artery, retracts it laterally, and reaches deep to palpate the ventral aspect of the cervical vertebral bodies (**a**); in this way the trachea and esophagus are splayed contralaterally off-midline (note the endotracheal tube on **a**). The needle is then inserted to contact the vertebral body just medial to the uncinate process (*red dot* on **b** and **c** at C4) and perforates the ventral cortex of the vertebral body and can be advanced to the middle third of the vertebral body toward midline (**b** and **c**)

is safer for the vertebral artery. C7 and T1 access is not recommended with large-caliber needles due to poor control of carotid (anteriorly located, not well palpable, and poorly mobilized) and vertebral arteries (course of the vertebral artery outside of foramen transversarium) at this level.

3.8.1.2 CT Guidance

The CT gantry is tilted along the CC axis of the vertebral body. A localization scan is performed, preferably with i.v. contrast to depict the course of the carotid artery and of the vertebral artery. A 22 G × 17 cm spinal needle is aligned with the gantry laser light to stay in-plane and is then inserted, under intermittent CT guidance, between the carotid artery and the trachea-esophagus to the target, avoiding major vessels and the esophagus. The hub is removed or cut off, and the shaft of the needle serves as a guidewire. An introducer trocar of desired caliber (usually 14–17 G) is then inserted coaxially over this guidewire to the target. Through the introducer, in a coaxial fashion, a biopsy cannula can be introduced and multiple biopsy passes can be performed (Fig. 3.24).

3.8.1.3 Special Considerations

Vascular anatomy in the neck can be quite variable; vascular loops, kinks, and retropharyngeal course of carotid arteries ("kissing carotids") may be poorly controllable with palpation and retraction. Pre-procedural awareness of the individual local vascular anatomy is therefore strongly recommended, especially when using fluoroscopic guidance.

3.8.2 Trans-pedicular Access

Due to the small size, proximity to the vertebral artery, and suboptimal fluoroscopic landmark definition of the cervical pedicles, this access is very seldom utilized to

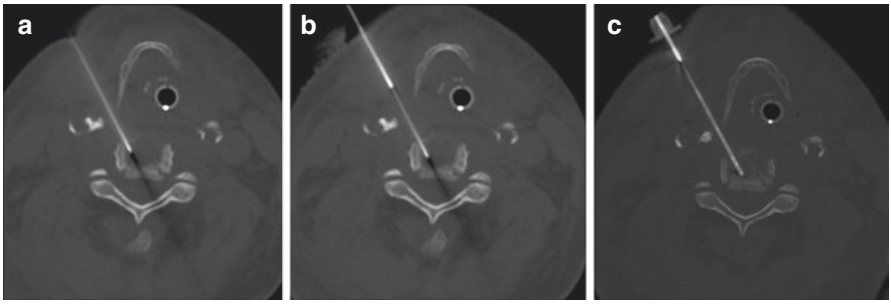

Fig. 3.24 Anterolateral cervical spine access with CT guidance: a 22 G–17 cm spinal needle is inserted between the carotid artery (note calcification of the carotid bifurcation) and the trachea and advanced to the vertebral body medial to the uncinate process (**a**); the needle, once the hub is removed, serves as a guidewire to advance a larger caliber access cannula with Seldinger technique to the anterior third of the vertebral body (**b** and **c**)

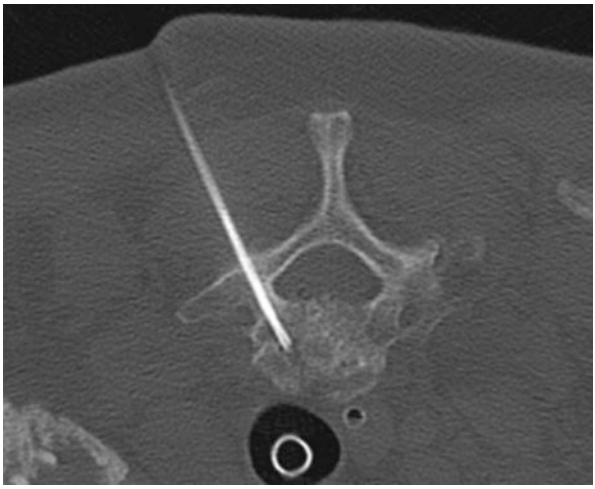

Fig. 3.25 Trans-pedicular access to the cervical vertebral body under CT guidance: this access at C7 was performed with a 14 G beveled-tip cannula. Care is taken not to violate the foramen transversarium (in this case no vertebral artery was coursing in the foramen at C7) and central canal. The needle has to be kept in-plane with the control axial slice, to avoid the risk of breaching the thin pedicle and violating the neuroforamen

access the cervical vertebral bodies, but when it is used, it is generally performed under CT guidance (Fig. 3.25).

3.8.3 Paramaxillary Access

It is used to access the vertebral bodies of C1–C3. It is a subzygomatic access through the masticator space between the vertical ramus of the mandible and the maxilla (alveolar process or maxillary sinus). It traverses the temporalis and pterygoid muscles, lateral to the pterygoid plates and the parapharyngeal space and medial to the upper cervical portion of the internal carotid artery and jugular vein. The anatomical space is large and allows a wide RL and CC access range. Along the path is the pterygoid venous plexus, the internal maxillary artery, and the maxillary branch of the trigeminal nerve, but complications have been reported very rarely. The patient is positioned supine. General anesthesia is strongly recommended. We exclusively perform this access under CT guidance, due to the superior visualization of vascular structures. Contrast-enhanced localization CT scan displays crucial locoregional vascular anatomy (mainly internal carotid artery) and allows safe planning of the right-to-left access obliquity. The CC obliquity of the access varies depending on the target structure. While the skin entry point has to be strictly subzygomatic (a more caudal entry may violate the buccal space), the head of the patient can be positioned in different degrees

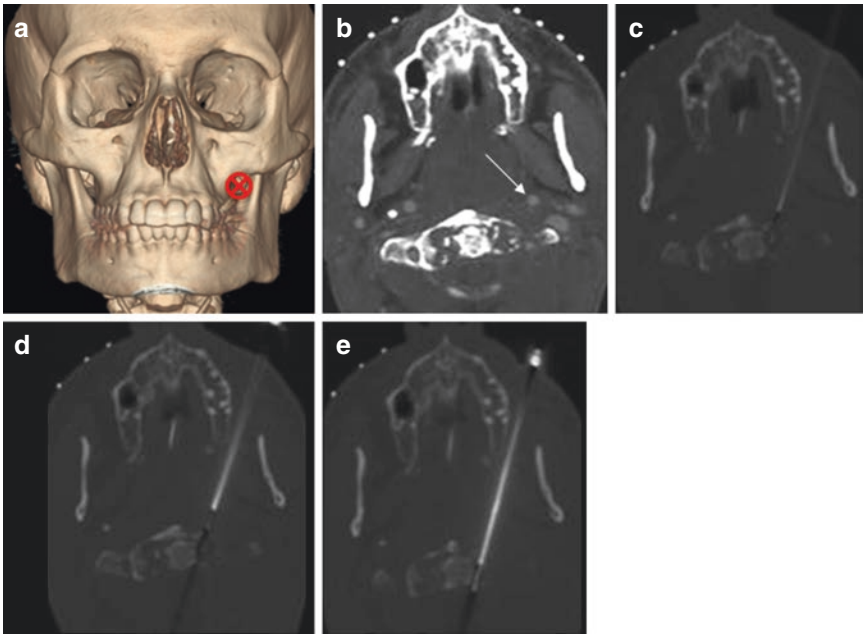

Fig. 3.26 Paramaxillary access to the upper cervical spine: The 3D volume-rendering frontal view CT image of the splanchnocranium (**a**) shows the entry point (*red crossed circle*) for paramaxillary subzygomatic approach to the upper (C0–C3) cervical spine. The localizing CT scan is usually performed after contrast injection (**b**) to show the local vasculature structures and plan the safest approach. A long 22 G spinal needle is first inserted (**c**) medial to the carotid artery (*arrow* on **b**) and then used as a k-wire to insert a bone access cannula (**d**). Through the cannula a coaxial biopsy device can be inserted under intermittent CT guidance (**e**)

of flexion/extension, and/or the CT gantry can be tilted in order to align the paramaxillary access to the desired deep target (skull base-clivus-C1-C2-C3). As an example, compared to a neutral head position, extension of the head allows a more cranial target to be reached through the same skin access. Once the desired image plane's angle is obtained, we strongly recommend alignment of the needle to the CT gantry's laser light, so that the whole needle path, from its skin entry point to the final target, is displayed on a single CT slice and can be safely advanced in-plane to the target, avoiding straying off-slice. We routinely first insert a 22 G × 17 cm spinal needle to serve as a guidewire for coaxial placement of a blunt tip 14–16 G trocar cannula to the target. Biopsy needles are then inserted coaxially through the cannula (Fig. 3.26).

3.8.3.1 Special Considerations

Attention should be paid not to traverse the buccal space and the pharyngeal mucosa, to diminish the potential risk of infection to the deep targeted structures.

3.8.4 Trans-oral Access

It is used to access the C1–C3 anterior bony elements. With the mouth opened, the tongue depressed or moved sideways, and the soft palate moved cranially, there is good visibility of the posterior oropharyngeal mucosa. Through the large mouth opening, the midline ventral aspect of the C1–C3 bony elements can be palpated and accessed traversing the mucosa and the thin retropharyngeal and prevertebral spaces. With different degrees of mouth opening, flexion-extension of the craniocervical junction and angle of needle access, the anterior elements from C1 to C4 can be targeted. Midline access is safe, while off-midline the internal carotid arteries run just lateral to the parapharyngeal space, ventral to the lateral masses of C1, and the vertebral arteries run in the C2 and C1 foramen transversarium. The patient is positioned supine, under general anesthesia, with the orotracheal tube positioned on one side of the mouth. A surgical mouth opener can be used, preferably if radiotransparent. Biplane fluoro-guidance is preferred to CT since it is less cumbersome and offers real-time control in a very delicate area. Complete asepsis in the oral cavity is not possible, but we use a diluted solution of Betadine to clean the mucosal surfaces; then we create a sterile passage inserting a tubular ultrasound probe cover into the mouth. The probe cover is then pierced at the closed end, where all the instruments and devices we might use during the procedure will pass without direct contact with the mucosal surfaces. The access is strictly midline. The needle is inserted in the mouth; a tongue depressor can be used to move the tongue and the soft palate out of the way. The needle is gently rested on the posterior wall of the pharynx, its position checked on two precise orthogonal views to ensure that the CC direction is correct and that the access is strictly midline prior to advancing the needle to the target (Fig. 3.27).

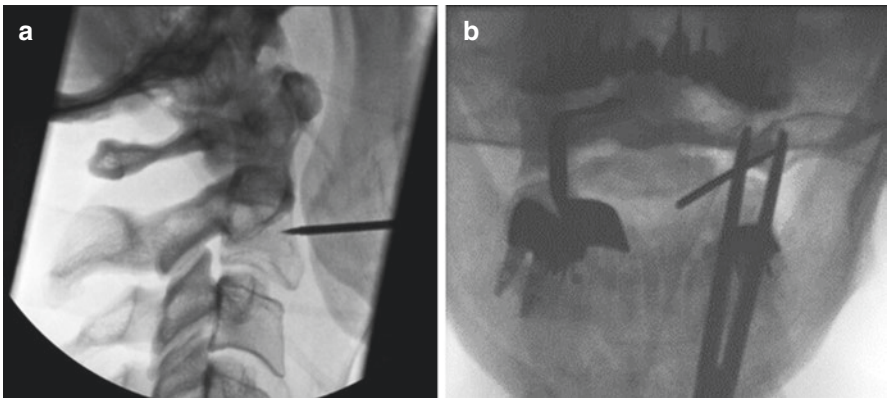

Fig. 3.27 Trans-oral approach to the upper cervical spine: biplane fluoroscopic guidance is strictly recommended to ensure the safest trans-oral approach; in fact real-time fluoroscopic control ensures the correct CC approach to the desired target and avoids straying off-midline where carotid and vertebral arteries course

3.8.4.1 Special Considerations

A retropharyngeal course of the internal carotid artery has to be ruled out before planning a trans-oral approach.

Suggested Readings

1. Clamp JA, Bayley EJ, Ebrahimi FV, Quraishi NA, Boszeyk BM. Safety of fluoroscopy guided percutaneous access to the thoracic spine. Eur. Spine J. 2012;21(Suppl 2):S207–11.
2. Murphy WA, Destouet JM, Gilula LA. Percutaneous skeletal biopsy 1981: a procedure for radiologists – results, review, and recommendations. Radiology. 1981;139:545–9.
3. Froelich JJ, Saar B, Hoppe M, Ishaque N, Walthers EM, Regn J, Klose KJ. Real-time CT-fluoroscopy for guidance of percutaneous drainage procedures. J. Vasc. Int. Rad. 1998;9:735–40.
4. Laredo JD, Bard M. Thoracic spine: percutaneous trephine biopsy. Radiology. 1986;160: 485–9.
5. Yaffe D, Greenberg G, Leitner J, Gipstein R, Shapiro M, Bachar GN. CT-guided percutaneous biopsy of thoracic and lumbar spine: a new coaxial technique. Am. J. Neuroradiol. 2003;24(10):2111.
6. Ashizawa R, Ohtsuka K, Kamimura M, et al. Percutaneous transpedicular biopsy of thoracic and lumbar vertebrae-method and diagnostic validity. Surg. Neurol. 1999;52:545–51.
7. Brenac F, Huet H. Diagnostic accuracy of the percutaneous spinal biopsy. Optimization of the technique. J. Neuroradiol. 2001;28:7–16.
8. Geremia G, Joglekar S. Percutaneous needle biopsy of the spine. Neuroimaging Clin. N. Am. 2000;10:503–33.
9. Pierot L, Boulin A. Percutaneous biopsy of the thoracic and lumbar spine: transpedicular approach under fluoroscopic guidance. Am. J. Neuroradiol. 1999;20:23–5.
10. Czervionke LF. Percutaneous spine biopsy. In: Fenton DS, Czervionke LF, editors. Image-guided spine intervention. Philadelphia: Saunders; 2003. p. 141–86.
11. Kennith FL, Kallmes DF, Horlocker TT. Recommendations for anticoagulated patients undergoing image-guided spinal procedures. Am. J. Neuroradiol. 2006;27:468–70.
12. Massari F, Rumboldt Z, Vandergrift W, Bonaldi G, Cianfoni A. Percutaneous image-guided C-spine procedures. Neurographics. 2014;4:62–77.
13. Cianfoni A, Boulter DJ, Rumboldt Z, Zapton T, Bonaldi G. Guidelines to imaging landmarks for interventional spine procedures: fluoroscopy and CT anatomy. Neurographics. 2011;01:38–47.
14. Boulter DJ, Rumboldt Z, Bonaldi G, Muto M, Cianfoni A. Tilting the gantry for CT-guided spine procedures. Radiol. Med. 2014;119(10):750–7.

CT/X-ray-Guided Augmentation Techniques in Cervical and Thoracic Spine

4

Giovanni Carlo Anselmetti

4.1 Introduction

Spine is the most common site of metastasis, with 50–80% of patients presenting with spinal lesions during the course of their disease [1, 2]. Due to a relatively large blood flow, the thoracic spine is a frequent site of metastasis. The cervical spine, by contrast, is less commonly involved, accounting for only 8–20% of all spinal metastases [1, 2]. In particular, metastases to the cervical junction (C1 and C2) are uncommon and represent less than 1% of all spinal metastases [1, 3].

Nonsurgical options for spinal metastases depend on tumor histology, presence of neurologic symptoms, as well as spinal stability [1, 4]. Recent progress in anticancer therapy [5] and newer radiotherapy techniques such as cyberknife radiosurgery [6, 7] or intensity-modulated stereotactic radiotherapy [8, 9] have improved the management of patients with spinal metastases. Unfortunately, a significant proportion of patients with spinal metastases will develop symptoms of bone progression during the course of the disease despite these therapies [10]. In particular, patients with cervical and thoracic metastases, because of the difficult anatomical localization, represent a subgroup where there are unmet medical needs. An osteolytic cervical or thoracic lesion, as well as an aggressive hemangioma with clinical signs of mechanical instability and uncontrolled pain, is, in most cases, suggestive of an impending fracture with high risk of severe consequences; in these patients, surgery [11–13] is a preferred option. However, surgical stabilization poses the risk of severe complications [12] considering also that these patients present frequently with poor clinical conditions and an advanced, multi-metastatic disease.

G.C. Anselmetti
Interventional Radiology Unit, Istituto Europeo per l'Oncologia (IEO),
Via Ripamonti 435, 20141 Milan, Italy

Interventional Radiology Unit, GVM Care & Research,
Villa Pia Hopsital, Strada Mongreno 180, 10132 Turin, Italy
e-mail: gc.anselmetti@fastwebnet.it

L. Manfrè (ed.), *Vertebral Lesions*, New Procedures in Spinal Interventional Neuroradiology, DOI 10.1007/978-3-319-52634-8_4

A less invasive procedure is represented by percutaneous vertebroplasty (PV), a technique originally described by Deramond in 1987 for the treatment of symptomatic vertebral hemangioma of C2 [14] that has evolved to become a standard of care for VCFs. Presently, PV is extensively applied for the palliative treatment of spine metastases in the thoracic and lumbar region [15–18]. Despite being less invasive than surgery, cervical and high level thoracic (above T6) spine PV remains a challenging procedure.

4.2 Technique

The procedure can be performed under local anesthesia and conscious sedation or general anesthesia. Usually sedation offers a perfect pain control during the procedure with lower risk compared to general anesthesia that, in our experience, is used in cervical transoral approach only. Intraprocedural antibiotic cover (e.g., 1 g of vancomycin hydrochloride and 100 mg of gentamycin immediately before the procedure) is mandatory in all patients. Oxygen saturation, pulse, and blood pressure are monitored throughout the procedure. Strict asepsis should be maintained during the whole procedure; the skin should be sterilized with povidone-iodine, whereas the oral cavity and posterior oropharynx should be cleansed with povidone-iodine if the transoral approach is employed.

A supine position is used for the cervical region and a prone position for the thoracic vertebrae.

The classical transpedicular route is preferred in the lower thoracic vertebrae, as it is inherently safe. This can be performed either by a monopedicular or bipedicular approach. An intercostovertebral route is preferred in the upper thoracic spine as the pedicle is too small or destroyed by the lesion; this approach usually requires a monolateral approach as the contralateral vertebral body can be reached by the needle with this approach. In the lower cervical vertebrae (C3–C7), the anterolateral approach is used; the needle path should avoid the carotid jugular complex. In the cervical junction (C1 and C2) the transoral route is preferred as it reduces the risk of injuries to the vertebral artery.

The combination of CT and fluoroscopy allows for precise needle placement (particularly in cervical and upper thoracic vertebrae, tumor cases, and difficult cases), reduces complications, and increases the comfort of the operator, as it allows for visualization in three dimensions with exact differentiation of anatomic structures. Fluoroscopy is provided by placing a mobile C-arm in front of the CT gantry. The use of CT allows for precise medial positioning of the needle tip in the anterior third of the vertebral body, thus allowing complete vertebral fill and no need for a contralateral access. Recently, new-generation angiographic suite (i.e., Allura Xper CT, Philips, The Netherlands in our experience) offers the integration of high-quality digital fluoroscopy and CT-like rotational acquisition that allows high definition and fast visualization of the correct needle placement with two-dimensional multiplanar reconstruction (2DMPR) coronal (Fig. 4.1) and sagittal (Fig. 4.2). Once satisfactory positioning of the needle is obtained, the imaging mode is switched to

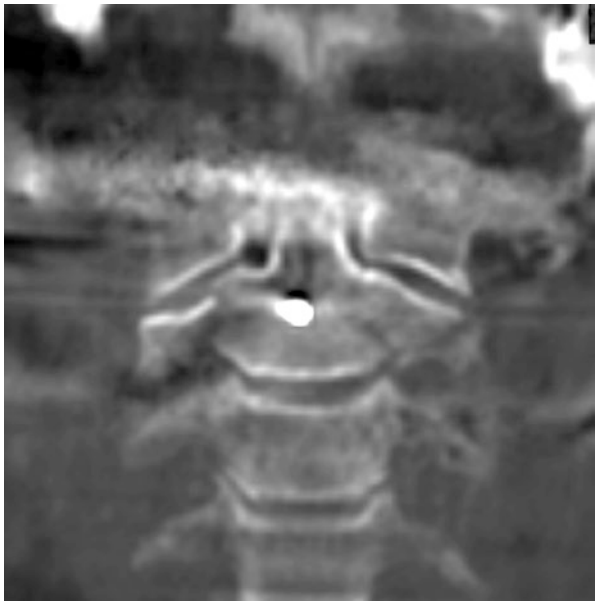

Fig. 4.1 2DMPR coronal reconstruction confirmed needle placement within the lesion

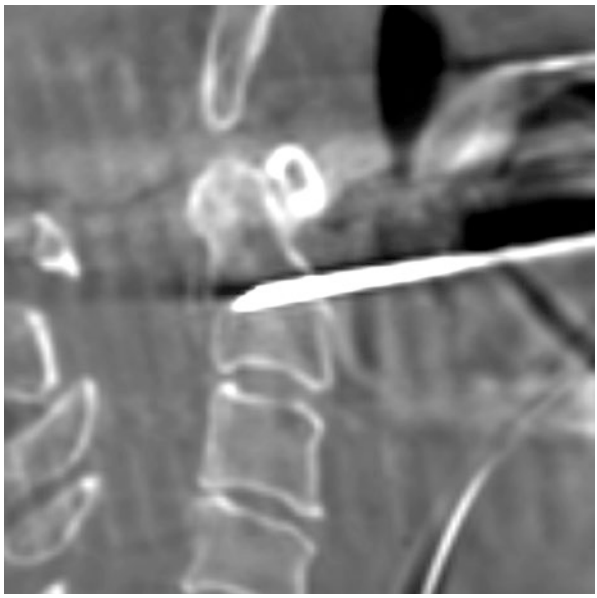

Fig. 4.2 2DMPR sagittal reconstruction

fluoroscopy for real-time visualization of cement injection. The use of a beveled needle (15 gauges for cervical and 13 gauges for thoracic) is always preferable for precise placement. After penetration of the cortex within the pedicle, the bevel of the needle is rotated toward the midline, allowing medial positioning; this allows bilateral filling of the vertebral body, obviating the need for the bilateral approach.

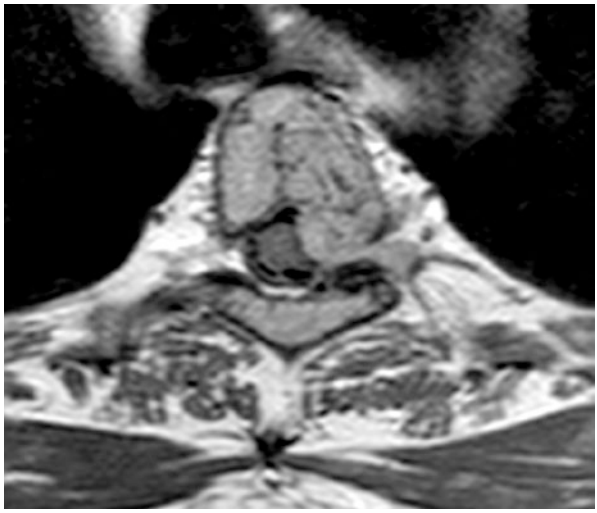

Fig. 4.3 Aggressive painful hemangioma of Th3

Preoperative planning requires radiographic studies to define fracture anatomy and assess posterior vertebral body wall deficiency (this is mandatory in tumoral lesions the often involve the vertebral wall); magnetic resonance (MR) is a must in all patient candidates for PV, as it provides both functional and anatomical information. T1-, T2-, and STIR-weighted sequences in axial and sagittal planes are required. If there is any doubt regarding the intactness of the posterior vertebral wall, a CT scan through the intended level(s) should be performed. It will also provide information regarding the location and extent of the lytic process, the visibility and degree of involvement of the pedicles, and the tumor extension or retropulsed bone fragment, which can increase the likelihood of major complications. A well-performed pre-procedural study helps to plan the procedure considering if more than one approach and multiple needles are required. When the tumoral lesion such an aggressive hemangioma (Fig. 4.3) is well identified in MR, additional CT scans can precisely evaluate the discontinuity of the cortical bone and the extension of the lesion to the vertebral posterior elements (Fig. 4.4). Digital fluoroscopy integrated with rotational acquisition and 2DMPR may allow precise positioning of three needles trough the pedicles and the spinous process in axial (Fig. 4.5) and sagittal view (Fig. 4.6). Bone cement injection is then performed under continuous digital fluoroscopy monitoring (Fig. 4.7) for early detection of possible cement leakages up to satisfactory bone lesion filling. The injection should be performed using a dedicated injection set (e.g., from Cemento-RE gun Optimed; Allegiance; Cook; Stryker; D-Fine) for a better-graduated control of the injection. Although the use of the injection sets increases the expense of the procedure, it is safer than freehand injection especially in the cervical and upper thoracic spine.

Injection of cement should be done under continuous lateral fluoroscopic control. The lateral view is preferred, as it allows for early detection of epidural leak; in such a case, the injection needs to be immediately stopped, and using the injection

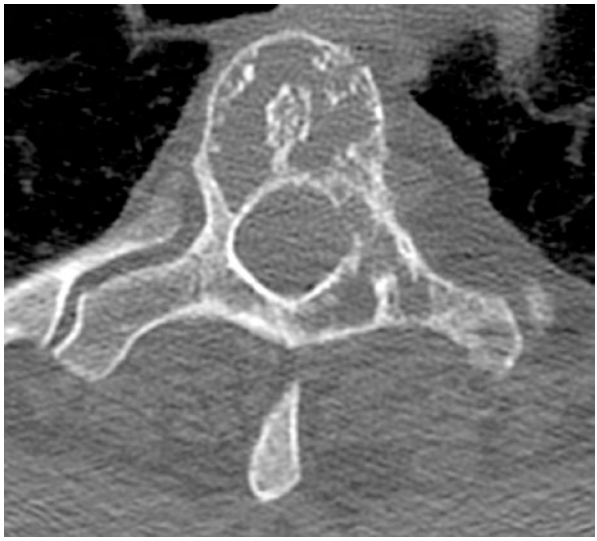

Fig. 4.4 Pre-procedural CT detects discontinuity of the cortical bone

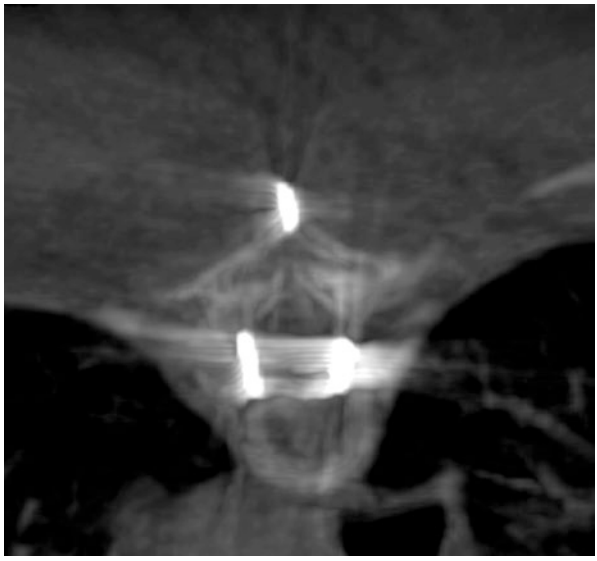

Fig. 4.5 Procedural 2DMPR axial shows the correct positioning of the needles

set, the pressure can be reversed by unscrewing the injector. Waiting for 1 min allows the cement to harden to seal the leak, changing the needle position or the bevel direction is useful to avoid further leakages, and the injection can be carried out again. If the leak still continues, the injection has to be terminated and the needle removed.

Postprocedural CT (Fig. 4.8) is always useful to evaluate the filling of the lesion and to assess the cement leakage and to detect possible complications; in our

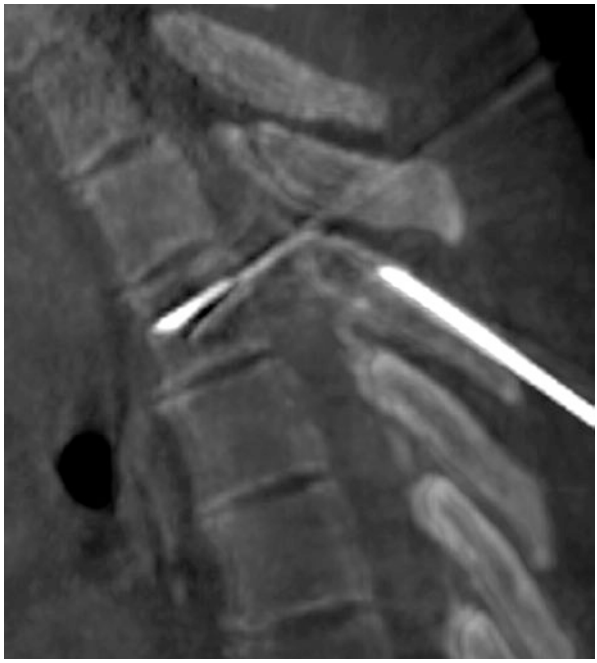

Fig. 4.6 Sagittal reconstruction confirms the correct placement of the needle within the spinous process of Th3

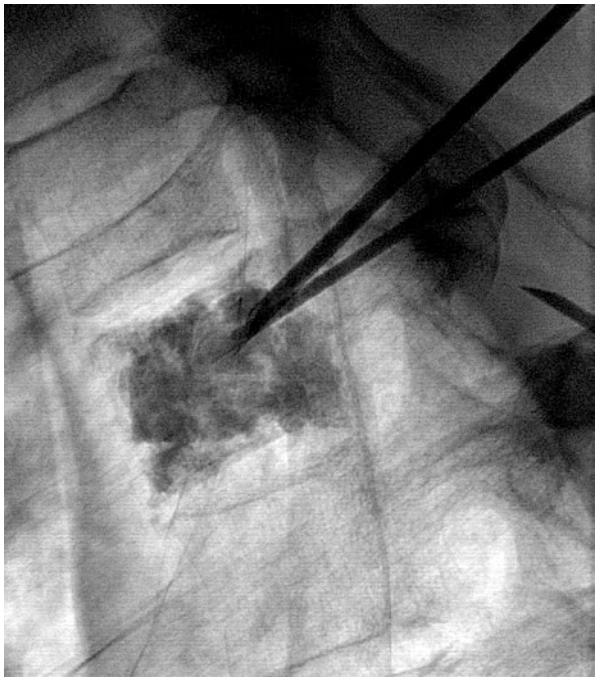

Fig. 4.7 Digital fluoro monitoring in lateral view during bone cement injection allows early detection of possible epidural leaks

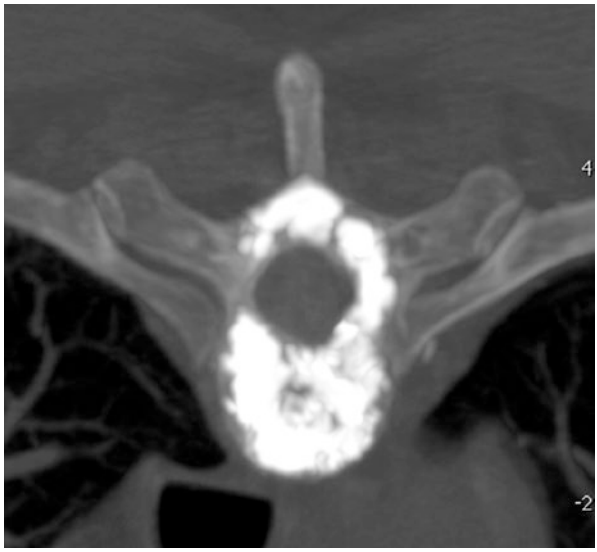

Fig. 4.8 Postprocedural CT scan evaluates lesion filling and the absence of epidural leakages and complications

experience, postprocedural CT scan is performed in all cases of cervical and upper thoracic spine vertebral augmentation. In neoplastic lesions, we try to fill the lesion fully in order to achieve both bone consolidation and thermal-chemical necrosis; if the aim of vertebroplasty is relief of pain only, smaller volumes (1.5–3 mL) are usually sufficient.

Before removing the patient from the angiographic cradle, it is safe to wait for cement hardening, generally from 20 to 30 min depending upon the bone cement characteristics indicated by the producer. The patient is maintained in the recumbent position for 2 h following the procedure (bone cement ultimate strength is usually achieved in 1 h) and then can be mobilized. The patient is usually discharged from the hospital the next procedural day.

4.3 Results

Cervical and upper thoracic vertebral augmentation is generally always feasible if correct indications are respected and safer combined fluoro-CT guidance is employed.

In our personal experience, 119 cervical (4 C1, 45 C2, 9 C3, 17 C4, 20 C5, 14 C6 and 10 C7) and 9629 thoracic vertebrae (from T1 to T12) were treated without any major complications and good clinical outcome. All the cases were performed with combined digital fluoroscopy and CT guidance in conscious sedation except for C1 and C2 where general anesthesia was employed. Some minor bone cement leakages occurred, but all of these were asymptomatic due to early identification by continuous fluoroscopic monitoring during injection. Vascular, spinal, or extraspinal tissue injuries were avoided by CT control during needle placement.

References

1. Jenis LG, Dunn EJ, An HS. Metastatic disease of the cervical spine. A review. Clin. Orthop. Relat. Res. 1999;359:89–103.
2. Sundaresan N, Boriani S, Rothman A, et al. Tumors of the osseous spine. J. Neuro-Oncol. 2004;69:273–90.
3. Sherk HH. Lesions of the atlas and axis. Clin. Orthop. Relat. Res. 1975;109:33–41.
4. Bilsky MH, Shannon FJ, Sheppard S, et al. Diagnosis and management of a metastatic tumor in the atlantoaxial spine. Spine (Phila Pa 1976). 2002;27:1062–9.
5. Tanvetyanon T, Hines Jr E. Long-term efficacy and safety of zoledronic acid in the treatment of skeletal metastases in patients with nonsmall cell lung carcinoma and other solid tumors. Cancer. 2005;103:1756–7; author reply 1757–1758
6. Gerszten PC, Welch WC. Cyberknife radiosurgery for metastatic spine tumors. Neurosurg. Clin. N. Am. 2004;15:491–501.
7. Tsai JT, Lin JW, Chiu WT, et al. Assessment of image-guided CyberKnife radiosurgery for metastatic spine tumors. J. Neuro-Oncol. 2009;94:119–27.
8. Bilsky MH, Yamada Y, Yenice KM, et al. Intensity-modulated stereotactic radiotherapy of paraspinal tumors: a preliminary report. Neurosurgery. 2004;54:823–30. discussion 830–821
9. Kuijper IT, Dahele M, Senan S, et al. Volumetric modulated arc therapy versus conventional intensity modulated radiation therapy for stereotactic spine radiotherapy: a planning study and early clinical data. Radiother. Oncol. 2010;94:224–8.
10. Meuser T, Pietruck C, Radbruch L, et al. Symptoms during cancer pain treatment following WHO-guidelines: a longitudinal follow-up study of symptom prevalence, severity and etiology. Pain. 2001;93:247–57.
11. Louis R. Anterior surgery of the upper cervical spine. Chir. Organi Mov. 1992;77:75–80.
12. Kingdom TT, Nockels RP, Kaplan MJ. Transoral-transpharyngeal approach to the craniocervical junction. Otolaryngol. Head Neck Surg. 1995;113:393–400.
13. Vieweg U, Meyer B, Schramm J. Tumour surgery of the upper cervical spine – a retrospective study of 13 cases. Acta Neurochir. 2001;143:217–25.
14. Galibert P, Deramond H, Rosat P, et al. Preliminary note on the treatment of vertebral angioma by percutaneous acrylic vertebroplasty. Neuro-Chirurgie. 1987;33:166–8.
15. Barragan-Campos HM, Vallee JN, Lo D, et al. Percutaneous vertebroplasty for spinal metastases: complications. Radiology. 2006;238:354–62.
16. McDonald RJ, Trout AT, Gray LA, et al. Vertebroplasty in multiple myeloma: outcomes in a large patient series. AJNR Am. J. Neuroradiol. 2008;29:642–8.
17. Weill A, Chiras J, Simon JM, et al. Spinal metastases: indications for and results of percutaneous injection of acrylic surgical cement. Radiology. 1996;199:241–7.
18. Wenger M. Vertebroplasty for metastasis. Med. Oncol. 2003;20:203–9.

CT/X-Ray-Guided Augmentation Techniques in Lumbar Spine

5

Gianluigi Guarnieri, Roberto Izzo, Giurazza Francesco, and Mario Muto

5.1 Introduction

Augmentation techniques (**AT**) include different percutaneous mini-invasive procedures such as vertebroplasty (**VP**) and assisted technique (AT) (kyphoplasty or kyphoplasty-like technique) for the treatment of symptomatic vertebral compression fractures (**VCFs**) due to osteoporosis diseases, primary or secondary vertebral tumors, and vertebral trauma [1].

The major target of all those techniques is pain relief, thanks to the simple cement injection (polymethylmethacrylate, **PMMA**) in the collapsed or abnormal soma stabilizing the movements of the trabecular and spongious microfractures (responsible for the pain), making more compact and resistant the vertebral body, improving life quality [1].

While VP consists in the simple cement injection, AT combines this analgesic and vertebral consolidation effect with the restoration of the physiological height of the collapsed vertebral body, reducing the kyphotic deformity and improving vertebral statics and trying to restore the physiologic curvature and biomechanics.

Reduction of the kyphotic deformity is the major target of all AT, thanks to the capacity of the system to restore the vertebral height [2]. Right now, many different devices have been developed by the industry obtaining a vertebral augmentation effect.

Electronic supplementary material The online version of this chapter (doi:10.1007/978-3-319-52634-8_5) contains supplementary material, which is available to authorized users.

G. Guarnieri, M.D. (✉) • R. Izzo • M. Muto, M.D.
Neuroradiology Service, Cardarelli Hospital, Naples, Italy
e-mail: gianluigiguarnieri@hotmail.it

G. Francesco
Radiology Department, Università Campus Bio-Medico di Roma, Rome, Italy

L. Manfrè (ed.), *Vertebral Lesions*, New Procedures in Spinal Interventional Neuroradiology, DOI 10.1007/978-3-319-52634-8_5

In 1998, balloon kyphoplasty technique was the first one to be developed consisting in delivering cement—**PMMA**—into a fractured vertebral body under fluoroscopic guidance after creation of a cavity within the vertebral body by a dedicated expandable balloon [3, 4].

Indeed many companies have developed many devices in order to obtain both vertebral high restoration and vertebral antalgic effects:

- Vertebral body stenting is another augmentation device where two metallic stents are placed in the vertebral body by bipeduncular approach creating a cavity where the cement can be injected in low-pressure condition [5].
- Metallic system placed into the vertebral body obtaining vertebral height restoration.

Statistically, the majority of porotic fractures are located at the lumbar segment due to the high biomechanical axial load at this level.

Even a recent meta-analysis has shown no statistical difference in terms of pain relief between VP and AT.

5.2 Patient Selection Criteria

Patient selection criteria are based on clinical pain evaluation associated to imaging correlation based mostly on MR abnormality [6].

Pain onset is an important parameter to consider because it can help in deciding whether the patient should be treated or not [7].

Patient affected by symptomatic VCF with intense, non-radicular, back pain on midline line, refractory to conventional medical treatment since 6–8 weeks (bracing, analgesic and bed rest) and strongly exacerbated by digital palpation of the spinous process of the affected vertebra, represent the first line of indication to treat by augmentation technique.

Pain syndrome can be evaluated by different methods such as the Visual Analog Scale (VAS), the Oswestry Disability Index (ODI), SF-36, and Roland-Morris Disability Questionnaire [8].

At clinical evaluation, it corresponds to an imaging pattern: VCF with more/less kyphosis deformation and hyperintensity signal alteration on T2-STIR MR sequence, corresponding to bone marrow edema and unhealed fracture [9].

In case of known MR contraindication, bone nuclear medicine scan is requested showing an unspecific vertebral body intense uptake requiring a MDCT correlation to confirm the diagnosis of porotic VCF.

MDCT with MPR is useful to differential benign porotic fracture versus neoplastic one, searching for the intravertebral vacuum sign or soft tissue abnormality.

In case of uncertain pattern on MDCT or MR morphology or signal intensity, a bone biopsy is mandatory to understand the nature of the lesion prior to perform AT.

Painless VCF, diffuse non-focal pain without MR evidence of altered trabecular bone signal, systemic or local infections, uncorrectable coagulation disorders, and allergy to PMMA are the exclusion criteria for AT [7].

Patient with porotic fracture on MR imaging with hyperintensity on T2-STIR sequence but without back pain is not indicated to the treatment. Patient with spine pain syndrome, VCF, and visibility on MR of hyperintensity on T2-STIR sequence is the one with the best and correct indication to perform VP [7].

AT are recommended when the vertebral height reduction is at least 30–40% or more of the normal anatomical morphology, especially in a young traumatic patient [1, 4, 7] to reduce kyphotic deformity.

For traumatic VCF at thoracolumbar level, AT is primarily indicated to achieve height augmentation and kyphosis reduction, and the treatment must be performed as soon as possible to avoid bone sclerotic response, especially in a young patient 2 weeks after trauma. According to Magerl classification—where VCFs are divided into three main categories according to trauma force, namely, (a) compression injury, (b) distraction injury, and (c) rotation injury—a main nonsurgical mini-invasive treatment is indicated for type A1 [10].

The management and indication to mini-invasive treatment at lumbar level in patients affected by neoplastic VCFs require a complete team and multidisciplinary approach between interventional neuroradiologist, radiotherapist, oncologist, neurosurgeons, and pain therapist.

The concept of oncologic instability is different compared to the traumatic one.

The aim of the treatment is antalgic effect and vertebral stabilization preventing also vertebral instability in case of bone disruption.

Malignant primary tumors or metastases, in fact, can disrupt the normal biomechanics of the spine via bone destruction or deformity resulting in a decrease in its load-bearing capacity. The load-bearing capacity is determined by a number of factors, including tumor size as well as cross-sectional area of the intact body and its bone mineral density. Krishaney [11] divided the vertebral body in 27 similar cubes. When the destruction of all the cubes within 1/3 of the axial soma occurs, it creates an instability due to a deficit of the anterior and middle column. In case of sagittal destruction only, the spinal stability is maintained and not altered. The location of the tumor (and hence bone destruction) within the vertebral body may also play a role in the patient's risk of fracture and instability. There is a distinct discrepancy between the thoracic and thoracolumbar or lumbar spine and spinal oncological instability. In fact, according to Taneichi, the most important risk factor of fracture of thoracic spine instability is the disruption of costovertebral joint and, only after, the vertebral body. The costovertebral joint and all thoracic muscular structure increase the stiffness and the resistance of the thoracic spine, maintaining the spinal biomechanics. In fact, at the thoracic level, it has been demonstrated that it is necessary to have about 50–60% vertebral disruption to have pathologic vertebral fracture and instability versus 35–40% at thoracolumbar and lumbar levels [12].

Spinal oncological instability classification [13] is based on patient symptoms and imaging criteria of the spine, and it is possible to predict the spine stability of neoplastic lesions deciding the indication of mini-invasive treatment. The classification system includes global spinal location of the tumor, type and presence of pain, bone lesion quality, spinal alignment, extent of vertebral body collapse, and posterolateral spinal element involvement.

By the combinations of all these elements, a score [13]—The Spinal Instability Neoplastic Score—comes out that can guide clinicians in identifying when patients with neoplastic disease of the spine may benefit from surgical treatment. A score between 0 and 6 results in spinal stability, between 7 and 12 results in possible instability, and between 13 and 18 results in oncological instability.

The indication treatment for patients affected by neoplastic lesions involving the spine has as target two major concepts:

- Pain treatment
- Stability treatment, especially for the spinal metastasis

5.3 Technique

All the procedures can be performed under local anesthesia or neuroleptanalgesia using fluoro-CT or fluoroscopy guidance in patient mostly in prone position.

To avoid cement leakage during injection, it is important to use high-quality fluoroscopy to achieve a complete anatomical control of the spine.

Bipeduncular approach is mandatory to perform assisted techniques and to reduce vertebral kyphosis deformation.

The technique to reach the peduncle is simple and easy to perform: in PA view, the first step is to archive the spinous process on the midline, and the second step is to see both vertebral endplates completely superimposed.

It is also possible to give a little obliquity to the projection to reach better the center of the vertebral body, especially in case you want to perform a simple VP with mono-lateral approach.

Once the correct imaging approach is obtained, a local anesthesia can be performed few centimeters laterally to the peduncle. Once it has been done, the needle is positioned in the vertebral body through a trans-peduncular approach reaching its posterior wall.

In AP view, the medial margin of the peduncle is an absolute anatomical landmark to check before to pass over the posterior wall of the vertebral body in LL view.

A metallic drill can also be used to model the trabecular bone such as other osteotomy cannula to lead the insertion of the balloon tamp or metallic implant without problems.

The drill is then removed and the balloons or the mechanical system can be inserted; the systems are connected, and under fluoroscopic guidance, the inflation of the balloon or the mechanical restoration can begin and be controlled. After creation of a cavity or a mechanic implant deployment, it is then possible to prepare and inject the cement. The amount of cement injected in the vertebral body is extremely variable: 2 to 4 mL for each peduncle depending on the size of lumbar metamer and on the grading of the collapsed vertebra; however, there is no absolute rule regarding the amount of cement to be injected [7] (Fig. 5.1a–h and Fig. 5.2a–d).

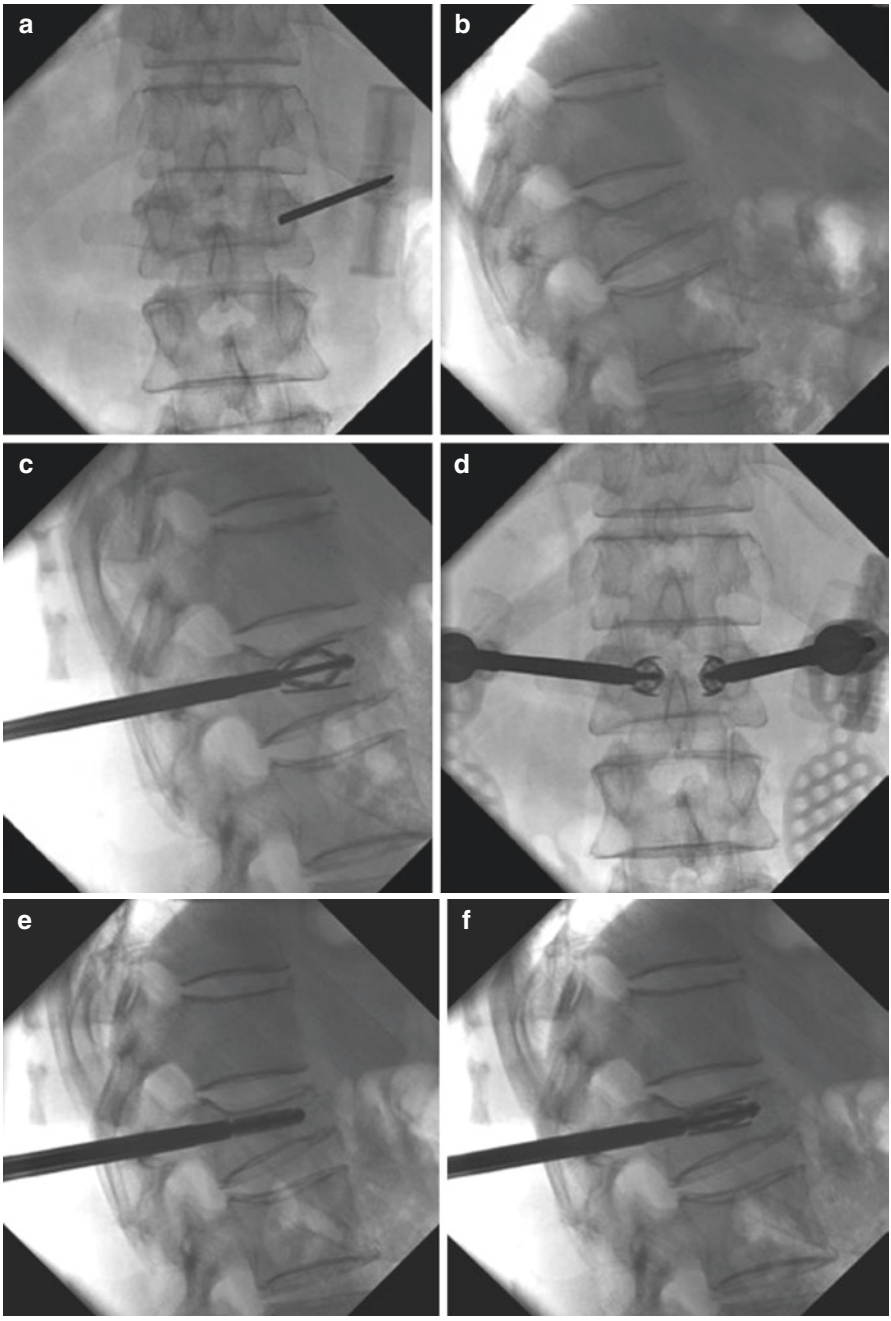

Fig. 5.1 (**a**–**b**) Male, 55 years old, affected by traumatic vertebral compression fracture at L1 level (Magerl A1 Fracture) treated by Spine Jack device. (**c**–**h**) PA and LL fluoroscopic control after placement of Spine Jack Device into L1 soma by bipeduncular approach with good augmentation effect

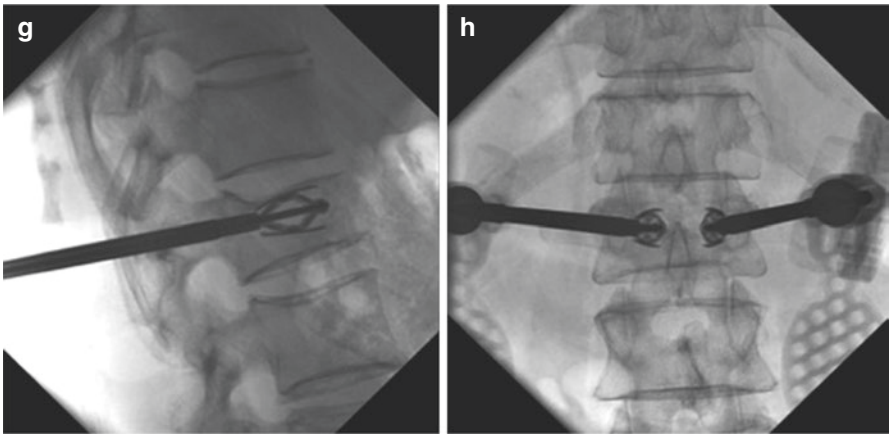

Fig. 5.1 (continued)

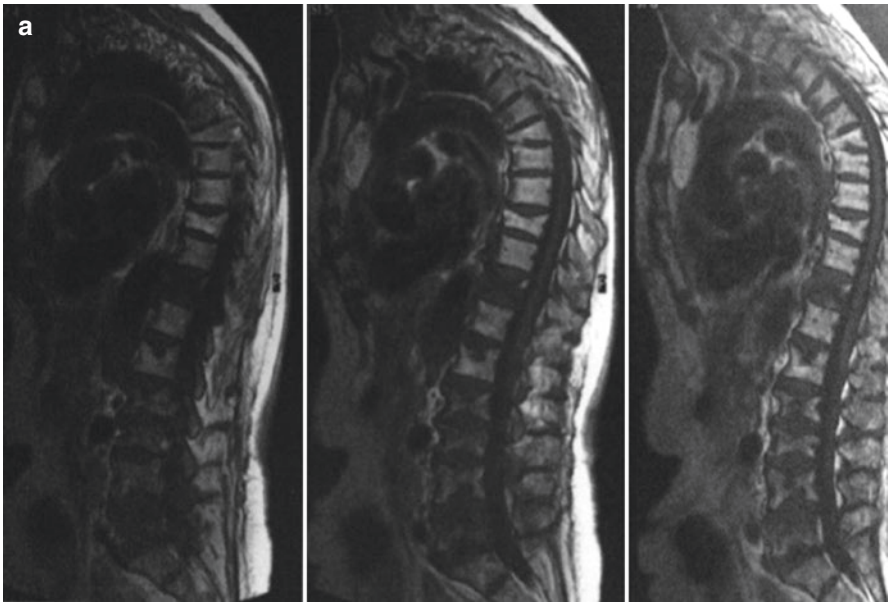

Fig. 5.2 The sagittal T1W(**a**), STIR(**b**),T2W(**c**) MRI showed multiple osteoporotic vertebral compression fractures at thoracolumbar level with hyperintense signal on STIR (intra-spongious edema) in a 75-year-old affected female who was resistant to medical therapy and treated with one session of multilevel vertebroplasty (**d**)

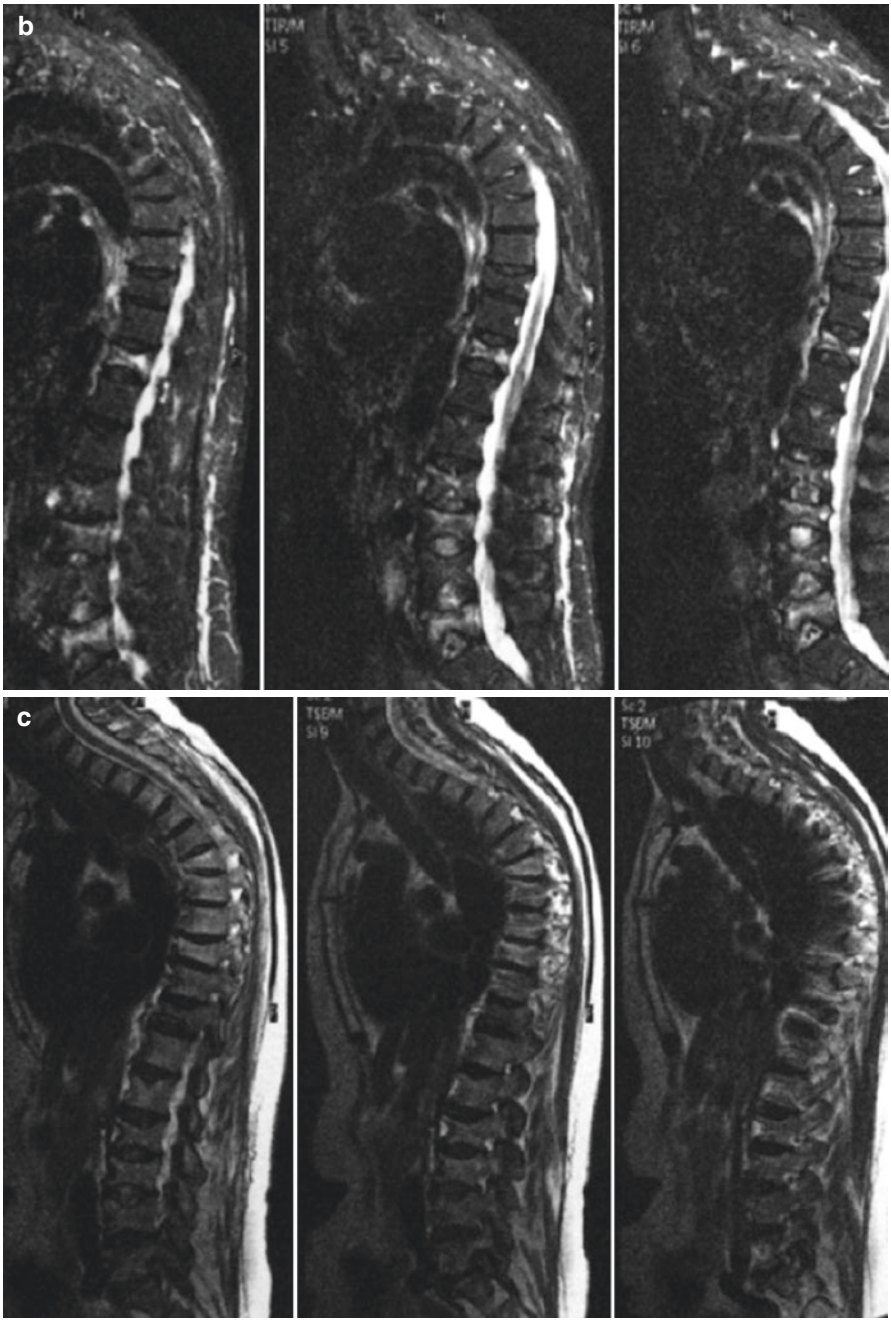

Fig. 5.2 (continued)

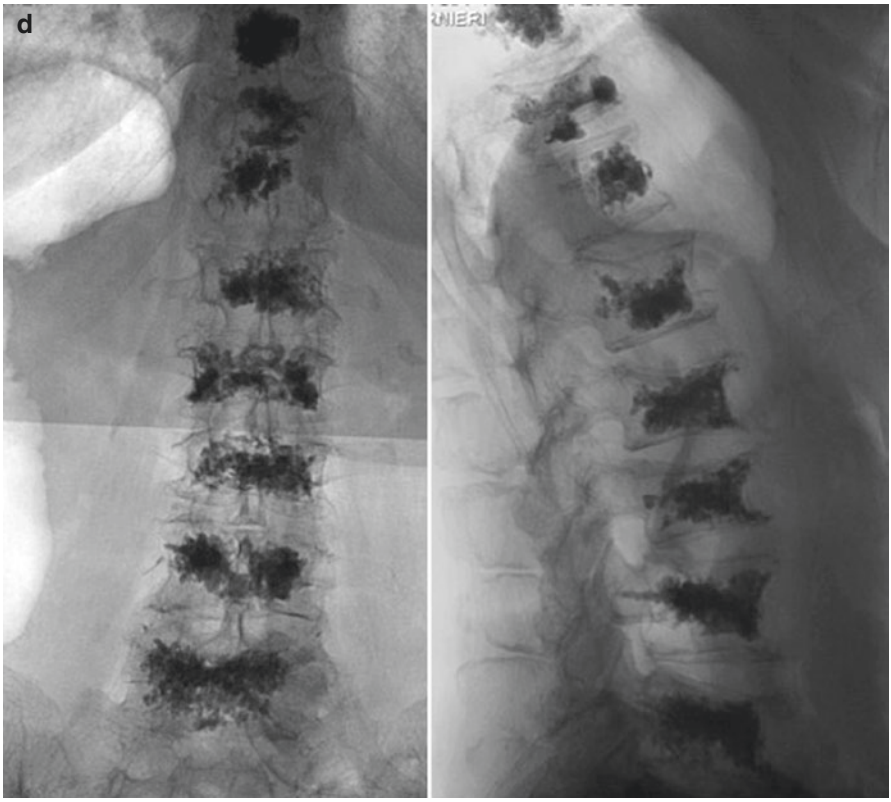

Fig. 5.2 (continued)

The cement must be injected through a slow injection system such as a bone filler or through 1 mL syringe to inject a quite high-viscosity cement, with less disk and venous leakage [7] and under continuous fluoroscopy control.

When the vertebral body is filled by cement with homogenous distribution, the procedure is concluded.

5.4 Discussion

The safety and the efficacy of those techniques are well established by several studies and trials [14–18], analyzing the outcome of technique about pain's reduction and kyphosis correction and complications, such as cement leakage, disk leakage, pulmonary embolism, and new vertebral fractures at adjacent or distant vertebral body.

The Fracture Reduction Evaluation (FREE) [19] multicenter randomized controlled trial compared the efficacy and safety of balloon kyphoplasty (149 patients for BKP-group) to nonsurgical management (151 patients for NSM group) over

24 months in patients with painful vertebral compression fractures (VCF). Compared with NSM, the BKP group had greater improvements in SF-36 physical component summary (PCS) scores at 1 month (5.35 points; 95% CI, 3.41–7.30; $P < 0.0001$) and when averaged across the 24 months (overall treatment effect 2.71 points; 95% CI, 1.34–4.09; $P = 0.0001$). The BKP group also had greater functionality by assessing timed up and go (overall treatment effect—2.49 s; 95% CI, −0.82 to −4.15; $P = 0.0036$). At 24 months, the change in index fracture kyphotic angulation was statistically significantly improved in the kyphoplasty group (average 3.13° of correction for kyphoplasty compared with 0.82° in the control, $P = 0.003$). Number of baseline prevalent fractures ($P = 0.0003$) and treatment assignment ($P = 0.004$) are the most predictive variables for PCS improvement; however, in patients who underwent BKP, there may also be a link with kyphotic angulation. In BKP, the highest quart for kyphotic angulation correction had higher PCS improvement (13.4 points) than the quart having lowest correction of angulation (7.40 points, $P = 0.0146$ for difference). The most common adverse events temporally related to surgery (i.e., within 30 days) were back pain (20 BKP, 11 NSM), new VCF (11 BKP, 7 NSM), nausea/vomiting (12 BKP, 4 NSM), and urinary tract infection (10 BKP, 3 NSM).

The Cancer Patient Fracture Evaluation (CAFE) study [20], a multicenter randomized controlled trial, compared balloon kyphoplasty (70 patients) versus nonsurgical fracture management (64 patients) for treatment of painful VCFs in patients with spine metastasis and one to three painful VCFs. The primary endpoint was back-specific functional status measured by the Roland-Morris Disability Questionnaire (RDQ) score at 1 month. The mean RDQ score in the kyphoplasty group changed from 17.6 at baseline to 9.1 at 1 month (mean change −8.3 points, 95% CI −6.4 to −10.2; $P < 0.0001$). The mean score in the control group changed from 18.2 to 18.0 (mean change 0.1 points; 95% CI −0.8 to 1.0; $P = 0.83$). At 1 month, the kyphoplasty treatment effect for RDQ was −8.4 points (95% CI −7.6 to −9.2; $P < 0.0001$). The most common adverse events within the first month were back pain (4 of 70 in the BK group and 5 of 64 in the control group) and symptomatic vertebral fracture (2 and 3, respectively). This trial showed that BK is an effective and safe treatment that rapidly reduces pain and improves function.

Eight nonrandomized trials of 422 patients and 1 randomized trial of 100 patients compared VP and KP [21]. In all eight studies, VP and KP reduced pain and improved QOL to a similar extent. Only one nonrandomized study suggested that KP is superior at relieving pain and improving QOL, with differences maintained over 1-year follow-up. KP was more effective at reducing the kyphotic wedge and increasing vertebral height. The largest meta-analysis available concluded that BKP decreased pain to a greater degree than VP (5.07 vs. 4.55 points on the VAS) and resulted in significantly better improvement in quality of life than both VP and NSM [21]. This meta-analysis includes all the level I data available on vertebral augmentation, and given this large amount of high-quality data, it is our contention that there is more than adequate information upon which to base treatment decisions. Both procedures are safe, with no reported complications [7].

The risk of cement leakage is certainly lower with AT, thanks to low-pressure condition of cement injection versus VP, while the incidence of new vertebral

fractured to adjacent or distant metamer is the same, mostly related to the porotic disease itself [7, 22].

Many studies suggested that AT produces a greater improvement in daily activity, physical function, and pain relief when compared to optimal medical management for osteoporotic VCFs by 6 months after intervention, while there is poor-quality evidence that AT results in greater pain relief for tumor-associated VCFs [23].

No significant difference is demonstrated between VP and KP in short- and long-term pain and disability, complications, and anatomic outcomes [24].

KP and VP are both safe and effective surgical procedures in treating osteoporotic VCF. KP has a similar long-term pain relief, function outcome, and new adjacent VCFs in comparison to VP. KP is superior to VP for the injected cement volume, the short-term pain relief, the improvement of short- and long-term kyphotic angle, and lower cement leakage rate. However, KP has a longer operation time and higher material cost than VP [25].

For traumatic patient, treated by AT, generally pain relief is achieved in the 90–95% of patients affected by A1 and A3 Magerl vertebral fractures, treated within 3 months from the trauma, depending on the type of fracture, and an increase in vertebral body height sufficient to allow early mobilization of the patient and restoration of the physiological distribution of postural forces avoiding bed rest and orthosis devices [7].

Conclusion

Vertebral augmentation is a well-established therapy for the treatment of spine pain due to porotic, neoplastic, and traumatic fractures.

Clinical history and a correct diagnostic approach with MR, CT, and nuclear medicine bone scan are mandatory in patient selection to obtain the best clinical results at 1-, 3-, and 12-month follow-up.

The rate of complications is very low and is related to the condition of the metamer to be treated, to operator experience, and fluoroscopy quality, and it is useful to remind that those complications are very often completely asymptomatic.

New materials with high-viscosity cement are now available to reduce this complications even with low cost.

References

1. Muto M, Marcia S, Guarnieri G, Pereira V. Assisted techniques for vertebral cementoplasty: why should we do it? Eur J Radiol. 2015;84(5):783–8.
2. McGirt MJ, Parker SL, Wolinsky JP, et al. Vertebroplasty and kyphoplasty for the treatment of vertebral compression fractures: an evidenced-based review of the literature. Spine J. 2009;9(6):501–8.
3. Garfin SR, Yuan HA, Reiley MA. New technologies in spine: kyphoplasty and vertebroplasty for the treatment of painful osteoporotic compression fractures. Spine. 2001;26(14):1511–5.

4. Pflugmacher R, Kandziora F, Schroder R, et al. Vertebroplasty and kyphoplasty in osteoporotic fractures of vertebral bodies: a prospective 1-year follow-up analysis. Rofo. 2005;177:1670–6.
5. Muto M, Greco B, Setola F, Vassallo P, Ambrosanio G, Guarnieri G. Vertebral body stenting system for the treatment of osteoporotic vertebral compression fracture: follow-up at 12 months in 20 cases. Neuroradiol J. 2011;24(4):610–9.
6. Kallmes DF, Heagerty PJ, Turner JA, Wilson DJ, Diamond TH, Ralston SH, et al. A randomized trial of vertebroplasty for osteoporotic spinal fractures. N Engl J Med. 2009;361(6):569–79.
7. Muto M, Guarnieri G, Lavanga A, Vassallo P, et al. Vertebroplasty and kyphoplasty: friends or foes? Radiol Med. 2008;113(8):1171–84.
8. Grotle M, Brox JI, Vøllestad NK. Concurrent comparison of responsiveness in pain and functional status measurements used for patients with low back pain. Spine. 2004;29(21):E492–501.
9. Ambrosanio G, Lavanga A, Vassallo P, Izzo R, Diano AA, Muto M. Vertebroplasty in the treatment of spine disease. Interv Neuroradiol. 2005;11:309–23.
10. Magerl F, Aebi M, Gertzbein SD, Harms J, Nazarian S. A comprehensive classification of thoracic and lumbar injuries. Eur Spine J. 1994;3(4):184–201.
11. Krishnaney AA, Steinmetz MP, Benzel EC. Biomechanics of metastatic spine cancer. Neurosurg Clin N Am. 2004;15:375–80.
12. Weber MH, Burch S, Buckley J, Schmidt MH, Fehlings MG, Vrionis FD, Fisher CG. Instability and impending instability of the thoracolumbar spine in patients with spinal metastases: a systematic review. Int J Oncol. 2011;38(1):5–12.
13. Fisher CG, Di Paola CP, Ryken TC, Bilsky MH, Shaffrey CI, Berven SH, Harrop JS, Fehlings MG, Boriani S, Chou D, Schmidt MH, Polly DW, Biagini R, Burch S, Dekutoski MB, Ganju A, Gerszten PC, Gokaslan ZL, Groff MW, Liebsch NJ, Mendel E, Okuno SH, Patel S, Rhines LD, Rose PS, Sciubba DM, Sundaresan N, Tomita K, Varga PP, Vialle LR, Vrionis FD, Yamada Y, Fourney DR. A novel classification system for spinal instability in neoplastic disease: an evidence-based approach and expert consensus from the Spine Oncology Study Group. Spine. 2010;35(22):E1221–9.
14. Voormolen MH, Mali WP, Lohle PN, Fransen H, Lampmann LE, van der Graaf Y, Juttmann JR, Jansssens X, Verhaar HJ. Percutaneous vertebroplasty compared with optimal pain medication treatment: short-term clinical outcome of patients with subacute or chronic painful osteoporotic vertebral compression fractures. The VERTOS study. AJNR Am J Neuroradiol. 2007;28(3):555–60.
15. Klazen CA, Lohle PN, de Vries J, Jansen FH, Buskens E, Mali WP, et al. Vertebroplasty versus conservative treatment in acute osteoporotic vertebral compression fractures (Vertos II): an open-label randomised trial. Lancet. 2010;376(9746):1085–92.
16. Klazen CA, Muller A, Fransen H, Elgersma OE, Mali WP, Verhaar HJ, et al. Percutaneous vertebroplasty is not a risk factor for new osteoporotic compression fractures: results from VERTOS II. AJNR Am J Neuroradiol. 2010;31(8):1447–50.
17. Venmans A, Lohle PN, van Rooij WJ. Pain course in conservatively treated patients with back pain and a VCF on the spine radiograph (VERTOS III). Skelet Radiol. 2014;43(1):13–8.
18. Comstock BA, Sitlani CM, Jarvik JG, Heagerty PJ, Turner JA, Kallmes DF. Investigational vertebroplasty safety and efficacy trial (INVEST): patient-reported outcomes through 1 year. Radiology. 2013;269(1):224–31.
19. Wardlaw D, Cummings SR, Van Meirhaeghe J, Bastian L, Tillman JB, Ranstam J, Eastell R, Shabe P, Talmadge K, Boonen S. Efficacy and safety of balloon kyphoplasty compared with non-surgical care for vertebral compression fracture (FREE): a randomised controlled trial. Lancet. 2009;373(9668):1016–24.
20. Berenson J, Pflugmacher R, Jarzem P, Zonder J, Schechtman K, Tillman JB, Bastian L, Ashraf T, Vrionis F, Cancer Patient Fracture Evaluation (CAFE) Investigators. Balloon kyphoplasty versus non-surgical fracture management for treatment of painful vertebral body compression fractures in patients with cancer: a multicentre, randomised controlled trial. Lancet Oncol. 2011;12(3):225–35.

21. Deramond H, Salioub G, Aveillana M, et al. Respective contributions of vertebroplasty and kyphoplasty to the management of osteoporotic vertebral fractures. Joint Bone Spine. 2006;73:610–3.
22. Peh WC, Gilula LA. Percutaneous vertebroplasty: indications, contraindications, and technique. Br J Radiol. 2003;76:69–75.
23. Eck JC, Nachtigall D, et al. Comparison of vertebroplasty and balloon kyphoplasty for treatment of vertebral compression fractures: a meta-analysis of the literature. Spine J. 2008;8:488–97.
24. Gu CN, Brinjikji W, Evans AJ, Murad MH, Kallmes DF. Outcomes of vertebroplasty compared with kyphoplasty: a systematic review and meta-analysis. J Neurointerv Surg. 2016;8(6):636–42.
25. Wang H, Sribastav SS, Ye F, Yang C, Wang J, Liu H, Zheng Z. Comparison of percutaneous vertebroplasty and balloon kyphoplasty for the treatment of single level vertebral compression fractures: a meta-analysis of the literature. Pain Physician. 2015;18(3):209–22.

CT-/X-Ray-Guided Augmentation Techniques in Sacrococcygeal Spine Augmentation

6

Todd S. Miller, Allan L. Brook, Joshua A. Hirsch, Ronil Chandra, A. Orlando Ortiz, and Luigi Manfrè

6.1 Introduction

Sacral insufficiency fractures are typically diagnosed in a frail elderly patient who experiences pain preventing or limiting ambulation [1–7]. Typically located in the sacral ala or S2 vertebral body, they may result from generalized osteopenia, focal osteolysis from cancer metastasis (after pelvic radiation treatment), or trauma. They may occur spontaneously or after minor trauma.

The diagnosis is often delayed because of clinical unfamiliarity and the fact that most transverse or nondisplaced sacral fractures are not clearly identified on conventional radiology [8–12]. Specifically, they often require advanced imaging techniques such as CT, MR imaging, or nuclear bone scintigraphy for accurate diagnosis and characterization. In addition, clinicians are more attuned to the possibility of lumbar spinal fractures, and sacral fractures may not be considered. Thus, not surprisingly, diagnosis may be delayed by weeks, leading to complications related to sacral fragment dislocation (Fig. 6.1a–c).

T.S. Miller, M.D. (✉) • A.L. Brook, M.D.
Montefiore Medical Center, Albert Einstein College of Medicine, Bronx, NY, USA
e-mail: tmiller@montefiore.org; abrook2214@aol.com

J.A. Hirsch, M.D. • R. Chandra, M.D.
Massachussets General Hospital, Boston, MA, USA
e-mail: hirsch@snisonline.org; ronilvchandra@gmail.com

A.O. Ortiz, M.D., M.B.A.
Clinical Professor of Radiology, State University of New York, Stony Brook, NY, USA

Department of Radiology, Winthrop-University Hospital, Mineola, NY, USA

L. Manfrè, M.D.
Minimal Invasive Spine Therapy, Cannizzaro Hospital,
Catania, Italy
e-mail: lmanfre@me.com

L. Manfrè (ed.), *Vertebral Lesions*, New Procedures in Spinal Interventional Neuroradiology, DOI 10.1007/978-3-319-52634-8_6

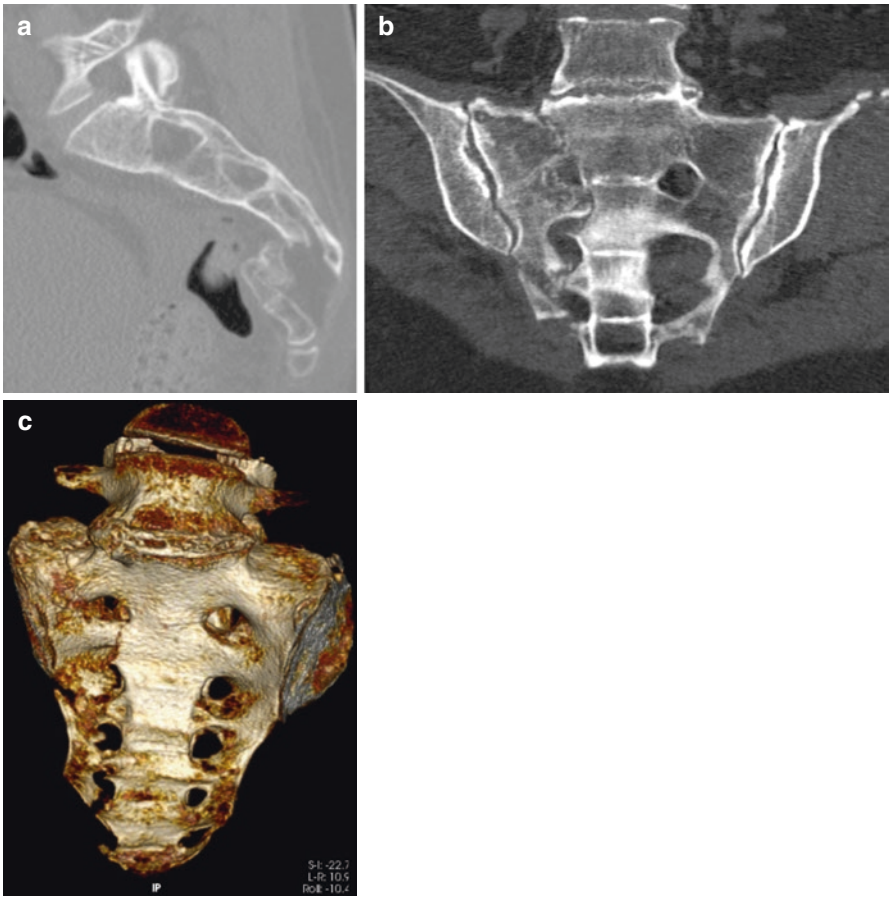

Fig. 6.1 Two cases of sacral fragment dislocation related to misdiagnosis. In patient on the left (**a**), the S4–S5 body of the sacrum has been dislocated anteriorly, due to the patient being allowed to sit in a chair without precautions. In the patient on the right (**b**, **c**), S1 and S2 anterior root compression related to sacral foramina narrowing secondary to a body-to-left wing dislocation

Historically, treatment has relied on a short period bed rest and analgesics, which is appropriate for most patients. However, a small number of patients may be refractory to medical management and require prolonged bed rest and escalating opioid analgesia. This may generate the well-known problems associated with bed rest in an elderly debilitated population, such as pneumonia, urinary tract infections, muscle wasting, and thrombophlebitis, and may also exacerbate underlying osteoporosis [13]. In addition, some patients may experience opioid side effects such as change in mental status, respiratory depression, constipation, and medication dependence.

Several alternatives for treatment exist. These include open surgical fixation, which is generally reserved for patients with displaced fractures or fracture/dislocations, as well as percutaneous cement fixation [12, 14–20]. This chapter will focus on treatment of sacral fractures with percutaneous sacroplasty using either fluoroscopic

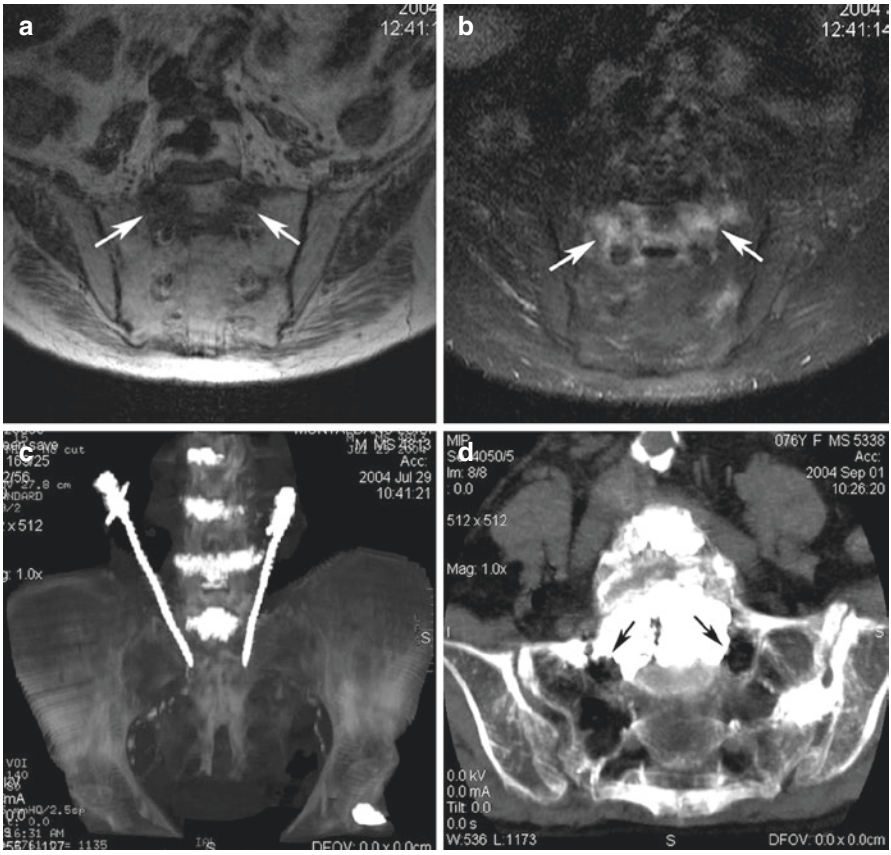

Fig. 6.2 Sacral osteoporotic symmetric fractures at the body-to-wing area S1–S2. On coronal T1SE (**a**) and T2STIR (**b**) images, abnormal signal intensity can be depicted through the joining area between the wing and the body of S1, while a crossover fracture line is appreciated at S1 body, just above the foramina area. Sacroplasty was performed introducing the needles bilaterally (**c**), and complete cementation of the fracture was performed (**d**)

or CT guidance. While no randomized controlled trials have been performed to assess sacroplasty, multiple cohort studies have reported reductions in pain scores and analgesic requirements, with minimal associated morbidity [7, 14, 17, 21, 22].

Although there is a vast clinical experience using cement to treat fractured vertebrae, the anatomy of the sacrum is far more complex which creates special challenges for treatment. The bone has a somewhat curved pyramidal appearance and is traversed by a central canal as well as neural foramina. Fracture lines in osteoporotic cases are typically of two varieties: parallel to the sacroiliac joints and traversing the horizontal bridges between the parallel columns of the neural foramina. [23] The fracture lines can be symmetrical (Figs. 6.2 and 6.3) or asymmetrical (Fig. 6.4). There may be multiple interconnected fractures or several distinct areas of fracture. The cortex may not be disrupted, or there may be frank cortical disruption or extensive tumor-related bone destruction. This is important to appreciate as cortical or

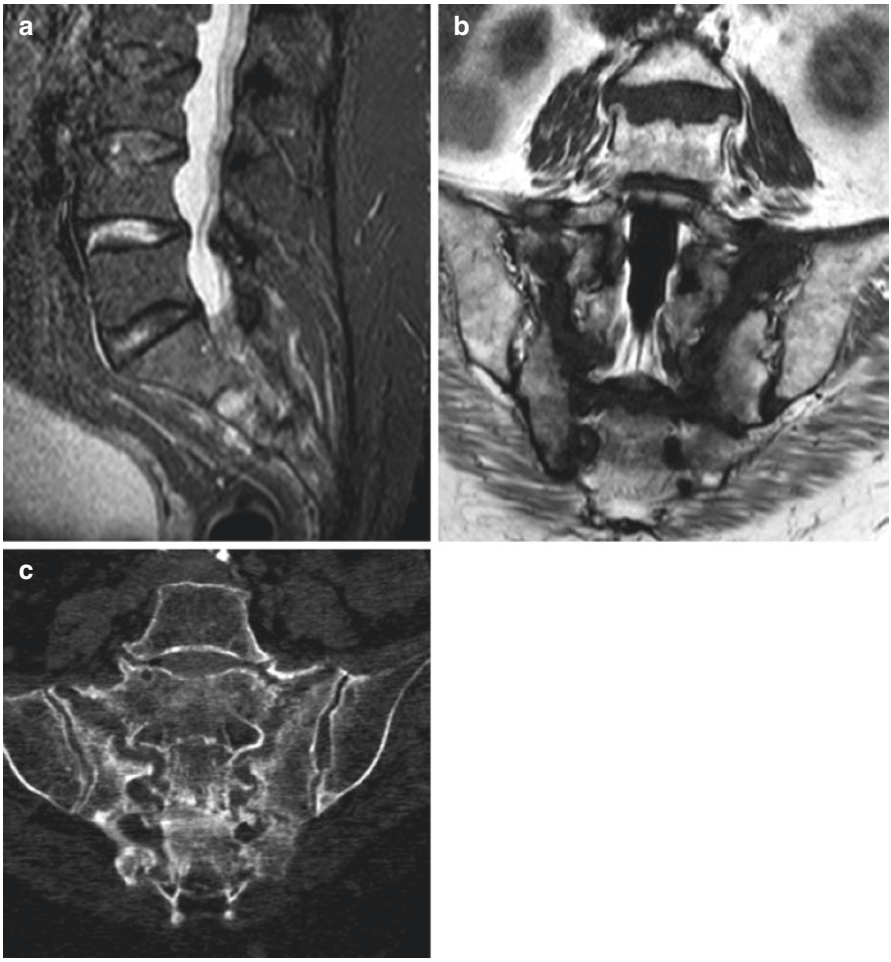

Fig. 6.3 Complete symmetrical fracture of the sacrum. On conventional midline sagittal T2STIR image, the fracture can be missed as small focal signal abnormality can be appreciated only inside the sacral body (**a**). Coronal T1SE sacral MR pictures show dramatic complete symmetrical fractures of the sacral wings (**b**). Bilateral fragment dislocation appreciated on 2D recon CT image demonstrates severe bilateral foraminal stenosis (**c**)

bone destruction is a risk factor for cement leakage. All extraosseous cement extravasation, in particular into the central canal, sacral neural foramina, sacroiliac joint, and vascular structures, should be avoided. Moreover, as well as for the rest of the spine, the sacrum can be affected by primary or secondary malignancies, with anarchic osteolysis of the wings and/or the body of the sacrum, increasing the risk of extra-sacral leakage.

In addition to sacral-related pain, pain originating from the coccyx is sometimes hard to delineate from that arising from the sacrum. Coccydynia accounts for less

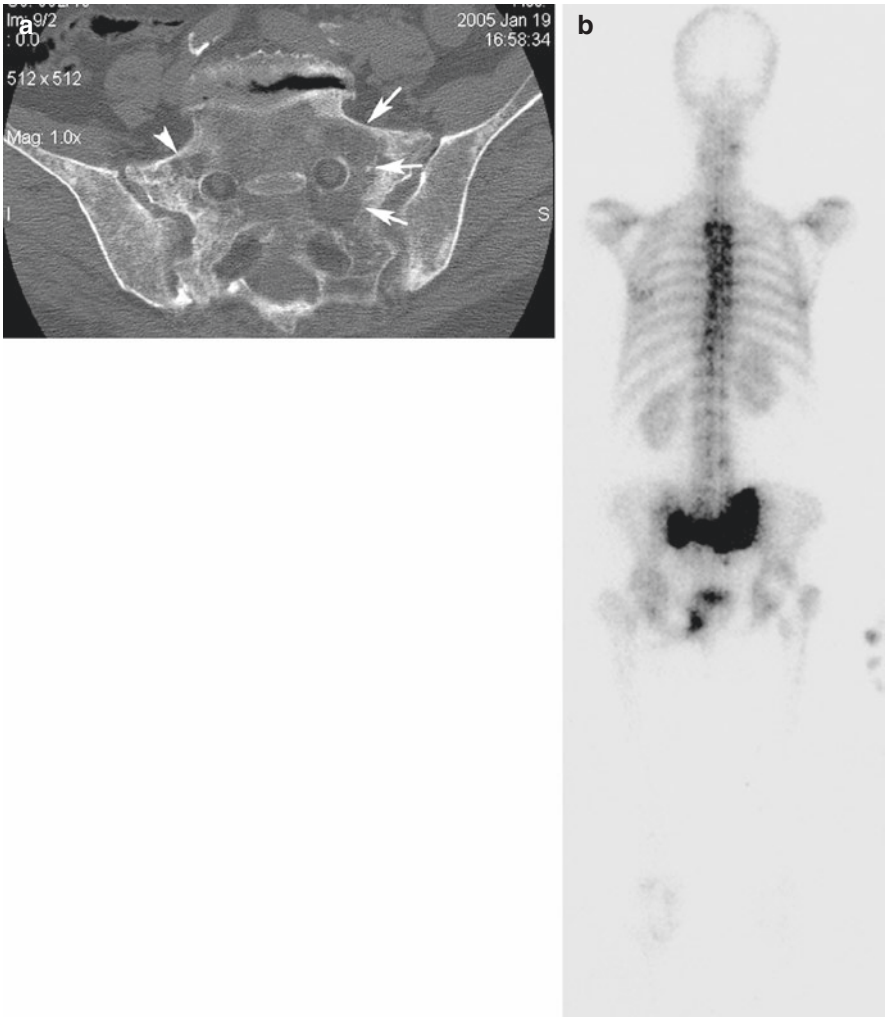

Fig. 6.4 Asymmetrical fracture of the sacrum. On coronal CT recon image on the left (**a**) and coronal bone scanning on the right (**b**), complete sacral fracture on the left side and small right-sided fracture can be appreciated

than 1% of all the causes of low back pain. A coccygeal fracture and/or subluxation can be extremely hard to diagnose, and even harder to tolerate for patients, causing drug abuse and psychological consequences (Figs. 6.5 and 6.6). Local anesthetic and steroid infiltration can solve the pain temporarily in 59% of cases, while manipulation and injection in 85%: unfortunately approximately 1/3 of the patients do not experience a stable pain solution [24]. Surgical coccygectomy can be proposed, but complications have been reported in ¼ of patients. [25]

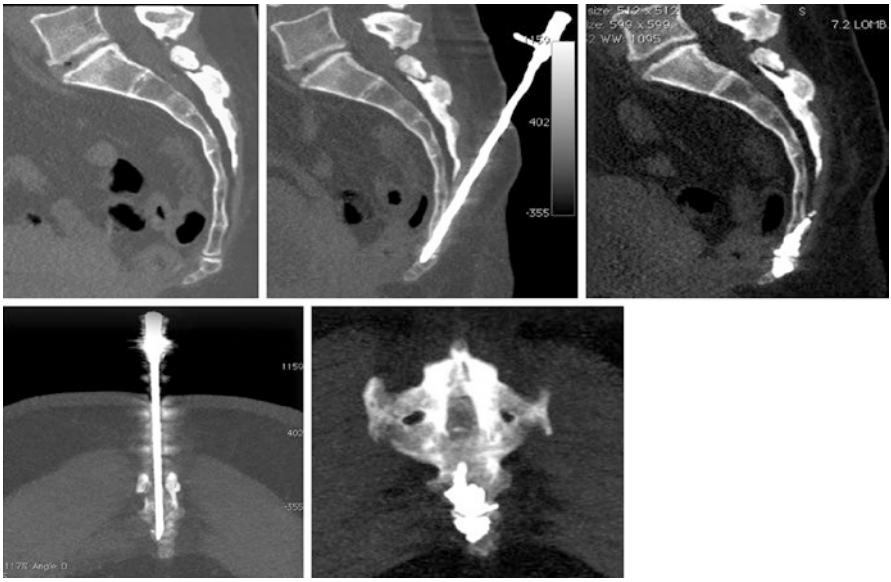

Fig. 6.5 Coccygeal subluxation in a 34-year-old woman. On sagittal 2D CT scan (*top left*), detachment of the coccyx from the sacrum is appreciated. To perform coccygeoplasty, a 13G Jamshidi needle has been introduced through the S4–S5 body directly into the coccyx (*top middle*, *left down*), and 2–3 cc of PMMA has been injected, re-attaching the coccyx to the sacrum (*top right* and *down right* images)

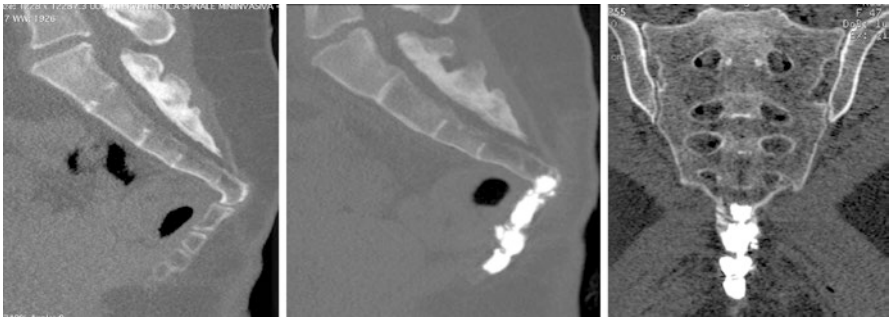

Fig. 6.6 Severe coccyx subluxation of very long coccygeal bone. On the left, several subluxation of coccygeal vertebra can be appreciated. On the right, complete PMMA bridge reconnecting the coccyx to the sacrum can be appreciated on sagittal (*middle*) and (*right*) scans

6.2 Patient Selection

Sacroplasty is indicated for the treatment of symptomatic/painful sacral fractures in the subset of patients where medical management has failed to provide pain relief [17]. Sacroplasty may be performed for primary or metastatic neoplasms of

the sacrum or benign cystic lesions of the sacrum such as aneurysmal bone cysts failing to respond to medical management [17, 26, 27]. Overall, 4 weeks is a reasonable trial of medical management, although earlier intervention is often considered for patients who are hospitalized for severe pain requiring intravenous analgesia.

Patient selection is critical in planning any image-guided intervention. It is important to recall that the natural history of most sacral fractures is benign and they tend to heal on their own. The population at risk for sacral fractures typically has severe or focal osteoporosis and is therefore at risk for delayed or failed healing. Treatment with appropriate osteoporotic therapy is essential. The practitioner must consider a particular patient's pain duration and intensity when considering treatment options. This decision becomes most straightforward for a patient who was able to ambulate independently and can no longer enjoy this freedom due to pain limitations. For patients who are able to ambulate but have new limitations on their ability to ambulate, the decision becomes less clear. As all procedures may generate complications, pain medication, time, and the hopes of healing may be the best option for some patients. However, if the pain medication requirements are too significant, or the patient's pain limits their ability to perform their daily activities, or pain persists beyond a tolerable time span, these patients may also be appropriate candidates for cement augmentation therapy. In those patients with persistent coccygodynia, with no significant improvement after conservative therapy, coccygeoplasty is an option (Figs. 6.5 and 6.6).

6.3 Considering Additional Pain Generators

It is important to note that patients with painful sacral fractures typically have multiple additional underlying pain generators [28]. The intense pain from the fracture may mask chronic pain or other new pains caused by the event that incited the initial sacral fracture. It is possible that a patient will have residual pain even with the most technically successful procedure. Additional interventions may be required to treat underlying spondylosis symptoms when unmasked after a successful sacral fracture treatment.

6.4 Pre-procedure Planning

6.4.1 History and Physical

Planning begins with a complete history and physical examination. As with all image-guided pain interventions, it is important to correlate the imaging findings with the patient's pain symptoms. This can be challenging for patients with intense pain, as they will have limited ability to cooperate for an examination. It is not unusual for a patient to resist any movement with a complete sacral fracture.

6.4.2 Clinical/Laboratory Assessment

Thorough review of clinical data is also important to exclude concurrent infection such as pneumonia or urinary tract infection. Identification of coagulopathy, thrombocytopenia, or metabolic abnormalities that would increase the risks of the planned procedures is also important. Thorough evaluation for the use of anticoagulants is a discussion that should be had with the care team in order to weigh the risks and benefits of discontinuing certain agents should this become necessary. As the use of prophylactic antibiotics periprocedurally is a best practice to limit the risk of infection, it is important to elicit an allergy history. There are only a few absolute contraindications to sacroplasty: active systemic infection, uncorrectable bleeding diathesis, insufficient cardiopulmonary health to safely tolerate sedation or general anesthesia, and known allergy to bone cement. Information relevant to each of these should be obtained during patient selection.

6.4.3 Imaging

Most patients being considered for sacroplasty have had plain X-rays. Although of limited use to detect sacral fractures, they should be reviewed to detect additional pelvic or hip fractures that may be overlooked in bedbound patients with distracting injuries. The gold standard test used to detect acute fractures of the spinal axis is MRI with T1-weighted sequences and short-tau inversion recovery (STIR) or T2-weighted fat saturation sequences that identify bone marrow edema, fracture lines, and neoplastic lesions. In osteoporotic fractures, MRI scan generally demonstrates diffuse signal abnormalities along the wing-to-body joining line (JL), in an "H" (when symmetrical fracture occurs) or "half-H" (asymmetrical fracture) shape, suggesting the diagnosis of sacral insufficiency fracture (Figs. 6.2, 6.3, and 6.4). CT scan may show nondisplaced fractures, and occasionally fractures that are weeks old may show sclerotic changes around fracture lines. Although CT is less sensitive than MRI in demonstrating acute sacral fracture, it remains crucial for a pre-op planning by demonstrating fracture dislocation and sacral foramina involvement which is a condition increasing the risk of PMMA extravasation (Figs. 6.1b and 6.3c). CT enhances the ability to delineate blastic from lytic masses identified on MRI. If an MRI is not possible, bone scans may demonstrate recent fractures with increased radiotracer uptake. Correlation with history is important to avoid missing a fracture if the bone scan is performed too early in the course of healing in a severely osteoporotic patient. SPECT or SPECT-CT imaging is useful to confirm anatomic localization of radiotracer uptake in the complex sacral anatomy.

6.5 Technique

6.5.1 Consent

Ideally an informed consent conversation should take place with the patient and their involved family. This is a good opportunity to fully explain and set expectations regarding pain relief and the potential of additional underlying pain generators that may be unmasked after a successful procedure [28]. The standard risks of bleeding or infection apply to all patients. Particular attention should be paid to those with underlying diabetes. A thorough clinical review to exclude common infection sources such as pneumonia and UTI is required. The use of periprocedural antibiotics as prophylaxis is a recognized best practice.

The possible complication of nontarget cement deposition with liquid agents is perhaps more likely in the sacrum than with vertebral augmentation. The complex anatomy can make nontarget cement deposition more difficult to detect. It is not unusual for overall cement volumes to be higher than those for lumbar vertebra as it is common to use multiple needles for cement injection. In frail patients, the subcutaneous tissues overlying the sacrum are quite thin, and the risk of a cement tail causing irritation is higher than in the lumbar spine. This unusual outcome should be anticipated as a potential complication and explained in advance [29].

6.6 Technique

6.6.1 CT vs. Fluoroscopic Guidance

When using fluoroscopy as a guidance modality, the complex sacral anatomy provides challenges for the operator [30]. The AP view is most clear. This allows for the operator to avoid the sacral neural canal as well as the neural foramina and sacroiliac joints. However, the lateral view can be troublesome in the pelvis. In larger patients, limited X-ray penetration may prevent adequate visualization of ventral cement. A small cement aliquot entering a venous structure may be difficult to detect. The contours of the sacrum may also make detection of extraosseous cement confusing or difficult. The benefits of real-time visualization of cement injection are to be balanced with the patient anatomy, the planned approach, and the limitations of the specific fluoroscopic equipment. If there is adequate visualization of the ventral surface of the sacrum, the procedure can be performed safely with fluoroscopic guidance.

CT guidance can help overcome the limits of fluoroscopy for optimal visualization of sacral anatomy during access with needle trocars and while injecting cement [30]. The canal and foramina as well as surrounding vascular structures can be

readily seen. This is balanced by the need to limit radiation dose and procedure time with limited anatomic coverage and intermittent scanning that can limit the detection of nontarget cement deposition out of the field of imaging. Utilizing small cement aliquots between images and thicker cement can mitigate this limitation. CT guidance provides the most flexibility with needle positioning and targeting visible fractures, centering needles in the midportion of lytic areas, and may be optimal for patients with complex cancer-related fractures and tumor deposits. Many metastatic lesions destroy the standard bony anatomy that guides safety and accuracy on plane films and makes CT beneficial for use in patients with infiltrating lesions.

6.7 Technique

6.7.1 Patient Positioning

For procedures using both CT guidance and fluoroscopic guidance, the patient is placed in the prone position on the table. This may be the most difficult and painful portion of the procedure. If available, partnering with an anesthesiologist and administration of intravenous analgesia and sedation may allow safe and comfortable patient transfer from supine to prone position with minimal physiologic stress. Proper cushioning and support is important for the safety and comfort of the patient. Thorough prepping and skin cleansing with antimicrobial scrubs is particularly important in this procedure given the proximity to the perineum. Sacroplasty can be performed using general anesthesia, monitored anesthesia care, intravenous anesthesia, intravenous sedation, and analgesia. Accurate and copious local anesthetic administration is vital to minimize pain during the procedure as to maximize post-procedure comfort. Collaboration among the operator, the anesthesiologist, and the patient helps determine the best anesthesia plan.

6.8 Technique

6.8.1 Cement and Needles

The minimum tools that are required for sacroplasty include bone needles (13, 11, 10.5, or 10 gauge) and medical-grade barium-opacified (at least 28% by weight) acrylic bone cement. The bone needles are usually 10 cm in length, but the approach may warrant the use of a longer needle (such as a 15-cm-length bone needle) [31]. The cement can be injected with small 1 mL handheld syringes, pre-filled cement delivery cannulas designed for coaxial use with the bone needle, or a commercially available cement delivery system. Recently, new biomaterials have been tested for bone regeneration, looking for the ideal tool to repair the human bone: new osteoconductive materials have been used to fix bone defects in osteoporotic patients and in neoplastic fractures (Fig. 6.7).

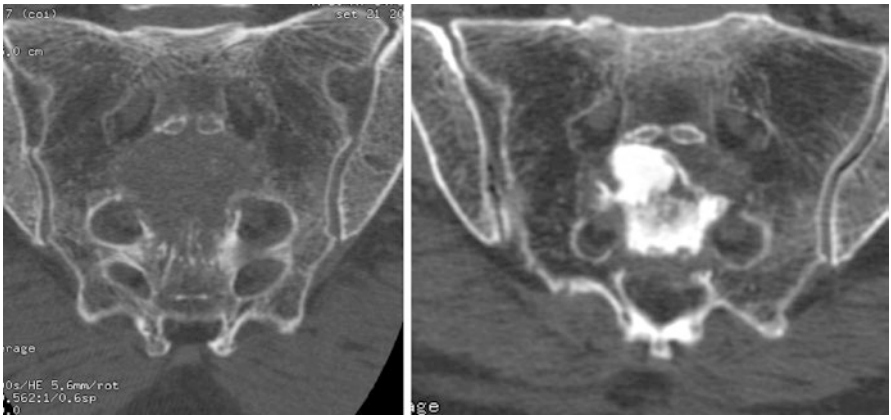

Fig. 6.7 Bone regeneration in a patient affected by multiple myeloma of the sacrum using osteoconductive injectable biomaterial (Cerament®). On the left, large osteolytic lesion mainly involving the body of S2 can be appreciated, despite the good pharmacological control of the disease. On the right, a dense compact bone regeneration can be appreciated after 45 days inside the area of the disease, recreating the original shape of sacral foramina

6.9 Technique

6.9.1 Planning and Approach

The approach for sacroplasty is determined by the location of the lesion. The goal is to place the bone needle adjacent to or within the fracture line or within a painful space-occupying sacral lesion. Given that the most frequent indication for this procedure is a painful osteoporotic sacral insufficiency fracture, a posterior approach is typically utilized [31].

6.9.2 Technique, Fracture Geometry

The fracture lines are commonly located within the sacral ala and are almost always oriented parallel to the ipsilateral sacroiliac joint in the transverse plane and course along the vertical axis of the sacrum. Bilateral sacral insufficiency fractures are more common than unilateral fractures [17]. The options for needle trajectory in these cases include horizontal, oblique, or longitudinal orientations. One or more needle placements may be required when the bone needle is placed along a horizontal trajectory relative to the fracture plane in the short axis of the sacrum [31].

When neoplastic osteolysis occurs, the goal of PMMA injection is completely restoring the sacral morphology, respecting sacral anatomy, and obtaining symmetrical bilateral stress-load through the iliac wings (Fig. 6.8a–d).

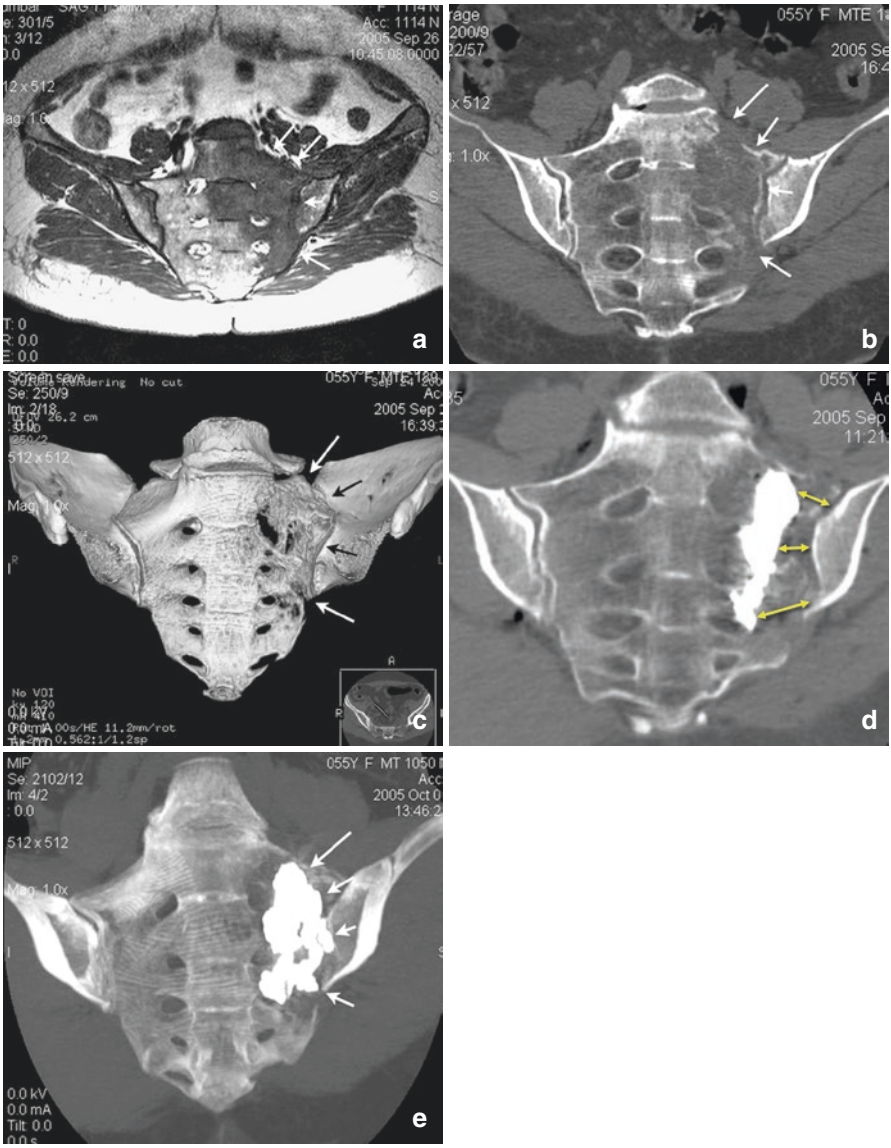

Fig. 6.8 Left wing and S1–S2 sacral body lymphoma. On coronal MR T1SEw scan (**a**), abnormal signal intensity of the left hemisacrum is appreciated. 2D (**b**) and 3D (**c**) coronal CT image demonstrates large osteolysis of the left sacrum. First PMMA injection was considered insufficient from a biomechanical point of view, according to residual lytic gap between the intrasacral PMMA and the iliac bone (*arrows* in **d**). A second PMMA injection was performed, to completely restore the sacroiliac joint (**e**)

6.10 Technique

6.10.1 Skin Puncture and Needle Targeting

The skin puncture site is anesthetized with a local anesthetic agent, and a small skin incision is made in order to facilitate bone needle insertion. A narrow gauge spinal needle is used to administer the anesthetic agent down to the level of the periosteum. This important step allows a greater margin of safety with more local analgesia allowing the operator to use less intravenous sedation for these typically frail patients [17]. Again, the extent and severity of the fracture may dictate how many bone needles are required with this short axis approach. In the majority of these cases, however, the procedure can be safely performed with a single needle (for each side) placed along a horizontal trajectory at the level of the sacral ala [31]. The needle tip is advanced into the anterior aspect of the sacral ala, within 10 mm of the anterior sacral cortex with a two-handed technique to prevent inadvertent "plunging" through the soft osteoporotic bone, taking great care not to breach the anterior sacral cortex (where vascular structures and soft tissue organs are located) or the lateral aspect of a neural foramen.

For the occasional fracture with a horizontal component that extends into and involves the S2 vertebra, the fracture can be approached from an oblique longitudinal trajectory or, rarely, a horizontal trajectory that courses through the fibrous portion of the sacroiliac joint (Fig. 6.9a–b).

A curved bone needle may also facilitate safe access to S1 component of the fracture. Some operators have opted to treat only the alar component of these fractures and have, anecdotally, reported a successful treatment [31]. Universal agreement does not exist about the need to treat the horizontal component of sacral fractures, and these require a more difficult approach to treatment. The weight bearing and shear forces of the sacrum in the midline are less well understood. As such, practice patterns differ.

In cases of sacral malignancy, the needle approach is chosen according to the best way to reach the core of the osteolytic area. Generally, a trans-alar route is performed to introduce the needle, paying attention to avoid the local sacral nerve (Fig. 6.10a–d). In patients with massive osteolysis, the procedure can be performed in different times/staged according to the area to be restored (Fig. 6.11a–f).

In the case of coccygeoplasty, the fragment should be aligned with the rest of the sacral axis: a small gauge needle (13G) is introduced through the midline sacral axis, penetrating through the coccyx, paying attention to fragments and areas of bone marrow edema or cystic changes (Figs. 6.6 and 6.7).

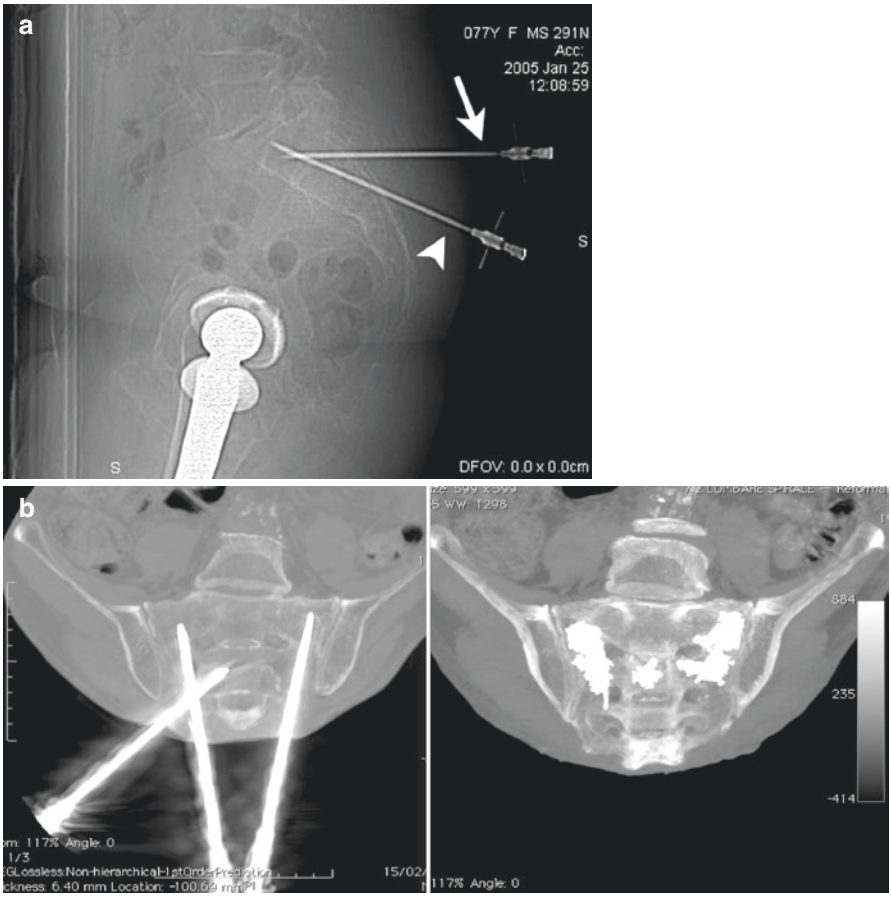

Fig. 6.9 Bilateral symmetric sacral fracture: different needle approaches on X-ray and CT guide. A couple of needles are oriented along the main axis of the sacrum, to fix the body-to-wing fractures, while a direct transversely oriented needle is centered into the body of S2 (**a**, **b** *left*). After PMMA injection, complete sacroplasty of the "H-shaped" fracture is obtained (**b** *right*)

6.11 Technique

6.11.1 Cement Injection

Once the bone needles are in place and any biopsies have been performed, acrylic bone cement is prepared and carefully injected. Cement injection requires meticulous imaging surveillance. Cement is injected in small aliquots of 0.3–0.5 mL, keeping in mind that many commercially available injection systems allow cement to flow from built-up pressure in the injector after the operator has stopped actively advancing the plunger. During cement injection, the bone needle cannula may be gradually withdrawn/repositioned in order to allow for cement deposition along the

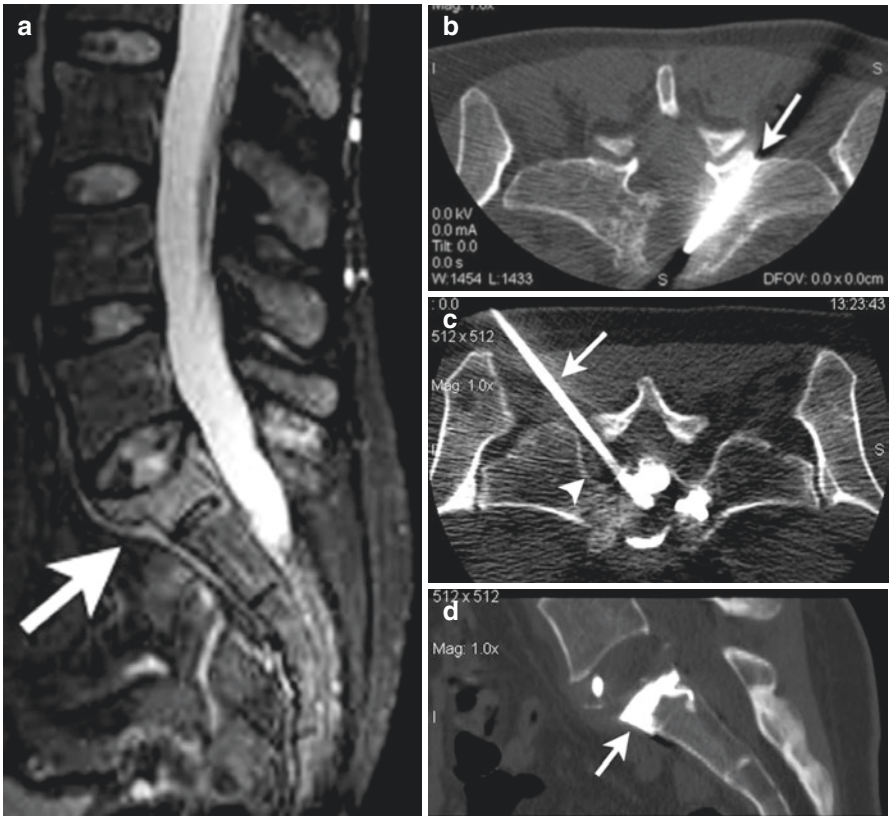

Fig. 6.10 S1 level breast cancer in a 41-year-old woman. On T2STIR MR scan, infiltration of the S1 vertebral body associated with superior endplate collapse can be appreciated (**a**). The needle can reach the S1 body directly through the right sacral wing (**b**) or via posterior I sacral foramina (**c**) reaching the same target and obtaining total cementation of the area (**d**)

intended destinations. The target for cement deposition is either in or near the fracture line or within the sacral mass. Endpoints for the termination of cement injection include adequate filling of the target lesion, cement approaching a sacral foramen or the spinal canal, cement extension outside of the sacrum (presacral or posterior sacral, or into the sacroiliac jonts), or cement extension into a parasacral vein with the potential for formation of a cement embolus [32]. A slow injection technique with specific stopping and observation points will increase the safety and efficacy of the procedure. If intraforaminal PMMA leakage occurs, the injection is stopped. The beveled needle can be rotated outside the foraminal area and pulled out a few millimeters. Then the PMMA injection can be restarted. Care must be taken to ensure that a tail does not form along the subcutaneous needle tract. These can be located where they cause irritation due to pressure from sitting or supine lying. This can be achieved by using coaxial pre-filled cement cannulas or by carefully using a trocar to push the residual cement from the cannula bore into the sacrum. If these

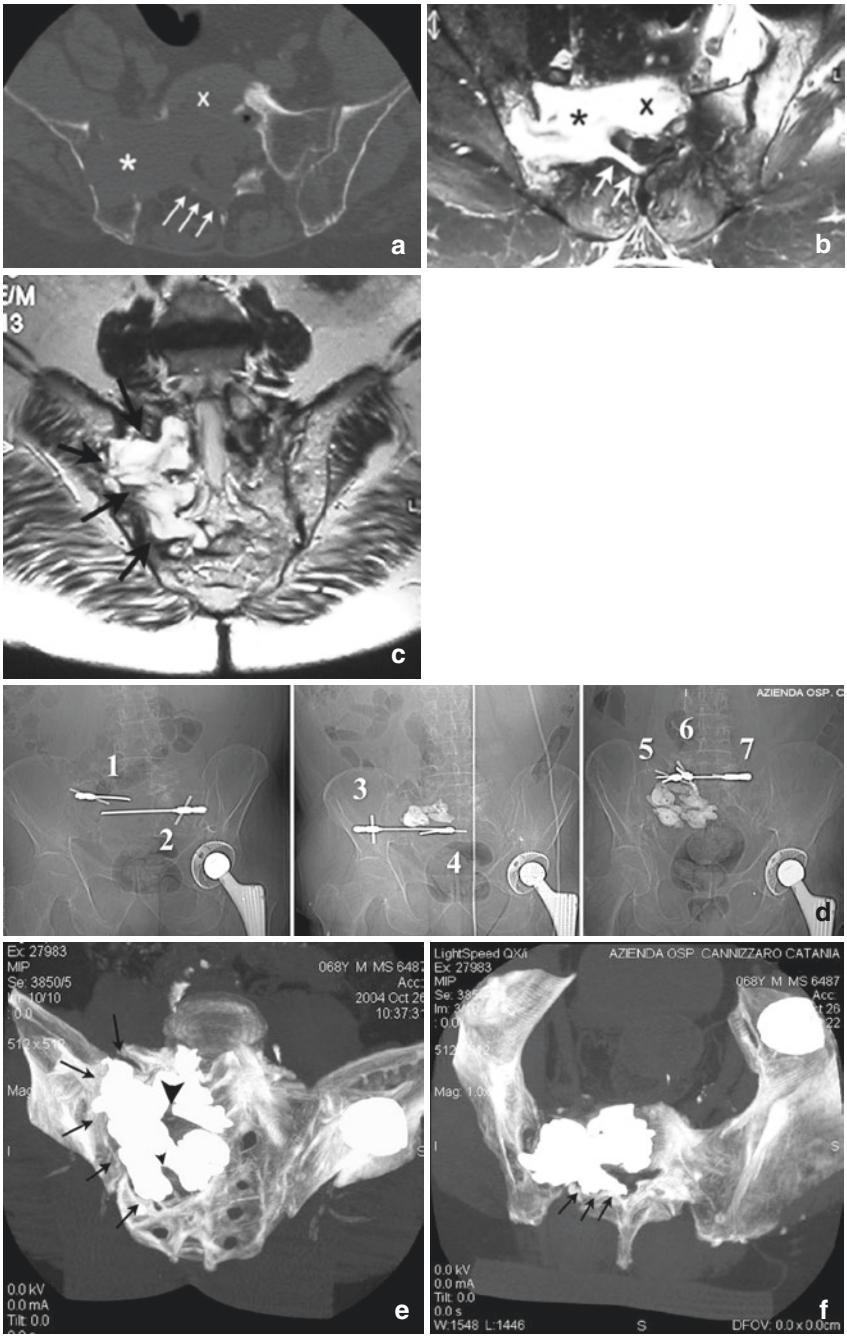

Fig. 6.11 Severe sacrum osteolysis related to multiple myeloma disease in a 58-year-old male. On axial CT (**a**), MR (**b**), and coronal (**c**) scans, full involvement of the right sacral wing, iliac bone, S1–S3 sacral body, as well as the posterior right wall of the sacral canal can be appreciated. A three-stage treatment was planned, using seven needles. After PMMA injection, full reconstruction of the sacrum and right iliac bone and recreation of the I and II right sacral foramina (**e**) and sacral canal (**f**) can be appreciated

are unavailable, the technique of waiting and allowing the cement to solidify within the cannula prior to rotating the bone needle in order to remove the uninjected cement with the bone needle prior to removal is an option. Care must be taken to limit the force used to remove the cannula in patients with demonstrated bone insufficiency.

In coccygeoplasty, the PMMA is slowly injected while simultaneously removing the needle from the fracture/defect, trying to create an artificial bridge that will create coccyx fixation [31].

6.11.2 Post-procedure and Follow-Up Care

After removal of the bone needle, the operator should firmly compress at the skin entry site for a few minutes prior to covering the site with a sterile dressing. This maneuver tends to minimize excess bleeding, swelling, and irritation at the puncture site(s). Carefully coordinating a team transfer of the patient to the stretcher occurs immediately after the procedure, where they should recover for 2–3 h. Additional analgesia may be required to alleviate immediate post-procedure pain, which usually resolves over 24–72 h. Most patients can be mobilized after 3 h, depending on their physical and clinical condition, and potentially discharged later the same day. If there is any clinical deterioration, cross-sectional imaging should immediately be performed. Post-procedure follow-up is critical. Pain and mobility levels and the need for analgesia should be assessed both in the short term (3–4 weeks) and longer term to assess treatment effectiveness.

6.12 Complications

As with any percutaneous procedure, infection and bleeding can occur. The needles used can injure any structure they transverse or puncture. Positioning the patient with severe osteoporosis can lead to new insufficiency fractures. Allergies to any medicines or materials must be recognized early and treated appropriately. Cement extravasation must be avoided and, if it occurs, recognized early and followed for clinical consequences. Experienced anesthesia teams are a necessity for patient safety. Treatment of the wrong segment or side of the sacrum or coccyx must be avoided. Displaying preprocedural imaging in the treatment room and preprocedure team communication is the standard of care.

6.13 Literature Review

A review of the medical literature on sacroplasty shows that this is a technically feasible procedure. The success rate of this procedure, in terms of pain relief, as demonstrated in case reports and patient series is extremely favorable [7, 14, 17, 19, 21, 22]. The incidence of major complications is rare and a review of the

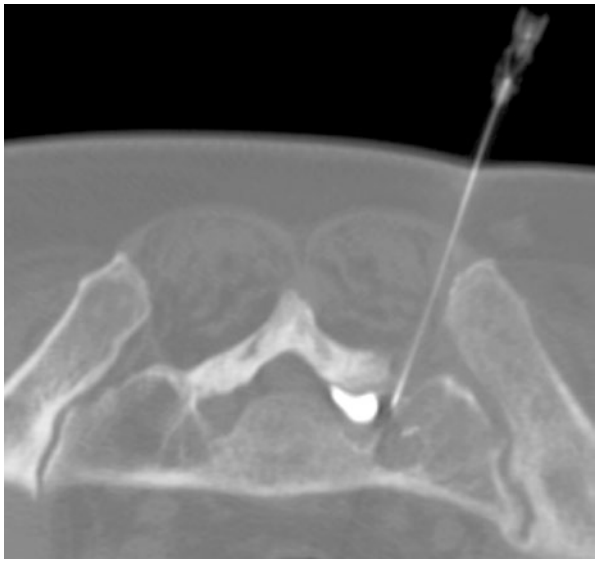

Fig. 6.12 Intraforaminal leakage in sacroplasty. Minimal PMMA intraforaminal leak can be appreciated on the right side, with painful sciatica. Transforaminal steroid injection was successful in resolving the temporary pain of the patient

literature has not identified any mortality nor permanent major morbidity. Rarely, surgical decompression has been performed for cement leakage into the central canal or sacral foramina [14, 33]. Sometimes the sciatica secondary to temporary irritation of the nerve by the PMMA can be controlled with simple steroid injection (Fig. 6.12). Sacroplasty helps to provide sacral stabilization and enables the patient to tolerate weight bearing after the procedure. The mechanism of pain relief is likely similar to that observed in augmented thoracic and lumbar vertebra and fracture stabilization through reduced micromotion with activities such as weight bearing. Indeed, the application of biomechanical engineering models with finite element analysis does show reduction of stress and micromotion at fracture sites following sacroplasty [11]. There appears to be no correlation between pain relief and the volume of injected cement. [31] Additionally, sacroplasty does not appear to restore the strength or stiffness of the sacrum as shown in biomechanical evaluations of a cadaveric sacrum [34]. With these ideas in mind, successful treatment with minimum complications may be achieved by injection of small volumes of cement and avoiding any extraosseous cement leakage.

Conclusions

Sacral insufficiency fractures are a frequent source of pain and disability in the elderly population, and diagnosis is often delayed. For the small subset of patients with painful fractures or sacral tumors refractory to medical therapy, sacroplasty offers a safe and effective treatment option.

References

1. Lourie H. Spontaneous osteoporotic fracture of the sacrum. An unrecognized syndrome of the elderly. JAMA. 1982;248(6):715–7. doi:10.1103/PhysRevD.15.2752.
2. Leroux JL, Denat B, Thomas E, Blotman F, Bonnel F. Sacral insufficiency fractures presenting as acute low-back pain. Biomechanical aspects. Spine. 1993;18(16):2502–6.
3. Grasland A. Sacral insufficiency fractures. Arch Intern Med. 1996;156(6):668. doi:10.1001/archinte.1996.00440060096012.
4. Finiels H, Finiels PJ, Jacquot JM, Strubel D. Fractures of the sacrum caused by bone insufficiency. Meta-analysis of 508 cases. Presse Med. 1997;26(33):1568–73.
5. Lin J, Lachmann E, Nagler W. Sacral insufficiency fractures: a report of two cases and a review of the literature. J Womens Health Gend Based Med. 2001;10(7):699–705.
6. Hosey RG, Fernandez MM, Johnson DL. Evaluation and management of stress fractures of the pelvis and sacrum. Orthopedics. 2008;31(4):383–5.
7. Gupta AC, Yoo AJ, Stone J, et al. Percutaneous sacroplasty. J Neurointerv Surg. 2012;4(5):385–9. doi:10.1136/neurintsurg-2011-010136.
8. Diel J, Ortiz O, Losada RA, Price DB, Hayt MW, Katz DS. The sacrum: pathologic spectrum, multimodality imaging, and subspecialty approach 1. Radiographics. 2001;21(1):83–104. doi:10.1148/radiographics.21.1.g01ja0883.
9. Ahovuo JA, Kiuru MJ, Visuri T. Fatigue stress fractures of the sacrum: diagnosis with MR imaging. Eur Radiol. 2004;14(3):500–5. doi:10.1007/s00330-003-1989-2.
10. Blake SP, Connors AM. Sacral insufficiency fracture. Br J Radiol. 2014; doi:10.1259/bjr/81974373;issue:issue:10.1259/bjr.2004.77.issue-922;page:string:Article/Chapter.
11. Lyders EM, Whitlow CT, Baker MD, Morris PP. Imaging and treatment of sacral insufficiency fractures. Am J Neuroradiol. 2010;31(2):201–10. doi:10.3174/ajnr.A1666.
12. Galbraith JG, Butler JS, Blake SP, Kelleher G. Sacral insufficiency fractures: an easily overlooked cause of back pain in the ED. Am J Emerg Med. 2011;29(3):359.e5–6. doi:10.1016/j.ajem.2010.04.015.
13. Jensen ME, McGraw JK, Cardella JF, Hirsch JA. Position statement on percutaneous vertebral augmentation: a consensus statement developed by the American Society of Interventional and Therapeutic Neuroradiology, Society of Interventional Radiology, American Association of Neurological Surgeons/Congress of Neurological Surgeons, and American Society of Spine Radiology. 2007;18:325–30. doi:10.1016/j.jvir.2007.01.014.
14. Pereira LP, Clarençon F, Cormier É, et al. Safety and effectiveness of percutaneous sacroplasty: a single-centre experience in 58 consecutive patients with tumours or osteoporotic insufficient fractures treated under fluoroscopic guidance. Eur Radiol. 2013;23(10):2764–72. doi:10.1007/s00330-013-2881-3.
15. Nebreda C, Vallejo R, Aliaga L, Benyamin R. Percutaneous sacroplasty and sacroiliac joint cementation under fluoroscopic guidance for lower back pain related to sacral metastatic tumors with sacroiliac joint invasion. Pain Pract. 2010:564–9. doi:10.1111/j.1533-2500.2010.00439.x.
16. Naderi S, Ilaslan H, Aslan A, Koc ON, Dalkilic T. Sacroplasty: report of three cases. Turk Neurosurg. 2010;20(3):418–22. doi:10.5137/1019-5149.JTN.2676-09.3.
17. Kortman K, Ortiz O, Miller T, et al. Multicenter study to assess the efficacy and safety of sacroplasty in patients with osteoporotic sacral insufficiency fractures or pathologic sacral lesions. J Neurointerv Surg. 2013;5(5):461–6. doi:10.1136/neurintsurg-2012-010347.
18. Kang SE, Lee JW, Kim JH, Park KW, Yeom JS, Kang HS. Percutaneous sacroplasty with the use of C-arm flat-panel detector CT: technical feasibility and clinical outcome. Skelet Radiol. 2010;40(4):453–60. doi:10.1007/s00256-010-0959-4.
19. Frey ME, DePalma MJ, Cifu DX, Bhagia SM, Daitch JS. Efficacy and safety of percutaneous sacroplasty for painful osteoporotic sacral insufficiency fractures: a prospective, multicenter trial. Spine. 2007;32(15):1635–40. doi:10.1097/BRS.0b013e318074d4e1.

20. Choi K-M, Song J-H, Ahn S-K, Choi H-C. Therapeutic considerations of percutaneous sacroplasty for the sacral insufficiency fracture. J Korean Neurosurg Soc. 2010;47(1):58. doi:10.3340/jkns.2010.47.1.58.
21. Moussazadeh N, Laufer I, Werner T, et al. Sacroplasty for cancer-associated insufficiency fractures. Neurosurgery. 2015;76(4):446–50. doi:10.1227/NEU.0000000000000658.
22. Dougherty RW, McDonald JS, Cho YW, Wald JT, Thielen KR, Kallmes DF. Percutaneous sacroplasty using CT guidance for pain palliation in sacral insufficiency fractures. J Neurointerv Surg. 2014;6(1):57–60. doi:10.1136/neurintsurg-2012-010599.
23. Baran S, Hak DJ, Stahel PF, editors. Sacral fractures: current strategies in diagnosis and management. Orthopedics. 2009;32(10):752–7. doi:10.3928/01477447-20090818-18.
24. Perkins R, Schofferman J, Reynolds J. Coccygectomy for severe refractory sacrococcygeal joint pain. J Spinal Disord Tech. 2003;16(1):100.
25. Fogel GR, Cunningham PYI, Esses SI. Coccygodynia: evaluation and management. J Am Acad Orthop Surg. 2004;12(1):49.
26. Nas OF, Kaçar E, Buyukkaya R, Şanal B, Erdogan C, Hakyemez B. Treatment of sacral aneurysmal bone cyst with percutaneous sacroplasty. Spine J. 2016;16(1):e1–2. doi:10.1016/j.spinee.2015.08.005.
27. Gupta AC, Chandra RV, Yoo AJ, et al. Safety and effectiveness of sacroplasty: a large single-center experience. Am J Neuroradiol. 2014;35(11):2202–6. doi:10.3174/ajnr.A4027.
28. Kamalian S, Bordia R, Ortiz AO. Post-vertebral augmentation back pain: evaluation and management. Am J Neuroradiol. 2012;33(2):370–5. doi:10.3174/ajnr.A2775.
29. Mathis JM, Deramond H, Belkoff SM, editors. Percutaneous vertebroplasty and kyphoplasty. New York: Springer; 2006. doi:10.1007/0-387-36083-2.
30. Ortiz AO, Natarajan V, Gregorius DR, Pollack S. Significantly reduced radiation exposure to operators during kyphoplasty and vertebroplasty procedures: methods and techniques. AJNR Am J Neuroradiol. 2006;27(5):989–94.
31. Kortman K, Mathis JM, Ortiz AO. Sacroplasty. In: Mathis JM, Deramond H, Belkoff SM, editors. Percutaneous vertebroplasty and kyphoplasty. New York: Springer; 2006. p. 197–209. doi:10.1007/0-387-36083-2_12.
32. Belkoff SM, Mathis JM, Jasper LE, Deramond H. The biomechanics of vertebroplasty. The effect of cement volume on mechanical behavior. Spine. 2001;26(14):1537–41.
33. Barber SM, Livingston AD, Cech DA. Sacral radiculopathy due to cement leakage from percutaneous sacroplasty, successfully treated with surgical decompression. J Neurosurg Spine. 2013;18(5):524–8. doi:10.3171/2013.2.SPINE12497.
34. Richards AM, Mears SC, Knight TA, Dinah AF, Belkoff SM. Biomechanical analysis of sacroplasty: does volume or location of cement matter? Am J Neuroradiol. 2009;30(2):315–7. doi:10.3174/ajnr.A1358.

CT/X-ray-Guided Techniques in Vertebral Tumors: Radio-ablation

7

Mario Raguso, Marco Morini, Roberto Fiori, and Salvatore Masala

7.1 Introduction

Primary spinal tumors are relatively rare, estimated around 10% of all cancers interesting spine [1]. The spine is instead the most common site of metastasis in patients with cancer: up to 70% of cancer patients develop secondary spinal disease [2]. New cases of spinal tumors are detected in North America with a rate of incidence near to 18000 patients/year [3].

Spinal metastasis usually arise from tumors of the breast, lung, prostate gland, and hemopoietic tissues (e.g., lymphoma or multiple myeloma). In addition, the spinal lesion represents the first symptomatic manifestation of cancer in 12 to 20% of patients [4, 5].

The dorsal and lumbar segments are the most frequently involved, respectively 70% and 20%, compared to those cervical and sacral; in 30% of cases the disease is multi-segmental [4, 6]. Spinal metastasis, like all spinal tumors, are classified according to their origin, clinical and histological behavior (malignant or benign), and anatomical distribution: secondary lesions are extradural in 94–99% of cases, intramedullary metastases are extremely rare with a rate of 0.5%, while intradural extramedullary tumors account for the remaining percentage [7].

The majority of systemic neoplasms metastasize to the spinal column through hematogenic spread. Vertebral bodies have in fact an intense vascularization especially in their posterior third [6]. Hematogenic spread is possible via arterial emboli to the abundant bone marrow of the vertebral bodies or via retrograde spread through the extradural Batson's venous plexus [1, 8]. The second mechanism involves mainly the prostatic gland tumors, which have a high incidence of metastasis to the

M. Raguso • M. Morini • R. Fiori • S. Masala, M.D. (✉)
Department of Diagnostic and Molecular Imaging, Interventional Radiology and Radiation Therapy, University "Tor Vergata", Viale Oxford, 81, Rome 00133, Italy

L. Manfrè (ed.), *Vertebral Lesions*, New Procedures in Spinal Interventional Neuroradiology, DOI 10.1007/978-3-319-52634-8_7

spinal column [8]. Hemopoietic neoplasms as multiple myeloma or lymphoma have a direct contiguous extension of the tumor into the epidural space [1, 8].

Finally tumor spread may be also by seeding through cerebrospinal fluid [1, 8].

Pain without trauma is the initial symptom in the majority of patients. Symptomatic lesions are more frequently in the thoracic region (70%) than in other spinal segments [9]. Therefore, in a patient with history of cancer, the appearance of a sudden and progressive spinal pain is suspicious for spinal metastases. The pain is referred as local and non-radicular; it worsens with rest and at night. This pain is usually elicited by palpation over the spinous process at the level of involvement.

The appearance of radicular symptoms and neurologic deficits, motor sensory or visceral, usually occurs secondarily to the extension of the lesion [6, 9].

Imaging techniques play an important role in the detection of spinal disease. Instrumental diagnosis includes techniques as plain radiography, computed tomography (CT), magnetic resonance (MR), and radionuclide imaging [6].

CT scanning provides a detailed study of the osseous architecture of the spinal axis. Physician detects also data regarding the extent of neoplastic destruction (Fig. 7.1) [6]. MR is the first imaging technique in the evaluation of the soft tissues, therefore is the method of choice for the study of the spinal cord. MR provides essential information for surgical planning, as the epidural and bone marrow tumor infiltration (Fig. 7.2) [10].

The treatment of symptomatic spinal metastasis has mainly a palliative function. We should always consider the goal of preserving or restoring, even partially, the neurological function [11, 12]. The therapeutic choice has to consider the clinical status of the patients, the presence of a single or multiple painful lesions, and the involvement of the neural structures [12]. While conservative therapies with analgesic and chemotherapy drugs are not always successful, radiotherapy (RT) and surgery are the most used therapeutic options for a radical treatment [11, 12].

RT is particularly effective in the treatment of various radiosensitive histological subtypes of metastasis, such as hemopoietic tumors, small-cell lung carcinoma, and prostate carcinoma [11, 13]. The standard radiation dose schedule consists of 20 to 30 Gy administered in five to ten treatment sessions to the interested area, usually beaming an area of two vertebral bodies; many variations are related to the general status of the patient and the extent of spinal tumor [14, 15].

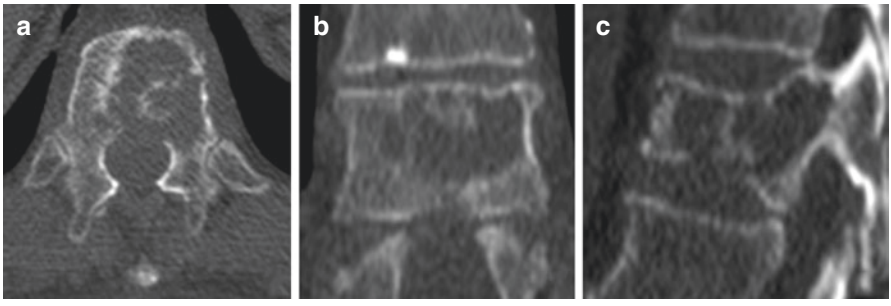

Fig. 7.1 An osteolytic lesion located within the D12 vertebral body in a 72-year-old patient with multiple myeloma: CT multiplanar reformation on axial (**a**), coronal (**b**), and sagittal (**c**) plans

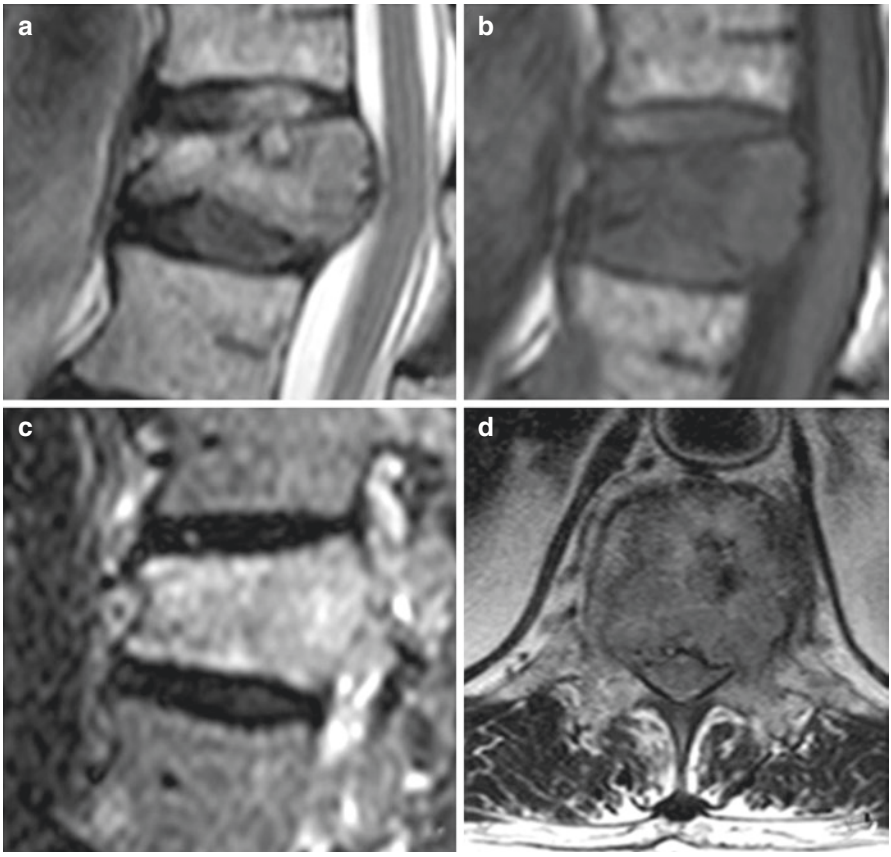

Fig. 7.2 MRI of the same patient: sagittal T2 weighted (**a**), sagittal T1 weighted (**b**), short-tau inversion recovery (STIR) (**c**), and axial T2-weighted (**d**) images show the osteolytic lesion, which caused vertebral collapse

While in conventional RT the dose is fractioned over the time, stereotactic RT has the rational to focus multiple doses at the same time on the volume of interest, with an important reduction of the radiation exposition for the surrounding soft tissues. The typical dose is 8–20 Gy in one to two sessions. Stereotactic RT has indication in patients when conventional RT has failed or surgery is not applicable [16, 17]. The disadvantage is the need of several re-treatments.

The aim of surgery is the decompression of the spinal cord and spinal roots and the stabilization of the spinal column [12]. Good results with the use of surgery need a careful patient selection. Surgical decompression and stabilization of the spinal axis is necessary in patients with pathological fracture and dislocation of the fragments in the vertebral canal [12]. In patients with no history of primary cancer, surgery should be performed with a diagnostic and therapeutic purpose. Finally, in patients in whom RT has failed to control the progression of symptoms or with a known radioresistant tumor, surgery should be considered [11]. Anyway some

studies suggest that infections drastically increased when surgery is performed after radiotherapy [18, 11].

Less invasive therapeutic options include augmentation techniques as vertebroplasty and kyphoplasty (the reader is directed to relative chapters) [19].

In recent years the technology development has provided techniques, as thermal ablation with radio frequency (RF) or cryoablation, in association with vertebral augmentation methods [20]. The goal is both the pain relief and a better quality of life in patients, whose poor clinical status does not allow the use of more invasive techniques.

In this chapter we will focus the attention on radiofrequency ablation (RFA).

7.2 Radiofrequency Heat Ablation

RFA was introduced in clinical practice to treat painful cancerous lesions, not approachable with traditional therapeutic methods [20]. RFA has the purpose to destroy or to stop the tumor progression, and it tries also to fire endosteal nerve endings, which are involved in the origin of pain as a result of their stimulation by chemicals such as prostaglandins and bradykinin, substance P, or histamine, released by the destroyed bone [20]. RFA of bone tumors has specific advantages, related to the electrical and thermal properties of the bone structure [21]. Trabecular bone conducts heat less well than the muscle. In addition, the cortical bone has heat insulating activity, which protects neighboring structures [21].

Osteoid osteomas were the first tumors treated by RFA more than 20 years ago, and nowadays percutaneous RFA has become the primary well-established approach as treatment of these benign lesions [22].

In the last 15 years, chondroblastoma was the second benign tumor considered for ablation. This rare tumor of children/young adults is usually located in the epiphyses/apophyses, and it is often painful [23]. When a small chondroblastoma is detected, RFA offered a shorter postoperative hospitalization and a lower rate of recurrence in comparison to surgery, especially if the proximity to cartilage and growth plates is taken into account [24, 25].

The role of RFA in treatment of painful metastasis is well established, particularly in the axial-loading locations of the spinal column or peri-acetabular region, mainly to avoid potential complications from tumor progression, primarily fracture [26].

7.2.1 Physics of Radiofrequency Ablation

The aim of RFA is the destruction of cancer cells with the use of high temperature. When an ablation electrode is applied to the target tissue, a high-frequency (200–1200 KHz) alternating current moves from the tip of the electrode into the surrounding tissue [27]. The indirect current causes local ionic agitation and subsequent frictional heat, with a significant increase in temperature. The frictional heat emitted from ionic agitation then spreads by convection, with the final results of enlarging the area of ablated tissue [28].

Some authors documented that injury to cells begins at 42 °C and the tissue composition influences the time of heat exposure required to achieve cell death [29, 30]. As the temperature increases above 42 °C, the necessary exposure time decreases exponentially. In vitro experiments with white eggs documented the size of the coagulum did not increase, if a time exposure between 60 and 90 seconds and a target temperature of 80 °C are adopted [31]. Other studies supported the hypothesis in vivo coagulation necrosis of cancer cells could be achieved in only 2 min at 51 °C [29]. Anyway some authors proved the cells die, resulting in tissue necrosis, when the temperature exceeds 60 °C [32]. The tissue temperature decreases rapidly with increasing distance away from the electrode [33]. Authors then supposed the use of a "higher-than-ideal temperatures", typically over 90–100 °C, for ablation of tissues with a greater distance from the RF source: hence, it should be used to obtain a complete coverage of the tumor by the ablation zone with an adequate margin, typically 1 cm otherwise the boundary of the treated cancer lesion [34].

The physician may preset some parameters to maximize the energy deposition inside the target tissue, as temperature, voltage, impedance, and pulse duration, and then to improve the efficacy of treatment [35]. Also the choice of the RF electrode may influence the results of treatment.

There are RFA systems with single or multiple clustered electrodes. A conventional RF electrode is a metal cylinder entirely covered, except its tip [36]. The coating has an insulating function. In the inner distal tip, a thermocouple is positioned with the aim of monitoring the tissue temperature. There are many types of electrodes, which differ substantially for the length and the thickness of the tip, and the choice depends on the characteristics of the lesion to be treated. The area of tissue coagulation necrosis is a sphere proportional to the square of the RF current and increases linearly in function of the tip length [37]. The surface area of the electrode tip is also many orders of magnitude smaller than the entire coated surface RF probe [28]. Hence, the density of the field lines that are forced through the electrode tip is huge. There is a major ionic agitation in the molecules of the neighbor tissues to the electrode tip, therefore a higher temperature increase [28].

In single-electrode RFA systems, a closed-loop circuit is created with the RF generator, a large dispersive electrode (ground pad), the patient, and a needle electrode in series [33]. Some RFA systems have hollow electrodes, whose cavity is flushed with saline solution to outside the tip with the aim of controlling impedance and temperature; other companies produce water-cooled electrodes, with the saline flush in a closed circuit and without an external flush. Water-cooled RF electrode was performed in order to prevent drying or charring of tissue at the interface with the electrode tip, because the impedance may increase with an insulator function and frictional heat cannot spread out [38]. The internal cooling then supports an increased power deposition in the target tissue and drives RF heating from the electrode-tissue interface deeper into the tissue to create more clinically relevant ablations. Some studies described the efficacy of monopolar RFA since 2000 [39, 40]; e.g., in a multicenter trial on 43 patients with painful osteolytic metastases treated by monopolar RFA, a significant reduction of pain in 95% of the patients was documented [41].

Some companies produce bipolar electrodes: two serially non-insulated metallic surfaces at the tip electrode act as double poles. Xavier Buy in 2005 described the

bipolar technique as a therapeutical method for vertebral tumors on three patients [42]. In 2014 Angelos Ng et al. reported good results in a cohort of 36 patients, and this was the first prospective study on the treatment of spinal tumor with bipolar RFA [43].

For larger tumors, a single electrode in different positions can be used to produce multiple overlapping lesions. RFA systems with multiple electrodes are more eligible because of their faster and wider coagulation than single-electrode systems [44, 45]. Multi-tine conventional or cooled electrode systems range from 3 to 12 active tips of variable size and cluster configurations, with a final ablation zone of 3–4 cm [44, 45]. Although the treatment time is reduced with the use of multi-tined electrodes, such systems are not indicated for the treatment of lesions neighboring neurovascular structures (spinal cord and spinal roots must be spared) [44, 45].

7.2.2 Patient Selection, Role of Imaging, and Technique

History of metastatic cancer is the first clue for physician. Clinical examination reveals acute pain, usually refractory to conservative therapies, and tenderness over the spine at or near the involved vertebral level [46].

Imaging techniques play an important role in detection of painful metastasis and their therapeutic planning, as in the follow-up period. Vertebral fractures are generated when the combination of the axial and rotational charges on the spine exceed the resistance offered by the vertebral body [47]. At X-ray examination the vertebral compressive fracture is defined as a reduction in height, which must be at least 20% beyond its initial dimensions [48]. CT examination is useful for the evaluation of the bone erosion. MR scans allow an evaluation of the soft tissues as neural and vascular structures. The presence of intra-spongious edema, particularly in fat suppression sequences, indicates a recent fracture [6, 10].

The contraindications to RFA consist of fractures with retropulsion of the fragments within neural foramen, spread of tumor within the epidural space, local infection, coagulative disorders, pain not related to vertebral collapse, asymptomatic fractures, and tumor involvement of pedicles, entry site in mini-invasive techniques of interventional radiology, or joint facets [49].

MR imaging is an invaluable modality in staging lesions before RFA and in the follow-up of ablated lesions. During follow-up, the administration of intravenous contrast is extremely helpful in delineating the extent of the ablation zone. Ablated tissue shows no enhancement, because it is necrotic [50]. Clinical examination must be addressed to evaluation of pain relief and improvement of quality of life.

RFA is performed under fluoroscopy or combined fluoroscopy/CT guidance, in local anesthesia or mild sedation. The patient is placed in prone position with two rolls of soft material inserted under the chest and the pelvis, to obtain the maximum extension of the spine. A stiff cannula of a diameter between 11 and 13 gauge is introduced with unilateral or bilateral trans-pedicular pathway (or intercostovertebral for thoracic vertebrae or posterolateral for the lumbar levels) in the vertebral body (Figs. 7.3 and 7.4) [51, 41]. A flexible working cannula (Fig. 7.5) is

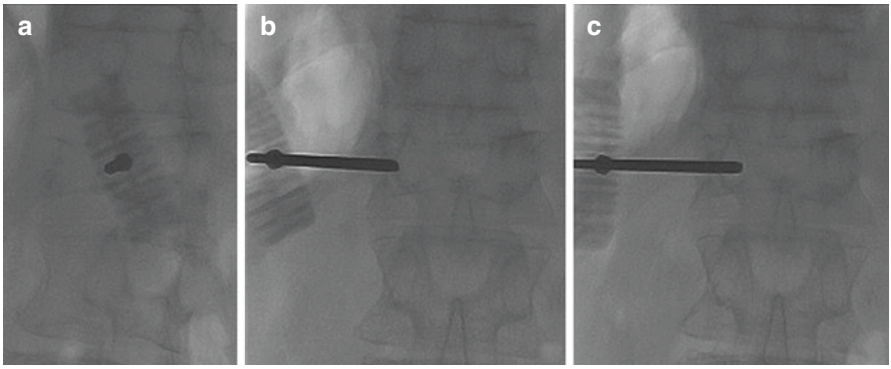

Fig. 7.3 Under left oblique (**a**) and anteroposterior (**b–c**) fluoroscopic views, the stiff cannula is positioned with trans-pedicular approach near to the posterior wall of the involved vertebral body

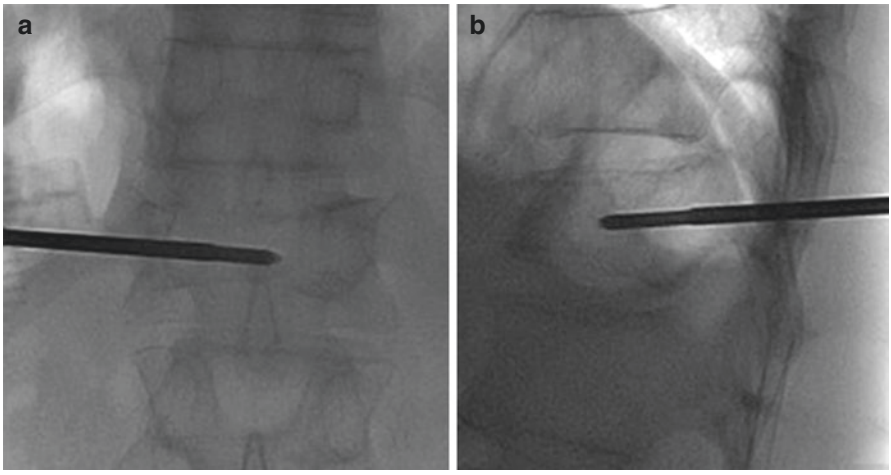

Fig. 7.4 Under anteroposterior (**a**) and lateral (**b**) fluoroscopic control, the introducer is positioned with a coaxial technique in the center of the vertebral body

introduced with the aim of creating a cavity within the tumor, to allow the subsequent introduction of RF electrode that is then positioned with a coaxial technique in the target lesion (Fig. 7.6).

Potential complications generally occur in the immediate or late post-procedural period and include general complications (infection, hematoma at the entry site) and those related to specific procedure. Skin heat injuries and damages to neurovascular structure or other closer soft tissues should be searched in the follow-up. Preventive thermal protection techniques include gas dissection (air or CO_2 in the soft tissues) or hydro-dissection with subcutaneous fluid injection as saline solution or the anesthetic drugs: they have an insulating function and increase the distance between the ablation zone and a certain structure [52]. Skin lesions can be avoided

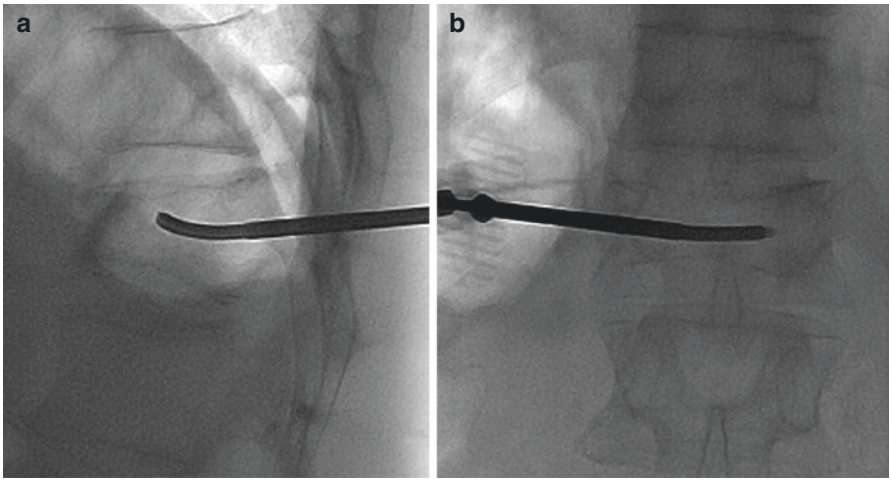

Fig. 7.5 Under lateral (**a**) and anteroposterior (**b**) fluoroscopic views, a flexible working cannula is introduced with the aim of creating a cavity within the tumor, to allow the subsequent introduction of RF electrode

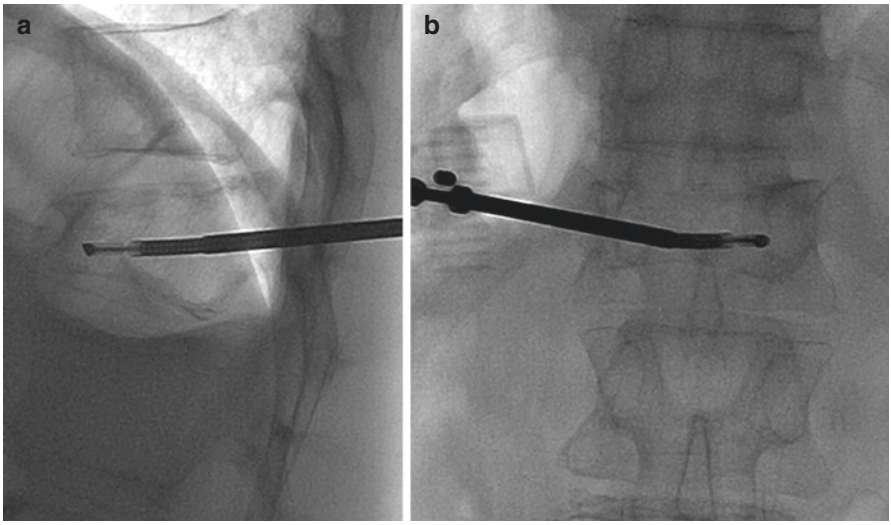

Fig. 7.6 After removing the flexible working cannula, the RF electrode is placed in the vertebral body. Lateral (**a**) and anteroposterior (**b**) fluoroscopic views

by positioning sterile gloves containing cooled fluid on the expected ablation zone [52]. Temperature monitoring includes different techniques as a thermocouple included in the RFA electrodes, in order to prevent injuries to closer soft tissues around the ablation zone [52].

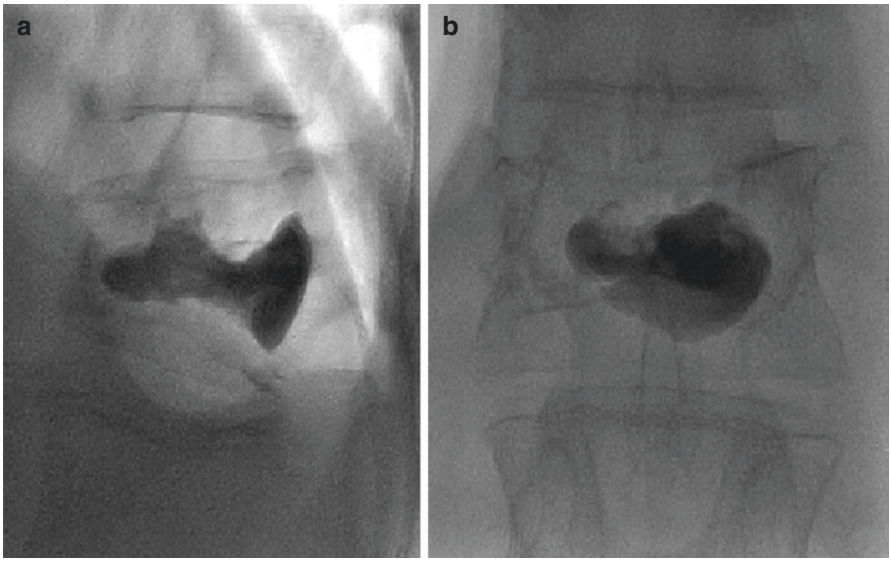

Fig. 7.7 After the RF ablation, bone augmentation may be performed. Lateral (**a**) and anteroposterior (**b**) fluoroscopic views show a homogeneous filling of PMMA in the vertebral body

Conclusion

RFA is a minimally invasive technique that is becoming increasingly popular for the treatment of specific cancers. The clinical status of patients, the intrinsic characteristics of the tumor, and radiological findings are essential for a better planning of the procedure.

RFA may be undertaken as a stand-alone treatment or in combination with injection of cement (Fig. 7.7) with the aim of bone augmentation, to provide an immediate post-procedural pain relief and to prevent future fractures.

References

1. Harrop JS, Schmidt MH, Boriani S, et al. Aggresive "benign" primary spine neoplasm: osteoblastoma, aneurysmal bone cyst, and giant cell tumor. Spine (Phila Pa 1976). 2009;34(22 Suppl):S39–47.
2. Jacobs WB, Perrin RG. Evaluation and treatment of spinal metastases: an overview. Neurosurg Focus. 2001;11(6):e10.
3. Gokaslan ZL, York JE, Walsh GL, et al. Transthoracic vertebrectomy for metastatic spinal tumors. J Neurosurg. 1998;89(4):599–609.
4. Abdu WA, Provencher M. Primary bone and metastatic tumors of the cervical spine. Spine (Phila Pa 1976). 1998;23(24):2767–77.
5. Solberg A, Bremnes RM. Metastatic spinal cord compression: diagnostic delay, treatment, and outcome. Anticancer Res. 1999;19(1B):677–84.
6. Guillevin R, Vallee JN, Lafitte F, et al. Spine metastasis imaging: review of the literature. J Neuroradiol. 2007;34(5):311–21.

7. Schick U, Marquardt G, Lorenz R. Intradural and extradural metastases. Neurosurg Rev. 2001;24(1):1–5. Discussion 6–7
8. Öge HK, Aydin S, Cagavi F, et al. Migration of pacemaker lead into the spinal venous plexus: case report with special reference to Batson's theory of spinal metastasis. Acta Neurochir (Wien). 2001;143(4):413–6.
9. Gerzsten PC, Welch WC. Current surgical management of metastatic spinal disease. Oncology (Williston Park). 2000;14(7):1013–24. Discussion 1024, 1029–30
10. Sciubba DM, Petteys RJ, Dekutoski MB, et al. Diagnosis and management of metastatic spine disease. A review. J Neurosurg Spine. 2010;13(1):94–108.
11. Zairi F, Marinho P, Allaoui M, et al. New advances in the management of thoracolumbar spine metastasis. Bull Cancer. 2013;100(5):435–41.
12. Filis AK, Aghayev KV, Doulgeris JJ, et al. Spinal neoplastic instability: biomechanics and current management options. Cancer Control. 2014;21(2):144–50.
13. Ippolito V, Micheletti E, Saccalani M, et al. Radiotherapy and spinal brace: still first-choice treatment for vertebral metastases from breast cancer. Chir Organi Mov. 1998;83(1–2):177–83.
14. Rhee WJ, Kim KH, Chang JS, et al. Vertebral compression fractures after spine irradiation using conventional fractionation in patients with metastatic colorectal cancer. Radiat Oncol J. 2014;32(4):221–30.
15. Maranzano E, Latini P, Perrucci E, et al. Short-course radiotherapy (8 Gy X 2) in metastatic spinal cord compression: an effective and feasible treatment. Int J Radiat Oncol Biol Phys. 1997;38(5):1037–44.
16. Sahgal A, Bilsky M, Chang EL, et al. Stereotactic body radiotherapy for spinal metastases: current status, with a focus on its application in the postoperative patient. J Neurosurg Spine. 2011;14(2):151–66.
17. Chawla S, Abu-Aita R, Philip A, et al. Stereotactic radiosurgery for spinal metastases: case report and review of treatment options. Bone. 2009;45(4):817–21.
18. Ghogawala Z, Mansfield FL, Borges LF. Spinal radiation before surgical decompression adversely affects outcomes of surgery for symptomatic metastatic spinal cord compression. Spine (Phila Pa 1976). 2001;26(7):818–24.
19. Bhatt AD, Schuler JC, Boakye M, et al. Current and emerging concepts in non-invasive and minimally invasive management of spine metastasis. Cancer Treat Rev. 2013;39(2):142–52.
20. Rosenthal D, Callstrom MR. Critical review and state of the art in interventional oncology: benign and metastatic disease involving bone. Radiology. 2012;262(3):765–80.
21. Dupuy DE, Hong R, Oliver B, et al. Radiofrequency ablation of spinal tumors: temperature distribution in the spinal canal. AJR Am J Roentgenol. 2000;175(5):1263–6.
22. Motamedi D, Learch TJ, Ishimitsu DN, et al. Thermal ablation of osteoid osteoma: overview and step-by-step guide. Radiographics. 2009;29(7):2127–41.
23. Martel Villagrán J, Bueno Horcajadas A, Ortiz Cruz EJ. Percutaneous radiofrequency ablation of benign bone tumors: osteoid osteoma, osteoblastoma, and chondroblastoma. Radiologia. 2009;51(6):549–58.
24. Lin PP, Thenappan A, Deavers MT, et al. Treatment and prognosis of chondroblastoma. Clin Orthop Relat Res. 2005;438:103–9.
25. Atalar H, Basarir K, Yildiz Y, et al. Management of chondroblastoma: retrospective review of 28 patients. J Orthop Sci. 2007;12(4):334–40.
26. Guarnieri G, Izzo R, Muto M. Current trends in mini-invasive management of spine metastases. Interv Neuroradiol. 2015;21(2):263–72. pii:1591019915582366. [Epub ahead of print].
27. Curley SA. Radiofrequency ablation of malignant liver tumors. Ann Surg Oncol. 2003;10(4):338–47.
28. Haines DE, Verow AF. Observations on electrode-tissue interface temperature and effect on electrical impedance during radiofrequency ablation of ventricular myocardium. Circulation. 1990;82(3):1034–8.
29. Dickson JA, Calderwood SK. Temperature range and selective sensitivity of tumors to hyperthermia: a critical review. Ann NY Acad Sci. 1980;335:180–205.

30. Seegenschmiedt MH, Brady LW, Sauer R. Interstitial thermoradiotherapy: review on technical and clinical aspects. Am J Clin Oncol. 1990;13(4):352–63.
31. Cosman Jr ER, Dolensky JR, Hoffman RA. Factors that affect radiofrequency heat lesion size. Pain Med. 2014;15(12):2020–36.
32. Mertyna P, Dewhirst MW, Halpern E, et al. Radiofrequency ablation: the effect of distance and baseline temperature on thermal dose requiredfor coagulation. Int J Hyperthermia. 2008;24(7): 550–9.
33. Davis KW, Choi JJ, Blankenbaker DG. Radiofrequency ablation in the musculoskeletal system. Semin Roentgenol. 2004;39(1):129–44.
34. Di Staso M, Zugaro L, Gravina GL, et al. Afeasibility study of percutaneous radiofrequency ablation followed by radiotherapy in the management of painful osteolytic bone metastases. Eur Radiol. 2011;21(9):2004–10.
35. Masala S, Fiori R, Raguso M, et al. Pulse-dose radiofrequency for knee osteoartrithis. Cardiovasc Intervent Radiol. 2014;37(2):482–7.
36. Tatli S, Tapan U, Morrison PR, et al. Radiofrequency ablation: technique and clinical applications. Diagn Interv Radiol. 2012;18(5):508–16.
37. Frezza EE. Therapeutic management algorithm in cirrhotic and noncirrhotic patients in primary or secondary liver masses. Dig Dis Sci. 2004;49(5):866–71.
38. Haemmerich D. Biophysics of radiofrequency ablation. Crit Rev Biomed Eng. 2010;38(1): 53–63.
39. Gronemeyer DH, Schirp S, Gevargez A. Image-guided radiofrequency ablation of spinal tumors: preliminary experience with an expandable array electrode. Cancer J. 2002;8(1): 33–9.
40. Schaefer O, Lohrmann C, Herling M, et al. Combined radiofrequency thermal ablation and percutaneous cementoplasty treatment of a pathologic fracture. J Vasc Interv Radiol. 2002; 13(10):1047–50.
41. Goetz MP, Callstrom MR, Charboneau JW, et al. Percutaneous image-guided radiofrequency ablation of painful metastases involving bone: a multicenter study. J Clin Oncol. 2004;22(2): 300–6.
42. Buy X, Basile A, Bierry G, et al. Saline-infused bipolar radiofrequency ablation of high-risk spinal and paraspinal neoplasms. AJR Am J Roentgenol. 2006;186(5 Suppl):S322–6.
43. Gazis AN, Beuing O, Franke J, et al. Bipolar radiofrequency ablation of spinal tumors: predictability, safety and outcome. Spine J. 2014;14(4):604–8.
44. Gulesserian T, Mahnken AH, Schernthaner R, et al. Comparison of expandable electrodes in percutaneous radiofrequency ablation of renal cell carcinoma. Eur J Radiol. 2006;59(2): 133–9.
45. Pereira PL, Trübenbach J, Schenk M, et al. Radiofrequency ablation: in vivo comparison of four commercially available devices in pig livers. Radiology. 2004;232(2):482–90.
46. Stallmeyer MJ, Zoarski GH, Obuchowski AM. Optimizing patient selection in percutaneous vertebroplasty. J Vasc Interv Radiol. 2003;14(6):683–96.
47. Mathis JM, Barr JD, Belkoff SM, et al. Percutaneous vertebroplasty: a developing standard of care for vertebral compression fractures. AJNR Am J Neuroradiol. 2001;22(2):373–81.
48. McKiernan F, Jensen R, Faciszewski T. The dynamic mobility of vertebral compression fractures. J Bone Miner Res. 2003;18(1):24–9.
49. Masala S, Fiori R, Massari F, et al. Kyphoplasty and vertebroplasty: new equipment for vertebral fractures treatment. J Exp Clin Cancer Res. 2003;22(4 Suppl):75–9.
50. Goldberg SN, Gazelle GS, Solbiati L, et al. Ablation of liver tumors using percutaneous RF therapy. AJR Am J Roentgenol. 1998;170(4):1023–8.
51. Garfin SR, Yuan HA, Reiley MA. New technologies in spine: kyphoplasty and vertebroplasty for the treatment of painful osteoporotic compression fractures. Spine (Phila Pa 1976). 2001;26(14):1511–5.
52. Tsoumakidou G, Buy X, Garnon J, et al. Percutaneous thermal ablation: how to protect the surrounding organs. Tech Vasc Interv Radiol. 2011;14(3):170–6.

CT/X-Ray Guided Techniques in Vertebral Tumors: Embolization

8

Fabio Baruzzi and Luca Valvassori

8.1 Part I: Embolization of Vertebral Tumors

8.1.1 Indication

Surgery is used in case of neurological dysfunction, as well as for stabilization of the spine, and local tumor excision, but it may have to face a significant intraoperative blood loss.

The presurgical endovascular treatment has therefore the goal of reducing the intraoperative blood loss by intra-arterial (locoregional) injection of embolic materials. Thus, surgery may result in a shorter operative time and, more likely, in a radical excision of the tumoral lesion or a smaller rate of tumor recurrences over time.

Normally, only hypervascular tumors are considered for endovascular treatment, including both benign (osteoblastomas, chondromas, osteomas) and malignant neoplasms (chordomas, sarcomas, multiple myelomas) [1].

But since up to 50% of cancer patients have spinal metastases, these are in fact the most frequent tumors affecting the spine. Hypervascular metastases include renal and thyroidal origin, sarcomas, melanomas, and multiple myelomas [2–4].

Tumor histology is generally consistent with CT and MR appearance, so that the need for a presurgical embolization may be required by the surgeons just based on this and on the tumor extension.

F. Baruzzi, M.D. (✉)
Department of Neuroradiology, Ospedale di Circolo di Varese, Varese, Italy
e-mail: fabio.baruzzi@tin.it

L. Valvassori, M.D.
Department of Neuroradiology, Ospedale Niguarda, Milano, Italy
e-mail: luca.valvassori@ospedaleniguarda.it

L. Manfrè (ed.), *Vertebral Lesions*, New Procedures in Spinal Interventional Neuroradiology, DOI 10.1007/978-3-319-52634-8_8

8.1.2 Diagnostic Angiography: Anatomical and Technical Considerations

From a general standpoint, the correct angiographic examination of the spine and the spinal cord (the two cannot be separated anatomically and functionally) must include the selective catheterization of intercostal and lumbar arteries of both sides, median sacral artery, hypogastric arteries, bilateral vertebral, ascending cervical and costo-cervical arteries, and occasionally external carotid branches: thus, a complete picture of the whole spine and its contents and relation with surrounding and functionally related structures is achieved.

More specifically, since the spinal cord is part of the central nervous system, the more cranial the lesions to image and treat, the more obligatory the study of cerebral circulation, due to the multiple connections between the two.

This complete study allows a fulfilling imaging of either the vertebral bony structures or the spinal cord vascularization.

Anatomically, the spinal cord is vascularized by an anterior spinal axis, fed by multiple and variable anterior radiculomedullary arteries arising at different levels from the dorsal branches of the intercostal and lumbar arteries, and a posterior spinal axis (which is in fact more a network on the posterior side of the spinal cord than a single artery running from rostral to caudal), fed by multiple posterior radiculomedullary arteries (Fig. 8.1).

This basic anatomy must always be kept in mind when approaching any vascular lesion of this system and even more when switching to any kind of endovascular treatment.

Occlusion of spinal arteries is obviously to be avoided, since the risk of causing an infarct and a severe medullary syndrome is high, much higher for the anterior axis, though, compared to the posterior arteries, because collateral circulation is unlikely to work if the occlusion is inside the axis itself, caused by injection of solid or liquid embolics.

From a pragmatic point of view, for local lesions involving one or two vertebral bodies in the dorsal or lumbosacral segments, it is probably enough to visualize some metameres above and below the lesions, to be sure to image all the possible feeders to the lesion together with the spinal arteries.

For more extensive diseases or when dealing with vascular malformation (AVMs, direct or dural fistulas, etc.), a complete examination must be accomplished.

Differently, anatomy and vascularization of the cervical spine are more complex. Caudal cervical bodies are fed by branches arising from the tireocervical arteries, whereas the median vertebrae are fed by arteries of the costocervical trunk.

The C1-C3 segment is vascularized also by vessels coming off the occipital artery. But anatomic variations are very frequent, so that imaging of all these arteries is needed before taking any diagnostic and therapeutic decision.

The extremely rich arterial network of the head, face, and neck makes it mandatory to check for possible collaterals, linking arteries of the external carotid to the vertebro-basilar and cervical medullary system.

If an endovascular treatment is planned, attention must be paid to possible non-target embolization of the brain [5].

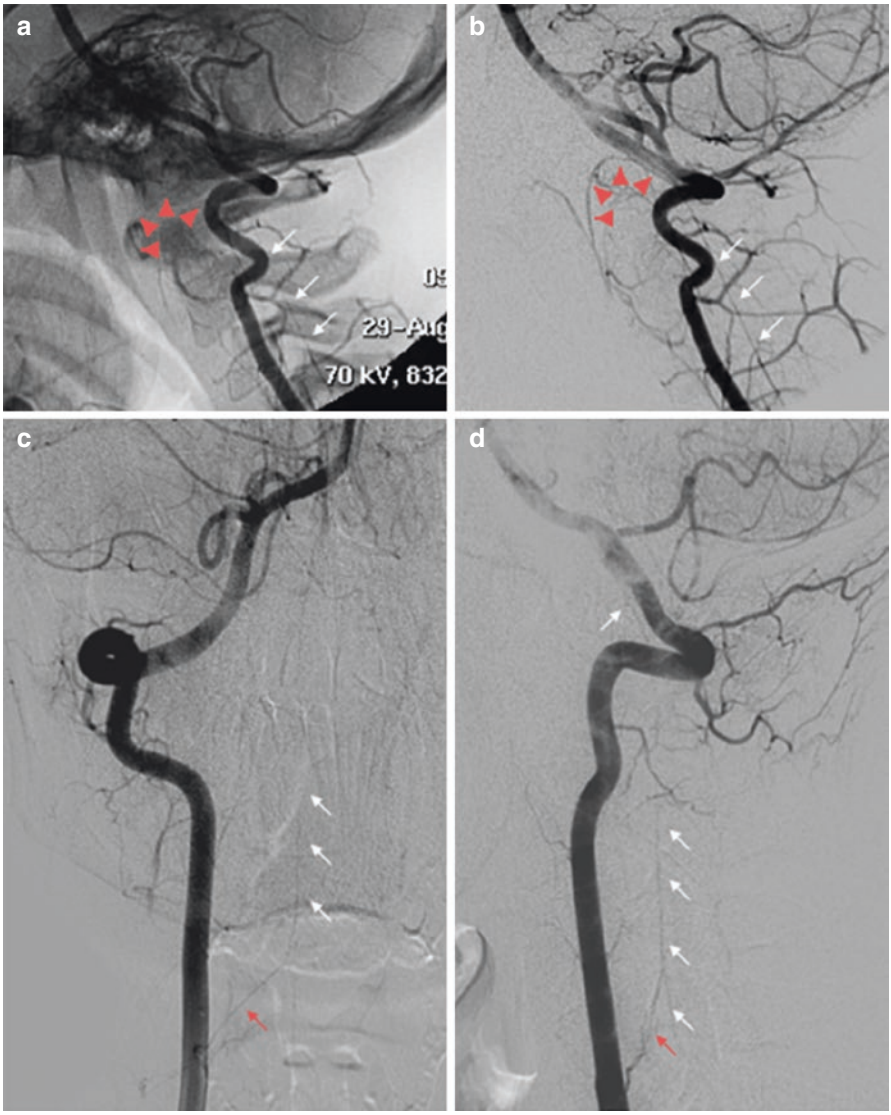

Fig. 8.1 Lateral non-subtracted and subtracted angiograms (**a**, **b**) show the course of anterior spinal artery (*white arrows*) emerging from the cisternal segment of the vertebral artery and descending on the anterior surface of the spinal cord. Odontoid arch anastomosis (*red arrowheads*) is one of the common connections between vertebral artery and ascending pharyngeal artery, branch of the external carotid artery. AP and lateral subtracted views (**c**, **d**) show a radiculo-medullary artery at C3 level feeding the anterior spinal artery

8.1.3 Endovascular Treatment

After transfemoral puncture, the diagnostic part of the procedure requires the choice of a correct catheter. Different curves are available, in accordance with the personal experience but also the diameter of the aorta, the presence of atheromatous plaque, and even its possible aneurysmatic dilation.

Djindjan, Simmons, Cobra, Headhunter or special (custom) curves are generally used.

Of note, the possibility to steam shape the catheters is often very useful to negotiate difficult origin of intercostals and lumbar arteries and large diameter aortas.

For presurgical procedures, once the diagnostic phase has shown a significant pathologic blush at the level of the tumor, injection of particulate embolic agents is almost always enough to obtain a useful and reasonably stable devascularization in the next 48–72 h, allowing the surgeon to perform a safer operation.

Different issues and concerns must be taken into consideration when it comes to the presurgical treatment of vertebral tumors.

The kind of surgery (debulking, "standard" resection, en bloc resection, and local stabilization, etc.) may require a different rate of devascularization, and the high flow shunts inside the tumoral tissue may need different embolic material and devices.

In our experience the use of PVA particles in the range of 150–350 microns of diameter results to be easy, safe, and effective.

Injection is realized at different dilution of the particles, according to operator's experience, until the flow in the feeder is almost absent and the pathological blush not visible anymore (Fig. 8.2).

Angiographic runs have to be taken at intervals during the procedure, to check for the state of the flow and especially for the appearance of spinal arteries or for collateral circulation, since the lesser the flow, the more likely the injection can open and jeopardize these vessels.

These particles tend to aggregate, thus occluding vessels larger in diameter than nominal and probably in a less homogeneous mixture [6].

On the other side, when using more recent products, such as calibrated microspheres, attention must be paid to oversize the diameter of the particles compared to PVA, because these embolics do not aggregate, are compressible and consequently injectable through smaller catheters compared to their nominal size, and, moreover, are very slippery and elastic, making it possible to easily pass through AV shunts and reach the venous drainage or, more risky, embolize collaterals as soon as they open: all these potential sources of complications will not be visible during fluoroscopy.

The use of liquid embolics, such as glue, Onyx, Phil, and solid materials as coils, has a very limited role in the treatment of vertebral tumors, unless a large mass has to be treated in a relatively safe anatomical region, like the sacral area (Fig. 8.3).

In other territories, the more complex procedure, even considering the higher stability of the devascularization, doesn't seem to carry a consistent benefit in the presurgical approach [7].

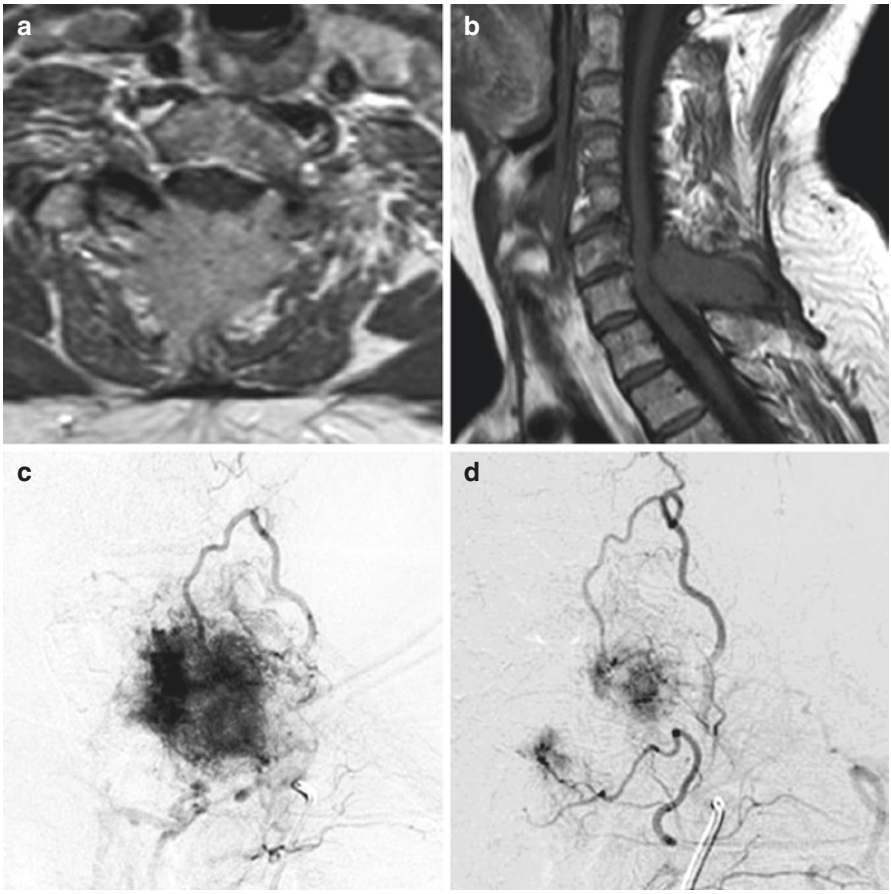

Fig. 8.2 Seventy-four-year-old woman with renal carcinoma's metastasis in C7 undergoing a preoperative endovascular treatment. Post-contrast axial T1-weighted (**a**) and sagittal T1-weighted (**b**) images show involvement of the posterior arch by the metastasis with compression of the spinal cord. DSA AP view (**c**) demonstrates the high vascularization of the lesion fed by branches of both the tireo-cervical trunks. AP angiogram (**d**), immediately after the embolization with PVA particles, shows a consistent reduction of blood supply in the lesion

Even if no randomized trial has been designed so far to show the usefulness of presurgical embolization in reducing intraoperative blood loss, this approach is widely accepted and many series support this concept [7].

Conceptually and technically, things are different when the anatomical region involved is the proximal cervical spine and when the lesion is large, thus not only entering the spinal canal but also surrounding one or both vertebral arteries.

In some of these cases, after considering histology, age, and comorbidity, an en bloc resection could highly improve patient's prognosis or even be the only possible solution, other than palliative surgery or embolization.

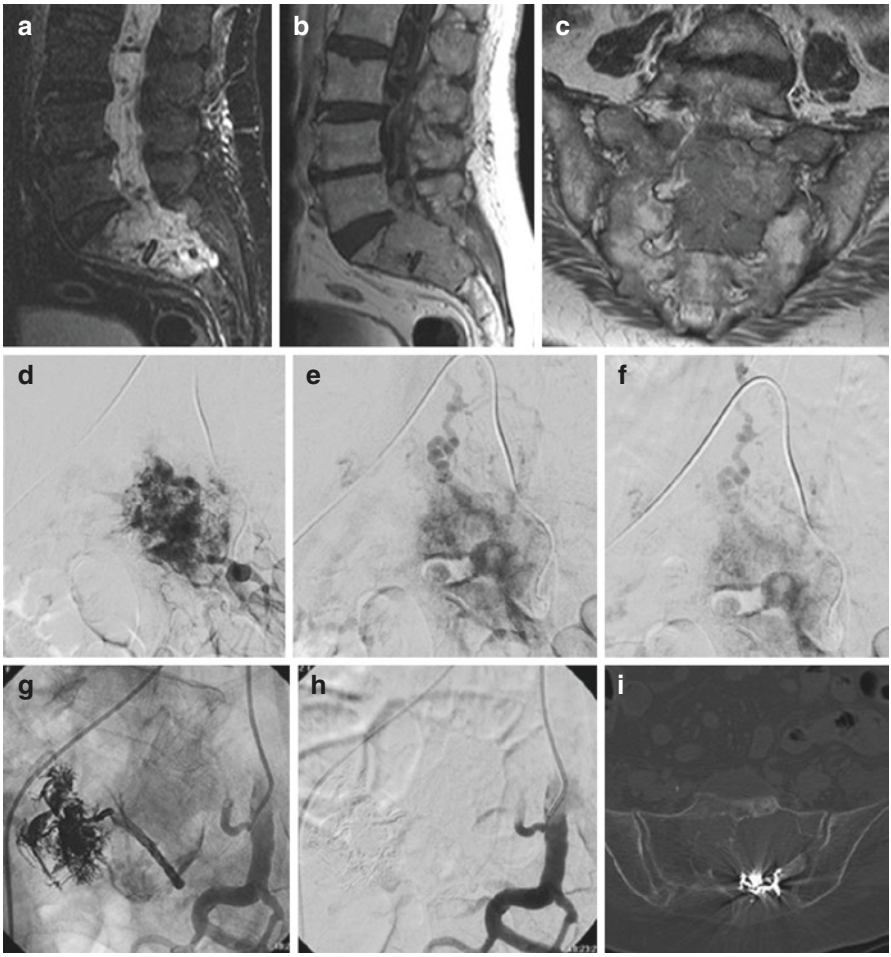

Fig. 8.3 Sixty-year-old patient presenting with progressive paraplegia, bilateral limb numbness, and back pain. MR images (**a**, **b**, **c**) reveal a huge mass of the sacrum with posterior extension to spinal canal and sacral foraminae. A-P angiographic runs (**d**, **e**, **f**) show high vascularization of the lesion with drainage into a vein inside the spinal canal. Patient undergoes a preoperative embolization (**g**, **h**) of the lesion with Onyx and with PVA particles with reduction of blood supply of the lesion. Non-enhanced CT (**i**) shows the results of the endovascular procedure

In these cases, PVA embolization needs very careful injection because the risk of nontarget embolization in this region is consistent, thus making it obligatory a preliminary six-vessel study (vertebral arteries, internal and external carotid of both sides) [8].

A less common requirement from the surgeon is the occlusion of one or even both vertebral arteries. Occlusion of the vertebral artery on one side (Figs. 8.4 and 8.5) at the distal cervical segment (C1-C2 level) can be easily accomplished, provided that the contralateral artery has a sufficient caliber , up to the vertebro-basilar junction, to provide blood flow for the basilar and the branches coming off it and also to feed the contralateral PICA, once the omolateral vertebral has been occluded.

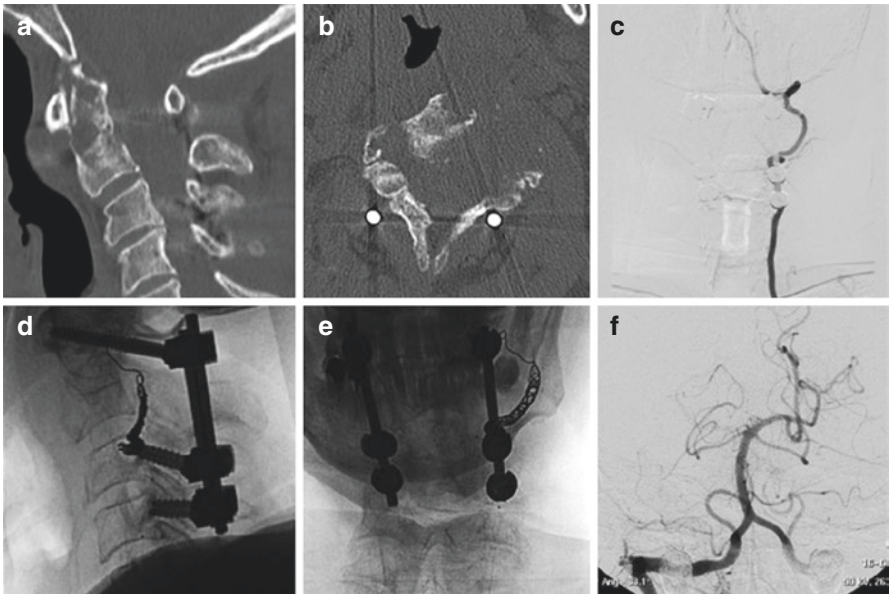

Fig. 8.4 Preoperative therapeutic vertebral artery occlusion in a 62-year-old man with the recurrence of a previously operated chordoma of C2 on the left side. Non-enhanced CT images (**a**, **b**) demonstrate the chordoma of C2 vertebral body extending to the odontoid process. Patient undergoes a preliminary DSA (**c**), after which occlusion of the left vertebral is realized with platinum coils (**d**, **e**). Right vertebral selective angiogram (**f**) shows a perfect flow in the basilar artery and a reverse flow feeding the distal left vertebral

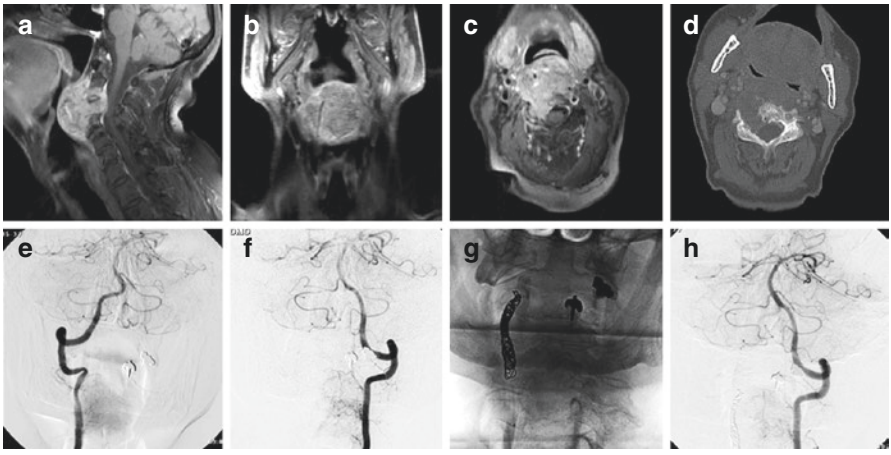

Fig. 8.5 Preoperative therapeutic vertebral artery occlusion in a patient suffering from a chordoma of C2. Post-contrast MR images (**a**, **b**, **c**) show a chordoma of C2-C3-C4 extending to the anterior and paraspinal soft tissues. Non-enhanced CT (**d**) better defines the erosion of the vertebral bodies. Patient undergoes a preliminary DSA (**e**, **f**), showing that both vertebral arteries, of good caliber, reach the basilar artery, thus allowing occlusion of the right one. Frontal single shot radiographs (**g**) and left vertebral artery selective angiogram (**h**) demonstrate the occlusion with platinum coils of the extracranial vertebral artery with good supply of posterior fossa circulation from left vertebral artery

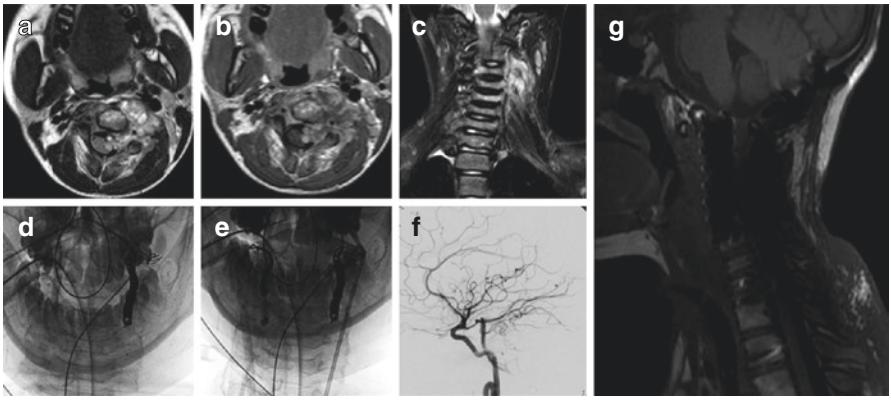

Fig. 8.6 Thirteen-year-old girl with an osteosarcoma of C2-C3 extending to the paraspinal soft tissues as shown in the MR images (**a**, **b**, **c**). The patient undergoes a preoperative endovascular occlusion of both vertebral arteries (**d**, **e**) after performing an occlusion test in order to evaluate the collateral supply from anterior circulation. Right internal carotid selective angiogram (**f**), acquired after occlusion of both vertebral arteries, demonstrates a good supply of the posterior circulation via the posterior communicating artery. Sagittal MR image shows the result of the reconstructive surgery (**g**)

If these criteria are respected, then it is possible to go on with the occlusion deploying detachable platinum coils, which best fit the need of the surgeon.

No clinical test occlusion is feasible nor needed at this level.

A reliable neurological examination would be impossible, since posterior fossa symptoms are often subtle and need complex movements and orders to be investigated. Moreover, angiographic evaluation, as for the carotids, has proved to be highly reliable and very easy to obtain.

More unusual is bilateral vertebral occlusion, more likely to be feasible in young patients (Fig. 8.6).

It is technically similar, but needing an angiographic balloon occlusion test, to make sure that the patency of the basilar and distal vertebral arteries is guaranteed by the reverse flow through one or two posterior communicating arteries. Provided the flow is consistent, the second vertebral may be occluded with coils, as well.

8.1.4 Anesthesiology

All the procedures can be carried out with patients awake, or with some degree of sedation, also depending on the clinical conditions, age, etc.

General anesthesia might be considered for specific situation, including very long procedures in old patient or patients suffering from untreatable back pain.

In some situation, whenever surgery is planned right after the endovascular procedure, a single anesthesia may be done.

8.1.5 Timing for Surgery

Since the effect of the presurgical treatment with particles is decreasing over time, it is generally accepted that surgery should not be delayed of more than 48–72 h from the endovascular treatment, knowing that the sooner, the better.

Beyond this time span, recanalization of embolized vessels as well as recruitment of other feeders might take place, making the "preparatory treatment" less effective [9, 10].

8.1.6 Complications

Complications of spinal tumor embolization are low [11].

Apart from those related to any endovascular access, i.e., problems due to vascular access (hematoma or pseudoaneurysm), radiation exposure, and reaction to contrast medium, most serious complications are those connected with the navigation in the metameric and supraortic arteries and with the injection of embolic agents.

Dissection and rupture of arteries is always possible but is a rare evenience.

More frightening, embolization of cerebral territories or spinal arteries can occur, whose rate can be kept low, if a complete study of the vascular territories is performed before injecting embolic material.

And also keeping in mind that the endovascular procedures are preparatory to a main surgery, therefore, morbidity must be kept low also by not pushing too much the technique.

Otherwise, the effort focused on making surgery easier and at lower risks is vanished.

8.2 Part II: Vertebral Hemangiomas Embolization

8.2.1 General Information

Vertebral hemangiomas are extremely frequent in the general population (incidence of 10% to 12%), often solitary (70%) and, less frequently, multiple (30%) [12], mostly involving the lumbar and dorsal spine. They are benign vascular lesions, almost always asymptomatic, and defined as vascular malformations, dysplasias [13], or hamartomas. Only 1% to 2% of these cases cause problems, such as localized pain (*symptomatic hemangiomas*), fractures, or neurological deficits caused by the growth of a soft extraosseous component [14] invading the spinal canal and thus compressing the spinal cord and/or spinal nerves (*aggressive hemangiomas*).

Symptomatic hemangiomas, with or without associated fracture, are now effectively and permanently treated with percutaneous vertebroplasty (VP) (Figs. 8.7 and 8.8) gold standard [15]: the complete filling and subsequent sclerosis of the hemangioma result in remission and full recovery [16].

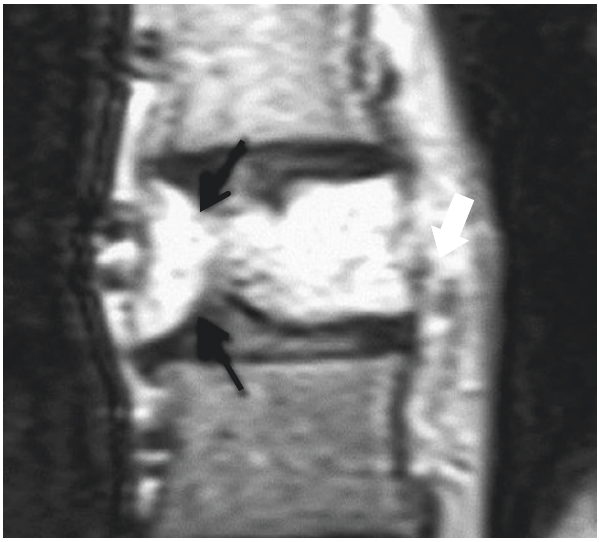

Fig. 8.7 Thirty-two-year-old female, T1-weighted coronal MR scan with gadolinium. Symptomatic vertebral hemangioma (thoracic back pain for more than 1 year) in T8 involving the entire vertebral body, with strong enhancement and minimal involvement of the left paravertebral side (*white arrow*). There is also a somatic fracture with sinking of both vertebral end plates (*black arrows*)

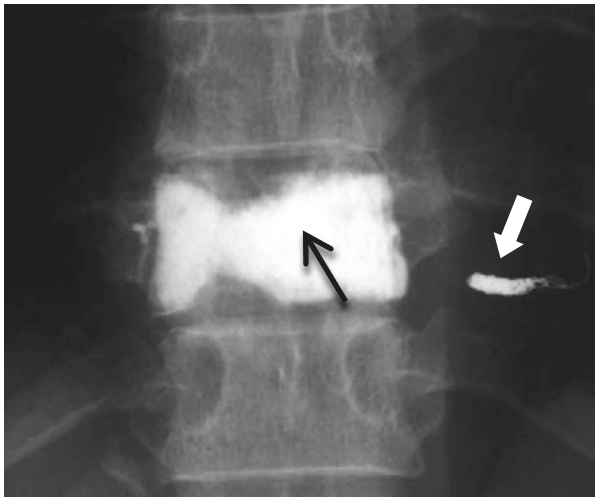

Fig. 8.8 AP follow-up radiograph of same patient post D8 hemangioma embolization and percutaneous vertebroplasty PMMA cementing material, highly radiopaque, entirely filled the hemangioma (*black arrow*); in the left paravertebral side is highlighted (*white arrow*) the employed coil for the pre-vertebroplasty embolization

Aggressive vertebral hemangiomas sometimes represent a complex diagnostic issue, since they can resemble, both clinically and radiologically, more harmful diseases, such as primary or metastatic bone tumors [17]; in these uncertain cases, performing a percutaneous biopsy under CT guidance or fluoroscopy is mandatory (Figs. 8.9 and 8.10).

The differential diagnosis for a potential spinal hemangioma includes multiple myeloma, aneurysmal bone cyst, bone metastases, lymphoma, osteosarcoma, and Paget's disease.

Aggressive vertebral hemangiomas with extraosseous tissue component, classified as Stage 3 according to Enneking [18], grow rather slowly over years or decades.

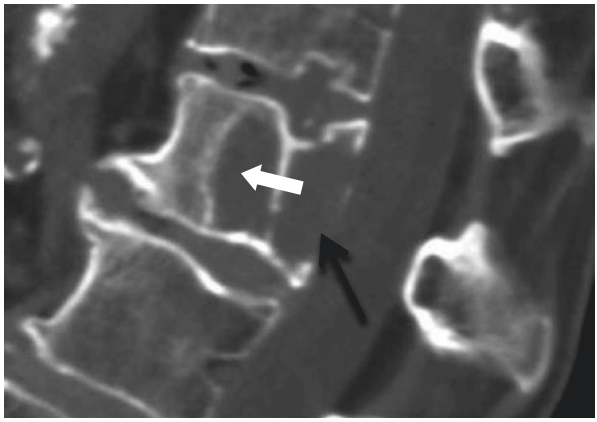

Fig. 8.9 Fifty-seven-year-old female, CT sagittal view of the bone architecture demonstrates a lesion in D12, showing structural rearrangement of the vertebral body with large lytic areas (*white arrow*), also involving posterior vertebral wall (*black arrow*). Since x-ray images are not pathognomonic, more than one diagnostic hypothesis can be suggested: vertebral hemangioma, myeloma, or another aggressive disease

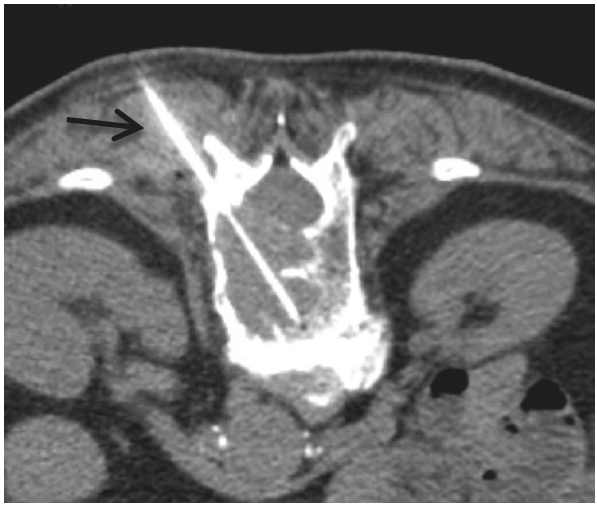

Fig. 8.10 Same patient of the previous figure. Guided biopsy by CT fluoroscopy, with semiautomatic guillotine 18G needle (*black arrow*); histology confirms expected diagnosis of aggressive vertebral hemangioma, subsequently treated by percutaneous vertebroplasty

Such growth is not due to mitosis [19] and over the year it will spread in the paravertebral area and/or invade the spinal canal. The consequent compression of nerve root or spinal cord is associated to neurological symptoms, usually progressive [20]. In a few cases, bleeding [21] or thrombosis located in the hemangioma will cause a rapid onset of the neurological symptoms.

Hence the aggressive hemangiomas require treatment, also when they represent an incidental finding, before they can cause neurological deficits thus requiring an urgent or emergency surgery (Fig. 8.11), such as decompressive laminectomy or vertebrectomy, associated or not with the excision of the extraosseous extension and sometimes anterior/posterior stabilization.

When promptly treated, a different approach can be applied instead of surgical intervention [22], radiotherapy (RT) [23], or sclerotherapy [24] (Fig. 8.12).

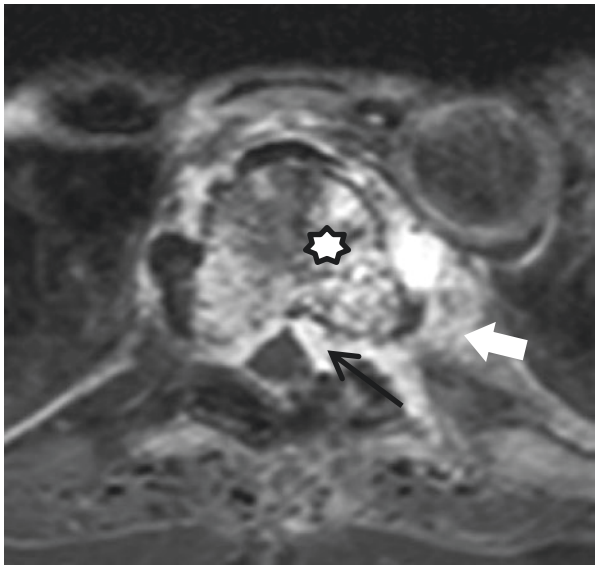

Fig. 8.11 Sixty-seven-year-old male, fast spin-echo T1 axial MR image with fat suppression after contrast, carried out after left hemilaminectomy and partial excision of hemangioma in the right epidural area in a hospitalized patient with paraparesis caused by spinal cord compression due to aggressive hemangioma in D5. MR image shows pathological enhancement due to residual hemangioma in the left epidural area (*black arrow*), in the left paravertebral area (*white arrow*), and into the vertebral body (*asterisk*)

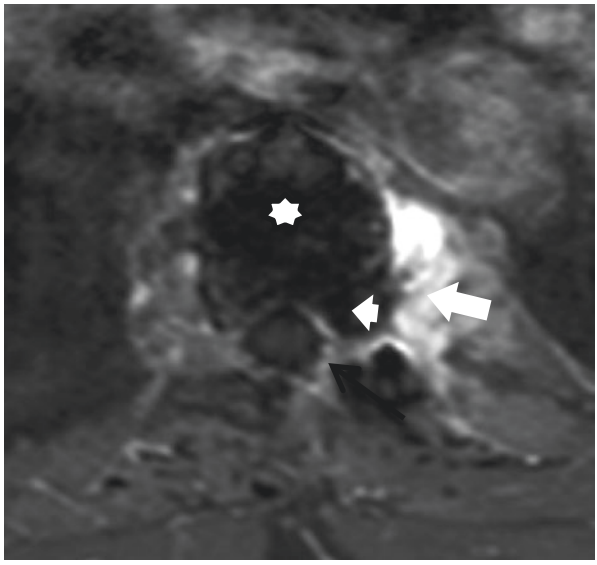

Fig. 8.12 MR follow-up performed 2 years after the VP + percutaneous embolization with **Onyx**, fast spin-echo T1 MR image with fat suppression with contrast: complete filling of the intraosseous component of the hemangioma (*asterisk*), marked reduction in epidural component (*black arrow*) caused by glue (*head white arrow*), and persistence of the left paravertebral extraosseous component (*white arrow*), unchanged

8.2.2 Embolization

The digital subtraction angiography (DSA) is useful during the treatment planning of aggressive hemangiomas because it highlights vascularization of both intra- and extraosseous components of the hemangioma. The arteriographic appearance [25] is usually a characteristic of dilatation of the arterioles of the vertebral body (Fig. 8.13), multiple blood pools in the capillary phase (Fig. 8.14),

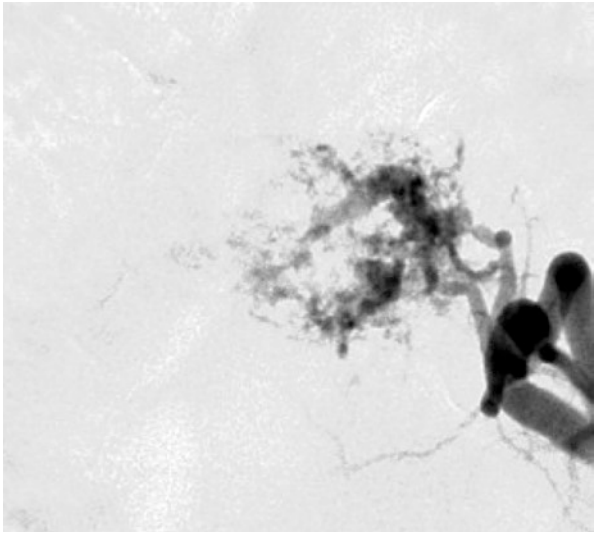

Fig. 8.13 Fifty-six-year old male, aggressive hemangioma in D7, asymptomatic, accidentally discovered because of a road accident; digital subtraction angiography (DSA), anterior-posterior angiogram, early arterial phase: note the tortuous and dilated afferent arterioles

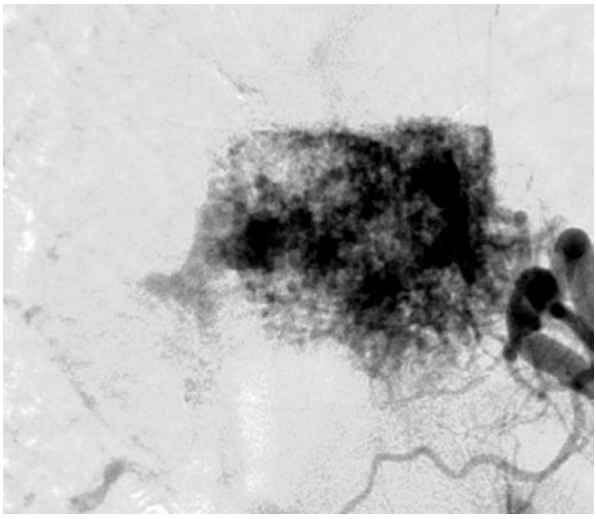

Fig. 8.14 Same patient that in Fig. 8.7, DSA, anterior-posterior angiogram: note multiple blood pools in the capillary phase

and, finally, intense opacification extending beyond the territory throughout the entire vertebral body.

The angiographic report is also necessary to identify the arterial supply of the spinal cord present in the surgical area, thus reducing the risk of spinal cord ischemia correlated to surgery [7]. Angiographic report may be useful in the contest of a differential diagnosis.

Preoperative intra-arterial embolization is often required by the neurosurgeon because it reduces perioperative morbidity related to the high risk of bleeding [26]; it is often realized using sponge fragments [27] or with polyvinyl alcohol (PVA),

channeled through microcatheters that allow the release of the embolic agent into the hemangioma vessel moving from the afferent arteries to the more distal branches.

PVA microspheres are often chosen for the variety of available sizes (from 50 up to 1000 microns), the ability to penetrate into the hemangioma and block to the vessels, and the ease in their surgical removal when necessary. PVA particles embolization (Figs. 8.15 and 8.16) has been even shown in several cases [28] of dramatic reduction of neurological symptoms; such reduction might be only temporary.

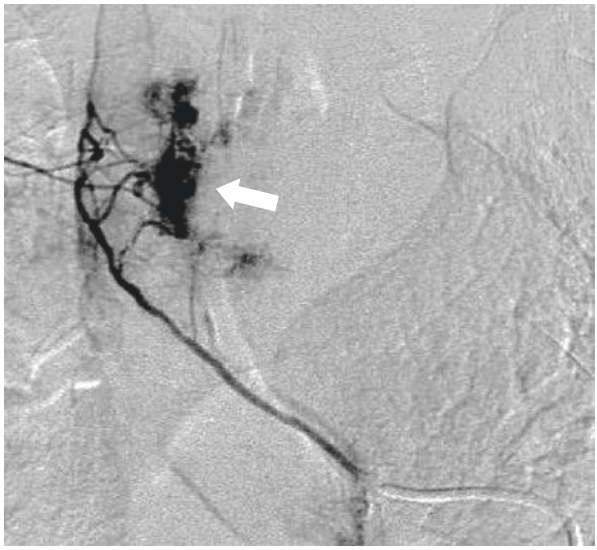

Fig. 8.15 Sixty-five-year-old male, aggressive vertebral hemangioma in D4 in a patient with progressive paraparesis, DSA, anterior-posterior angiogram: note impregnation (*white arrow*) of the arteriole and capillaries with contributions from branches of the right intercostal artery

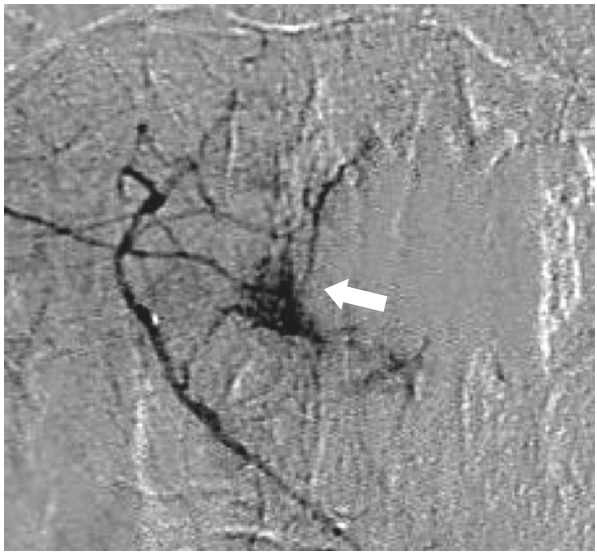

Fig. 8.16 DSA, AP angiogram after embolization with PVA: marked reduction in the vascularization of the hemangioma with minimal residual blush (*white arrow*) and marked clinical improvement; later the patient was subjected to percutaneous vertebroplasty of the intraosseous component of the hemangioma, with further clinical improvement

The usefulness of preoperative embolization is unquestionable, while its role as the sole method of treatment of vertebral hemangiomas is still controversial.

Despite technologic advancements and the experience of even the most skilled interventionalists, *endovascular embolization* is not always feasible. Excessive vascular tortuosity will not allow the microcatheter to navigate distally and steadily in certain cases. If the Adamkiewicz artery (Fig. 8.17) comes from the intercostal arteries related to the hemangioma, it is unsafe to perform embolization (Fig. 8.18). Also, embolization is not feasible when the vessels related to the hemangioma constitute a network of arterioles too thin to be catheterized.

In 1996, Cotten et al. [29] proposed a combined treatment for complex hemangiomas with epidural extension: first endovascular embolization was provided, then VPL of the soma was performed to stabilize the vertebra, and, at last, through an

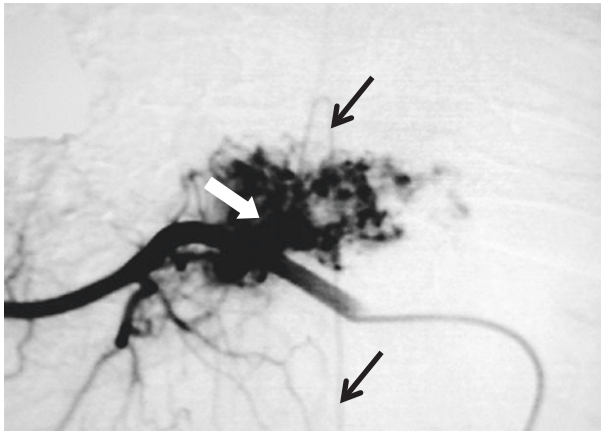

Fig. 8.17 Aggressive vertebral hemangioma in D8, same case of and Fig. 8.2, DSA, AP angiogram: the medullary preoperative angiography showed a great vascularity of the hemangioma (*white arrow*); unfortunately, the embolization from the right intercostal artery was prevented by the presence of Adamkiewicz's artery (*black arrows*), thus it was performed from the left intercostal with great success

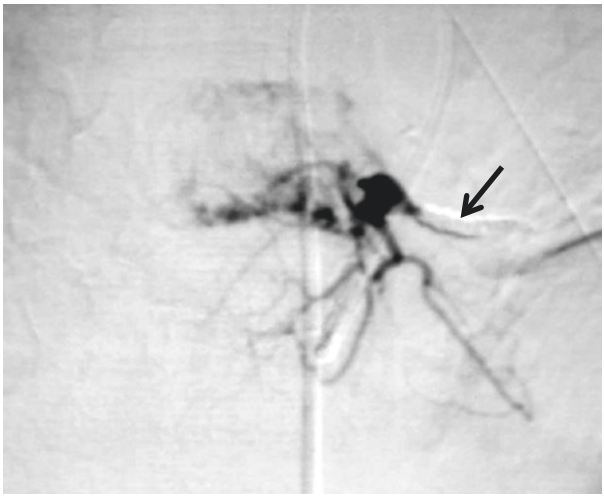

Fig. 8.18 Same case study: DSA, final check after the embolization of the left hemivertebra in D8 with PVA (contour 250–350 microns) performed from the left intercostal artery (*black arrow*): good devascularization of the hemangioma

18G needle inserted in the posterolateral portion of the soma was made a percutaneous injection of *N-butyl, cyanoacrylate*, causing thrombosis of the epidural component of the hemangioma. At the end, surgery was performed with decompressive hemilaminectomy and excision of the embolized hemangioma and residual component: the intervention was carried out safely, with little bleeding.

More recently, some aggressive hemangiomas have been preoperatively embolized intravascularly [30, 31], by means of specific microcatheters (*Rebar or Echelon*), using liquid glues such as Onyx. These aqueous glues are beneficial because they allow a more controlled and faster injection, thus limiting the radiation exposure and obtaining a resolving sclerosis.

For preoperative purposes, the percutaneous transpedicular embolization of aggressive vertebral hemangiomas by *N*-butyl cyanoacrylate has been proposed [32] resulting in a good sclerotization of epidural hemangioma component.

8.2.3 Percutaneous Embolization with Onyx

By developing these previously mentioned experiences, a method has recently been introduced that allows to overcome the anatomical and technical issues found during the attempts of the endovascular embolization by associating the percutaneous embolization with Onyx to the VPL (Figs. 8.19 and 8.20), not only with preoperative but also for therapeutic purposes as the only definitive treatment. This technique, therefore, allows to overcome the neurosurgeons' unwillingness to operate symptomatic or aggressive vertebral hemangiomas without neurological symptoms,

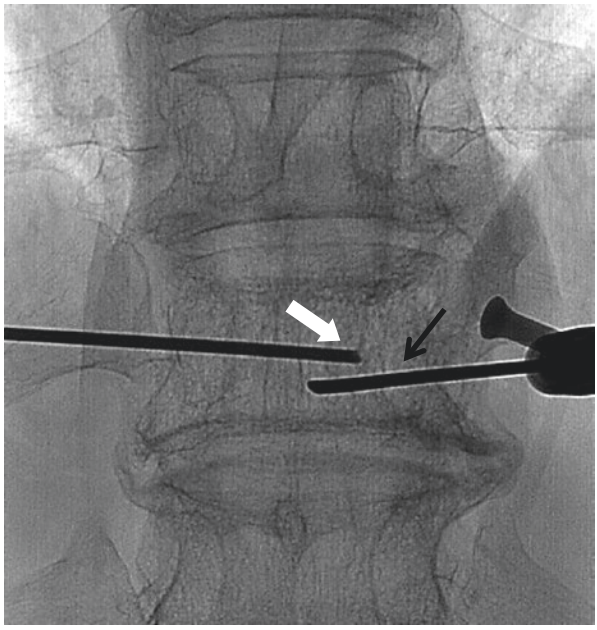

Fig. 8.19 Fifty-six-year-old male, aggressive vertebral hemangioma in the D10; AP radiograph: trocar positioning for VPL (15G.) in the central part of the soma (*white arrow*) and the supporting trocar (15G.) (*black arrow*) for the microcatheter to perform percutaneous embolization of the epidural component of the hemangioma

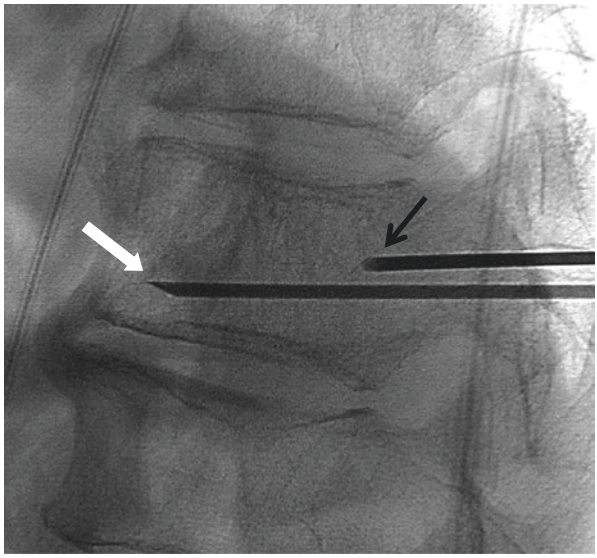

Fig. 8.20 Aggressive vertebral hemangioma in D10, same patient of Fig. 8.13, lateral radiograph: the trocar tip for the VPL (*white arrow*) is very distal, 1/3 of the anterior of the vertebral body, while the supporting trocar (*black arrow*) for the microcatheter is quite posterior, adjacent to the vertebral wall

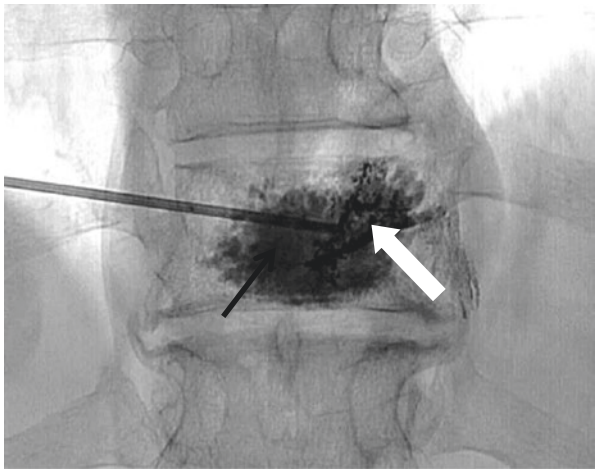

Fig. 8.21 Same patient as before, AP radiograph; VPL has been completed (*black arrow*) and the trocar is removed while injecting the Onyx (recognizable because of its higher radiopacity than PMMA) that fills the vascular channels of epidural sector of the hemangioma (*white arrow*)

because of the fear of bleeding, the complexity of surgery, and the difficulty in obtaining the expected radicality.

A series of treatments of aggressive vertebral hemangiomas with extraosseous component in epidural and/or paravertebral side (Enneking SII-SIII) has been performed [33], by means of a combined percutaneous approach (Fig. 8.21). It consists in performing a VPL of the vertebral body (and if necessary of the peduncles and posterior arch) thus filling the intraosseous component of the hemangioma with PMMA-based cement (Fig. 8.22) and proceeding with the percutaneous embolization by Onyx of the extraosseous component, in epidural and/or paravertebral side, thus causing a sclerosis of the hemangioma and arresting its growth.

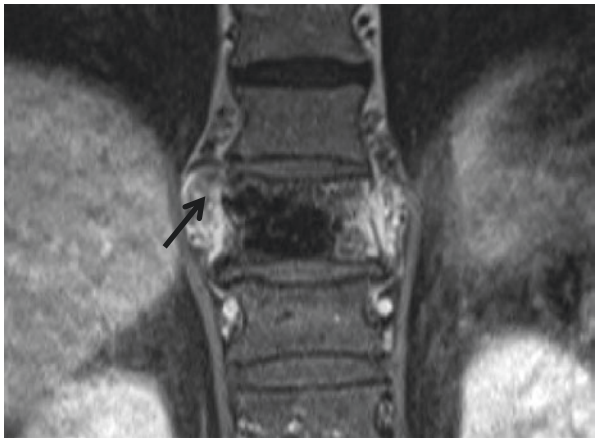

Fig. 8.22 Same patient, MR follow-up after VPL + percutaneous embolization with Onyx, T1 coronal fast spin-echo MR image with fat suppression with contrast: good coverage of the cancellous of the vertebral body with PMMA, recognizable by the hyposignal; a little residual amount of the hemangioma in the right paravertebral side (*black arrow*) is remarkable. Clinically, the patient got a remission of the back pain lasting for more than 1 year.

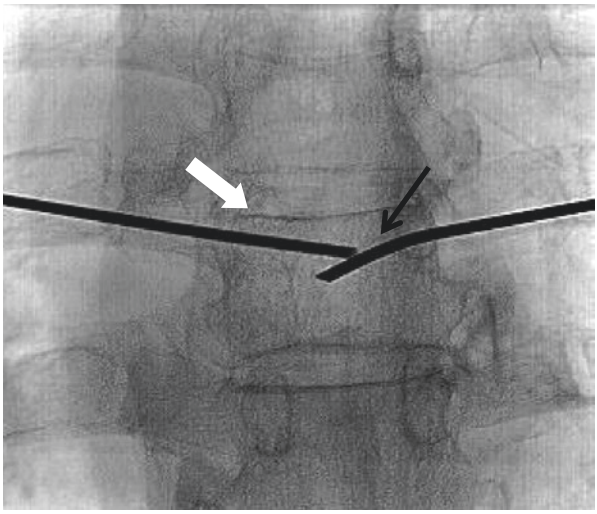

Fig. 8.23 Same patient that in Fig. 8.5 (aggressive hemangioma in the D5 already treated with hemilaminectomy), AP radiograph: trocar positioning for VPL (*black arrow*) in the soma (15G) and trocar (15G) carrying (*white arrow*) the microcatheter (Echelon) for percutaneous embolization of epidural component of hemangioma

The procedure is performed in the angiography room with biplanar angiography under local anesthesia and sedoanalgesia, in-patient hospital.

A trocar for VPL (15G. or 13G.; 10 to 12 cm long) is placed with transpedicular approach for the lumbar vertebrae, preferably transcostovertebral for dorsal vertebrae, and then the tip of this trocar is pushed much further, in 1/3 anterior of the soma, on the midline (Fig. 8.23), to fill as much as possible the vertebral body (Fig. 8.24) with PMMA, yet avoiding cement overflow over the back wall (Fig. 8.25).

Then, an 18 G needle (15 cm long) is placed (or another 15G. needle for VPL if the bone to be crossed seems too compact) with transpedicular (or transcostovertebral) contralateral access (Fig. 8.23) tilting the path so much to reach the midline as posteriorly as possible (Fig. 8.24).

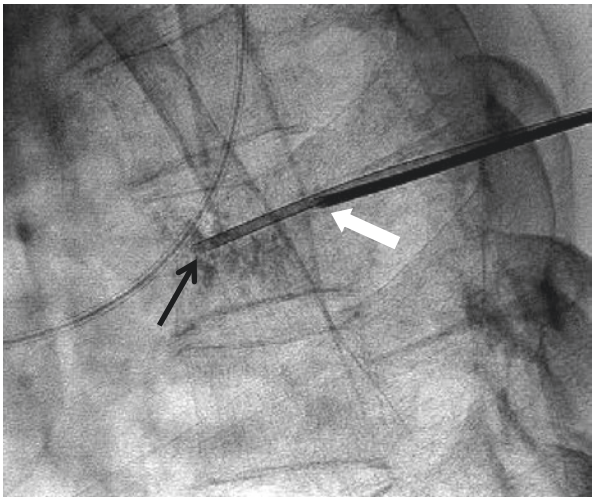

Fig. 8.24 Same case of the previous picture, LL radiograph, by means of the trocar for VPL (*black arrow*) placed in the 1/3 anterior of the vertebral body: you can see an initial filling with PMMA; the trocar (*white arrow*) carrying the microcatheter for the following embolization is in really posterior side, adjacent to the vertebral wall

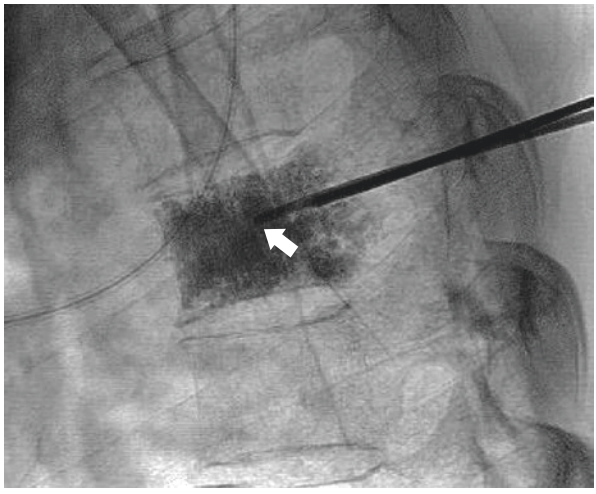

Fig. 8.25 Same case of the previous picture, LL radiogram follow-up: the trocar for VPL (*white arrowhead*) was gradually retracted into the 1/3 posterior of the soma allowing the complete filling of the vertebral body with PMMA, up to the back wall

On the trocar, a Y tap is mounted with a K50 side fitting in order to run tests with contrast medium, while from the main gate a compatible Onyx catheter (ECHELON) is introduced, whose end is pushed just beyond the tip of the needle carrier.

In the first stage, the PMMA is injected into the vertebral body from the trocar, filling the best possible, until the cement reaches the limit of the posterior wall (Fig. 8.25), being careful to any possible leak into unwanted locations, uncommon occurrence, however, for the treatment of the vertebral hemangiomas [34].

Then comes the second stage with the filling of the extraosseous component with Onyx, useful to perform pretests (Fig. 8.26) with contrast medium (Iopamiro 300); the contrast medium, being the vertebral body almost completely occupied by the

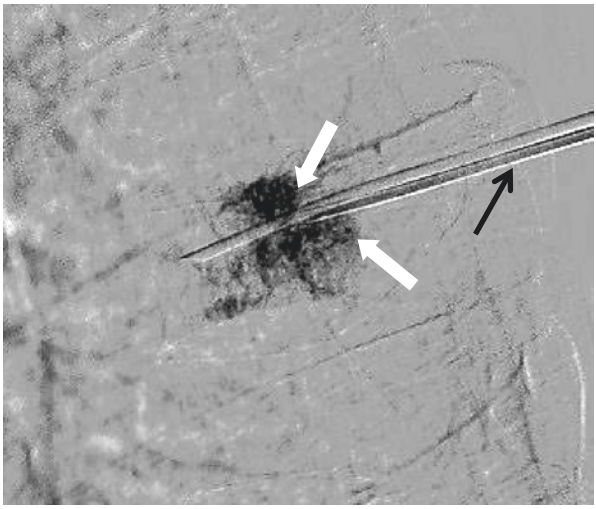

Fig. 8.26 Same case of the previous picture, LL radiogram: through the trocar for embolization (*black arrow*), the operation is performed by injecting contrast medium (Iopamiro 300), resulting in opacification especially in the epidural region of the hemangioma (*white arrows*); these images are useful to guide the following embolization with Onyx

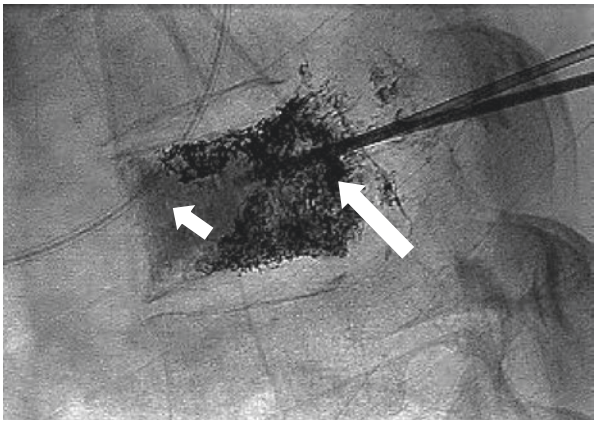

Fig. 8.27 Same case of the previous picture, LL radiogram: after the embolization the Onyx can be appreciated for the marked radiopacity in the epidural compartment of the hemangioma (*white arrow*), while in 2/3 anterior of the soma the less radiopaque PMMA is quite clear (*white arrowhead*)

cement, expands posteriorly into the epidural compartment of the hemangioma, prefiguring thus, as an improper road map, the distribution of the glue that will follow. Next, the injection of Onyx is performed, whose progression is closely monitored with biplane fluoroscopy.

When the filling (this phase, besides, can give rise to local pain) is considered sufficient (Fig. 8.27), roughly comparable to the distribution of the contrast medium during the test, the injection is suspended and a further test (or a final test) is performed, whose outcome (no or poor opacification of residual hemangioma) affects the end of the procedure (Fig. 8.28).

Upon completion, it is useful to perform contrast-enhanced MRI and possibly a CT scan targeted at high resolution with MPR, to evaluate the final result. These controls are also essential for subsequent follow-up, mostly to truly identify possible signs of thrombosis/sclerosis of any remaining portions of the hemangioma not

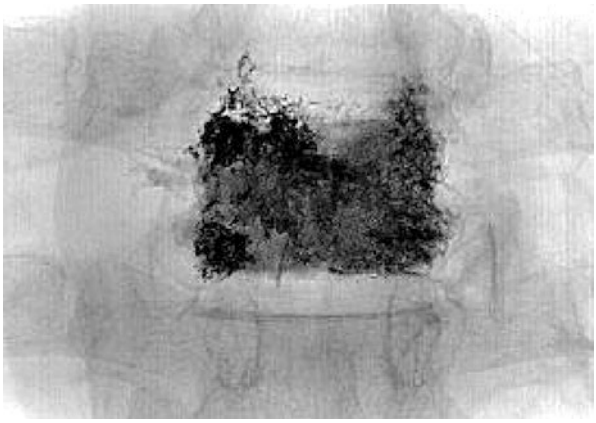

Fig. 8.28 Same case as before, AP final radiogram, after trocar removal at the end of VPL and embolization with Onyx: the vertebral body and epidural compartment of the hemangioma are filled with PMMA and Onyx respectively, recognizable by the different radiopacity

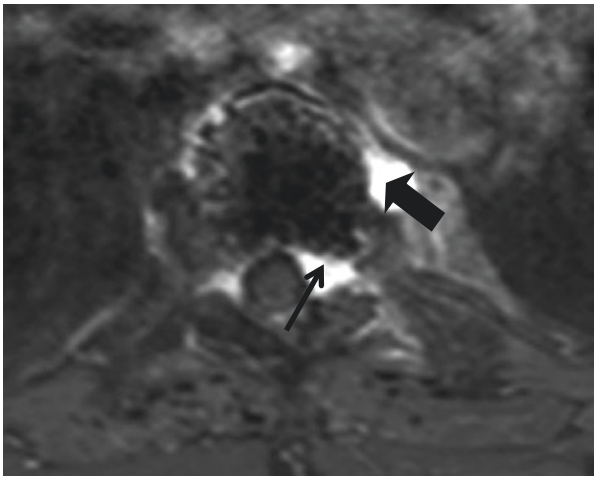

Fig. 8.29 Same case as before, MR follow-up 2 years after the procedure, fast spin-echo MR image with fat suppression with contrast: it shows minimal residual of the hemangioma in the left lateral epidural side (*black arrow*) and in the left paravertebral side (*black arrowhead*)

completely embolized (Fig. 8.29) or to confirm the stability of the result achieved (Fig. 8.30).

Overall, the procedure lasts about 45 to 100 min, depending on the complexity of the case treated and in particular on the importance of extraosseous component of the hemangioma.

In the absence of severe neurological symptoms requiring necessarily a surgical intervention in a short time or even in emergency, aggressive hemangiomas also with epidural component tend to have an extremely slow growth and poor evolutivity [25], which allows to deal with them by carefully planning the most appropriate treatment which may include more than one method with no obligation to immediately reach a final result.

Above all, it is sufficient to stabilize the fracture by strengthening the vertebra and fill the hemangioma in all its components, intraosseous and extraosseous, so as to block the growth, thus obtaining clinical remission. The clinical and radiological stability and

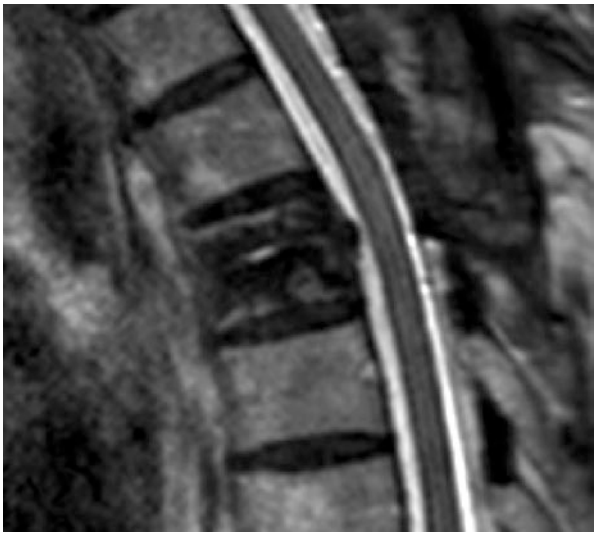

Fig. 8.30 Same case as before, MR follow-up, T2 sagittal: complete filling of the hemangioma in the vertebral body and normal morphology and signal of the dorsal spinal cord; MR imaging has remained unchanged over time, and the patient is still asymptomatic

then the absence of symptoms allow to follow the patient over time, with follow-up very distant in time, completing the treatment, when necessary, in the later stages, when the presence of a worrying residual makes it necessary a further surgery.

References

1. Hsu W, Kosztowski TA, Zaidi HA, et al. Multidisciplinary management of primary tumors of the vertebral column. Curr Treat Options Oncol. 2009;30:107–25.
2. Harel R, Angelov L. Spine metastases: current treatment and future directions. Eur J Cancer. 2010;46:2696–707.
3. Prince EA, Ahn SH. Interventional management of vertebral body metastases. Semin Intervent Radiol. 2013;30:278–28.
4. Rehak S, Krajina A, Ungermann L, et al. The role of embolization in radical surgery of renal cell carcinoma spinal metastases. Acta Neurochir. 2008;150(11):1177–81.
5. Geibprasert S , Pongpech S, Armstrong D, Krings T. Dangerous Extracranial–Intracranial Anastomoses and Supply to the Cranial Nerves: Vessels the Neurointerventionalist Needs to Know AJNR. Am J Neuroradiol. 2009;30:1459–68
6. Yamamoto A, Imai S, Kobatake M, et al. Evaluation of tris-acryl gelatine microsphere embolization with monochromatic X Rays: comparison with polyvinyl alcohol particles. J Vasc Interv Radiol. 2006;17:1797–802.
7. Owen RJ. Embolization of muscoloskeletal bone tumors. Semin Interv Radiol. 2010;27:111–2.
8. Choi IS, Berenstein A. Surgical neuroangiography of the spine and spinal cord. Radiol Clin N Am. 1988;26:1131–41.
9. Barton PP, Waneck RE, Karnel FJ, et al. Embolization of bone metastases. J Vasc Interv Radiol. 1996;7(1):81–8.
10. Berkefeld J, Scale D, Kirchner J, et al. Hypervascular spinal tumors: influence of the embolization technique on perioperative hemorrhage. Am J Neuroradiol. 1999;20(5):757–63.
11. Wilson MA, Cooke DL, Ghodke B, et al. Retrospective analysis of preoperative embolization of spinal tumors. AJNR Am J Neuroradiol. 2010;31:656–60.
12. Acosta FL Jr, Sanai N, Cloyd J, Deviren V, Chou D, Ames CP. Treatment of Enneking stage 3 aggressive vertebral hemangiomas with intralesional spondylectomy. J Spinal Disord Tech. 2011;24(4):268–75.

13. Blecher R, Smorgick Y, Anekstein Y, Peer A, Mirovsky Y. Management of symptomatic vertebral hemangioma: follow-up of 6 patients. J Spinal Disord Tech. 2011;24(3):196–201.
14. Rich JA, Donahue TC, Mick TJ. Symptomatic expansile vertebral hemangioma causing conus medullaris compression. J Manipulative Physiol Ther. 2005;28(3):194–8.
15. Brunot S, Berge J, Barreau X, Ménégon P, Dousset V. Long term clinical follow up of vertebral hemangiomas treated by percutaneous vertebroplasty. J Radiol. 2005;86(1):41–7.
16. Guarnieri G, Ambrosanio G, Vassallo P, Pezzullo MG, Galasso R, Lavanga A, Izzo R, Muto M. Vertebroplasty as treatment of aggressive and symptomatic vertebral hemangiomas: up to 4 years of follow-up. Neuroradiology. 2009;51(7):471–6.
17. Alexander J, Meir A, Vrodos N, Yau YH. Vertebral hemangioma: an important differential in the evaluation of locally aggressive spinal lesions. Spine. 2010;35(18):E917–20.
18. Jawad MU, Scully SP. Enneking classification: benign and malignant tumors of the musculoskeletal system. Clin Orthop Relat Res. 2010;468(7):2000–2.
19. Karaeminogullari O, Tuncay C, Demirors H, Akin K, Sahin O, Ozyurek A, Tandogan NR. Multilevel vertebral hemangiomas: two episodes of spinal cord compression at separate levels 10 years apart. Eur Spine J. 2005;14:706–10.
20. Fox MW, Onofrio BM. The natural history and management of symptomatic vertebral hemangiomas. J Neurosurg. 1993;78:36–45.
21. Castel E, Lazennec JY, Chiras J, Enkaoua E, Saillant G. Acute spinal cord compression due to intraspinal bleeding from a vertebral hemangioma: two case-reports. Eur Spine J. 1999;8(3):244–8.
22. Urrutia J, Postigo R, Larrondo R, Martin AS. Clinical and imaging findings in patients with aggressive spinal hemangioma requiring surgical treatment. J Clin Neurosci. 2011;18(2):209–12.
23. Heyd R, Seegenschmiedt MH, Rades D, Winkler C, Eich HT, Bruns F, Gosheger G, Willich N, Micke O, German Cooperative Group on Radiotherapy for Benign Diseases. Radiotherapy for symptomatic vertebral hemangiomas: results of a multicenter study and literature review. Int J Radiat Oncol Biol Phys. 2010;77(1):217–25.
24. Doppmann JL, Oldfield EH, Heiss JD. Symptomatic vertebral hemangiomas: treatment by means of direct intralesional injection of ethanol. Radiology. 2000;214(2):341–8.
25. Laredo JD, Reizineb D, et al. Vertebral hemangiomas: radiologic evaluation. Radiology. 1986;161:183–9.
26. Kato S, Kawahara N, Murakami H, Demura S, Yoshioka K, Okayama T, Fujita T, Tomita K. Surgical management of aggressive vertebral hemangiomas causing spinal cord compression: long-term clinical follow-up of five cases. J Orthop Sci. 2010;15(3):350–6.
27. Benati A, Da Pian R, Mazza C, et al. Preoperative embolisation of a vertebral haemangioma compressing the spinal cord. Neuroradiology. 1974;7(3):181–3.
28. Raco A, et al. Vertebral hemangiomas with compression: the role of embolization in five cases. Surg Neurol. 1990;34:164–8.
29. Cotten A, Deramond H, Cortet B, Lejeune JP, Leclerc X, Chastanet P, Clarisse J. Preoperative percutaneous injection of methyl methacrylate and *N*-butyl cyanoacrylate in vertebral hemangiomas. AJNR Am J Neuroradiol. 1996;17:137–42.
30. Hurley MC, Gross BA, Surdell D, Shaibani A, Muro K, Mitchell CM, Doppenberg EM, Bendok BR. Preoperative Onyx embolization of aggressive vertebral hemangiomas. AJNR Am J Neuroradiol. 2008;29(6):1095–7.
31. Sedora-Roman NI, Gross BA, Reddy AS, Ogilvy CS, Thomas AJ. Intra-arterial Onyx embolization of vertebral body lesions. J Cerebrovasc Endovasc Neurosurg. 2013;15(4):320–5.
32. Yao KC, Malek AM. Transpedicular *N*-butyl cyanoacrylate-mediated percutaneous embolization of symptomatic vertebral hemangiomas. J Neurosurg Spine. 2013;18(5):450–5.
33. Baruzzi F. Gli angiomi: trattarli? Quando e come? Presentazione al XXVII Congresso nazionale A.I.N.R., L' Aquila 18–21 settembre 2013.
34. Evangelopoulos DS, Kontovazenitis P, Kokkinis K, Glynos M, Korres DS, Sapkas G. Cement leakage in a symptomatic vertebral hemangioma: a case report and review of the literature. Cases J. 2009;2:7148.